Investigating the assembly and egress of arenaviruses

Owen Byford

Supervisor: Dr John N. Barr

Submitted in accordance with the requirements for the degree of

Doctor of Philosophy

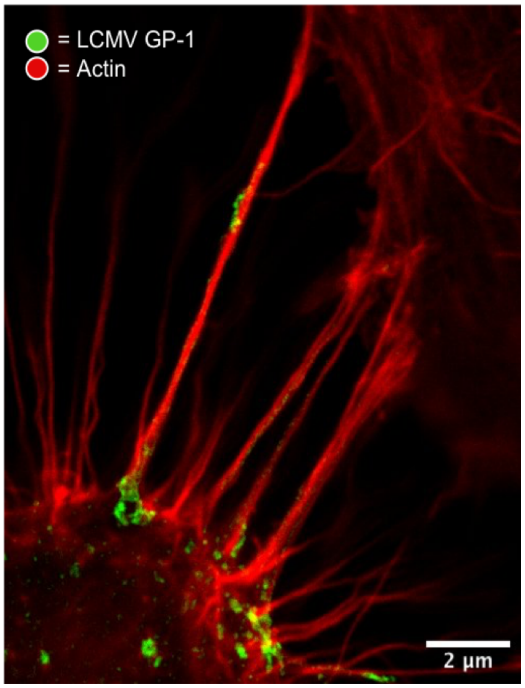

The University of Leeds

The Astbury Centre for Structural Molecular Biology

March 2025

Intellectual property and publication statement

The candidate confirms that the work submitted is his own and that appropriate credit has been given where reference has been made to the work of others.

To my friends and family, I couldn't have done it without you

I think I did pretty well, considering I started out with nothing but a bunch of blank paper

Steve Martin

Acknowledgements

Chapter 2: The siRNA screen was performed by myself, but as part of the MBIOL degree. Dr. Amelia Shaw assisted in the generation of the rLCMV-GP1-FLAG mutant.

Chapter 4: VLP generation and LC-MS analysis was performed by Dr. Allison Groseth, Marine-Noel Klamke, Richard Küchler and Axel Karger (Friedrich-Loeffler-Institut, Germany).

Chapter 4: S343A and S343E S-segment plasmids were generated by Dr. Amelia Shaw and Lee Kipling

Chapter 4: CK-869 treatment alongside LCMV-Arm and LCMV-WE strains was performed by Dr. Allison Groseth and Marine-Noel Klamke (Friedrich-Loeffler-Institut, Germany).

Foremost, I would like to thank John for his guidance and support throughout the 5 years within the group! Without the enthusiam and time spent invested in all my projects, the two publications would not have been possible. I also would like to thank Juan, who has also played a significant role in my scientific development over the years. Thank you for being patient with me while trying to teach me everything related to EM and STA. I would like to acknowledge Martin who has helped me with useful suggestions for the multiple PhD aims throughout. I would like to acknowledge the assistance of the Bio-Imaging and EM facilities who have invested time to help train me on their equipment.

A huge thanks goes to Prof. Roger Hewson and UKHSA funding scheme. Your support and funding has ensured that I have been able to follow my passion and complete this PhD.

To my Barr family that have kept me from insanity I will be sad to leave you all. We started as a Barr star: Much love to my work mama Amelia, your advice throughout my PhD has been instrumental. I think we did alright at working

together to make sure the tools you developed in your PhD were put to good use! My crazy looney work sister Cherrie (who I always clearly destined to meet), I don't think I would have laughed half as much without you. From running to get white roll after you've dropped coffee on your keyboard (AGAIN!) to your ability to each your body weight in noodles, you never failed to make me smile. Auntie Hayley, your bubbly positive energy always cheered me up if I was having a bad science day. I don't think my lab bench will ever be as organised as yours, but then I don't think you'll ever be as organised as me with work lunches (even if it is your new years resolution). Auntie Ellie, thanks for being the Troy to my Gabriella, and allowing me to harmonise with you, VTC has not been the same since you left. Thanks to the new members of the Barr family, Ros, Kate and Sophia for your fresh outlook and renewed energy.

To my friends and family, thanks for supporting me throughout all my studies. To my Dad and Grandma, thanks for believing in me even when I didn't, and pushing me to take opportunities you didn't have. To the Mellor's, thanks for always welcoming me as one of the family and for everything you do for me, Toby and Cooper. A particularly important thank you to Toby. From creating a lovely home to be able to write the thesis stress free, to helping me co-parent for our wild child puppy Cooper, I couldn't have done it without you! Although we might now both be Dr. so we can continue to disagree on which is the real one; I'm aware they don't ask for PhDs when there is a flight emergency. Finally, to the newest addition to our family, Cooper, you have been an adorable distraction during my write-up period. You've grown up so fast, but please stop now as you are suppose to only be a medium Australian Labradoodle not a large!

Contents

List of Figures

List of Tables

Abbreviations

4-AP 4-Aminopyridine

a-DG a-Dystroglycan

agRNA Antigenomic strands

AHF Argentine haemorrhagic fever

AMAV Amapari virus

AP-4 Adapter protein 4

ARF-1 ADP-ribosylation factor 1

BFA Brefeldin A

BSA Bovine serum albumin

BSL Biosafety level

BUNV Bunyamwera virus

CCHFV Crimean-Congo Haemorrhagic fever virus

CHAPV Chapare virus

CK2 Casein kinase 2

CKDs Cyclin-dependent kinases

CLKs CDC-like kinases

co-IP Co-immunoprecipitation

COP-I Coat protein complex I

CSF Cerebrospinal fluid

DAAs Direct acting antivirals

DDX3 DEAD-Box Helicase 3

DIs Defective interfering particles

DMEM Dulbecco modified Eagle medium

dpi Days post infection

dpt Days post transfection

EBOV Ebola virus

EBV Epstein-Barr virus

eIF Eukaryotic initiation factor

eIF2a Eukaryotic initiation factor 2a

eIF4E Eukaryotic initiation factor 4E

ELISA Enzyme-linked immunosorbent assay

EM Electron microscopy

ER Endoplasmic reticulum

ESCRT Endosomal sorting complex required for transport

ExoN Exonuclease

F-actin Filamentous-actin

FBS Fetal bovine serum

FDA Food and Drug Administration

FFA Focus forming assay

FISH Fluorescent in situ hybridisation

GBF-1 Golgi BFA-resistant guanine nucleotide exchange factor 1

GEF Guanine exchange factor

GP-1 Glycoprotein-1

GP-2 Glycoprotein-2

GPC Glycoprotein precursor

GPs Glycoproteins

GSKs Glycogen synthase kinases

GTOV Guanarito virus

HAZV Hazara virus

HCV Hepatitis C virus

HF Haemorrhagic fever

HIV-1 Human immunodeficiency virus 1

HLRV Hailar virus

hpi Hours post infection

hpt Hours post transfection

IAV Influenza A virus

IF Immunofluorescence

IFN-1 Interferon-I

IFN-b Interferon-beta

IGR Intergenic region

IKKe IB kinase-related kinase e

IRF3 Interferon regulatory factor 3

JUNV Junín virus

kDa Kilodaltons

L Large

LACV La Crosse virus

LASV Lassa virus

LC-MS Liquid chromatography–mass spectrometry

LCMV Lymphocytic choriomeningitis virus

LCMV-eGFP LCMV expressing eGFP

LHF Lassa haemorrhagic fever

LUJV Lujo virus

MACV Machupo virus

MAPKs Mitogen-activated protein kinases

MAVS Mitochondrial antiviral signalling protein

MDA-5 Melanoma differentiation-associated protein 5

MG Mini-genome

MOI Multiplicity of infection

MOPV Mopeia virus

MVBs Multivesicular bodies

NHE Na(+)/H(+) exchanger

NMMII Non-muscle myosin II

NP Nucleoprotein

NRP-2 Neuropilin-2

NS2 Nonstructural 2

nt Nucleotide

NW New World

OW Open reading frame

OW Old World

PBS Phosphate buffered saline

PFA Paraformaldehyde

PICV Pichinde Virus

PKR Protein Kinase R

PM Plasma membrane

PML Promyelocytic leukemia protein

RdRp RNA-dependent RNA polymerase

RIG-I Retinoic acid-inducible gene I

RING Really interesting new gene

RT-PCR Reverse transcription polymerase chain reaction

RTCs Replication transcription complexes

RVFV Rift Valley Fever virus

rVSV Recombinant Vesicular stomatitis virus

S Small

SABV Sabiá virus

SARS Severe acute respiratory syndrome

SFM Serum-free media

SKI-1/S1P Subtilisin kexin isozyme-1/site-1 protease

SNV Sin Nombre virus

SSP Stable signal peptide

STED Stimulated emission depletion

TAM Tyro3, Axl, and Mer

TCRV Tacaribe virus

TfR1 Transferrin receptor 1

TGC Total green cell count

TGN Trans-Golgi network

TIIE Total integrated intensity of eGFP expression

TLR Toll-like receptors

TMV Tobacco mosaic virus

TNTs Tunnelling nanotubes

TOA Time-of-addition

Tsg101 Tumor susceptibility gene 101

UTRs Untranslated regions

VLP Virus-like particle

vRNP Viral ribonucleoprotein

Z Matrix protein

Abstract

There are around 70 segmented RNA viruses contained within the *Arenaviridae* family, and multiple members are associated with fatal haemorrhagic fevers, including Lassa and Junín viruses. Established LCMV strains are biosafety level (BSL) 2 pathogens, and can model for these serious pathogens since fatality is only common within immunocompromised populations. Here, the project details three aims which collectively investigate the later stages of arenavirus multiplication. Firstly, an siRNA library, which targeted cellular trafficking components, identified coat protein 1 (COPI) coatomer and adapter protein 4 (AP-4) complexes as important during LCMV infection. Immunofluorescence (IF) was performed for cells infected with an infectious recombinant LCMV harbouring a FLAG tag within GP-1, which identified close co-localisation of COPA, AP4E1 and viral proteins. Additionally, the inhibitor Brefeldin A (BFA) was applied to LCMV infection, which suggests that COPI and AP-4 complexes are critical for efficient virion production.

Secondly, it was noted during live-cell imaging that cells initially infected with LCMV result in infection of neighbouring cells, with discrete foci formed. IF analysis revealed LCMV structural proteins co-localise within cell-cell connections resembling tunnelling nanotubes (TNT-like). Fluorescent *in situ* hybridisation was applied and identified that TNT-like connections also contain genomic sense RNA. Strikingly, blocking the extracellular route of infection (post initial entry) through application of a potent neutralising antibody did not abolish progression of LCMV infection, and thus implied intracellular connections could account for around half of infection events.

Finally, we investigated the phosphorylation of LCMV NP during infection. We noted that CK-869 caused an increased post-translational modification of NP. Through investigations, we reveal that S343 is phosphorylated, and we established infectious NP phospho-ablantant (S343A) and phospho-mimetic (S343E) mutants. Here, we identified that S343 phosphorylation of NP is not a viral-dependent process, and acts in an anti-viral manner within the mouse macrophage RAW264.7 cell line. Mechanistically, we suggest that phosphorylation of NP may trigger lysosomal degradation, reporting co-localisation of NP and LAMP-1 during S343E infected cultures. Additionally, we reveal that S343 NP phosphorylation is LCMV strain

specific, which may contribute to difference in pathogenicity.

Taken together, these results increase our knowledge surrounding the later stages of arenavirus multiplication, which may contribute to the development of effective preventatives or therapeutics.

Chapter 1

Introduction

A virus is defined as an infectious agent that requires a host organism to replicate and multiply [1]. In fact, all living organisms discovered to date can be infected by at least one virus [2]. The first virus to be discovered was Tobacco mosaic virus (TMV), which was isolated by Dimitri Ivanovski and Martinus Beijerinck in the 1890s. Within these studies, it was shown that a distinct pathogen exists which was filterable through Chamberland filter-candle, unlike bacteria [3]. However, it was not until 1931, when Ernst Ruska developed the electron microscope (EM), that visualising viruses became possible. Between the 1930s and 1990s, many viruses were visualised by EM, presenting large variety in shape and size, which was the original basis for classification.

1.1 Arenavirus Introduction

1.1.1 Arenavirus discovery

This thesis will focus on the *Arenaviridae* family, specifically the assembly and egress stages of infection. Regarding arenavirus discovery, in 1933 the first arenavirus was isolated, arising from a patient with a suspected case of St. Louis encephalitis. However, it was determined through the inoculation of mice and monkeys that the causative agent in this instance was a novel virus termed Lymphocytic choriomeningitis virus (LCMV), given the presence of infiltrating lymphocytes in the choroid plexus [4]. The first strain of the virus was isolated by Charles Armstrong in 1933, and subsequently termed LCMV Armstrong (LCMV-Arm) strain, however two other LCMV strains were later isolated [4]. Erich Traub in 1935 isolated a virus from persistently infected mice, with symptoms described strikingly similar to those reported by Armstrong [5]. Later the virus isolated by Traub was confirmed

as LCMV (Traub strain), and the ability to persistently infect the common house mouse (*Mus musculus*) was described [6]. In 1935, a third strain was isolated from a human patient suffering from aseptic meningitis, termed LCMV-WE stain [7].

The subsequent arenavirus species to be identified were not isolated until the late 1950s. For example, Tacaribe virus (TCRV) was isolated from *Artibeus* fruit bats during rabies virus surveillance in Trinidad [8]. Within this study, investigations to isolate TCRV from a rodent host were unsuccessful, leading to the proposal that Jamaican fruit bats may act as a reservoir for arenaviruses [8]; however, later work has disputed this, since TCRV infection was found to cause fatality of Jamaican fruit bats, and bat-bat transmission was not observed despite close contact for a 45-day period [9]. TCRV has also been isolated from mosquitos and ticks, thus the natural host for TCRV remains to be elucidated. In terms of pathogenicity, unlike LCMV, TCRV does not naturally cause human infection.

The ability of arenaviruses to cause serious human pathogenicity was not recognised until 1958, with the isolation of Junín virus (JUNV) [10]. Initially, clinical symptoms remain typical to viral infection including fever, chills, headache, and anorexia. JUNV infection then progresses to Argentine haemorrhagic fever (HF), symptoms of which, in severe cases can include bleeding under the skin, internal organs, or from mouth, eyes, or ears. The mortality rate of untreated individuals of JUNV is around 15-30%. Since its discovery, JUNV has been determined to cause annual outbreaks of HF, with between 300 and 1,000 cases each year [11, 12].

In 1959, the first case of Bolivian HF was described, with the causative agent Machupo virus (MACV), another arenavirus, isolated in 1963 [13]. Between 1962 and 1964, there were significant MACV outbreaks, with over 1000 infected patients, of which 180 deaths were recorded (case-fatality rate of 20%). Of most significance, the next arenavirus to be discovered was Lassa virus (LASV), in 1969. It was determined that LASV was the causative agent of a Lassa HF (now commonly known as Lassa fever), which had been prominent in Nigeria since the 1950s [14]. Today, LASV possess the biggest threat of all arenavirus species, with nearly 60 million people word-wide at risk of infection and around 3 million cases annually, which result in an estimated 67,000 deaths [14].

Subsequent to the identification of LASV, there have been numerous novel

arenaviruses discovered as the cause of localised HF outbreaks in South America. Guanarito virus (GTOV) was isolated in 1989 and identified as the cause of Venezuelan HF. Between 1989-91 only 15 cases were confirmed, however to date there has now been nearly 800 total suspected cases, with a mortality rate of 26% [15]. Sabiá virus (SABV) was identified in 1990, and results in Brazilian HF. Only 5 cases of SABV have been reported so far, three naturally-acquired and two laboratory-acquired, with a mortality of 60% [16–20]. Since there is no routine reverse transcription polymerase chain reaction (RT-PCR) diagnostic testing for SABV, including the area in which SABV cases were recorded, it is likely that infected individuals go unnoticed, and thus the danger of SABV to human health remains unknown. Subsequently, between 2003 to 2004 there was an isolated case with only one individual infected with the arenavirus Chapare virus (CHAPV) [21]. However, a second outbreak occurred between 2019 and 2020 with a further 9 cases [21, 22]. Overall, the mortality rate for the cases of CHAPV is 50%, highlighting the potential virulence.

Finally, Lujo virus (LUJV) was discovered in 2008 following five cases of infected individuals from Lusaka (Zambia) and Johannesburg (South Africa) suffering from HF. All cases of LUJV all began from an index case which transmitted the virus to health care workers during hospitalisation [23, 24]. Overall, the mortality rate for these cases was 80% [23–26]. Again, the true global threat of LUJV is unknown, mainly since routine diagnostics are not available [25].

Collectively, the discovery of new arenaviruses is continuous, with new species being isolated have potential to cause serious human disease. The current recognised arenavirus that poses the biggest threat to global health is LASV, and thus this species is listed as a 'priority pathogen' by the WHO; this is defined as a disease with epidemic potential and/or with no or insufficient countermeasures [27].

1.1.2 Classification

The taxonomy of viruses was updated by the ICTV in 2023, with major changes for bunyavirus species classification. Previously, all families containing bunyaviruses, including *Arenaviridae*, were classified within the *Bunyavirales* order. The recent reorganisation created the *Bunyaviricetes* class, dividing species into two new orders,

namely *Elliovirales* and *Hareavirales* (Figure 1.1).

The *Elliovirales* and *Hareavirales* orders were created to split the previous order *Bunyavirales* into two, based on the RNA-dependent RNA polymerase (RdRp), which exists for each species as part of two distinguishable clades (ICTV, 2023). There are now 592 species classified within the *Bunyaviricetes* class, with 5 families able to cause serious human disease, namely *Hantaviridae*, including Sin Nombre virus (SNV), *Peribunyaviridae*, including La Crosse virus (LACV), *Arenaviridae*, including Lassa virus (LASV), *Nairoviridae*, including Crimean-Congo Haemorrhagic fever virus (CCHFV) and *Phenuiviridae*, including Rift Valley Fever virus (RVFV).

1.1.3 *Arenaviridae* family classification

Species within the *Arenaviridae* family are sub-divided into five genera based on the sequence similarity of the RdRp and nucleoproteins (NP); *Antennavirus*, *Hartmanivirus*, *Innmovirus*, *Mammarenavirus*, *Reptarenavirus*. The host range differs between each genera, including fish (*Antennavirus*), mammals (*Mammarenavirus*) and reptiles (*Reptarenavirus* and *Hartmanivirus*). The host range for *Innmovirus* species is yet to be determined, since the only virus species, Hailar virus (HLRV), was identified through high-throughput sequencing of river sediment samples in China. Collectively, the *Arenaviridae* family currently contains 69 species, all of which are described in Table 1.1.

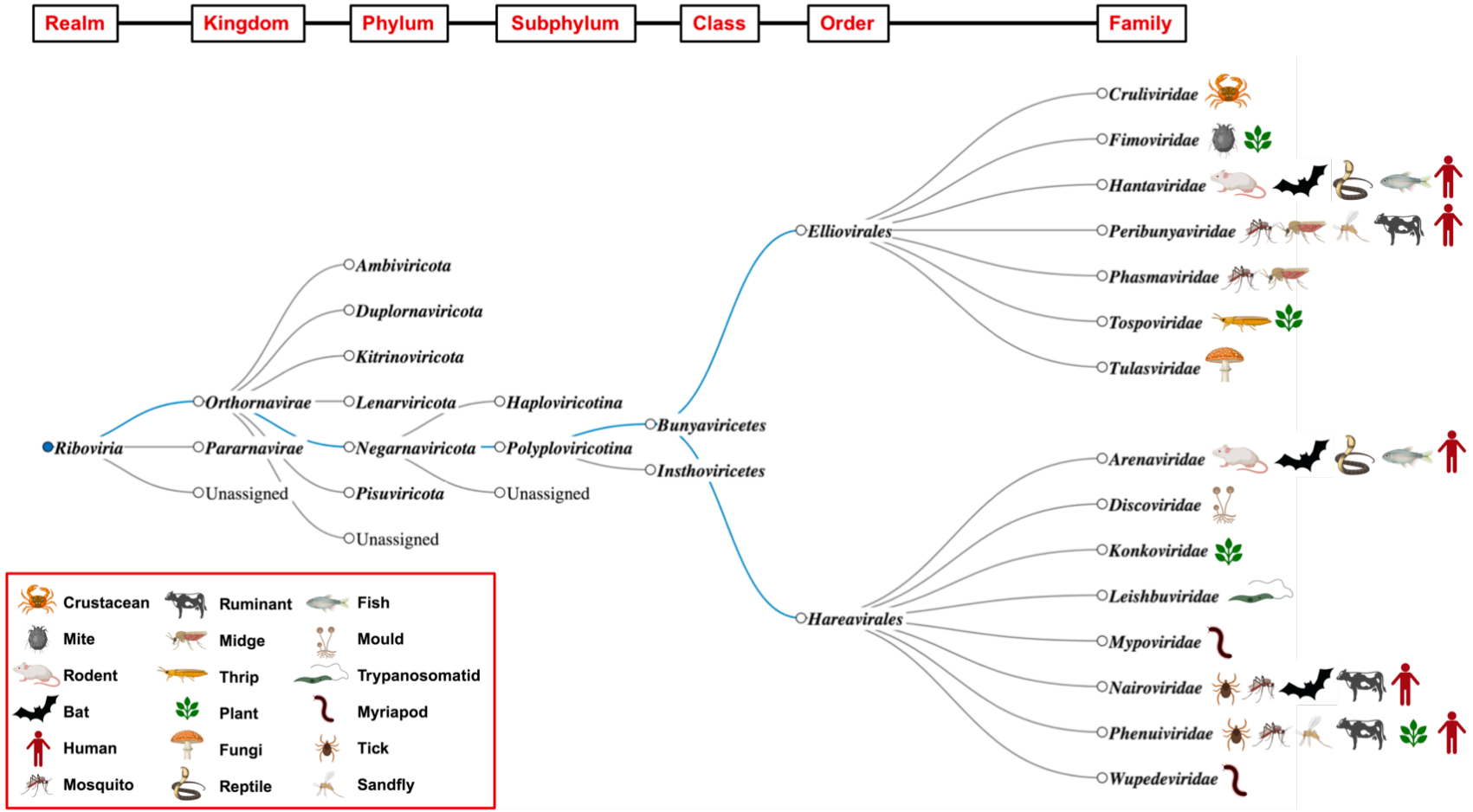

Figure 1.1: Phylogenetic tree of the *Bunyaviricetes* class. Bunyaviruses are classified based on the sequence similarity of the RNA-dependent RNA polymerase (RdRp). For each family, infectable known hosts are shown (see key).

Table 1.1: ICTV-Accepted Taxonomic Organisation of the *Arenaviridae* Family.

Genus	Species	Viruses	Abbr.
Antennavirus	*Antennavirus hirsutum*	Wēnlǐng frogfish arenavirus 2	WlFAV-2
	Antennavirus salmonis	Salmon pescarenavirus 1	SPAV1
	Antennavirus salmonis	Salmon pescarenavirus 2	SPAV2
	Antennavirus striale	Wēnlǐng frogfish arenavirus 1	WlFAV-1
Hartmanivirus	*Hartmanivirus brazilense*	SetPatVet virus 1	SPVV1
	Hartmanivirus haartmani	Haartman Institute snake virus 1	HISV1
	Hartmanivirus haartmani	Haartman Institute snake virus 2	HISV2
	Hartmanivirus helvetiae	Dante Muikkunen virus 1	DaMV1
	Hartmanivirus patriae	Andere Heimat virus 1	aHeV1
	Hartmanivirus quadrati	Big electron-dense squares virus 1	BESV1
	Hartmanivirus scholae	Old schoolhouse virus 1	OScV1
	Hartmanivirus scholae	Old schoolhouse virus 2	OScV2
	Hartmanivirus turici	Veterinary pathology Zurich virus 1	VPZV1
	Hartmanivirus turici	Veterinary pathology Zurich virus 2	VPZV2
	Hartmanivirus unni	Universidad Nacional virus 1	UnNV1
Inmmovirus	*Innmovirus hailarense*	Hailar virus	HLRV
Mammarenavirus	*Mammarenavirus abaense*	Abà-Miányáng virus	AMYV
	Mammarenavirus alashanense	Alxa virus	ALXV
	Mammarenavirus allpahuayoense	Allpahuayo virus	ALLV
	Mammarenavirus amapariense	Amaparí virus	AMAV
	Mammarenavirus aporeense	Aporé virus	APOV
	Mammarenavirus batangense	Batáng virus	BTTV
	Mammarenavirus bearense	Bear Canyon virus	BCNV
	Mammarenavirus beregaense	Berega virus	BEGV
	Mammarenavirus bituense	Bitu virus	BITV
	Mammarenavirus brazilense	Sabiá virus	SBAV
	Mammarenavirus caliense	Pichindé virus	PICHV
	Mammarenavirus cameroonense	Souris virus	SOUV
	Mammarenavirus chapareense	Chapare virus	CHAPV
	Mammarenavirus choriomeningitidis	Lymphocytic choriomeningitis virus	LCMV
	Mammarenavirus choriomeningitidis	Dandenong virus	DANV
	Mammarenavirus cupixiense	Cupixi virus	CUPXV
	Mammarenavirus dhati-welelense	Dhati Welel virus	DHWV
	Mammarenavirus flexalense	Flexal virus	FLEV
	Mammarenavirus gairoense	Gairo virus	GAIV
	Mammarenavirus ganziense	Ganzi virus	GNZV
	Mammarenavirus guanaritoense	Guanarito virus	GTOV
	Mammarenavirus ippyense	Ippy virus	IPPYV
	Mammarenavirus juninense	Junín virus	JUNV
	Mammarenavirus kitaleense	Kitale virus	KTLV
	Mammarenavirus kwanzaense	Kwanza virus	KWAV
	Mammarenavirus lassaense	Lassa virus	LASV
	Mammarenavirus latinum	Latino virus	LATV
	Mammarenavirus lijiangense	Lìjiāng virus	LIJV
	Mammarenavirus loeiense	Loei River virus	LORV
	Mammarenavirus lujoense	Lujo virus	LUJV
	Mammarenavirus lunaense	Luna virus	LUAV
	Mammarenavirus lunaense	Luli virus	LULV

Continuation of Table 1.1

Genus	**Species**	**Viruses**	**Abbr.**
	Mammarenavirus lunkense	Lunk virus	LNKV
	Mammarenavirus machupoense	Machupo virus	MACV
	Mammarenavirus mafigaense	Mafiga virus	MAFV
	Mammarenavirus marientalense	Mariental virus	MRLV
	Mammarenavirus mecsekense	Mecsek Mountains virus	MEMV
	Mammarenavirus merinoense	Merino Walk virus	MRWV
	Mammarenavirus mopeiaense	Mopeia virus	MOPV
	Mammarenavirus mopeiaense	Morogoro virus	MORV
	Mammarenavirus ngerengerense	Ngerengere virus	NGEV
	Mammarenavirus okahandjaense	Okahandja virus	OKAV
	Mammarenavirus oliverosense	Oliveros virus	OLVV
	Mammarenavirus paranaense	Paraná virus	PRAV
	Mammarenavirus piritalense	Pirital virus	PIRV
	Mammarenavirus praomyidis	Mobala virus	MOBV
	Mammarenavirus ryukyuense	Ryukyu virus	RYKV
	Mammarenavirus solweziense	Solwezi virus	SOLV
	Mammarenavirus songeaense	Songea virus	SOGV
	Mammarenavirus tacaribeense	Tacaribe virus	TCRV
	Mammarenavirus tamiamiense	Tamiami virus	TMMV
	Mammarenavirus tietense	Tietê virus	TIEV
	Mammarenavirus wenzhouense	Wēnzhōu virus	WENV
	Mammarenavirus whitewaterense	Whitewater Arroyo virus	WWAV
	Mammarenavirus whitewaterense	Big Brushy Tank virus	BBRTV
	Mammarenavirus whitewaterense	Catarina virus	CTNV
	Mammarenavirus whitewaterense	Skinner Tank virus	SKTV
	Mammarenavirus whitewaterense	Big Tonto Creek virus	TTCV
	Mammarenavirus xapuriense	Xapuri virus	XAPV
Reptarenavirus	*Reptarenavirus aurei*	Golden Gate virus	GOGV
	Reptarenavirus californiae	CAS virus	CASV
	Reptarenavirus commune	Tavallinen suomalainen mies virus 2	TSMV2
	Reptarenavirus giessenae	University of Giessen virus 1	UGV1
	Reptarenavirus giessenae	University of Giessen virus 2	UGV2
	Reptarenavirus giessenae	University of Giessen virus 3	UGV3
	Reptarenavirus rotterdamense	ROUT virus	ROUTV
	Reptarenavirus rotterdamense	University of Helsinki virus 1	UHV1

1.1.4 Epidemiology and geographical distribution

The *Mammarenavirus* family contains members that can be described as either Old World (OW) or New World (NW) arenaviruses. Mammarenaviruses were initially assigned as OW or NW based on the geographical origin and serological classification, but have now been shown to exhibit distinction at the phylogenetic level [28] (Figure 1.2). Except for LCMV (which is distributed worldwide), OW mammarenaviruses are distributed throughout Africa within populations of rodents from the Muridae family [39–41], but also rodent or shew species throughout Asia [42]. There is no further distinct classification of the OW arenaviruses, and only three viruses are known to cause human infection: LCMV, LASV, and LUJV. NW mammarenaviruses are located throughout America, with the natural host being the *Cricetidae* family, *Sigmodontinae* subfamily, of *Muridae* family mice, except for TCRV and Ocozocoautla de Espinosa virus (OCEV), whereby the viruses have been isolated from *Artibeus* bats (TCRV), *Amblyomma americanum* ticks (TCRV) and *Peromyscus mexicanus* mice (OCEV) [43–46].

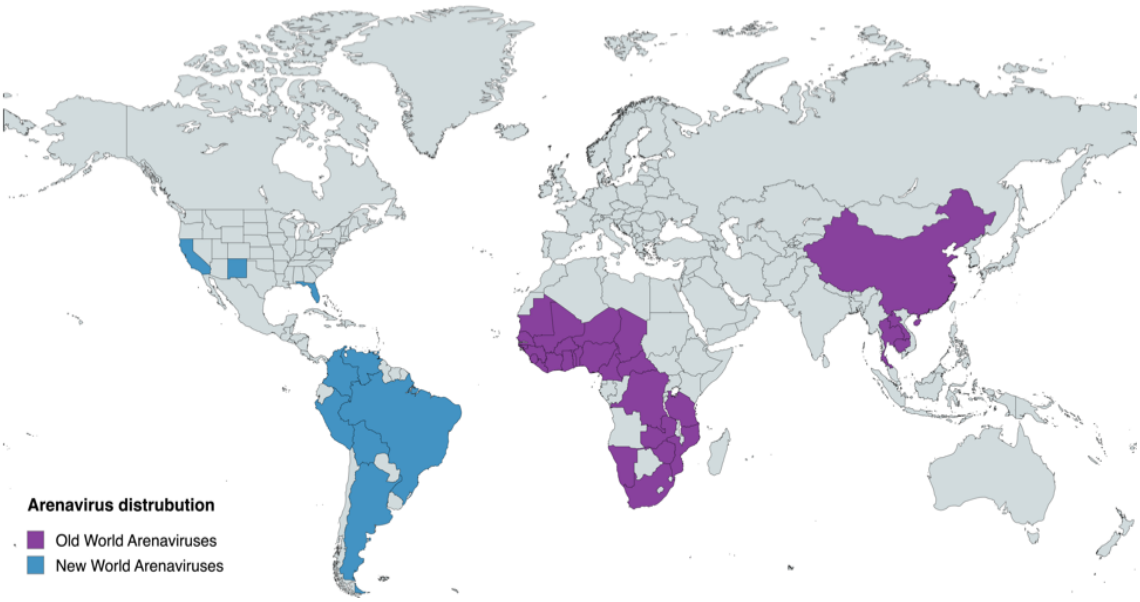

Figure 1.2: Geographical representation of countries where mammarenavirus species are endemic. Old World mammarenavirus (purple) species are located mainly within sub-Saharan Africa, with a select range of species also present in China, Thailand, Laos and Cambodia. New World mammarenavirus (blue) species are widespread within South America, with most South American countries and three states of the United states of America (California, New Mexico and Florida) possessing mammaarenavirus species. It is likely that other countries possess undetected mammarenavirus species. Figure created using mapchart.net and information from the literature [29–38].

Since NW viruses are more genetically diverse, they are divided into four separate lineages: clades A, B, C and D (A/Rec). Clade B contains the NW mammarenaviruses which possess the biggest threat to humans, with five members able to cause haemorrhagic fever: JUNV, MACV, GTOV, SABV and CHAPV. Since TCRV is a clade B virus, yet does not cause human disease, this virus remains a useful model for the highly pathogenic related species (Figure 1.3).

1.1.5 Virus emergence

Emerging and re-emerging infectious diseases present a serious threat to public health, and human factors contribute to the increase in incidence. In relation to arenaviruses, agricultural practices from increased farming demands have contributed significantly to increasing arenavirus zoonotic events. Human infection of arenaviruses with the ability to cause HF, occurs via zoonosis, routinely from rodent-human transmission. The viruses JUNV, MACV and LASV have all emerged due to increased agriculture [12, 48, 49]. For JUNV, the removal of pampas grass for planting of maize allowed the natural rodent host of JUNV, *Calomys musculinus*, to thrive; since JUNV can be transmitted via inhalation of aerosols produced from rodent excreta, the increased incidence of Argentine HF began, particularly affected farmers [50]. Although JUNV remains restricted to Argentina, populations of *C. musculinus* now cover 150,000 km^2, an area conferring that over 5 million individuals are now at risk [51, 52]. Through comparable practices, due to increased contact with *Calomys callosus* and *Mastomys natalensis*, the emergence of MACV and LASV has also occurred [53–55].

As evidenced, the emergence of mammarenaviruses frequently correlates to the increased geographical distribution of the natural reservoir. LCMV is a demonstration of this; the isolation of LCMV worldwide is due to the presence of the common house mouse (Mus musculus) on every continent apart from Antarctica [56]. Serological studies indicate that LCMV infections occur frequently, and the pathogen goes underrecognised. In the US, serology studies have demonstrated that 5% of American adults have antibodies against LCMV, implying prior exposure [57, 58]. In Finland, two human serological studies corroborate this, also indicating an LCMV seroprevalence for adults of approximately 5% [59, 60].

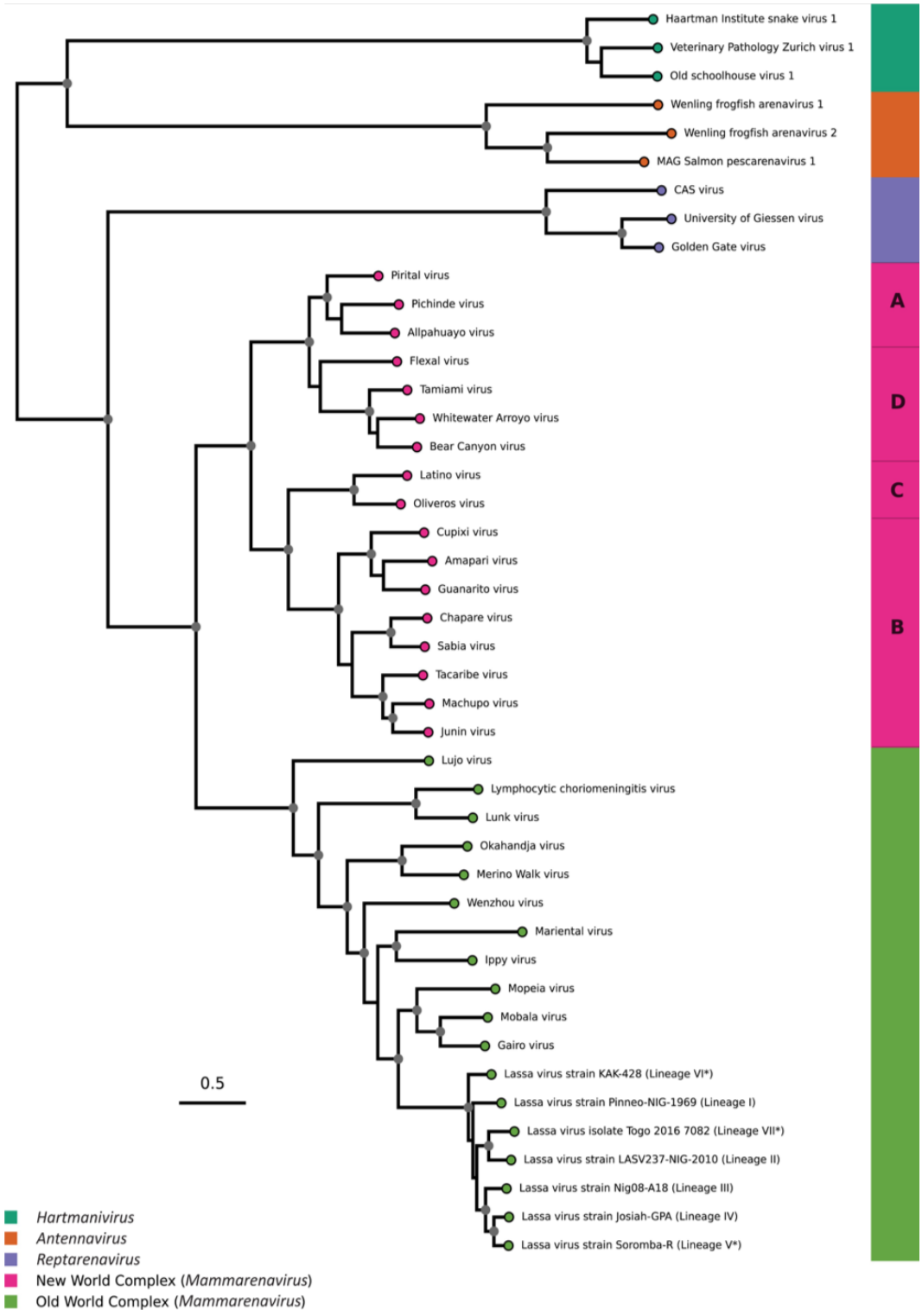

Figure 1.3: Phylogenetic tree of the Arenaviridae family. The sequence of L protein was utilized for grouping. Clustering of OW (green) and NW (pink) mammarenaviruses is shown, alongside divergence nodes with likely common ancestors. For NW mammarenaviruses, species belonging to each clade are highlighted. To highlight the likelihood of divergence, representative species from *Hartmaniviridae* (teal), *Antennaviridae* (orange) and *Reptarenaviridae* (purple) genera are included. This figure was taken from [47].

1.1.6 Pathogenicity and disease

Haemorrhagic fever (OW arenaviruses)

As mentioned above, specific arenaviruses species can cause serious human disease and fatality. The OW arenavirus LASV is of particular concern since it causes 10,000 deaths annually in West Africa [61]. However, symptoms from LASV infection can range from fever, cough, sore throat, malaise and gastrointestinal upset to more severe presentation such as pleural effusion, irreversible hearing loss, neurological sequelae, mucosal bleeding, hepatitis, pulmonary oedema, respiratory distress and shock [62–64]. The irreversible hearing loss as a result of LASV infections affects 30% of infected individuals, and is currently a leading cause of morbidity throughout west Africa [65]. LUJV is the only other OW arenavirus species able to cause HF. Generally, the symptoms of LASV and LUJV are identical, yet LUJV results in additional clinical presentations including rash, chest pain, myalgia and increased liver aminotransferases [66].

LCMV pathogenicity

Although LCMV does not cause HF, it can cause serious complications for infected individuals, and is regarded as an underrecognised source of meningitis and meningoencephalitis [56]. Infection occurs through inhalation of infected rodent saliva, urine, faeces or nasal secretions [67]. The stability of the virus outside of the natural reservoir has not been examined but is regarded to be short-term [4]. Upon inhalation, LCMV replication first proceeds in the lung tissues, and then disseminates by the bloodstream to other organs, resulting in a systemic infection [68]. Subsequent to systemic infection, LCMV infects the meninges, choroid plexus and ventricular ependymal linings. The disease resulting from LCMV infection typically persists for 1-3 weeks, yet in severe cases this may extend for several months [69]. The initial LCMV symptoms are non-specific and include fever, headache, malaise, myalgia, anorexia and gastrointestinal upset [56]. Later stages of LCMV infection result in more severe neurological presentations associated with aseptic meningitis and meningoencephalitis including photophobia, fever and nuchal rigidity [70–72]. These resulting symptoms and neurological characteristic of the

meningitis determine the viruses name [56, 73]. LCMV remains unacknowledged since the overall mortality of acquired infections is less than 1%. However, given the seroprevalence of 5%, LCMV still represents a significant threat, particularly if spontaneous mutations or recombination events increase pathogenicity [57–60].

Since LCMV is underrecognised, one serious complication of LCMV is transmission through transplantation of infected tissues [74, 75]. Since organ transplantation requires immunosuppressive therapy to ensure organ rejection does not occur, the immune system is compromised at clearing LCMV infection. Thus, in the fourteen reported cases, eleven of the organ recipients died [74–76]. In a clustering of cases in 2008, the LCMV-infected donor did exhibit symptoms including fever and cerebrospinal fluid (CSF) lymphocytosis, but serology was negative for the viruses routinely tested, allowing the organ donations. To date, LCMV screening is still not performed during organ donation, and there is no specific Food and Drug Administration (FDA)-approved test for donor screening [75].

In addition to the discussed acquired LCMV infections, the virus may also be transmitted congenitally. Here, the foetus acquires LCMV transplacentally or in rare instances through maternal vaginal secretions or blood [56]. LCMV infects the brain of the developing foetus, resulting in significant neurological changes including microencephaly, periventricular calcifications, hydrocephalus, cerebellar hypoplasia, focal cerebral destruction, and gyral dysplasia [56]. Unlike acquired infection, congenital infection often causes severe outcomes [56]. Overall, the mortality rate of infants that contract prenatal LCMV infection is estimated to be between 30 – 35% [56, 77]. Additionally, all survivors have neurological morbidities including vision impairment, mental retardation, spastic quadriparesis, ataxia and epilepsy [78]. The difference in outcome for infection has been related to the age of the developing host at the time of infection since the brain morphology rapidly changes during this time [79].

Haemorrhagic fever (NW arenaviruses)

To date, five NW arenaviruses that cause HF have been identified: JUNV, MACV, GTOV, SABV and CHAPV. In general, the mild symptoms of NW HF are similar to LASV and LUJV, but can also include mild hypotension, conjunctivitis,

petechial haemorrhage of the soft tissues, lethargy, and irritability [80]. OW and NW arenaviruses that cause HF also share many of the same severe symptoms. However, one key difference is that LASV infection often results in patients suffering from hepatitis, yet hepatitis is a rare outcome in cases of NW HF arenaviruses. Another difference is that JUNV, GTOV or MACV infection often confers a higher probability that patients will suffer from neurological symptoms, haemorrhaging, leukopenia, and thrombocytopenia compared to LASV [81].

1.1.7 Diagnostics

Regarding mammarenaviruses that cause HF, epidemiology and clinical manifestations are often used for diagnosis rather than laboratory testing. There are currently no commercially available tests for mammarenaviruses, thus patient sampling is not routinely performed. If required, large public health laboratories can perform RT-PCR or serology testing to confirm some specific mammarenavirus infections [82]. Specifically, LASV infection can be confirmed utilising RT-PCR of patient serum, but the high level of genetic variability means this can be challenging, and certain strains may be reported as a false negative [83]. Serological diagnostic via enzyme-linked immunosorbent assay (ELISA) is more commonly utilised; detection of mammarenavirus-reactive IgG antibodies or sandwich-capture methods whereby novel monoclonal antibodies can detect specific NP of mammarenaviruses [82]. Since testing of patients is only requested in severe cases, it remains challenging to estimate the exact number of cases for each mammarenavirus species, and thus the overall threat posed.

1.1.8 Treatments

Currently, there are no specific FDA-approved inhibitors against mammarenaviruses. However, ribavirin, a synthetic guanosine nucleoside, has been used in some cases. Experimentally, in human cases, ribavirin has been shown to be advantageous for MACV and JUNV infections if administered early [84, 85]. Additionally, a study concluded that the use of ribavirin for LASV infection decreased mortality [86]. However, a recent subsequent analysis of the same data provided contradictory conclusions and suggests that in certain groups

the mortality rate for LASV patients was increased when treated with ribavirin [87, 88]. Investigations have shown that there are significant harmful side effects of ribavirin treatment, with 61% of patients treated for severe acute respiratory syndrome secondary to coronavirus infection exhibiting hemolytic anemia [89]. Additionally, hypocalcemia and hypomagnesmia were reported in 58% and 46% of patients, respectively. Thus, these side effects, combined with the lack of substantial evidence of ribavirin efficacy, reveal that there is a need for specific mammarenavirus treatments [89].

Direct acting antivirals (DAAs)

Direct acting antivirals (DAAs) offer an efficient way to tackle viral infections. However, since DAAs apply a selection pressure, viral mutations may arise, resulting in treatment resistance. When used in combination, multiple DAAs may restrict the ability of resistance mutations. The successful use of DAAs for treatment of human immunodeficiency virus 1 (HIV-1) highlight the importance of understanding the host cell requirements of viruses. Currently, with early diagnosis and DAAs which target multiple different stages of infection, HIV-1 may be suppressed to undetectable levels, with no HIV-1 related symptoms, and an estimated life expectancy comparable to the general population [90].

In relation to mammarenaviruses, important gaps in our knowledge surrounding the stages of virus multiplication remain, particularly the later stages including assembly, egress and budding; thus, this limits the ability for the development of specific DAAs and effective therapeutics. However, since more information is available regarding arenavirus entry, some potential mammarenavirus inhibitors have been identified targeting glycoprotein-mediated receptor binding, internalisation, endocytosis or membrane fusion [91].

Repurposing of FDA-approved compounds

Recently, a potential avenue for future treatment of arenaviruses was published [92]. Here, broad-spectrum potassium ion channel inhibitors were used during *in vitro* LCMV infection and revealed that K^+ ions were required during LCMV entry [92]. Using biochemical approaches in tissue culture, it was shown that K^+

ions were not required for GP-1-mediated receptor binding or fusion, and thus suggested that K^+ ions were required during arenavirus uncoating to mediate viral ribonucleoproteins (vRNPs) release [92]. Interestingly, within this study, quinine, quinidine and 4-Aminopyridine (4-AP) were shown to be effective against LCMV, and all of these compounds are already FDA-approved for other conditions. Quinine has approved use in the treatment of malaria, whilst quinidine (NUEDEXTA) may be used for treatment of Pseudobulbar Affect and 4-AP is used in treatment of walking-related motor issues in multiple sclerosis. It remains undetermined if these inhibitors are broad-spectrum arenavirus antivirals, or if at the current FDA-approved concentrations the compounds have efficacy, yet this should be further examined with animal models [92]. Other FDA-approved compounds that target voltage-gated calcium channels have been shown to effectively inhibit JUNV [93]. Here, gabapentin, used in the treatment of epilepsy, inhibited JUNV virus-cell fusion blocking entry, and when applied to a mouse model prevented JUNV infection [93]. Additionally, verapamil, utilised to prevent chest pain, also inhibited JUNV infection, alongside reducing infection of LCMV and LASV pseudoviruses [93, 94]. Collectively, these results highlight how existing FDA-approved compounds could potentially be applied to arenavirus treatments, but further clinical trials are required to ensure their efficacy.

Naturally isolated compounds

A promising alternative for arenavirus therapies is the use of naturally-isolated compounds that exhibit anti-viral properties. A botanical screen comprised of 1058 naturally-occurring compounds, discovered that casticin and bergamottin inhibit LASV pseudoviruses [95]. Casticin was established to inhibit GP-2-mediated fusion, and this mechanism of inhibition was retained for several pseudotyped NW and OW arenaviruses [95]. Bergamottin was shown to have potency due to disrupting the endocytic trafficking of LASV, with the compound also having efficacy against LCMV [95]. Beside these, other compounds including capsaicin and tangeretin have also been shown to inhibit arenavirus entry stages [96, 97]. Since all of the naturally derived compounds discussed were established utilising arenaviruses pseudoviruses, and thus assess only entry stages, it is plausible that a large number of unidentified compounds also exist that target the later stages of arenaviruses multiplication.

Immune serum

One mode of therapy that been historically utilised in cases of Argentine HF (AHF) is the transfer of immune serum to infected patients. Initially, serum was administered due to being advantageous in treatment of other viral infections including hepatitis, rubella, poliomyelitis, mumps and measles; yet it was not until the 1970s that efficacy for this specific treatment of JUNV was examined [11]. Between 1974 and 1978, 188 JUNV patients entered a double-blind trial whereby one group received normal plasma, and the other group received immune plasma. The case fatality for the patients that received the normal plasma was 16.5%, yet this was only 1.1% in those that received the immune plasma [98]. In this study, 500 mL of immune serum was administered to JUNV patients within the first 8-days of symptoms onset, thus the effectiveness of late-administration was unknown. The advantageous benefit to immune serum was thought to be based on specific neutralising antibodies against JUNV, since viremia was shown to be reduced for patients subsequent to immune serum transfusion [99]. Following the publishing of this study, in JUNV endemic regions, the early use of immune plasma was endorsed by doctors and nurses.

Vaccines

Alongside the lack of specific FDA-approved therapeutics, there are also currently no FDA-approved licenced vaccines for mammarenaviruses. Despite not being FDA-approved, a live-attenuated JUNV vaccine (Candid #1) is used in endemic regions, and has had significant impact on reducing the number of AHF cases [100]. Candid #1 is a strain of JUNV that was serially passaged between non-host animals and cultured cells, which can provide protection against lethal JUNV infection [100, 101]. In model systems the vaccine was shown to have an estimated effectiveness of 98.1% [100, 102]. In 1992, the vaccine became available, but only in Argentina, and has been continued to be administered seasonally to at-risk agricultural workers. Since the vaccination scheme began, nearly 250,000 vaccinations have been administered, and the number of AHF cases has decreased [11]. However, despite limiting JUNV infection and AHF, Candid #1 is unlikely to become FDA-approved or licenced for global use, since Candid #1 is a live-attenuated JUNV vaccine with

the potential for reversion, which has been shown to be possible in a cell culture system [103]. A non-revertant Candid #1 modified by reverse genetics (K33S Candid #1) has been proposed in an animal model system, but this is yet to be translated to large-scale use [104].

Besides Candid #1, many other potential vaccine candidates are under development, but the vast majority of these are in preclinical stage, with only a small proportion currently in phase I trials [105]. One vaccine candidate already in phase I trials is the DNA vaccine candidate INO-4500. This vaccine expresses LASV glycoprotein precursor (GPC), which induces a strong immune response, and confers 100% lethal LASV protection for cynomolgus non-human primates [106]. Another promising avenue is the use of recombinant vesicular stomatitis virus (rVSV) within vaccines, which provide long-term immunity. [104, 105]. This system has been utilised for LASV (rVSVΔG-LASV-GPC), and the vaccine candidate is currently in phase I trials. The rVSVΔG-LASV-GPC vaccine has already been shown to protect non-human primates and guinea pigs against lethal LASV, through generation of neutralising antibodies against the LASV GPC, and an immune response driven by T-cell activation [107–110]. One particular challenge for any mammarenavirus vaccine is the high genetic variability, even for a single species. In the case of LASV, seven different linages exist, and these are antigenically distinct; neutralising antibodies generated against LASV lineage IV do not protect against linage I [111]. Thus, ensuring any mammarenavirus vaccine can protect against all variants of the desired species could limit progression of vaccine candidates.

1.2 Molecular biology of arenaviruses

1.2.1 Arenavirus virion architecture

Arenavirus virions visualised via cryo-electron microscopy do not conform to defined shapes, and depending on species can be spherical, oval or pleomorphic. In general, the diameter of virions ranges between 40 to 200 nm [112]. The viral particles are enveloped, with a cell-derived membrane that are coated by randomly arranged glycoproteins [113, 114]. Underneath the viral membrane, the matrix protein (Z) forms an additional layer [113, 115, 116] connecting with the vRNPs, which are

made of vRNA coated with NPs, and interacting with the L (Figure 1.4). The name arenavirus originates since the particles were visualised with a "sandy" (Latin, arena) interior, due to the reported presence of ribosomes [117]. However, verification for functional cellular ribosomes packaged within particles is limited and requires further clarification.

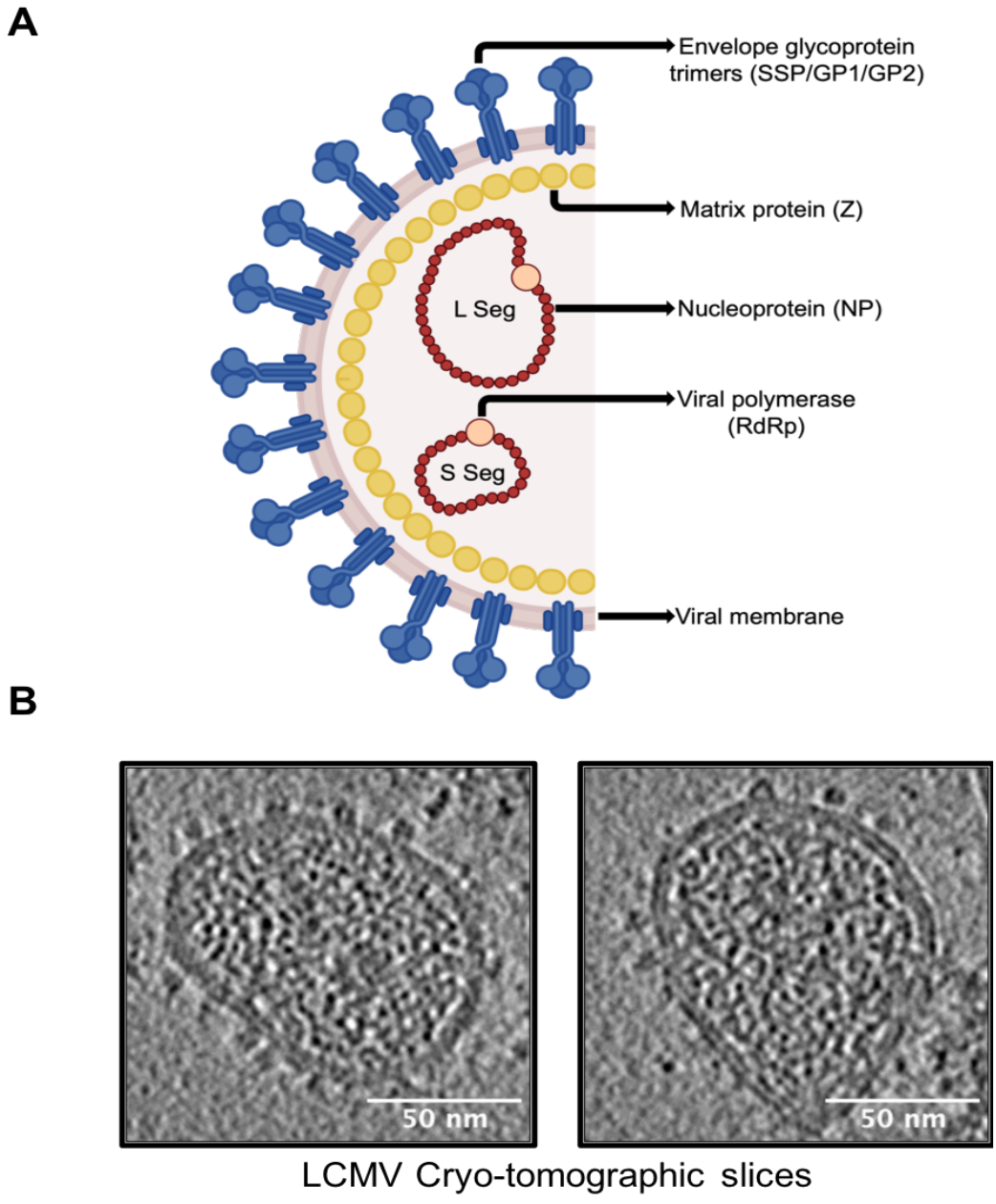

Figure 1.4: Schematic of arenavirus virion. (A) The S and L vRNAs are wrapped by NP (red), and together with L (pink) form vRNPs, which packages vRNA into infectious progeny virions. The Z protein (yellow) forms a layer between the viral membrane and vRNPs. The viral spike protrusions are trimers of SSP/GP-1/GP-2 and decorate the surface of virions. (B) Cryo-tomographic slices of purified LCMV virions. Scale bar, 50 nm (A. Shaw, unpublished).

1.2.2 Arenavirus genome

The arenaviruses genome consists of distinct ambi-sense RNA segments, with mammarenaviruses possessing small (S) and large (L) segments. Utilising the ambi-sense strategy, the S and L segments have two non-overlapping open reading frames (ORF) of opposite polarity, which are separated by an intergenic region (IGR) (Figure 1.5).

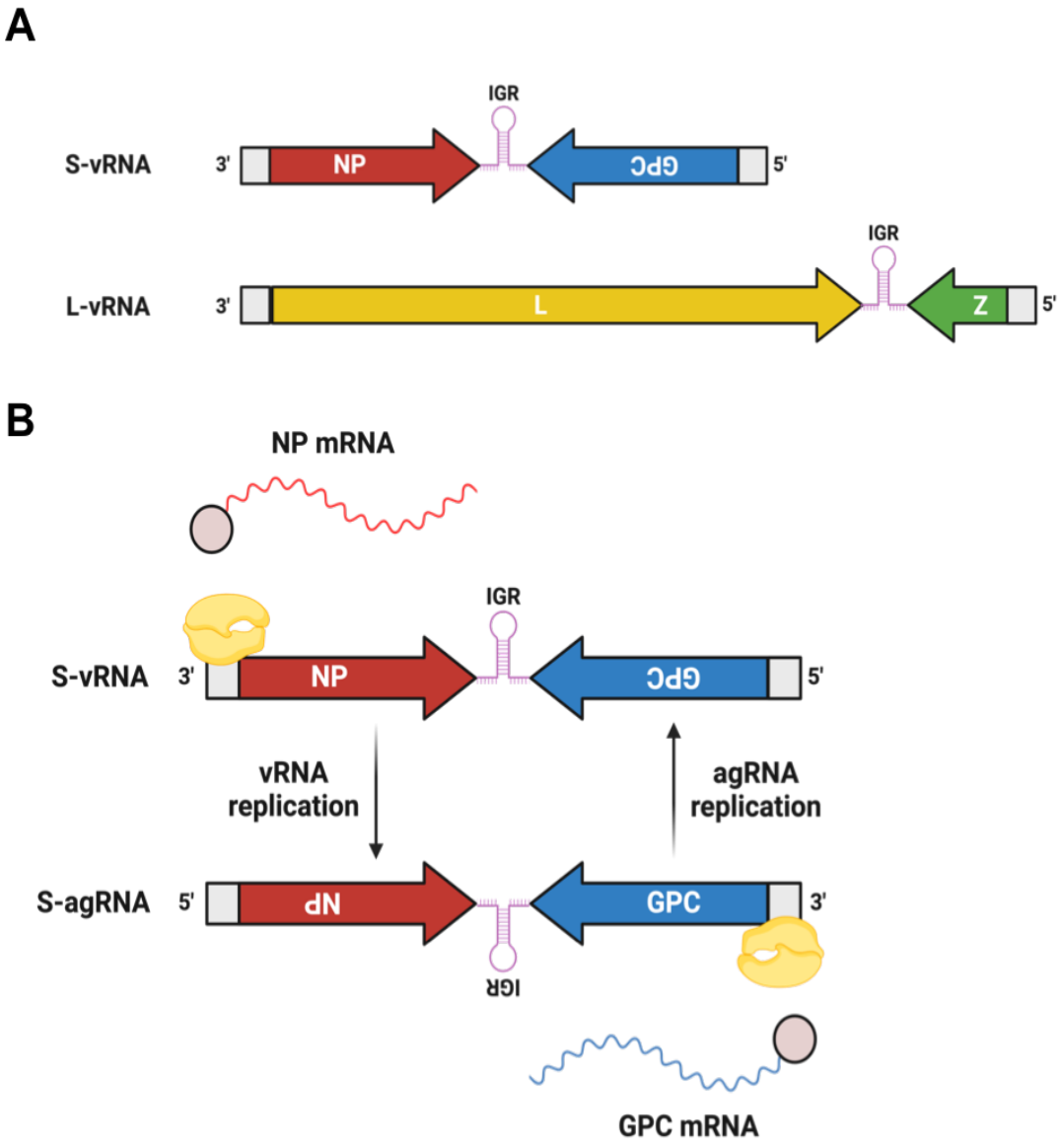

Figure 1.5: Schematic of arenavirus ambi-sense genome and the coding strategy (A) The S vRNA is responsible for encoding NP (red) and GPC (blue) mRNA, with each gene separated by an intergenic region (IGR). The L vRNA encodes mRNA for the L (yellow) and Z (green) viral proteins. (B) Input S and L vRNA (3' – 5') can directly produce positive-sense mRNA for NP and L but requires the synthesis of complimentary agRNAs to encode L and Z mRNA (ambi-sense strategy), respectively. Figures created with BioRender.

In terms of gene expression, the 3' ORFs of input S and L vRNAs act as templates for the transcription of the NP and L mRNAs, respectively. Replication of the S and L vRNAs allows for the generation of antigenomic strands (agRNA), which are full length complementary RNA molecules; these S and L agRNAs then act as templates during transcription of the GPC and Z mRNAs, respectively.

Intergenic region (IGR)

The IGR regions of arenaviruses RNA is predicted to form stem loops, which provide a termination signal during L-dependent transcription of viral mRNAs [118]. The sequence homology of IGRs between arenaviruses species varies, even for closely related species such as LASV and LCMV [119]. However, despite this, structurally the IGRs of LCMV and LASV are predicted to be similar, suggesting that the stem loops structures formed are essential for L termination, rather than consensus sequences [119]. Interestingly, studies have also shown that switching of the IGR regions, such as replacing the LCMV L segment IGR for the S segment IGR, can result in viral attenuation in vivo [119, 120]. Thus, the RNA stem loop structures formed are specific to each arenavirus species, but also between S and L segments. For the production of agRNA from vRNAs, the termination signals within the IGRs are bypassed by L. The mechanism for how this bypassing occurs is currently unknown, however it has been proposed that the RdRp termination signals may be blocked via accumulation of NP following initial mRNA transcription and translation [121]. Interestingly, a recent study has identified a subpopulation of genomes within native LCMV infection that contain a common specific deletion within the S segment IGR. It was established that the accumulation of these S IGR deleted genomes contributes to viral interference, through decreased production of glycoprotein production [122].

Untranslated regions (UTRs)

At the 5' and 3' ends of both the S and L vRNAs are untranslated regions (UTRs). The highly conserved 19 nucleotide (nt) region of the 3'-terminal of the UTRs has been identified as an essential viral promoter [123, 124]. The 3' and 5' ends of each RNA segment are almost entirely complementary, with 13 to 19 nt being important

for base pairing allowing for promoter function [124]. The base pairing of this region is predicted to form a thermodynamically stable panhandle structure, which controls RNA synthesis [123]. The first 12 nt have been implicated for base-specific interactions with the replication complex [124]. Additional base-pairing within the S segment UTRs has recently been identified; abrogation of the 20-40 nt of the 5' termini and the 20-38 nt of the 3' termini pairing greatly affected viral propagation [125].

1.2.3 The nucleocapsid protein (NP)

Since arenaviruses have an extremely limited protein encoding capacity, with only four viral proteins expressed (NP, GPC, L and Z), NP has evolved to be a multifunctional protein during arenavirus infection. The NP of arenavirus species is the most abundant viral protein expressed within infected cells, and aside from encapsidating the vRNA, it has multiple different roles including viral transcription and genome replication [121], immune modulation [126–128] and formation of replication transcription complexes (RTCs) [129].

Nucleopcapsid structure

NP is formed by two separate protein domains: an amino terminal domain (N-terminal) and a carboxy terminal domain (C-terminal) [130]. Connecting the N- and C-terminal domains is a 30 aa linker sequence, which structurally remains unresolved due to its high flexibility (Figure 1.6). For LCMV NP-NP multimerisation, the N-terminal regions 1-50 aa and 308-358 aa have been shown to be essential, however these regions are not involved in virion production [131]. The N-terminal domain of LASV NP contains an RNA-binding site, as shown by X-ray crystallography of LASV NP in complex with ssRNA (expression host derived) [132]. Within this work, it was suggested that the NP-RNA interaction is controlled through a gating mechanism, which is a result of conformational changes in the N-terminal domain [132]. The C-terminal domain of NP contains a 3'-5' exonuclease (ExoN) domain with specific activity against dsRNA, to prevent downstream interferon-I (IFN-I) activation. The ExoN belongs to the DEDDh family of 3'-5' exonucleases, consisting of two β-sheets and eight α-helices [133].

Finally, a linker sequence is encoded at the C-terminus of NP, following the ExoN domain [117].

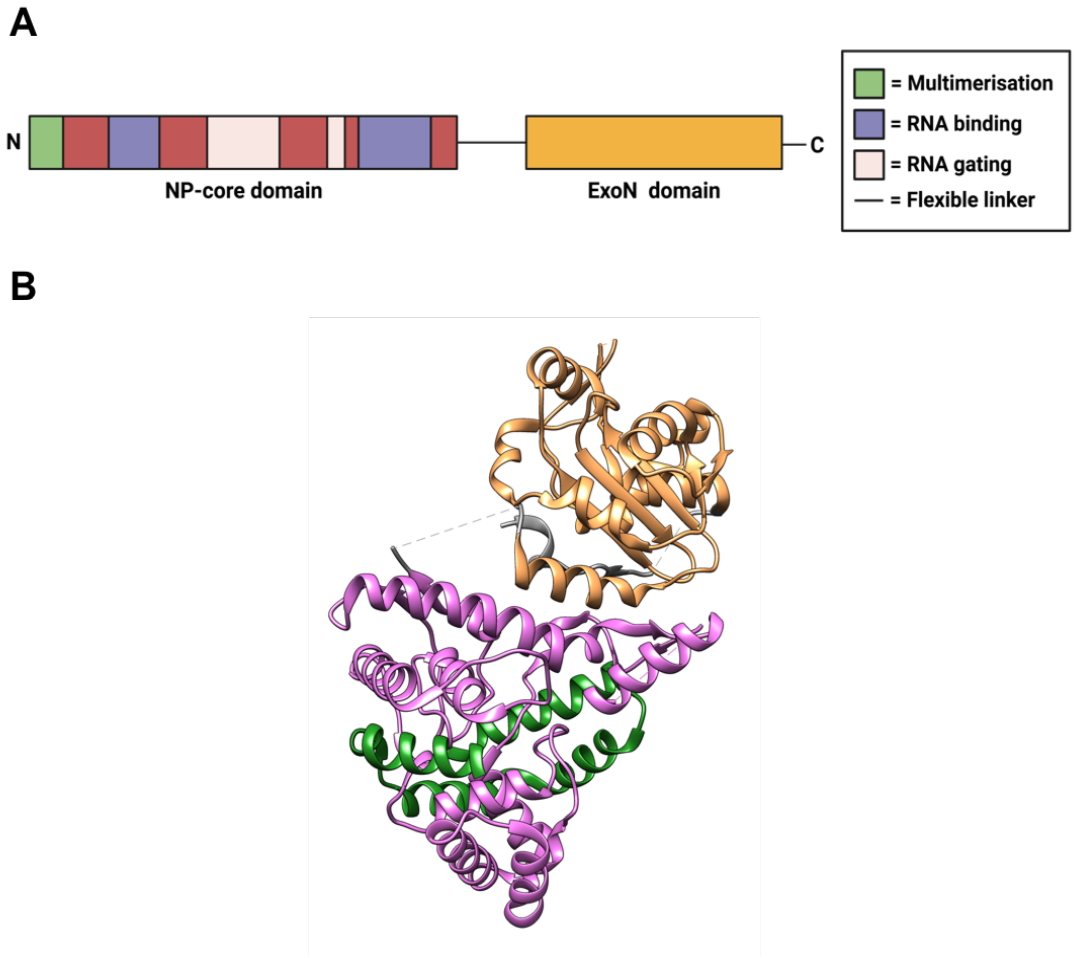

Figure 1.6: Schematic depicting arenavirus NP domains and structure. (A) NP has two domains, the N-terminal core domain and the C-terminal ExoN domain. NP also encodes for two highly flexible linker regions; the first linker separates the core and ExoN domains, and the other is at the C-terminus of the protein. Different regions of the NP core domain have been identified to be important for a range of functions including NP-NP multimerisation (green), RNA binding (blue) and RNA gating (light pink). Figure created with BioRender, using information from [130]. (B) Structure of full-length NP (PDB 3MWP) represented in ribbon. The NP-core domain (pink), ExoN domain (orange), the proposed multimerisation region within the NP-core (green) and flexible linkers (grey) are represented. Figure was made using Chimera X.

Nucleocapsid function

Formation of vRNPs

The viral mRNA first transcribed from the input S vRNA encodes for NP (LCMV; 63 kDa), while input L vRNA first encodes for the L protein mRNA (LCMV; 200 kDa). Once translated, NP encapsidates newly synthesised genomic

vRNA, and associates with the L protein, to form vRNP complexes. Importantly, vRNPs alone can facilitate viral persistence whereby cells remain infectious despite the lack of production of virions or defective interfering particles (DIs) [134]. The precise orientation and number of NP monomers within vRNP complexes remains to be elucidated. For Pichinde Virus (PICV), a dataset of vRNPs from purified virions has been examined via negative staining EM, showing a flexible filament composed of NP monomers of 4 to 5 nm diameter that constitute filamentous vRNPs of 12 to 15 nm in diameter; these vRNPs appeared to exhibit helical arrangement [135]. Recently, vRNP-like structures for MOPV were also visualised via negative staining EM [136]. Here, MOPV NP was bacterially expressed and purified and subsequently co-eluted alongside bacterial RNA [136]. The observed vRNP-like structures had a diameter of 15 ± 1 nm, formed by circular NP 'rings' (heptamers) [136]. Finally, MACV vRNPs from a mini-genome (MG) system were visualised, and this dataset highlighted the diversity and flexibility of arenavirus vRNPs (Figure 1.7) [137].

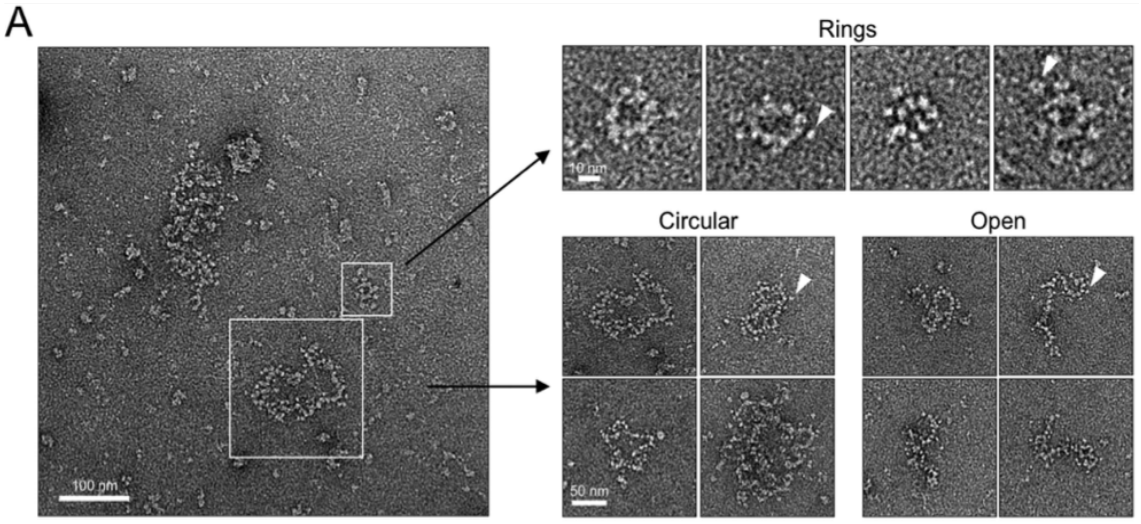

Figure 1.7: MACV vRNPs are highly flexible. MACV vRNPs were isolated from MG expressing cells and visualised via negative-stain EM. Three classes of vRNPs were reported: rings (top), circular (bottom left) and open (bottom right). Purification of vRNPs was performed alongside L, and L is likely represented by the larger globular particles (white arrowheads). Figure taken from [137].

These MACV vRNPs likely adopt the authentic organisation since NP and L were included alongside the MG plasmid, which retained the 3' and 5' UTRs [137]. However, high-resolution imaging of these vRNPs was not performed, and further investigations are required to elucidate the native arrangement of arenavirus vRNPs.

Formation of RTCs

A further function of arenavirus NP is for the formation of RTCs, which are discrete cytosolic puncta whereby RNA synthesis occurs [129]. Within this study, it was determined that JUNV (Candid #1 strain) and TCRV RTCs were associated with cellular membranes and contain full-length vRNA and agRNA [129]. In relative amounts, mRNA was found to be modest, thus suggesting that the function of RTCs is primarily for RNA synthesis, and mRNA is rapidly distributed elsewhere for translation by cellular ribosomes [129]. The RTCs of NW arenaviruses are distinct in comparison to positive sense-RNA viruses, which form large multivesicular structures. The NP of JUNV was suggested to assist in formation of RTC since transfection of JUNV NP alone was sufficient for formation of puncta which were consistent with the previously observed RTCs [129].

The evidence for RTC reliance during OW arenavirus infection is more limited, but evidence suggests RTCs are formed within LCMV infection [138]. Intriguingly, it was shown that eukaryotic initiation factor 4E (eIF4E) co-localises with RTCs of LCMV, suggesting that initial translation of arenavirus mRNAs may commence within the RTCs [138]. An interesting finding from these investigations was the proposal that LCMV RTC formation was dependent on phosphorylation of NP at T206, since RTCs were not observed after transfection of a phospho-ablatant NP mutant (substituting threonine to alanine; T206A) (Figure 1.8) [138]. Furthermore, within this study, MG analysis indicated that T206A NP was functional for MG transcription and replication, corroborating the role of NP phosphorylation at residue T206 for RTC establishment [138]. It is important to note, throughout these findings, T206 remained a predicted site of phosphorylation, and mass spectrometry analysis attempting to identify the phosphorylation during native LCMV infection was unsuccessful. Thus, addition of a phosphate group on NP may be a dynamic process, with on-off switching regulating different stages of LCMV multiplication [138]. The host cell kinase responsible for NP T206 phosphorylation was not identified.

Immune modulation

The differing pathogenicity of OW and NW arenavirus species often relates to the ability of NP to interfere with immune signalling pathways [139]. One conserved

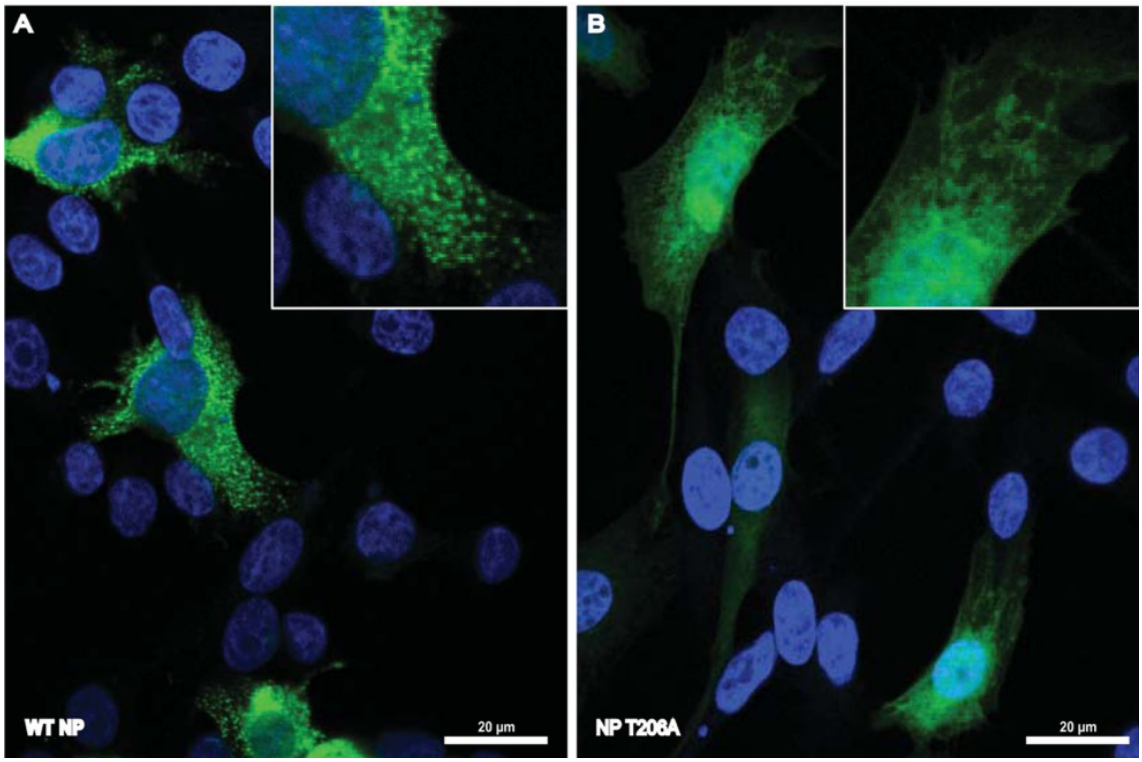

Figure 1.8: Phosphorylation of residue T206 is involved in LCMV RTC formation. IF was performed on BHK-21 cells transfected with WT NP (A) and T206A NP (B; phospho-ablatant), staining for NP (green) and DAPI (blue). This figure was taken from [138].

feature, for pathogenic and non-pathogenic arenaviruses, is IFN-I inhibition and dsRNA degradation [140]. The previously discussed ExoN C-terminal region of NP is responsible for binding to dsRNA, preventing IFN-I activation. Based on alanine substitutions, the highly conserved D382 and G385 residues within the ExoN of NP (amino acid numbering based on LCMV) were highlighted as being critical for prevention of IFN-I induction [141]. Additionally, the NP ExoN catalytic residues were identified and examined, whereby mutagenesis experiments utilising PICV revealed a decrease in IFN-I activation [142, 143]. Whilst this ability appears to be highly conserved, the pathogenic NW species MACV and JUNV retain the ExoN motifs but lack the ability to degrade dsRNA [144]. Interestingly, LASV NP can degrade the dsRNA accumulated during JUNV infection, however this is dependent on L; thus, this implies the ExoN domain of NP is not sufficient for dsRNA degradation [144]. In addition to the ExoN activity, NP is also able to directly bind to innate immunity signalling pathways members retinoic acid-inducible gene I (RIG-I) and melanoma differentiation-associated protein 5 (MDA-5), preventing the translocation of interferon regulatory factor 3 (IRF3) to the nucleus, and thus reducing downstream IFN-β production [127, 139, 145]. Additionally, the NP of

LCMV, LASV, WWAV, LATV and JUNV have all been shown to interact with IκB kinase (IKK)-related kinase IKKϵ, which is proposed to sequester the ability of the IKKϵ to phosphorylate IRF3 [146]. The C-terminal ExoN region of NP was shown to bind to the kinase domain of IKKϵ, which was shown in vitro to be sufficient at preventing phosphorylation of IRF3 [146].

For JUNV and MACV, the NP ExoN domain is unable to degrade dsRNA, resulting in activation of the host dsRNA sensor Protein kinase R (PKR). In an alternative mechanism to control this pathway, JUNV NP has been shown to directly bind to PKR preventing the phosphorylation of eukaryotic translation initiation factor 2a (eIF2a) [147]. Silencing of PKR did not influence viral propagation, suggesting the role of the JUNV NP-PKR interaction may be solely to prevent activation of antiviral pathways [147]. Interestingly, the NP-PKR interaction was shown to be specific to JUNV NP, since LCMV NP did not prevent eIF2a phosphorylation [147]. LCMV NP has also been shown to interact with DDX3, a DEAD (Asp-Glu-Ala-Asp)-box ATP-dependent RNA helicase [148]. Intriguingly, DDX3 has previously been reported to cause activation of IFN-I [149, 150], however, in the context of LCMV infection, DDX3 was shown to suppress IFN-I, alongside having a pro-viral impact on LCMV and LASV RNA synthesis [148]. The binding of DDX3 was also shown to be conserved between OW and NW arenaviruses, since JUNV NP was also identified as a DDX3 binding partner [148].

In relation to immune modulation, but also persistence, NW arenavirus NPs have also been shown to subvert the apoptosis mechanisms of infected cells [151–154]. For JUNV NP, it has been shown that cleavage at DVKD and QEHD motifs within NP, by cellular caspases, results in two truncated forms of NP [154]. It was established, that mutation of the caspase motifs with JUNV NP was sufficient to enhance apoptosis; it was proposed that the cleavage events of viral NP could act as a decoy, meaning that the caspases no longer cleave their native cellular targets, consequently inhibiting apoptosis [151, 154]. Recently, this work has been extended to show that another isoform of JUNV NP is expressed from alternative translation of NP mRNA (in-frame M80 ATG) [155], and all three NP isoforms were found to contribute at preventing apoptosis [155]. Within the first study, the non-pathogenic NW arenavirus TCRV was also examined, which was observed to exhibit increased levels of apoptosis [154]. Interestingly, TCRV did not generate

the same truncated NP products despite the caspase cleavage motif DVKD being conserved. The reasons for this remain unknown, but it suggests that other viral or cellular components are required. Taken together, this suggests that the capacity of NW arenaviruses NP to sequester cellular caspases for cleavage may impact the inhibition of apoptosis, potentially impacting pathogenicity [154]. The apoptosis subversion of OW arenaviruses is less defined, yet both LCMV and LASV infection seemingly does not result in the induction of apoptosis in cell culture [156, 157].

1.2.4 The L protein (L)

Research surrounding arenavirus L protein primarily focuses on the RdRp domain, and its requirement for transcription and replication of vRNA and agRNA. Nevertheless, the L protein does have other functions including; binding of the Z protein (discussed in Z function section) [158–160], endonuclease activity [161] and interacting with a range of host cell proteins [162].

L protein structure

The L mRNA encodes for the 250 kDa L protein, the largest of any arenavirus protein, and is composed of approximately 2200 aa residues. The L protein contains three domains which have been named based on the similarities with influenza A virus (IAV) RdRp [163]; the N-terminal PA-like domain (JUNV L numbering; 1-709 aa), the RdRp domain (709-1608 aa) in the middle and the C-terminal PB2-like domain (1608-2210 aa) [158] (Figure 1.9). X-ray crystallography for the full-length of any arenavirus L protein is not determined, yet JUNV L has been solved with only 400 aa of the C-terminal PB2-like domain absent [158]. The analysis showed that the RdRp domain is located at the core of the structure, with the N-terminal PA-like and C-terminal PB2-like domains tightly interacting with the RdRp thumb domain [158]. The endonuclease region was also reported to bind to the finger domain and the α-ribbon domain of the RdRp [158].

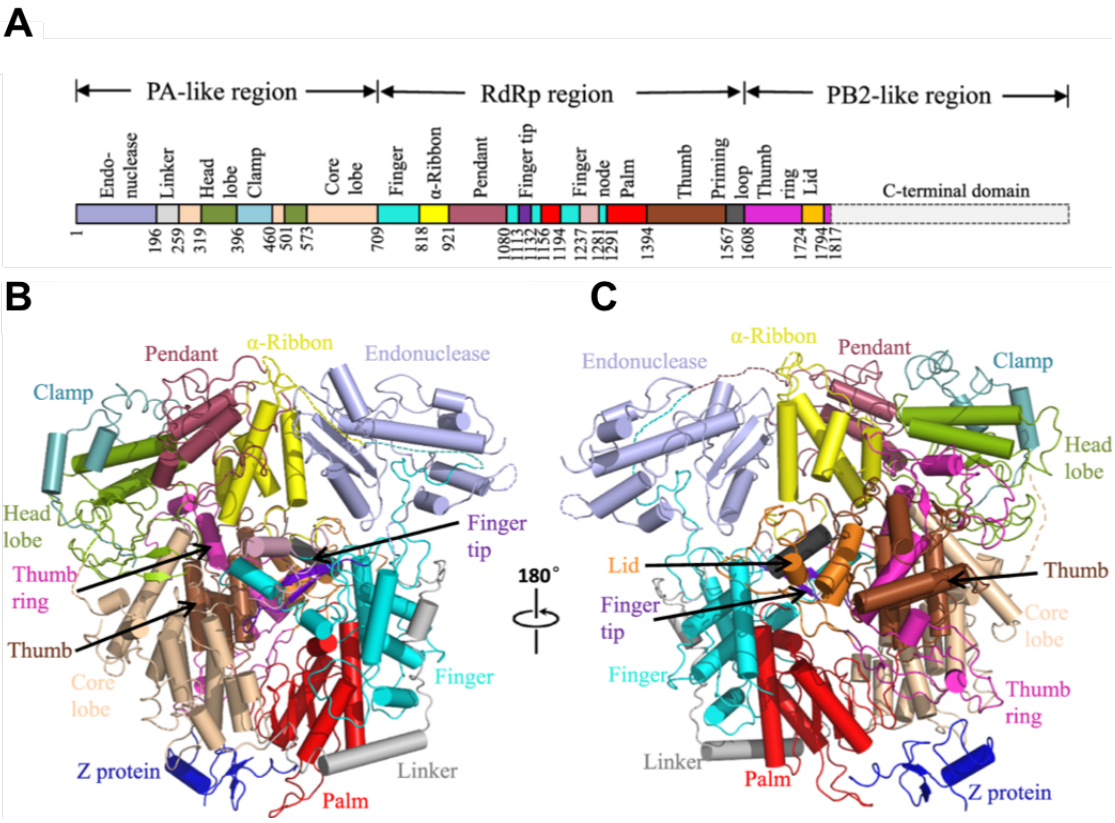

Figure 1.9: Schematic and structure of JUNV L protein, which is divided into three functional domains.(A) Domain I; PA-like region, Domain II; RdRp region, Domain III; PB2-like region. Each feature within the domains is colour-coded, with the C-terminal (unsolved) region represented by dotted lines. (B, C) Cartoon depiction of the solved JUNV L-Z complex. The structures are colour-coded according to (A), with unsolved regions connected via dashed lines. (C) is identical to (B), but with rotation along the vertical axis by 180°. This figure was taken from [158].

L protein function

vRNA transcription and genome replication

The L protein of arenaviruses is first responsible for input vRNA transcription. Subsequent to this, L performs genome replication, generating full-length agRNAs, which act as templates for transcription of GPC and Z mRNA. Conserved regions within the 3' and 5' of vRNA act as promoters to allow binding of L and initiation of RNA synthesis [164]. For MACV L, the promoter ssRNA motif was identified as 3' N1-2HKUG 5' which was critical for recognition of L [165]. In the case of LASV, a separate study found the first 1-12 nucleotides of S vRNA are required for L interaction, while residues 13-19 are important for 3'-5' base pairing required for efficient promoter function [124]. Specifically for genome replication, it is proposed that initiation occurs in a prime-and-realign mechanism [166]. A detailed account of

this mechanism of RNA synthesis is beyond the scope of this thesis, but briefly, an incoming GTP molecule is added to the template strand at position +2 (opposite to a C base), which extends to form a GC dinucleotide. Realignment subsequently occurs, with the latter moved on the template to positions -1 and +1, and the synthesised RNA then acts as a primer for elongation [166]. In support of this model, the product of MACV replication was determined to be a single nucleotide longer than the template, and thus only L drives attachment of the nontemplated G [166, 167]. Although the mechanism has not been fully understood, manganese ions rather than magnesium ions have also been shown to increase the speed at which the RNA is synthesised by LASV L [166].

Endonuclease and cap-snatching activity

A short 196 aa region (NL1) with the N-terminal PA-like domain of LCMV L has been reported by X-ray crystallography [161]. Within this study, it was identified that despite no clear sequence homology, LCMV NL1 and IAV PA_N are structurally related [161]. The IAV PA_N is well-established to have endonuclease activity and closely resembles resolvases and type II restriction endonucleases [168–170]. It has also been suggested that IAV PA_N is the endonuclease that is responsible for cap-snatching by cleavage of host mRNA [170]. It is assumed that the L protein of arenaviruses contains an endonuclease that can also perform host cell cap-snatching, given the structural similarities between NL1 and PA_N [171]. However, whilst there is no direct evidence of this, functional analysis has implied the C-terminus domain of LASV L could play a role in cap-snatching [172]. Conversely, structural and co-IP analysis of the C-terminal region of CASV L protein, a reptarenavirus, has suggested, biochemically and structurally, that the proposed cap-binding site within the C-terminus is not functional [171]. This work also demonstrated that LASV L C-terminus was unable to bind m^7GTP or capped RNA, thus suggesting the inability to cap-snatch within this region is conserved [171].

Host protein interactions

Several host cell proteins have also been identified to interact with LCMV L, through the application of co-IP and proteomics [162]. Globally, these host cell proteins were consistent with routine function of L during arenavirus infection and involved RNA-biology associated proteins i.e., ribosomal and RNA-binding

proteins, ribonucleoprotein, and splicing [162]. However, interactions of L with other proteins involved in different cellular pathways were identified, namely DDX3X, IGF2BP1, NKRF and TRIM21 [162]. Within this study, DDX3X, NKRF and TRIM21 knockout (KO) cell lines were generated, and when infected with LCMV had differing responses. In the case of NKRF and TRIM21 KO cells, LCMV could replicate to higher titres compared to WT, yet DDX3X KO resulted in a decrease in titre [162]. The pro-viral effect of DDX3X KO is consistent given NP-DDX3 is involved in suppressing the IFN-I response (see above) [148]. The anti-viral effect of TRIM21 was assessed via mouse investigations, infecting Trim21$^{-/-}$ and WT mice with LCMV [156], with higher viral titres of LCMV (clone 13) found in the spleen, liver and kidney of Trim21$^{-/-}$ mice when compared to WT [162].

1.2.5 The glycoprotein (GP)

The GPC mRNA is expressed from the S agRNA, requiring replication in order to be generated. The GPC polypeptide generated contains a N-terminal stable signal peptide (SSP) upon translation. GPC (75 kDa) is further cleaved by cellular subtilisin kexin isozyme-1/site-1 (SKI-1/S1P) generating sub-units GP-1 (44 kDa) and GP-2 (35 kDa) but retaining the associated SSP [173, 174] (Figure 1.10). LASV GPC SKI-1/S1P-mediated cleavage was reported to occur within the endoplasmic reticulum (ER) [173], yet LCMV GPC cleavage occurs either in the Golgi or post-Golgi compartments [176]. Thus, it is essential for infectious arenavirus virion production that SKI-1/S1P mediated GPC cleavage occurs, yet where this occurs within the secretory pathway may differ between species [176, 177].

Glycoprotein structure

GPC cleavage products SSP/GP-1/GP-2 remain associated on the viral membrane surface as a tripartite complex [178]. The LCMV surface glycoprotein in the pre-fusion conformation has been solved via crystallography [179], with the *in situ* LCMV organisation recently reported [175]. The native pre-fusion conformation of LASV glycoprotein for Josiah (lineage IV) has also been solved independently [180], and in complex with antibodies [181–183].

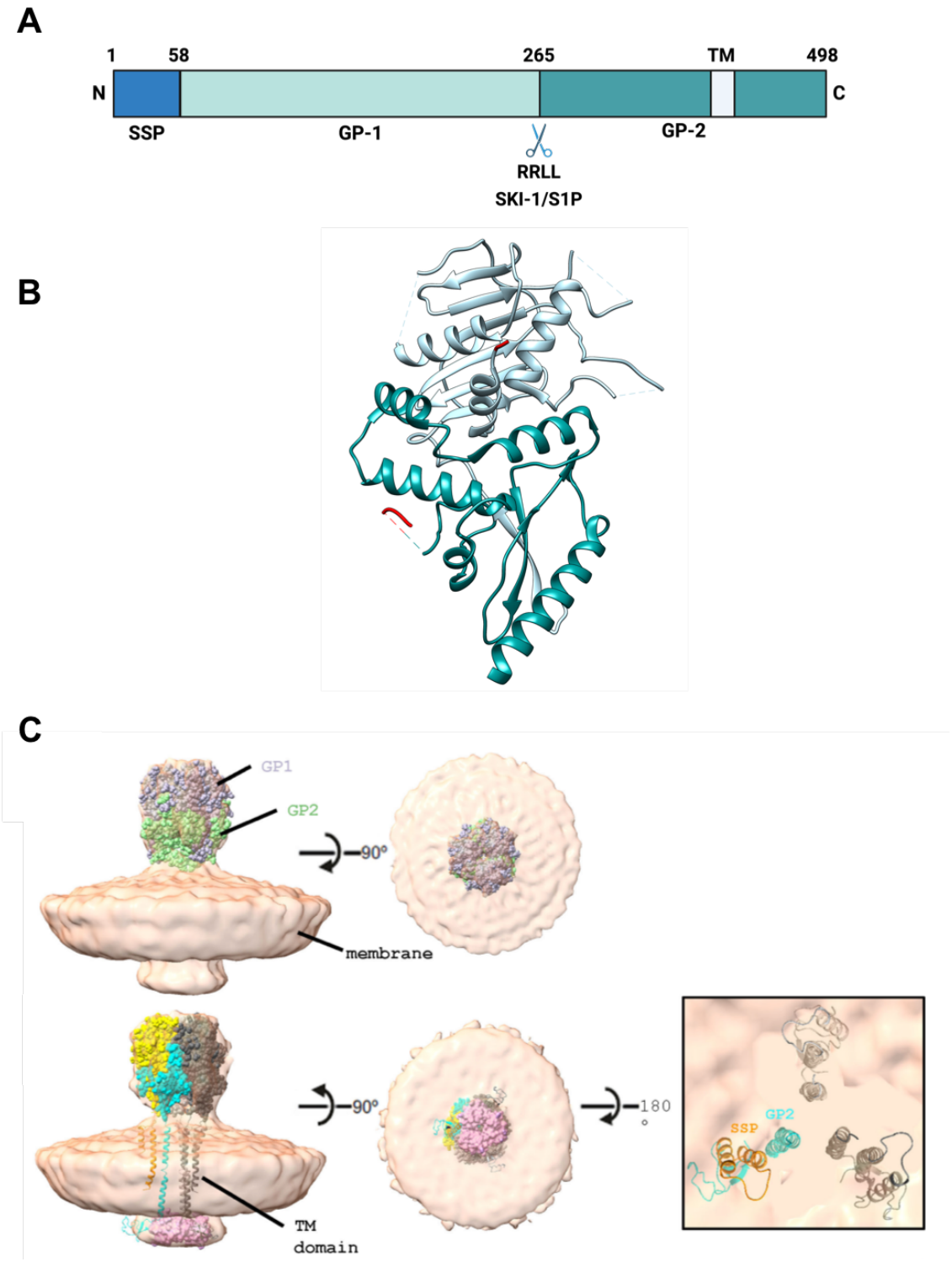

Figure 1.10: Schematic and structure of LCMV glycoprotein. (A) Representation of LCMV GPC, which is cleaved into subunits SSP (6 kDa), GP-1 (44 kDa) and GP-2 (35 kDa). The SKI-I/S1P cleavage site between GP-1 and GP-2 (RRLL) is highlighted. The transmembrane domain (TM) within GP-2 is shown (B). Structure of LCMV GP-1/GP-2 (PDB 8DMI) represented in ribbon. GP-1 (light blue) and GP-2 (dark blue) are represented alongside the cleavage site (red) (C) Cryo-electron tomography was performed on LCMV virions, and sub-tomogram averaging (STA) resulted in an *in situ* LCMV glycoprotein volume (pink). A known crystal structure of LCMV glycoprotein was fitted (8DMI) into the volume. Side, top and bottom views are depicted, with LCMV GP-1 (grey), GP-2 (green) and SSP (orange) shown. (C) was taken from [175].

SSP structure

It was established through mutagenesis of the cleavage site that GPC cleavage at the N-termini (position 59) results in a peptide of 58 aa, which showed characteristics consistent with a signal peptidase [184–186]. Since SSP is highly flexible, structural analysis of arenavirus SSP has been inconclusive. However, it is recognised that SSP contains two hydrophobic regions. A study on JUNV SSP topology revealed that SSP spans the membrane twice, with both the N- and C- termini located towards the cytosol [186].

GP-1 structure

GP-1 contains an N-terminal β-strand, with a β-sheet and a helix-loop [179]. The region of GP-1 that interacts with GP-2 is the N-terminal β-strand (β1), which together with two strands of GP-2 form a three-stranded anti-parallel β-sheet [179]. Interestingly, the GP-1 core of LCMV and MACV are structurally similar, as well as the core of JUNV GP-1 [179, 187]. However, LCMV and LASV GP-1 structurally have major differences, which is thought-provoking considering they are closely related [179, 188]. For example, the N- and C- termini of LCMV GP-1 are oriented towards the GP1-GP2 interface, yet the opposite occurs for the termini of LASV GP-1 [179]. Additionally, there are significant disparities in the "helix-loop" lower faces, with the LASV GP-1 helices of this region being oriented almost perpendicular to LCMV GP-1 [179].

GP-2 structure

The fusion domains of arenaviruses are within GP-2, and the related amino acids (W264, G277, Y278 and L280) are highly conserved [179, 189]. Arenaviruses contain two fusogenic regions within GP-2; an N-terminal fusion peptide (LCMV numbering; 266-272 aa), which is characteristic to class I viral fusion peptides [190], and also an internal fusion loop (289-300 aa) [189]. Thus, the GP-2 of arenaviruses is similar to the glycoprotein of Ebola virus (EBOV), with both being characterised as class I fusion proteins since they form alpha helix-rich trimers in their post-fusion states [191]. Nevertheless, both possess internal fusion loops which are typically associated with class II or III fusion peptides [190, 192, 193]. Within the solved crystal structures (pre-fusion), the fusion peptide is 'shielded' via hydrophobic and hydrophilic inter-protomer contacts of a loop of GP-1 [179].

Glycoprotein function

SSP function

As aforementioned, SSP is a signal peptidase. However, there are key differences in the arenavirus SSP that make them distinct from cellular signal peptidases. Firstly, the typical length for a signal peptidase is between 18-30 aa, thus the 58 aa arenavirus SSP is significantly larger [194]. Secondly, cellular signal peptidases contain a single hydrophobic region [195], yet the SSP of arenaviruses contains two discrete hydrophobic domains [196]. Finally, the half-live of SSP was shown to be 6 hours in cells, which is remarkably stable [196]. SSP has been shown to have two main roles during arenavirus infection: involvement in cellular-viral membrane fusion and maturation of the SSP/GP-1/GP-2 tripartite complex.

Whilst the exact mechanism is disputed, it is well established that the SSP of arenavirus GPC is required for glycoprotein maturation [184, 185, 197]. One proposed theory is that SSP ensures correct folding of GPC, which ensures recognition of S1P/SKI-1 for cleavage [184, 197]. An alternative supported hypothesis is that the SSP allows trafficking of GPC to Golgi compartments whereby the S1P/SKI-1 cleavage occurs [185]. Both of these models would result in the formation of the SSP/GP-1/GP-2 tripartite complex. Concurrently, it is possible that SSP may function somewhat differently between arenavirus species, since the first hypothesis was predominately based on LASV, whereby the second was based on JUNV; as mentioned above, S1P/SKI-1 mediated GPC cleavage occurs in differing locations for LASV and LCMV, thus this could justify the apparent disparities for the SSP function [176, 177]. Mutational analysis utilising JUNV SSP highlighted that residue C57 (introduced mutations; C57A and C57S) is essential for SSP to associate with the GPC complex [198]. Interestingly, this requirement represents a likely conserved feature of arenaviruses SSP, since residue C57 is present in all NW and OW SSP sequences [198]. Further investigations have revealed that the cytoplasmic domain of GP-2 is essential for the incorporation of SSP within SSP/GP-1/GP-2 tripartite complexes, and three residues (His-459, Cys-467, and Cys-469) may interact with SSP C57 to form an intersubunit zinc-binding center [199].

Intriguingly, JUNV SSP has also been implicated in pH-dependent membrane

fusion [200]. Again, mutagenesis studies on JUNV SSP established that although the SSP mutant K33A (lysine to alanine substitution) was proficient during the processes of GPC transcription, translation, cleavage, assembly, and plasma membrane trafficking, it was non-functional during pH-dependent membrane fusion [200]. Alterations to SSP residue K33 resulted in changes to the optimal pH which was required to trigger membrane fusion, since K33Q (lysine to glutamine) had an optimal pH of 4.5 compared to pH 5.0 - 5.5 for K33 (WT) [200]. Thus, although further mechanistic investigations are required, it is proposed that SSP contributes to pH sensing and the activation of membrane fusion [194, 200]. Additionally, myristylation at the N-terminal glycine of SSP has been shown, by alanine substitution (G2A), to be required for efficient membrane fusion activity [201].

GP-1 function

The arenavirus GP-1 is involved in host cell receptor binding [202, 203]. The target receptor for LCMV (immunosuppressive strains), LASV and NW clade C viruses is α-dystroglycan (α-DG), which is utilised as the major receptor for GP-1-mediated attachment to cells [204, 205]. The mechanistic binding of GP-1 to α-DG is conserved between LASV and LCMV since both require the same regions of the N-terminal globular and central mucin-type domains of α-DG [206, 207]. The conservation of high-affinity binding of α-DG between arenaviruses has been mapped via sequence comparison to a leucine or isoleucine at position 260, alongside an adjacent bulky amino acid with an aromatic ring at position 259 [205]. The amino acid at position 260 for GP-1 of LCMV has been linked to receptor switching or affinity, with evidence from over 35 strains, implying that this directly causes differences in LCMV pathogenicity and immune response generated as a consequence of infection [208]. However, not all strains of LCMV enter cells through binding of α-DG; one strain was shown to retain a high-affinity for α-DG, but cells that were absent of this receptor were still permissible to infection [209]. Additionally, there are multiple LCMV strains (non-immunosuppressive) that have low or no affinity to α-DG, and thus must enter cells via alternative mechanisms [209]. Other receptors have also been shown to be involved in OW arenavirus entry. For example, the tyrosine kinases (Axl and HGFR) have been implicated in LASV macropinocytosis-related entry, suggesting an additional functional entry pathway

during OW arenavirus infection [210]. OW arenaviruses also require GP-1 to switch receptors in the late endosomes in order to mediate membrane fusion (discussed in fusion of 1.2.7 section).

For NW arenaviruses within clade A and B, with different alternative entry mechanisms, transferrin receptor 1 (TfR1) was suggested as an alternative receptor [211]. However, further studies have highlighted that while the pathogenic NW arenaviruses JUNV, MACV and GTOV rely heavily on TfR1, alternative unknown pathways could exist since non-pathogenic TCRV and Amapari virus (AMAV) do not require TfR1 for entry [212]. Taken together, multiple receptors have been identified in which GP-1 binds with high-affinity to mediate entry for differing arenavirus species, however these often represent the main mode of attachment and it is typical for there to be alternative mechanisms.

GP-2 function

The arenavirus GP-2 undergoes significant irreversible conformational changes subsequent to environmental cues such as pH, which drives the fusion of viral and host membranes [190, 191, 213]. As mentioned above, the post-fusion conformation of LCMV and CASV GP-2 have been solved, resembling that of class I fusion proteins [190, 191, 214]. The structure of class I proteins is beyond the scope of the current work, but briefly, energy released through the conformational change allows the merging of the viral and host membranes to mix, allowing a pore to be formed. Progressive widening of this pore eventually allows the release of viral genetic material resulting in cell infection [215].

Glycosylation

The first indication that glycosylation may play an important role in arenavirus GPC processing was through the use of tunicamycin, a glycosylation inhibitor, which prevents cleavage of LCMV GPC into the required respective subunits [216]. It was later identified that GP-1 and GP-2 are glycosylated, with 11 conserved (at least 50%) N-glycosylation sites [217]. Interestingly, mutagenesis investigations found that sites T87 and S97 are essential, with alanine substitutions in cDNA rendering recovery of rLCMV impossible [217]. This was corroborated by *in vitro* findings showing that when GP-1 with T87 and S97 mutations was transfected into cells,

expression levels were diminished and mutated GPC could not be cleaved, and thus was non-functional during fusion [218]. It was proposed that these glycans may be required to solubilise the glycoprotein [217, 218]. Where glycosylation mutants were successfully recovered, upon passaging, three reverted to WT (S116, T234 and S373) [218]. The S116 mutant was particularly unstable, and reverted to WT within 24 hpi, suggesting another essential role of glycans at this residue during infection [218]. Collectively, all glycosylation mutations introduced, other than T126A and T173A, had diminished viral fitness. Thus, while further work is required to understand the mechanistic function for each site, this highlights overall the importance of glycosylation of arenavirus GP-1 and GP-2 [217]. Similar mutagenesis experiments were performed with LASV, showing that certain glycosylation sites were important for SKI-1/S1P mediated GPC cleavage [219]. The glycosylation of MACV GP-1 has recently been investigated, and interestingly, it was identified that native infection results in additional glycans at N83 and N166, which confer higher resistance to neutralising antibodies and virulence in animals [220]. Disruption of these sites resulted in attenuation of MACV in animals, without significant disruption to GPC expression, cleavage, or viral fitness in cell culture [220]. Thus, it was suggested that pathogenicity as a result of the glycans may be a consequence of neutralising antibodies against GPC, since the generated mutants were more sensitive to neutralising antibodies. Additionally, infection with the glycosylated mutants also elicited a higher neutralising antibody response [220].

1.2.6 The matrix protein (Z)

The mammarenavirus L agRNA acts as a transcript for the mRNA encoding for a small zinc finger protein known as the viral matrix protein (Z). The arenavirus Z is 90 aa (15 kDa), yet despite this has multiple functions including forming a structural layer within virions [116, 221], inhibiting viral replication (binding of L) [167, 222], budding [115, 223], binding host cell proteins [224–227] and immune modulation [228, 229].

Z structure

A partial structure of JUNV Z has been solved, in complex with L (Figure 1.11) [158]. The Z protein can be divided into three discrete domains, the N-terminal regions, the middle really interesting new gene (RING) domain and a C-terminal region [158, 230]. The structure of Z is two anti-parallel β-strands and one α-helix, which form one or two zinc fingers depending on species [158, 227].

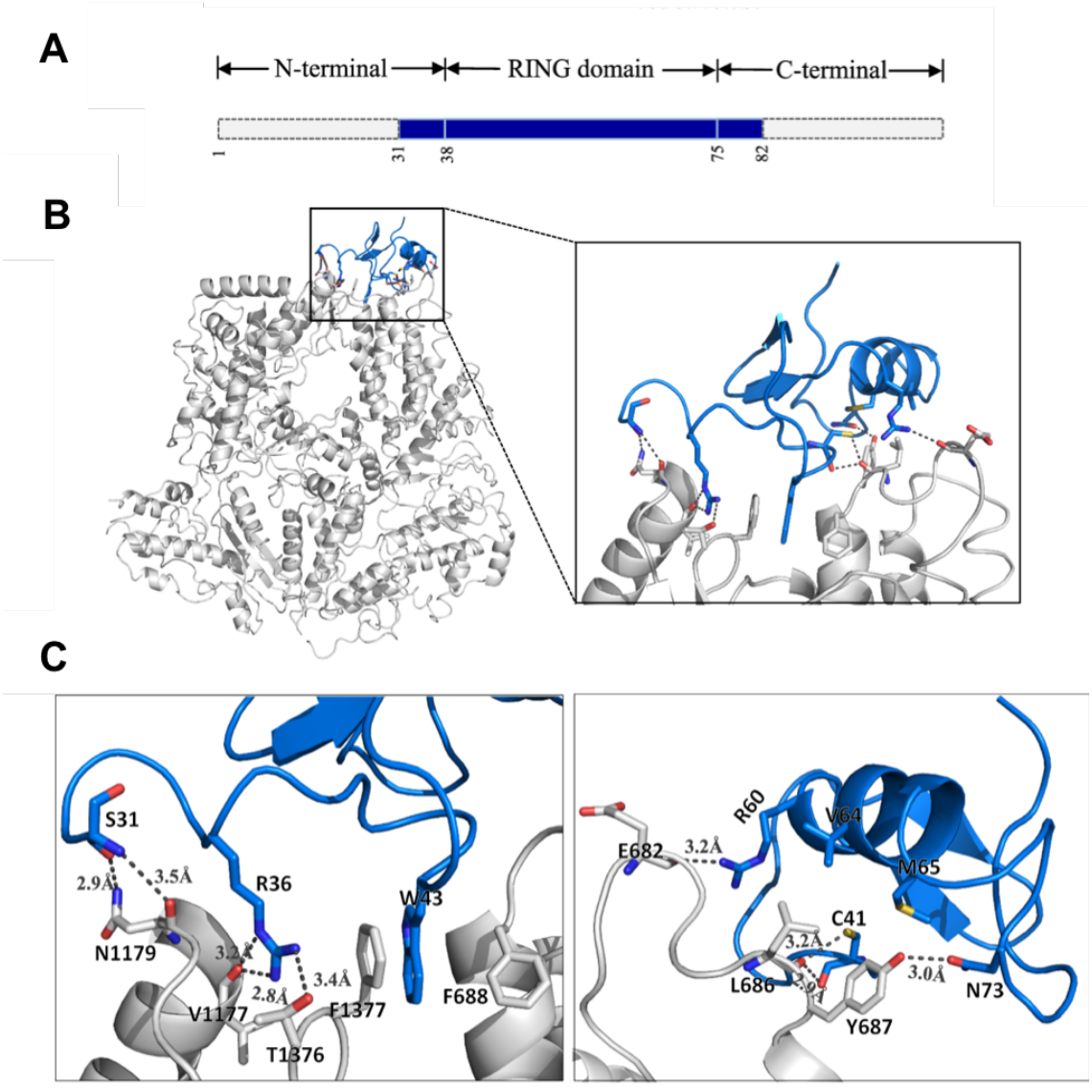

Figure 1.11: Schematic and structure (in complex with L) of JUNV Z. (A) Schematic representation of Z, which is divided in three regions: the N-terminal region, the RING (really interesting new gene) domain and the C-terminal region. Only the RING domain was fully resolved (blue) with the majority of both the N- and C-terminus yet to be elucidated (grey dotted lines). (B) Cartoon highlighting the identified JUNV Z (blue) and L (grey) interaction, alongside a zoomed image (right). (C) Magnified view of the JUNV Z-L interfaces, with residue numbers involved in this interaction shown. These figures were taken from [158].

Z function

Incorporation within virions

Through immunological and biochemical studies, it was identified that Z is packaged within LCMV virions, and associates closely with NP [116]. Since then, it is assumed that Z forms a small dense layer between NP and the viral lipid bilayer [221]. However, the resolution was limited within those images, thus the exact native orientations and abundances of Z and NP remain to be determined. During virion incorporation, Z was revealed to interact with the SSP of the glycoprotein [231]. Interestingly, the Z-SSP interaction was dependent on myristylation, a lipid modification, of Z. Mutational studies of Z (G2A) using both IF and co-IP indicated that abolishment of the Z myristylation site disrupts the Z-GPC interaction [231, 232]. It was proposed that the myristylation of Z allows the protein to localise to the inner lipid leaflet of the plasma membrane, in close contact with SSP/GP-1/GP-2 [231]. It has been shown by co-IP and IF for some arenavirus species that Z may also bind to NP, and thus potentially regulates vRNP incorporation into virions [223, 225, 228, 233, 234]. Taken together, these Z-NP and Z-GPC interactions imply that the critical role of Z during arenavirus infection is as a key viral factor for assembly, allowing all viral proteins to locate to the same sub-cellular locations prior to egress.

Inhibition of viral replication

Interestingly, mini-genome studies have shown that co-transfection of arenavirus Z inhibits viral replication and RNA synthesis [222]. Subsequent findings have clarified the mechanism for how Z is able to inhibit viral replication and RNA synthesis [167]. It was established that MACV Z forms a complex with L, which locks the polymerase in a catalytic inactive state [167]. The investigations revealed that L binds to the viral RNA promoter, but the interaction with Z prevents RNA synthesis [167]. It was proposed that the L-Z interaction may act as a mechanism to ensure that L is packaged into infectious progeny virions, which then allows the polymerase to reinitiate RNA synthesis following the release of vRNPs into the cytosol of newly infected cells [167]. Intriguingly, it was established that JUNV Z, but not LCMV Z, was able to inhibit RNA synthesis when applied to the MACV replicon-based system [167].

Z-mediated budding

Virus-like particle (VLP) studies have been applied to arenaviruses, suggesting Z is involved in budding [223, 235]. Mutational analysis of the PPPY motif of LCMV Z highlighted that whilst this region is not involved in transcription or replication, it is important for VLP production [223]. These hypotheses have recently been clarified, revealing that the PPXY domains play a role in budding, but mainly in context of defective interfering (DI) particle production, rather than for the generation of infectious particles [236]. It was proposed that the PPXY motif may mediate DI production which instead function for LCMV persistence, allowing the evasion from the immune response [236]. A follow-up study established that the Nedd4 family ubiquitin ligases directly interact with LCMV Z, and are responsible for Z ubiquitination at K10 and K77 [226]. In corroboration, the ubiquitination of Z was not essential for infectious virion production, but instead played a role in DI particle production [226]. This finding is likely to be conserved since the same Nedd4 family ubiquitin ligases were shown to interact with LASV and MOPV Z [237].

Binding host cell proteins

The ability of arenavirus Z protein to bind Nedd4 ubiquitin ligases [226] has been discussed above, however Z also interacts with several other cellular proteins. The first host cell protein shown to directly interact with any arenavirus protein was the promyelocytic leukemia protein (PML), which was shown to bind LCMV/LASV Z [238]. When examined via IF, the arenavirus Z protein causes a nucleus-to-cytoplasmic redistribution of PML [224, 238]. It was later established that Z/PML negatively regulates mRNA translation, by interacting with and repressing eIF4E [224, 239]. It was proposed that Z may sequester PML for viral replication. Additionally, the interaction between LCMV Z and eIF4E may inhibit the production of cyclin D1; this in turn may justify in the observed slower growth of infected cells, which allows the progression of chronic infection [239].

Immune modulation

How NP modulates the immune system has been explained above, but for GTOV, JUNV, MACV and SABV Z has also been shown to modulate the immune system during arenavirus infection [229]. It was first identified that Z of NW

arenaviruses, but not OW, independently lead to decreased production of IFN-β mRNA [229]. Mechanistically, it was established that JUNV Z binds RIG-I, which prevented downstream immune activation by inhibiting the formation of RIG-I/Mitochondrial antiviral signalling protein (MAVS) complexes [229]. JUNV Z was also recognised for its role in preventing NF-κB activation, and for blocking nuclear translocation of IRF-3 [229]. Collectively, these Z interactions confer a decreased production of IFN-β induction, contributing to the mechanisms for how JUNV evades the host innate immune response.

Arenaviruses lacking Z

Interestingly, arenavirus species that belong to the *Antennavirus*, *Hartmanivirus* and *Innmovirus* genera do not encode a Z protein [240]. It is intriguing to speculate how these viruses ensure that all proteins are incorporated into virions, given the discussed established roles of Z. It is plausible that species of these genera do not perform assembly and egress in the same manner as mammarenaviruses/reptarenaviruses. One possible explanation for these arenavirus species could be that budding potentially occurs at the Golgi, as for other bunyaviruses such as Bunyamwera virus (BUNV) [241–243], and thus Z is not required to recruit the other viral proteins at the plasma membrane. Additionally, species of the *Antennavirus* and *Innmovirus* genera code for proteins of unknown function [244–246]. It could be hypothesised that the uncharacterised proteins retain some of the established Z functions, but this remains to be determined.

1.2.7 Arenavirus replication cycle

The arenavirus replication cycle can be broadly divided into discrete stages; entry (encompassing receptor-mediated binding and initial endocytosis), fusion, uncoating, replication (encompassing vRNA transcription and agRNA synthesis/transcription), virion assembly and egress/budding (Figure 1.12). Particular stages of the arenavirus multiplication including entry, fusion and replication are well characterised, yet many questions remain for other stages particularly uncoating, assembly and egress. Here provided are the details surrounding each stage, alongside current gaps in knowledge.

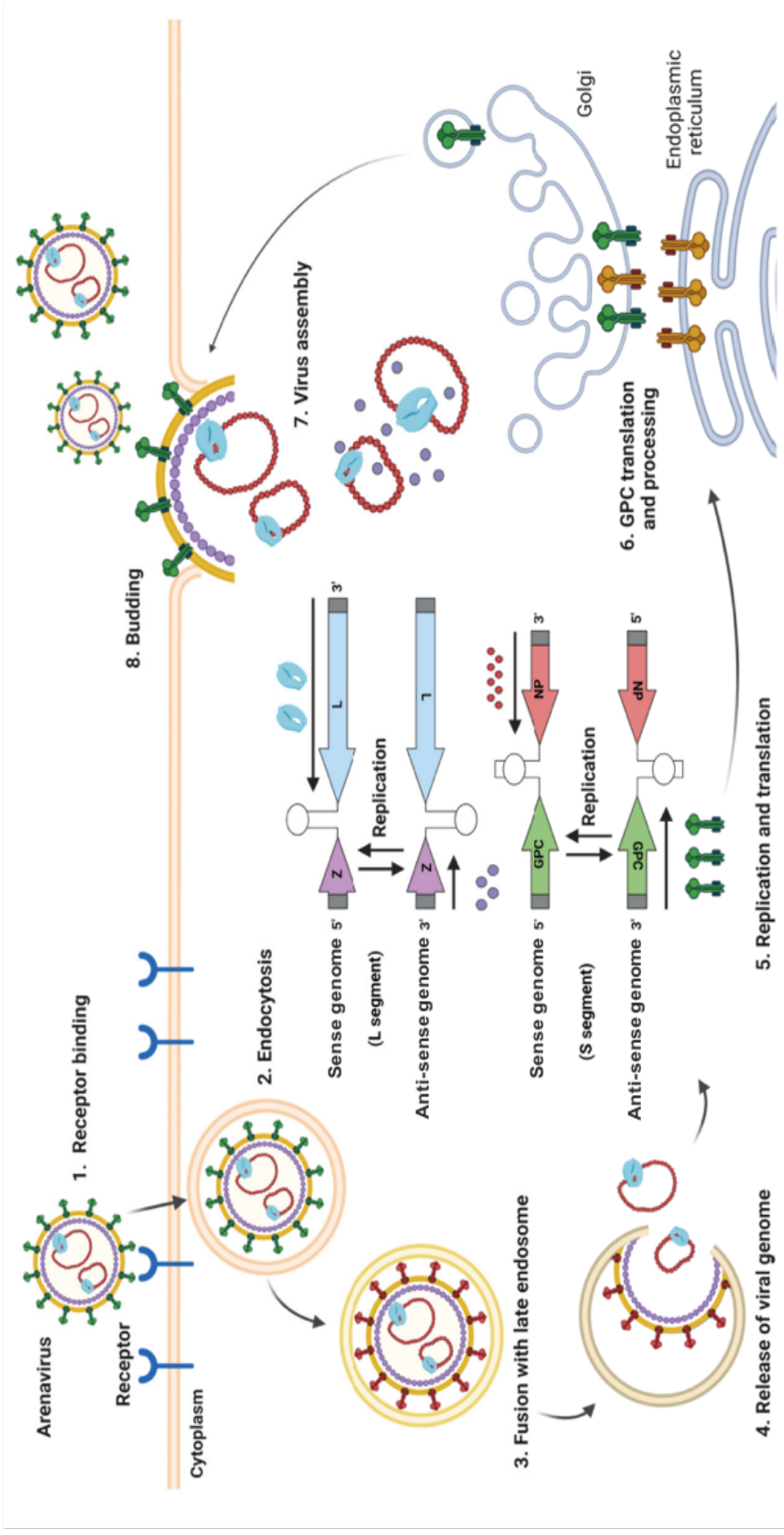

Figure 1.12: The stages of mammarenavirus multiplication. 1. GP-1-mediated cellular receptor binding. 2. Virion internalisation via endocytosis. 3. GP-2-mediated viral-cellular membrane fusion (late endosome). 4. Uncoating to release vRNPs into the cytosol. 5. vRNA transcription to generate NP and L mRNA, and vRNA replication which generates agRNA. Transcription of the agRNA generates mRNA for GPC and Z, and all mRNAs translation utilises host cell ribosomes. agRNA serve as templates for the production newly synthesised vRNA utilised for infectious progeny. 6. GPC is processed within the endoplasmic reticulum (ER), whereby cleavage of SSP occurs. Subsequently, GPC (retaining SSP) is trafficked to the Golgi, whereby cleavage by SKI-I/S1P results in SSP/GP-1/GP-2 trimers. 7. All viral proteins localise to the site of assembly at the plasma membrane, likely mediated by interactions with Z. 8. Egress occurs which allows infectious progeny virions to bud into the extracellular medium. This figure was taken from [105].

OW and NW attachment

The GP-1 from the glycoprotein trimer on the viral membrane is responsible for the initial attachment of viruses to their respective receptors for entry [202, 203]. As previously discussed, α-DG has been identified as the receptor utilised for entry of LASV, LCMV (certain strains), MOPV, MOBV and other Clade C NW arenaviruses [204, 205] (Figure 1.13). Although closely related to LASV, LUJV utilises a different entry mechanism, likely due to the evolution of GP-1 [26, 247]. Further investigations characterised the cell surface receptor as neuropilin (NRP)-2, which GP-1 binds with high affinity to the N-terminal domain [248]. Thus, LUJV is evidence that the cell surface receptor utilised by arenaviruses is not a restricting factor of evolution and may in turn act as an evolutionary pressure.

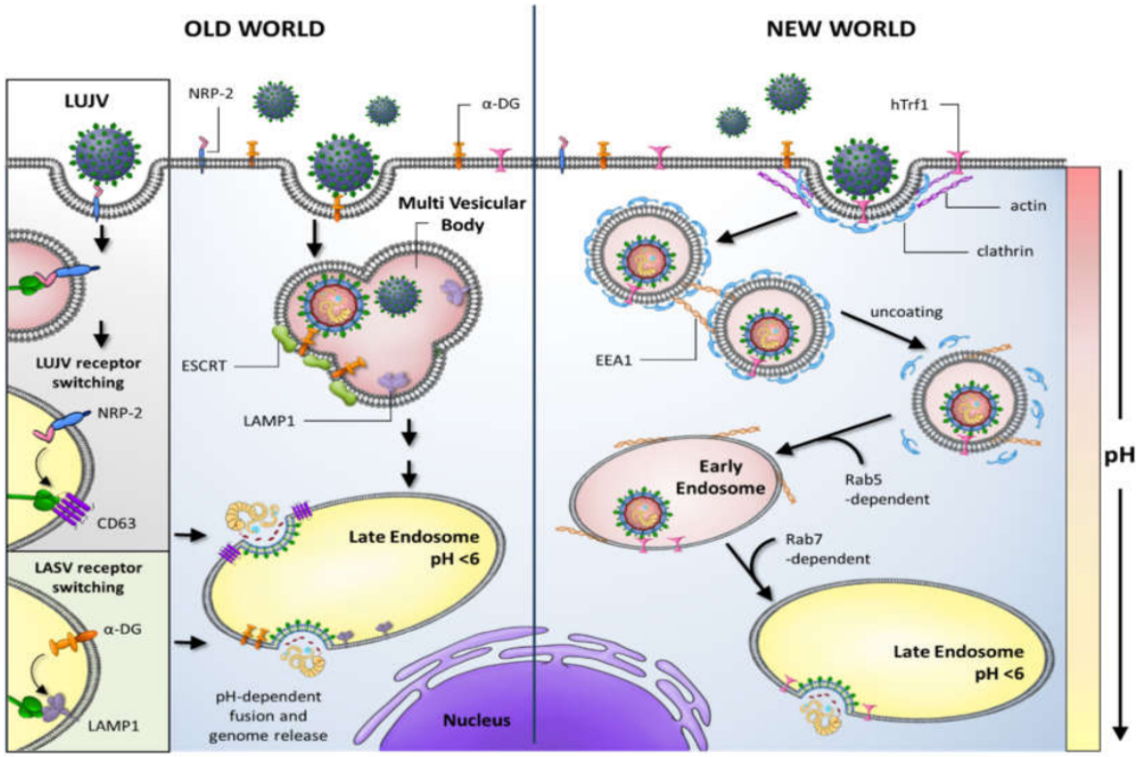

Figure 1.13: Schematic illustrating the differing entry mechanisms between OW and NW mammarenaviruses. OW mammarenavirus species binding requires cellular receptors α-dystroglycan (α-DG) or neurophilin (NRP)-2, while the majority of NW mammarenaviruses require human transferrin receptor 1 (hTrf1). OW mammarenavirus entry is clathrin- and caveolin-independent, whilst NW mammarenaviruses utilise clathrin-mediated endocytosis. NW mammarenaviruses then follow the endosomal pathway. Although not well defined, OW mammarenaviruses have been shown to utilise multi vesicular bodies, which in turn traffic to late endosomes. Upon environmental cues such as decreasing pH, viral-cellular membrane fusion occurs in the late endosome, and subsequent uncoating allows the release of vRNPs into the cytoplasm. This figure was taken from [139].

Broadly, for Clade A and B NW arenaviruses the cellular receptor TfR1 has been implicated as a required cellular receptor [211]. However, the non-pathogenic TCRV, which is phylogenetically closely related to JUNV and MACV, and the non-pathogenic AMAV, which is closely related to GTOV, do not require TfR1 for entry [212]. TCRV and AMAV have been shown to be dependent on T-cell immunoglobulin and mucin domain 1 (TIM1) as an entry factor [249]. Interestingly, it was established that non-pathogenicity of humans for both TCRV and AMAV relates to the inability of the viruses to recognise and attach to the human TfR1 orthologue, despite retaining the ability to bind the rodent host TfR1 [250, 251]. For AMAV, it has been uncovered that a single residue mutation would permit binding of the human TfR1, thus highlighting a selection pressure which could permit AMAV human infections [250, 252]. Collectively, this highlights the species specificity of TfR1, and how this influences the host range of each virus. In corroboration, the rodent hosts utilised by JUNV, MACV and GTOV differ, and this is dependent on the ability of each virus to specifically bind the different murine TfR1 orthologues [253]. Furthermore, for JUNV, MACV and GTOV only six amino acids are required for binding of murine TfR1. Therefore, selection pressure could result in mutations which would allow JUNV, MACV or GTOV to infect a wider range of rodent species, thus increasing the potential for the incidence of rodent-human transmission [253].

Taken together, the range of cellular receptors utilised by mammarenaviruses are well established. However, it could be important to fill current gaps in our knowledge by identifying the receptors for species of other genera including *Antennavirus*, *Hartmanivirus*, *Innmovirus* and *Reptarenavirus*. For example, the glycoproteins of *Reptarenavirus* are distinct from other arenaviruses, and instead they share similarity to the glycoproteins of filoviruses and retroviruses [254]. However, the receptor for any *Reptarenavirus* species is unknown. Alongside this, it has been established that pseudotyped reptarenaviruses can infect mammalian cell lines [255]. By understanding the different range of receptors for these genera, it may be possible to uncover the reasons for each host range restriction, which may uncover the likelihood of human spillover.

OW endocytosis

Following receptor-mediated attachment, virions undergo internalisation via the endocytic network [256]. The endocytic pathways utilised by OW and NW arenaviruses differs, consistent with the use of different receptors [257]. The exact mechanism utilised by OW arenaviruses for endocytosis is unclear, with contradictory evidence, but it is agreed that OW arenaviruses utilise an unusual pathway, since the typical mechanisms of endocytosis, clathrin and caveolin, are not utilised by LCMV during internalisation [257–259]. Within these investigations it was also proposed that LCMV-endocytosis does not require of dynamin, ARF6, flotillin or actin [257–259]. Recently, targeted siRNA and use of the inhibitor Na(+)/H(+) exchanger (NHE), ethyl-isopropyl amiloride have provided evidence that LCMV internalisation is dependent on NHE, actin and Pak1, proposing that macropinocytosis could be utilised as a route of entry [260]. Additionally, it has been shown that LCMV passes through Rab7-containing endosome [92]. Here, IF analysis performed after treatment with potassium ion channel inhibitors, which prevented virion uncoating, showed NP/Z representing trapped incoming virions co-localised with Rab7 [92]. Taken together, this highlights the current disparities regarding how OW arenavirus endocytosis occurs, and further clarification is required to pinpoint the exact mechanism.

NW endocytosis

The evidence surrounding endocytosis of NW arenaviruses is very limited, since only JUNV has been examined [257, 261]. JUNV was revealed to utilise clathrin-mediated endocytosis [257, 261]; alongside the use of specific inhibitors [261] and double-negative clathrin-related proteins [257], JUNV particles were visualised via EM within vesicles resembling clathrin-coated vesicles [261].

Fusion

To release vRNPs into the cytosol to initiate infection, arenaviruses undergo GP-2 mediated viral-cellular membrane fusion. Fusogenic conformational changes of GP-2 are triggered by low endosomal pH and interactions with endocytic co-receptors. For LASV, a pH-dependent receptor switch from α-DG to LAMP1 (also known

as CD107a) occurs, which promotes membrane fusion [262, 263]. Since LAMP1 subcellular localisation is restricted to the late endosomes and lysosomes, this also provides evidence for which endocytic compartments LASV fusion occurs [264, 265]. Interestingly, despite being closely related, both LCMV and LUJV do not require LAMP1 for fusion. Instead, CD164 and CD63 have been identified as the required secondary co-receptors required to promote fusion for LCMV and LUJV, respectively [248, 262, 266, 267]. No secondary receptor for any NW arenavirus has been identified so far, and this might suggest that receptor switching to mediate fusion could be specific to OW arenavirus entry. Since neutralising antibodies that target the receptor switching stage of fusion could be utilised for an effective therapeutic strategy [268], understanding the remains gaps in our knowledge on arenavirus entry could be important for development of novel treatment approaches.

Uncoating

For most bunyaviruses, fusion of the viral-cellular membranes permits the release of vRNA into the cytosol, initiating the downstream processes of infection. Interestingly, arenaviruses are unique in that an additional step termed uncoating is required to mediate the process of vRNP release. Recently, it has been shown that arenaviruses viral membrane becomes permeable during fusion, by using a system that detects quenching of an intraviral pH-sensor in acidic endosomes prior to virus fusion [269]. Separate work has shown that LAMP1 causes dilations of the LASV GPC-mediated fusion pores [270, 271]. Collectively, these investigations propose that fusion pores and membrane permeability may play a role in uncoating by ensuring the acidification of interior of virions subsequent to fusion [269–271]. Foundation for this is reasonable, since the M2 viroporin of IAV has ion channel activity and is important for uncoating of the matrix and nucleoprotein [272, 273]. In addition to this, it was recently shown that K^+ ions are essential for early LCMV infection, being required between 0 - 3 hpi [92]. It was established that K^+ ions are not required for receptor attachment, endocytosis, binding of CD164 or GPC-mediated fusion [92]. However, in the presence of potassium channel inhibitors, incoming LCMV virions became trapped within Rab7/CD164-positive late endosome, with inhibition of subsequent NP translation [92]. Thus, a model was proposed whereby K^+ ions are required for arenavirus uncoating, being required

for dissociation of Z and NP during fusion or post-fusion stages, which allows infection to progress through the release of vRNPs into the cytosol (Figure 1.14) [92]. Collectively, investigations surrounding uncoating have primarily focused on OW arenaviruses, with the assumption that the mechanism of uncoating for NW arenaviruses is similar. However, since NW arenaviruses utilise a different entry mechanism, and seemingly do no require secondary receptors, investigations should corroborate whether the uncoating requirements are conserved between OW and NW arenaviruses.

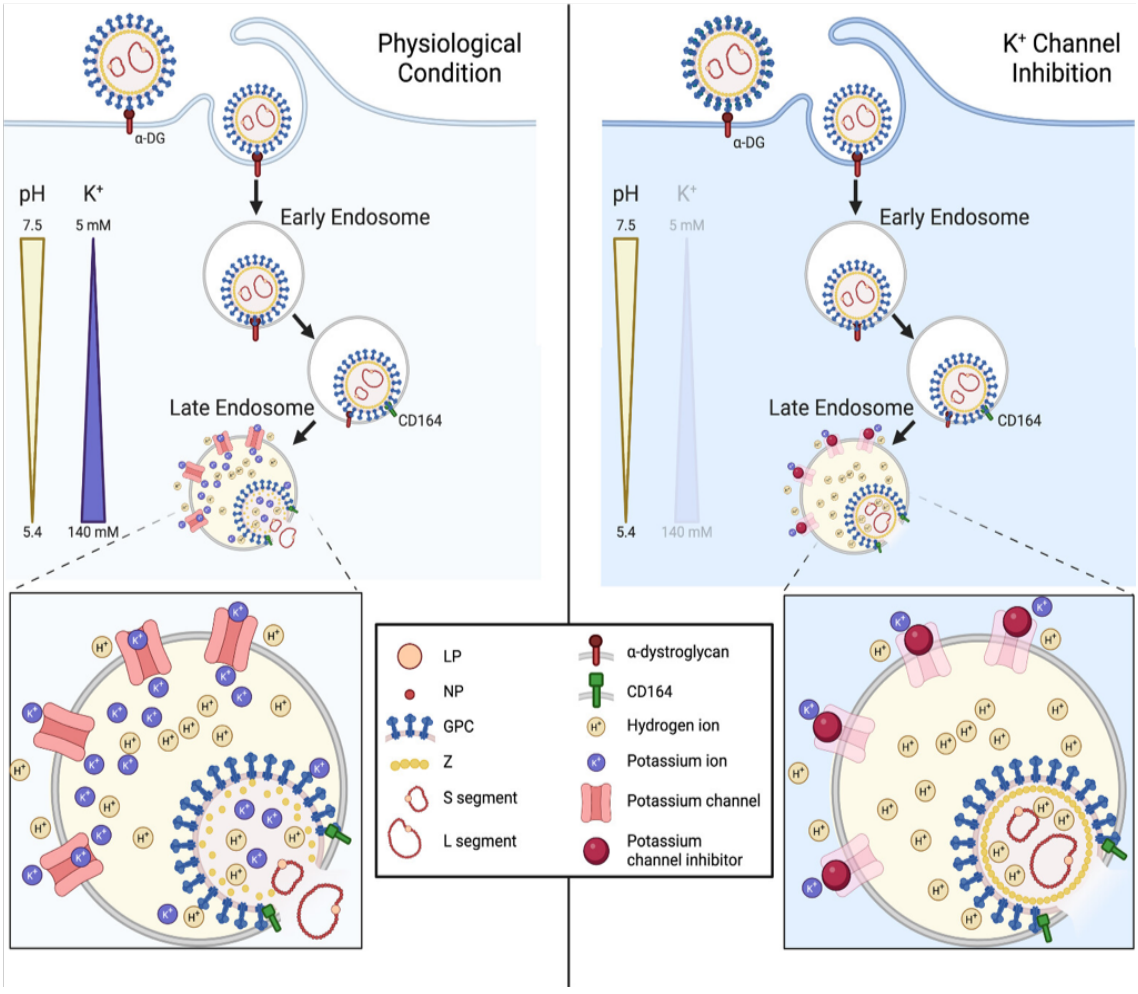

Figure 1.14: Schematic depicting the proposed role of potassium ions during uncoating. Under normal physiological conditions, hydrogen and potassium ions present at the late endosome ensure that fusion and uncoating occur, respectively, resulting in the release of vRNPs into the cytoplasm to initiate infection. However, in conditions whereby potassium ions are depleted, fusion can still occur but uncoating is inhibited. This figure was taken from [92].

Replication – Transcription and agRNA synthesis

Since input vRNA are ambi-sense polarity, the initial process inside the cytosol is transcription of input negative-sense ORFs of vRNA S and L, resulting in postive-sense NP and L mRNAs, respectively. However, in order for transcription to occur, a process term 'cap-snatching' whereby the cap structures of cellular mRNAs are cleaved (possibly by the endonuclease activity of L) and utilised as primers for viral mRNA synthesis is required [274–276]. While the cap-snatching mechanism of arenaviruses is poorly characterised, it may have similarities to the cap-snatching mechanism of IAV, which is more established. Briefly, the RdRp of IAV has two important regions for cap-snatching: the cap-binding of PB2 and the endonuclease of PA [277]. Within the nucleus, the endonuclease domain of IAV cleaves the caps of cellular mRNA. The capped RNA primer is then added to the vRNA to allow initiation of transcription. The length of cap-snatched primers is between 10 and 13 nucleotides and is determined by cleavage consensus sequences [278, 279]. For IAV, the process of cap-snatching has also been shown to be reliant on the cellular DNA-dependent RNAPII, with pharmalogical inhibition of RNAPII preventing IAV primary transcription [280]. Overall, whilst it is expected arenaviruses cap-snatching may share some characteristics with IAV, major differences exist meaning this requires specific investigations. Firstly, the cap-snatching for arenaviruses must occur in the cytoplasm rather than the nucleus. Secondly, the capped cap-snatched primer of arenaviruses is significantly shorter than IAV, being only 4 – 5 nt [281, 282]. Finally, RNAPII is active within discrete puncta localised to the nucleoplasm, thus it is unlikely that arenaviruses would require this cellular polymerase for cap-snatching [283]. Overall, the process of cap-snatching for arenaviruses is not well defined, and further investigations are required to establish the precise mechanisms.

Additionally, the arenavirus GPC and Z mRNAs cannot be transcribed from initial vRNAs since these genes are positive polarity. Following the production of NP and L mRNA, agRNAs are synthesised, which subsequently act as templates for GPC and Z mRNA transcription. The characteristics of agRNA are not well defined and the abundance of agRNA during arenavirus infection unknown. Additionally, it has not been clearly examined whether the agRNA are packaged into infectious or DI particles.

Assembly - Viral protein trafficking

Arenavirus mRNA is translated in the cytosol utilising host ribosomes, with eukaryotic translation initiation factors (eIF) 4A and 4GI shown to be required for translation of JUNV mRNA [284]. Interestingly, for LCMV, Z has been shown to bind ribosomal proteins and eIF-4E [285]. It was established through IF and co-IP that Z can modulate cell translation, repressing host cell protein production in an eIF-4E-dependent mechanism [285]. This could provide a way in which arenaviruses manipulate the host cell to drive translation of viral mRNAs specifically. Once translated, the viral proteins are processed within the cell to allow assembly and egress to occur. As discussed, GPC is initially processed in the ER, before being trafficked to the Golgi, and then subsequently trafficked to the plasma membrane. For NP, which alongside L forms part of the newly synthesised vRNP, trafficking from the cytosol to the site of RNA synthesis occurs. Since Z-NP interactions are well defined [223, 225, 228, 233, 234], it has been proposed that vRNP-Z complexes may traffic together to the plasma membrane. However, arenavirus protein trafficking within the cells needs further characterisation and could prove new avenues for the development of effective therapeutics. Many key questions remain; firstly, what are the cellular vesicles or components responsible for trafficking of GPC from the ER to the Golgi? Secondly, how do the SSP/GP-1/GP-2 trimers traffic between the cis-Golgi to trans-Golgi network? In addition, how are the glycoprotein trimers then transported from the trans-Golgi network to the plasma membrane? And during this process, what allows SSP/GP-1/GP-2 to be embedded in the cell membrane correctly? Finally, how do newly formed vRNPs traffic from the cytoplasm to the site of assembly, and what cellular components are involved?

Egress

It is widely accepted that budding and egress of infectious arenavirus virions occurs at the plasma membrane. Polarisation of cells has also been shown to be important for virus budding, with JUNV revealed to produce 100-fold higher progeny virus from apical membranes of polarised epithelial cells when compared to the basolateral [286]. This was corroborated with LASV, showing that GP of LASV preferentially localises to the apical membranes of polarised membranes, with a 200-fold increase

in virion production compared to the basolateral membranes [287]. It is generally accepted that the Z-NP and Z-SSP interactions ensure that vRNPs are packaged into infectious progeny during the budding process [223, 225, 228, 231–234], although the succession of this is yet to be established. In any case, Z is regarded as important during the budding process. However, given budding has contradictory evidence surround the requirement of the PPXY domain of Z and ESCRT components, further investigations are required to understand the exact mechanisms of egress [223, 226, 228, 236, 288].

1.3 References

[1] Payne S. Introduction to Animal Viruses. In: Viruses. Elsevier; 2017. p. 1–11. doi:10.1016/B978-0-12-803109-4.00001-5

[2] Shannon E. Greene, Ann Reid. Viruses Throughout Life & Time: Friends, Foes, Change Agents. Washington (DC): American Academy of Microbiology.; 2013.

[3] Lecoq H. Découverte du premier virus, le virus de la mosaïque du tabac : 1892 ou 1898 ? Comptes Rendus de l'Académie des Sciences - Series III - Sciences de la Vie. 2001;324(10):929–933. https://www.sciencedirect.com/science/article/pii/S0764446901013683. doi:https://doi.org/10.1016/S0764-4469(01)01368-3

[4] Armstrong C, Lillie RD. Experimental Lymphocytic Choriomeningitis of Monkeys and Mice Produced by a Virus Encountered in Studies of the 1933 St. Louis Encephalitis Epidemic. Public Health Reports (1896-1970). 1934;49(35):1019. doi:10.2307/4581290

[5] Traub E. A Filterable Virus Recovered from White Mice. Science. 1935;81(2099):298–299. doi:10.1126/science.81.2099.298

[6] Traub E. Epidemiology of the Lymphocytic choriomeningitis in a mouse stock observed for four years. Journal of Experimental Medicine. 1939;69(6):801–817. doi:10.1084/jem.69.6.801

[7] Scott TFM, Rivers TM. Meningitis in man caused by a filterable virus. Journal of Experimental Medicine. 1936;63(3):397–414. doi:10.1084/jem.63.3.397

[8] Downs WG, Anderson CR, Spence L, Aitken THG, Greenhall AH. Tacaribe Virus, a New Agent Isolated from Artibeus Bats and Mosquitoes in Trinidad, West Indies. The American Journal of Tropical Medicine and Hygiene. 1963;12(4):640–646. doi:10.4269/ajtmh.1963.12.640

[9] Cogswell-Hawkinson A, Bowen R, James S, Gardiner D, Calisher CH, Adams R, Schountz T. Tacaribe Virus Causes Fatal Infection of An Ostensible Reservoir Host, the Jamaican Fruit Bat. Journal of Virology. 2012;86(10):5791–5799. doi:10.1128/JVI.00201-12

[10] Parodi AS, Greenway DJ, Rugiero HR, Frigerio M, De La Barrera JM, Mettler N, Garzon F, Boxaca M, Guerrero L, Nota N. Concerning the epidemic outbreak in Junin. El Dia medico. 1958;30(62):2300–1.

[11] Enria DA, Briggiler AM, Sánchez Z. Treatment of Argentine hemorrhagic fever. Antiviral Research. 2008;78(1):132–139. doi:10.1016/j.antiviral.2007.10.010

[12] Maiztegui JI. Clinical and epidemiological patterns of Argentine haemorrhagic fever. Bulletin of the World Health Organization. 1975;52(4–6):567–75.

[13] Charrel RN, Lamballerie X de. Arenaviruses other than Lassa virus. Antiviral Research. 2003;57(1–2):89–100. doi:10.1016/S0166-3542(02)00202-4

[14] Richmond JK, Baglole DJ. Lassa fever: epidemiology, clinical features, and social consequences. BMJ (Clinical research ed.). 2003;327(7426):1271–5. doi:10.1136/bmj.327.7426.1271

[15] Logue J, Richter M, Johnson RF, Kuhn JH, Weaver W. Overview of Human Viral Hemorrhagic Fevers. In: Defense Against Biological Attacks. Cham: Springer International Publishing; 2019. p. 21–54. doi:10.1007/978-3-030-03071-1_2

[16] Nastri AC, Duarte-Neto AN, Casadio LVB, Souza WM de, Claro IM, Manuli ER, Selegatto G, Salomão MC, Fialkovitz G, Taborda M, et al. Understanding Sabiá virus infections (Brazilian mammarenavirus). Travel Medicine and Infectious Disease. 2022;48:102351. doi:10.1016/j.tmaid.2022.102351

[17] Ellwanger JH, Chies JAB. Keeping track of hidden dangers - The short history of the Sabiá virus. Revista da Sociedade Brasileira de Medicina Tropical. 2017;50(1):3–8. doi:10.1590/0037-8682-0330-2016

[18] Barry M, Russi M, Armstrong L, Geller D, Tesh R, Dembry L,

Gonzalez JP, Khan AS, Peters CJ. Treatment of a Laboratory-Acquired Sabiá Virus Infection. New England Journal of Medicine. 1995;333(5):294–296. doi:10.1056/NEJM199508033330505

[19] Coimbra TLM, Nassar ES, de Souza LTM, Ferreira IB, Rocco IM, Burattini MN, Travassos da Rosa APA, Vasconcelos PFC, Pinheiro FP, LeDuc JW, et al. New arenavirus isolated in Brazil. The Lancet. 1994;343(8894):391–392. doi:10.1016/S0140-6736(94)91226-2

[20] Vasconcelos PF da C, Travassos da Rosa AP de A, Rodrigues SG, Tesh R, Travassos da Rosa JFS, Travassos da Rosa ES. Laboratory acquired infection by the virus SP H 114202 (Arenavirus: Arenaviridae): clinical and laboratory findings. Revista do Instituto de Medicina Tropical de São Paulo. 1993;35(6):521–525. doi:10.1590/S0036-46651993000600008

[21] Delgado S, Erickson BR, Agudo R, Blair PJ, Vallejo E, Albariño CG, Vargas J, Comer JA, Rollin PE, Ksiazek TG, et al. Chapare Virus, a Newly Discovered Arenavirus Isolated from a Fatal Hemorrhagic Fever Case in Bolivia. PLoS Pathogens. 2008;4(4):e1000047. doi:10.1371/journal.ppat.1000047

[22] Loayza Mafayle R, Morales-Betoulle ME, Romero C, Cossaboom CM, Whitmer S, Alvarez Aguilera CE, Avila Ardaya C, Cruz Zambrana M, Dávalos Anajia A, Mendoza Loayza N, et al. Chapare Hemorrhagic Fever and Virus Detection in Rodents in Bolivia in 2019. New England Journal of Medicine. 2022;386(24):2283–2294. doi:10.1056/NEJMoa2110339

[23] Sewlall NH, Richards G, Duse A, Swanepoel R, Paweska J, Blumberg L, Dinh TH, Bausch D. Clinical Features and Patient Management of Lujo Hemorrhagic Fever. PLoS Neglected Tropical Diseases. 2014;8(11):e3233. doi:10.1371/journal.pntd.0003233

[24] Paweska JT, Sewlall NH, Ksiazek TG, Blumberg LH, Hale MJ, Lipkin WI, Weyer J, Nichol ST, Rollin PE, McMullan LK, et al. Nosocomial Outbreak of Novel Arenavirus Infection, Southern Africa. Emerging Infectious Diseases. 2009;15(10):1598–1602. doi:10.3201/eid1510.090211

[25] Simulundu E, Mweene AS, Changula K, Monze M, Chizema E, Mwaba P, Takada A, Ippolito G, Kasolo F, Zumla A, et al. Lujo viral hemorrhagic fever: considering diagnostic capacity and preparedness in the wake of recent Ebola

and Zika virus outbreaks. Reviews in Medical Virology. 2016;26(6):446–454. doi:10.1002/rmv.1903

[26] Briese T, Paweska JT, McMullan LK, Hutchison SK, Street C, Palacios G, Khristova ML, Weyer J, Swanepoel R, Egholm M, et al. Genetic Detection and Characterization of Lujo Virus, a New Hemorrhagic Fever–Associated Arenavirus from Southern Africa. PLoS Pathogens. 2009;5(5):e1000455. doi:10.1371/journal.ppat.1000455

[27] WHO. Prioritizing diseases for research and development in emergency contexts. 2024. [accessed 2025 Jan 6]. https://www.who.int/activities/prioritizing-diseases-for-research-and-development-in-emergency-contexts

[28] Bowen MD, Peters CJ, Nichol ST. Phylogenetic Analysis of theArenaviridae:Patterns of Virus Evolution and Evidence for Cospeciation between Arenaviruses and Their Rodent Hosts. Molecular Phylogenetics and Evolution. 1997;8(3):301–316. doi:10.1006/mpev.1997.0436

[29] Radoshitzky SR, Bào Y, Buchmeier MJ, Charrel RN, Clawson AN, Clegg CS, DeRisi JL, Emonet S, Gonzalez J-P, Kuhn JH, et al. Past, present, and future of arenavirus taxonomy. Archives of Virology. 2015;160(7):1851–1874. doi:10.1007/s00705-015-2418-y

[30] Fulhorst CF, Bennett SG, Milazzo ML, Murray HL, Webb JP, Cajimat MNB, Bradley RD. Bear Canyon Virus: An Arenavirus Naturally Associated with the California Mouse (*Peromyscus californicus*). Emerging Infectious Diseases. 2002;8(7):717–721. doi:10.3201/eid0807.010281

[31] Fulhorst CF, Bowen MD, Ksiazek TG, Rollin PE, Nichol ST, Kosoy MY, Peters CJ. Isolation and Characterization of Whitewater Arroyo Virus, a Novel North American Arenavirus. Virology. 1996;224(1):114–120. doi:10.1006/viro.1996.0512

[32] Jennings WL, Lewis AL, Sather GE, Pierce L V., Bond JO. Tamiami Virus in the Tampa Bay Area. The American Journal of Tropical Medicine and Hygiene. 1970;19(3):527–536. doi:10.4269/ajtmh.1970.19.527

[33] Calisher CH, Tzianabos T, Lord RD, Coleman PH. Tamiami Virus, a New Member of the Tacaribe Group. The American Journal of Tropical Medicine and

Hygiene. 1970;19(3):520–526. doi:10.4269/ajtmh.1970.19.520

[34] Reignier T, Oldenburg J, Flanagan ML, Hamilton GA, Martin VK, Cannon PM. Receptor use by the Whitewater Arroyo virus glycoprotein. Virology. 2008;371(2):439–446. doi:10.1016/j.virol.2007.10.004

[35] Blasdell KR, Duong V, Eloit M, Chretien F, Ly S, Hul V, Deubel V, Morand S, Buchy P. Evidence of human infection by a new mammarenavirus endemic to Southeastern Asia. eLife. 2016;5. doi:10.7554/eLife.13135

[36] Asogun DA, Günther S, Akpede GO, Ihekweazu C, Zumla A. Lassa Fever. Infectious Disease Clinics of North America. 2019;33(4):933–951. doi:10.1016/j.idc.2019.08.002

[37] Flannery B, Cain M, Ly H. Recent Discoveries of Novel Mammarenaviruses Infecting Humans and Other Mammals in Asia and Southeast Asia. Virulence. 2023;14(1). doi:10.1080/21505594.2023.2231392

[38] Sarute N, Ross SR. New World Arenavirus Biology. Annual Review of Virology. 2017;4(1):141–158. doi:10.1146/annurev-virology-101416-042001

[39] Olayemi A, Cadar D, Magassouba N, Obadare A, Kourouma F, Oyeyiola A, Fasogbon S, Igbokwe J, Rieger T, Bockholt S, et al. New Hosts of The Lassa Virus. Scientific Reports. 2016;6(1):25280. doi:10.1038/srep25280

[40] Kronmann KC, Nimo-Paintsil S, Guirguis F, Kronmann LC, Bonney K, Obiri-Danso K, Ampofo W, Fichet-Calvet E. Two Novel Arenaviruses Detected in Pygmy Mice, Ghana. Emerging Infectious Diseases. 2013;19(11):1832–1835. doi:10.3201/eid1911.121491

[41] Monath TP, Newhouse VF, Kemp GE, Setzer HW, Cacciapuoti A. Lassa Virus Isolation from Mastomys natalensis Rodents during an Epidemic in Sierra Leone. Science. 1974;185(4147):263–265. doi:10.1126/science.185.4147.263

[42] Blasdell KR, Becker SD, Hurst J, Begon M, Bennett M. Host Range and Genetic Diversity of Arenaviruses in Rodents, United Kingdom. Emerging Infectious Diseases. 2008;14(9):1455–1458. doi:10.3201/eid1409.080209

[43] Gómez RM, Jaquenod de Giusti C, Sanchez Vallduvi MM, Frik J, Ferrer MF, Schattner M. Junín virus. A XXI century update. Microbes and Infection. 2011;13(4):303–311. doi:10.1016/j.micinf.2010.12.006

[44] Sayler KA, Barbet AF, Chamberlain C, Clapp WL, Alleman R, Loeb JC, Lednicky JA. Isolation of Tacaribe Virus, a Caribbean Arenavirus, from Host-Seeking Amblyomma americanum Ticks in Florida. PLoS ONE. 2014;9(12):e115769. doi:10.1371/journal.pone.0115769

[45] Cajimat MNB, Milazzo ML, Bradley RD, Fulhorst CF. Ocozocoautla de Espinosa Virus and Hemorrhagic Fever, Mexico. Emerging Infectious Diseases. 2012;18(3):401–405. doi:10.3201/eid1803.111602

[46] Milazzo ML, Barragán-Gomez A, Hanson JD, Estrada-Franco JG, Arellano E, González-Cózatl FX, Fernández-Salas I, Ramirez-Aguilar F, Rogers DS, Bradley RD, et al. Antibodies to Tacaribe Serocomplex Viruses (Family *Arenaviridae*, Genus Arenavirus) in Cricetid Rodents from New Mexico, Texas, and Mexico. Vector-Borne and Zoonotic Diseases. 2010;10(6):629–637. doi:10.1089/vbz.2009.0206

[47] Hastie KM, Melnik LI, Cross RW, Klitting RM, Andersen KG, Saphire EO, Garry RF. The Arenaviridae Family: Knowledge Gaps, Animal Models, Countermeasures, and Prototype Pathogens. The Journal of Infectious Diseases. 2023;228(Supplement_6):S359–S375. doi:10.1093/infdis/jiac266

[48] Richmond JK. Lassa fever: epidemiology, clinical features, and social consequences. BMJ. 2003;327(7426):1271–1275. doi:10.1136/bmj.327.7426.1271

[49] Vainrub B, Salas R. Latin American hemorrhagic fever. Infectious disease clinics of North America. 1994;8(1):47–59.

[50] Ka-Wai Hui E. Reasons for the increase in emerging and re-emerging viral infectious diseases. Microbes and Infection. 2006;8(3):905–916. doi:10.1016/j.micinf.2005.06.032

[51] Kumar S, Yadav D, Singh D, Shakya K, Rathi B, Poonam. Recent developments on Junin virus, a causative agent for Argentine haemorrhagic fever. Reviews in Medical Virology. 2023;33(2). doi:10.1002/rmv.2419

[52] Barradas JS, Errea MI, D'Accorso NB, Sepúlveda CS, Damonte EB. Imidazo[2,1-b]thiazole carbohydrate derivatives: Synthesis and antiviral activity against Junin virus, agent of Argentine hemorrhagic fever. European Journal of Medicinal Chemistry. 2011;46(1):259–264. doi:10.1016/j.ejmech.2010.11.012

[53] Safronetz D, Lopez JE, Sogoba N, Traore' SF, Raffel SJ, Fischer ER, Ebihara H, Branco L, Garry RF, Schwan TG, et al. Detection of Lassa Virus, Mali. Emerging Infectious Diseases. 2010;16(7):1123–1126. doi:10.3201/eid1607.100146

[54] Sogoba N, Feldmann H, Safronetz D. Lassa Fever in West Africa: Evidence for an Expanded Region of Endemicity. Zoonoses and Public Health. 2012;59(s2):43–47. doi:10.1111/j.1863-2378.2012.01469.x

[55] Patterson M, Grant A, Paessler S. Epidemiology and pathogenesis of Bolivian hemorrhagic fever. Current Opinion in Virology. 2014;5:82–90. doi:10.1016/j.coviro.2014.02.007

[56] Bonthius DJ. Lymphocytic Choriomeningitis Virus: An Underrecognized Cause of Neurologic Disease in the Fetus, Child, and Adult. Seminars in Pediatric Neurology. 2012;19(3):89–95. doi:10.1016/j.spen.2012.02.002

[57] Riera L, Castillo E, Saavedra M del C, Priotto J, Sottosanti J, Polop J, Ambrosio AM. Serological study of the lymphochoriomeningitis virus (LCMV) in an inner city of Argentina. Journal of Medical Virology. 2005;76(2):285–289. doi:10.1002/jmv.20357

[58] Stephensen CB, Blount SR, Lanford RE, Holmes K V., Montali RJ, Fleenor ME, Shaw JFE. Prevalence of serum antibodies against lymphocytic choriomeningitis virus in selected populations from two U.S. cities. Journal of Medical Virology. 1992;38(1):27–31. doi:10.1002/jmv.1890380107

[59] Alburkat HAT, Pulkkinen E, Virtanen J, Vapalahti O, Sironen T, Jääskeläinen AJ. Serological and molecular screening of arenaviruses in suspected tick-borne encephalitis cases in Finland. Epidemiology and Infection. 2024;152:e20. doi:10.1017/S0950268824000128

[60] Fevola C, Kuivanen S, Smura T, Vaheri A, Kallio-Kokko H, Hauffe HC, Vapalahti O, Jääskeläinen AJ. Seroprevalence of lymphocytic choriomeningitis virus and Ljungan virus in Finnish patients with suspected neurological infections. Journal of Medical Virology. 2018;90(3):429–435. doi:10.1002/jmv.24966

[61] Günther S, Lenz O. Lassa Virus. Critical Reviews in Clinical Laboratory Sciences. 2004;41(4):339–390. doi:10.1080/10408360490497456

[62] Moraz M-L, Kunz S. Pathogenesis of arenavirus hemorrhagic fevers. Expert

Review of Anti-infective Therapy. 2011;9(1):49–59. doi:10.1586/eri.10.142

[63] Cummins D. Acute Sensorineural Deafness in Lassa Fever. JAMA: The Journal of the American Medical Association. 1990;264(16):2093. doi:10.1001/jama.1990.03450160063030

[64] Cashman KA, Wilkinson ER, Zeng X, Cardile AP, Facemire PR, Bell TM, Bearss JJ, Shaia CI, Schmaljohn CS. Immune-Mediated Systemic Vasculitis as the Proposed Cause of Sudden-Onset Sensorineural Hearing Loss following Lassa Virus Exposure in Cynomolgus Macaques. mBio. 2018;9(5). doi:10.1128/mBio.01896-18

[65] Mateer EJ, Huang C, Shehu NY, Paessler S. Lassa fever–induced sensorineural hearing loss: A neglected public health and social burden. PLOS Neglected Tropical Diseases. 2018;12(2):e0006187. doi:10.1371/journal.pntd.0006187

[66] Paweska JT, Sewlall NH, Ksiazek TG, Blumberg LH, Hale MJ, Lipkin WI, Weyer J, Nichol ST, Rollin PE, McMullan LK, et al. Nosocomial Outbreak of Novel Arenavirus Infection, Southern Africa. Emerging Infectious Diseases. 2009;15(10):1598–1602. doi:10.3201/eid1510.090211

[67] Lehmann-Grube F. Portraits of Viruses: Arenaviruses. Intervirology. 1984;22(3):121–145. doi:10.1159/000149543

[68] Danes L, Benda R, Fuchsova M, [Experimental inhalation infection of monkeys of the *Macacus cynomolgus* and Macacus rhesus species with the virus of Lymphocytic choriomeningitis (WE)]. Bratislavske lekarske listy. 1963;2:71–9.

[69] Jahrling PB, Peters CJ. Lymphocytic choriomeningitis virus. A neglected pathogen of man. Archives of pathology & laboratory medicine. 1992;116(5):486–8.

[70] Barton LL, Hyndman NJ. Lymphocytic Choriomeningitis Virus: Reemerging Central Nervous System Pathogen. Pediatrics. 2000;105(3):e35–e35. doi:10.1542/peds.105.3.e35

[71] Asnis DS, Muana O, Kim DG, Garcia M, Rollin PE, Slavinski S. Lymphocytic Choriomeningitis Virus Meningitis, New York, NY, USA, 2009. Emerging Infectious Diseases. 2010;16(2):328–330. doi:10.3201/eid1602.091347

[72] Bonthius DJ, Karacay B. Meningitis and encephalitis in children. Neurologic Clinics. 2002;20(4):1013–1038. doi:10.1016/S0733-8619(02)00016-6

[73] L.L. Barton, N.R. Friedman. The Neurological Manifestations of Pediatric

Infectious Diseases and Immunodeficiency Syndromes. American Journal of Neuroradiology. 2009;30(10):E153–E153. doi:10.3174/ajnr.A1761

[74] Fischer SA, Graham MB, Kuehnert MJ, Kotton CN, Srinivasan A, Marty FM, Comer JA, Guarner J, Paddock CD, DeMeo DL, et al. Transmission of Lymphocytic Choriomeningitis Virus by Organ Transplantation. New England Journal of Medicine. 2006;354(21):2235–2249. doi:10.1056/NEJMoa053240

[75] Centers for Disease Control and Prevention (CDC). Brief report: Lymphocytic choriomeningitis virus transmitted through solid organ transplantation–Massachusetts, 2008. MMWR. Morbidity and mortality weekly report. 2008;57(29):799–801.

[76] MacNeil A, Ströher U, Farnon E, Campbell S, Cannon D, Paddock CD, Drew CP, Kuehnert M, Knust B, Gruenenfelder R, et al. Solid Organ Transplant–associated Lymphocytic Choriomeningitis, United States, 2011. Emerging Infectious Diseases. 2012;18(8):1256–1262. doi:10.3201/eid1808.120212

[77] Wright R, Johnson D, Neumann M, Ksiazek TG, Rollin P, Keech R V., Bonthius DJ, Hitchon P, Grose CF, Bell WE, et al. Congenital Lymphocytic Choriomeningitis Virus Syndrome: A Disease That Mimics Congenital Toxoplasmosis or Cytomegalovirus Infection. Pediatrics. 1997;100(1):e9–e9. doi:10.1542/peds.100.1.e9

[78] Bonthius DJ, Wright R, Tseng B, Barton L, Marco E, Karacay B, Larsen PD. Congenital lymphocytic choriomeningitis virus infection: spectrum of disease. Annals of Neurology. 2007;62(4):347–355. doi:10.1002/ana.21161

[79] Bonthius DJ, Nichols B, Harb H, Mahoney J, Karacay B. Lymphocytic choriomeningitis virus infection of the developing brain: critical role of host age. Annals of Neurology. 2007;62(4):356–374. doi:10.1002/ana.21193

[80] Harrison LH, Halsey NA, McKee Jr, KT, Peters CJ, Oro JGB, Briggiler AM, Feuillade MR, Maiztegui JI. Clinical Case Definitions for Argentine Hemorrhagic Fever. Clinical Infectious Diseases. 1999;28(5):1091–1094. doi:10.1086/514749

[81] Pfau CJ. Arenaviruses. 1996.

[82] Fukushi S, Tani H, Yoshikawa T, Saijo M, Morikawa S. Serological Assays Based on Recombinant Viral Proteins for the Diagnosis of Arenavirus Hemorrhagic Fevers.

Viruses. 2012;4(10):2097–2114. doi:10.3390/v4102097

[83] Ölschläger S, Lelke M, Emmerich P, Panning M, Drosten C, Hass M, Asogun D, Ehichioya D, Omilabu S, Günther S. Improved Detection of Lassa Virus by Reverse Transcription-PCR Targeting the 5' Region of S RNA. Journal of Clinical Microbiology. 2010;48(6):2009–2013. doi:10.1128/JCM.02351-09

[84] Weissenbacher MC, Laguens RP, Coto CE. Argentine Hemorrhagic Fever. 1987. p. 79–116. doi:10.1007/978-3-642-71726-0_4

[85] Kilgore PE, Peters CJ, Mills JN, Rollin PE, Armstrong L, Khan AS, Ksiazek TG. Prospects for the Control of Bolivian Hemorrhagic Fever. Emerging Infectious Diseases. 1995;1(3):97–100. doi:10.3201/eid0103.950308

[86] McCormick JB, King IJ, Webb PA, Scribner CL, Craven RB, Johnson KM, Elliott LH, Belmont-Williams R. Lassa Fever. New England Journal of Medicine. 1986;314(1):20–26. doi:10.1056/NEJM198601023140104

[87] Salam AP, Cheng V, Edwards T, Olliaro P, Sterne J, Horby P. Time to reconsider the role of ribavirin in Lassa fever. PLOS Neglected Tropical Diseases. 2021;15(7):e0009522. doi:10.1371/journal.pntd.0009522

[88] Salam AP, Duvignaud A, Jaspard M, Malvy D, Carroll M, Tarning J, Olliaro PL, Horby PW. Ribavirin for treating Lassa fever: A systematic review of pre-clinical studies and implications for human dosing. PLOS Neglected Tropical Diseases. 2022;16(3):e0010289. doi:10.1371/journal.pntd.0010289

[89] Knowles SR, Phillips EJ, Dresser L, Matukas L. Common Adverse Events Associated with the Use of Ribavirin for Severe Acute Respiratory Syndrome in Canada. Clinical Infectious Diseases. 2003;37(8):1139–1142. doi:10.1086/378304

[90] Trickey A, Zhang L, Sabin CA, Sterne JAC. Life expectancy of people with HIV on long-term antiretroviral therapy in Europe and North America: a cohort study. The Lancet Healthy Longevity. 2022;3:S2. doi:10.1016/S2666-7568(22)00063-0

[91] Iyer K, Yan Z, Ross SR. Entry inhibitors as arenavirus antivirals. Frontiers in Microbiology. 2024;15. doi:10.3389/fmicb.2024.1382953

[92] Shaw AB, Tse HN, Byford O, Plahe G, Moon-Walker A, Hover SE, Saphire EO, Whelan SPJ, Mankouri J, Fontana J, et al. Cellular endosomal potassium ion flux regulates arenavirus uncoating during virus entry. mBio. 2024;15(7).

doi:10.1128/mbio.01684-23

[93] Lavanya M, Cuevas CD, Thomas M, Cherry S, Ross SR. siRNA Screen for Genes That Affect Junín Virus Entry Uncovers Voltage-Gated Calcium Channels as a Therapeutic Target. Science Translational Medicine. 2013;5(204). doi:10.1126/scitranslmed.3006827

[94] Sarute N, Ross SR. CACNA1S haploinsufficiency confers resistance to New World arenavirus infection. Proceedings of the National Academy of Sciences. 2020;117(32):19497–19506. doi:10.1073/pnas.1920551117

[95] Liu Y, Guo J, Cao J, Zhang G, Jia X, Wang P, Xiao G, Wang W. Screening of Botanical Drugs against Lassa Virus Entry. Journal of Virology. 2021;95(8). doi:10.1128/JVI.02429-20

[96] Tang K, He S, Zhang X, Guo J, Chen Q, Yan F, Banadyga L, Zhu W, Qiu X, Guo Y. Tangeretin, an extract from Citrus peels, blocks cellular entry of arenaviruses that cause viral hemorrhagic fever. Antiviral Research. 2018;160:87–93. doi:10.1016/j.antiviral.2018.10.011

[97] Tang K, Zhang X, Guo Y. Identification of the dietary supplement capsaicin as an inhibitor of Lassa virus entry. Acta Pharmaceutica Sinica B. 2020;10(5):789–798. doi:10.1016/j.apsb.2020.02.014

[98] Maiztegui J, Fernandez N, De Damilano A. Efficacy of immune plasma in treatment of Argentine haemorrhagic fever and association between treatment and a late neurological syndrome. The Lancet. 1979;314(8154):1216–1217. doi:10.1016/S0140-6736(79)92335-3

[99] Enria DA, de Damilano AJ, Briggiler AM, Ambrosio AM, Fernández NJ, Feuillade MR, Maiztegui JI. [Late neurologic syndrome in patients with Argentinian hemorrhagic fever treated with immune plasma]. Medicina. 1985;45(6):615–20.

[100] Enria DA, Oro JGB. Junin Virus Vaccines. 2002. p. 239–261. doi:10.1007/978-3-642-56055-2_12

[101] McKee KT, Oro JGB, Kuehne AI, Spisso JA, Mahlandt BG. Safety and Immunogenicity of a Live-Attenuated Junin (Argentine Hemorrhagic Fever) Vaccine in Rhesus Macaques. The American Journal of Tropical Medicine and Hygiene. 1993;48(3):403–411. doi:10.4269/ajtmh.1993.48.403

[102] Maiztegui JI, McKee Jr, KT, Oro JGB, Harrison LH, Gibbs PH, Feuillade MR, Enria DA, Briggiler AM, Levis SC, Ambrosio AM, et al. Protective Efficacy of a Live Attenuated Vaccine against Argentine Hemorrhagic Fever. The Journal of Infectious Diseases. 1998;177(2):277–283. doi:10.1086/514211

[103] York J, Nunberg JH. Epistastic Interactions within the Junín Virus Envelope Glycoprotein Complex Provide an Evolutionary Barrier to Reversion in the Live-Attenuated Candid#1 Vaccine. Journal of Virology. 2018;92(1). doi:10.1128/JVI.01682-17

[104] Gowen BB, Hickerson BT, York J, Westover JB, Sefing EJ, Bailey KW, Wandersee L, Nunberg JH. Second-Generation Live-Attenuated Candid#1 Vaccine Virus Resists Reversion and Protects against Lethal Junín Virus Infection in Guinea Pigs. Journal of virology. 2021;95(14):e0039721. doi:10.1128/JVI.00397-21

[105] Saito T, Reyna RA, Taniguchi S, Littlefield K, Paessler S, Maruyama J. Vaccine Candidates against Arenavirus Infections. Vaccines. 2023;11(3):635. doi:10.3390/vaccines11030635

[106] Andrade VM, Cashman K, Rosenke K, Wilkinson E, Josleyn N, Lynn G, Steffens J, Vantongeren S, Wells J, Schmaljohn C, et al. The DNA-based Lassa vaccine INO-4500 confers durable protective efficacy in cynomolgus macaques against lethal Lassa fever. Communications Medicine. 2024;4(1):253. doi:10.1038/s43856-024-00684-8

[107] Cross RW, Woolsey C, Prasad AN, Borisevich V, Agans KN, Deer DJ, Geisbert JB, Dobias NS, Fenton KA, Geisbert TW. A recombinant VSV-vectored vaccine rapidly protects nonhuman primates against heterologous lethal Lassa fever. Cell Reports. 2022;40(3):111094. doi:10.1016/j.celrep.2022.111094

[108] Safronetz D, Mire C, Rosenke K, Feldmann F, Haddock E, Geisbert T, Feldmann H. A Recombinant Vesicular Stomatitis Virus-Based Lassa Fever Vaccine Protects Guinea Pigs and Macaques against Challenge with Geographically and Genetically Distinct Lassa Viruses. PLOS Neglected Tropical Diseases. 2015;9(4):e0003736. doi:10.1371/journal.pntd.0003736

[109] Stein DR, Warner BM, Soule G, Tierney K, Frost KL, Booth S, Safronetz D. A recombinant vesicular stomatitis-based Lassa fever vaccine elicits rapid and long-term protection from lethal Lassa virus infection in guinea pigs. npj Vaccines.

2019;4(1):8. doi:10.1038/s41541-019-0104-x

[110] Marzi A, Feldmann F, Geisbert TW, Feldmann H, Safronetz D. Vesicular Stomatitis Virus–based Vaccines against Lassa and Ebola Viruses. Emerging Infectious Diseases. 2015;21(2). doi:10.3201/eid2102.141649

[111] Buck TK, Enriquez AS, Schendel SL, Zandonatti MA, Harkins SS, Li H, Moon-Walker A, Robinson JE, Branco LM, Garry RF, et al. Neutralizing Antibodies against Lassa Virus Lineage I. mBio. 2022;13(4). doi:10.1128/mbio.01278-22

[112] Grande-Pérez A, Martin V, Moreno H, de la Torre JC. Arenavirus Quasispecies and Their Biological Implications. 2015. p. 231–275. doi:10.1007/82_2015_468

[113] Neuman BW, Adair BD, Burns JW, Milligan RA, Buchmeier MJ, Yeager M. Complementarity in the Supramolecular Design of Arenaviruses and Retroviruses Revealed by Electron Cryomicroscopy and Image Analysis. Journal of Virology. 2005;79(6):3822–3830. doi:10.1128/JVI.79.6.3822-3830.2005

[114] Schlie K, Maisa A, Lennartz F, Stroher U, Garten W, Strecker T. Characterization of Lassa Virus Glycoprotein Oligomerization and Influence of Cholesterol on Virus Replication. Journal of Virology. 2010;84(2):983–992. doi:10.1128/JVI.02039-09

[115] Strecker T, Eichler R, Meulen J ter, Weissenhorn W, Dieter Klenk H, Garten W, Lenz O. Lassa Virus Z Protein Is a Matrix Protein Sufficient for the Release of Virus-Like Particles. Journal of Virology. 2003;77(19):10700–10705. doi:10.1128/JVI.77.19.10700-10705.2003

[116] Salvato MS, Schweighofer KJ, Burns J, Shimomaye EM. Biochemical and immunological evidence that the 11 kDa zinc-binding protein of lymphocytic choriomeningitis virus is a structural component of the virus. Virus Research. 1992;22(3):185–198. doi:10.1016/0168-1702(92)90050-J

[117] Rowe WP, Murphy FA, Bergold GH, Casals J, Hotchin J, Johnson KM, Lehmann-Grube F, Mims CA, Traub E, Webb PA. Arenoviruses: Proposed Name for a Newly Defined Virus Group. Journal of Virology. 1970;5(5):651–652. doi:10.1128/jvi.5.5.651-652.1970

[118] Pinschewer DD, Perez M, de la Torre JC. Dual Role of the Lymphocytic Choriomeningitis Virus Intergenic Region in Transcription Termination

and Virus Propagation. Journal of Virology. 2005;79(7):4519–4526. doi:10.1128/JVI.79.7.4519-4526.2005

[119] Iwasaki M, Cubitt B, Sullivan BM, de la Torre JC. The High Degree of Sequence Plasticity of the Arenavirus Noncoding Intergenic Region (IGR) Enables the Use of a Nonviral Universal Synthetic IGR To Attenuate Arenaviruses. Journal of Virology. 2016;90(6):3187–3197. doi:10.1128/JVI.03145-15

[120] Cai Y, Iwasaki M, Motooka D, Liu DX, Yu S, Cooper K, Hart R, Adams R, Burdette T, Postnikova EN, et al. A Lassa Virus Live-Attenuated Vaccine Candidate Based on Rearrangement of the Intergenic Region. mBio. 2020;11(2). doi:10.1128/mBio.00186-20

[121] Pinschewer DD, Perez M, de la Torre JC. Role of the Virus Nucleoprotein in the Regulation of Lymphocytic Choriomeningitis Virus Transcription and RNA Replication. Journal of Virology. 2003;77(6):3882–3887. doi:10.1128/JVI.77.6.3882-3887.2003

[122] Hackbart M, López CB. Characterization of non-standard viral genomes during arenavirus infections identifies prominent S RNA intergenic region deletions. mBio. 2024;15(10). doi:10.1128/mbio.01612-24

[123] Perez M, de la Torre JC. Characterization of the Genomic Promoter of the Prototypic Arenavirus Lymphocytic Choriomeningitis Virus. Journal of Virology. 2003;77(2):1184–1194. doi:10.1128/JVI.77.2.1184-1194.2003

[124] Hass M, Westerkofsky M, Muller S, Becker-Ziaja B, Busch C, Gunther S. Mutational Analysis of the Lassa Virus Promoter. Journal of Virology. 2006;80(24):12414–12419. doi:10.1128/JVI.01374-06

[125] Taniguchi S, Yoshikawa T, Shimojima M, Fukushi S, Kurosu T, Tani H, Fukuma A, Kato F, Nakayama E, Maeki T, et al. Analysis of the Function of the Lymphocytic Choriomeningitis Virus S Segment Untranslated Region on Growth Capacity In Vitro and on Virulence In Vivo. Viruses. 2020;12(8):896. doi:10.3390/v12080896

[126] Ortiz-Riaño E, Cheng BYH, de la Torre JC, Martínez-Sobrido L. The C-Terminal Region of Lymphocytic Choriomeningitis Virus Nucleoprotein Contains Distinct and Segregable Functional Domains Involved in NP-Z Interaction

and Counteraction of the Type I Interferon Response. Journal of Virology. 2011;85(24):13038–13048. doi:10.1128/JVI.05834-11

[127] Zhou S, Cerny AM, Zacharia A, Fitzgerald KA, Kurt-Jones EA, Finberg RW. Induction and Inhibition of Type I Interferon Responses by Distinct Components of Lymphocytic Choriomeningitis Virus. Journal of Virology. 2010;84(18):9452–9462. doi:10.1128/JVI.00155-10

[128] Loureiro ME, Zorzetto-Fernandes AL, Radoshitzky S, Chi X, Dallari S, Marooki N, Lèger P, Foscaldi S, Harjono V, Sharma S, et al. DDX3 suppresses type I interferons and favors viral replication during Arenavirus infection. PLOS Pathogens. 2018;14(7):e1007125. doi:10.1371/journal.ppat.1007125

[129] Baird NL, York J, Nunberg JH. Arenavirus infection induces discrete cytosolic structures for RNA replication. Journal of virology. 2012;86(20):11301–10. doi:10.1128/JVI.01635-12

[130] Papageorgiou N, Spiliopoulou M, Nguyen T-H Van, Vaitsopoulou A, Laban EY, Alvarez K, Margiolaki I, Canard B, Ferron F. Brothers in Arms: Structure, Assembly and Function of Arenaviridae Nucleoprotein. Viruses. 2020;12(7):772. doi:10.3390/v12070772

[131] Ortiz-Riaño E, Cheng BYH, de la Torre JC, Martínez-Sobrido L. Self-Association of Lymphocytic Choriomeningitis Virus Nucleoprotein Is Mediated by Its N-Terminal Region and Is Not Required for Its Anti-Interferon Function. Journal of Virology. 2012;86(6):3307–3317. doi:10.1128/JVI.05503-11

[132] Hastie KM, Liu T, Li S, King LB, Ngo N, Zandonatti MA, Woods VL, de la Torre JC, Saphire EO. Crystal structure of the Lassa virus nucleoprotein–RNA complex reveals a gating mechanism for RNA binding. Proceedings of the National Academy of Sciences. 2011;108(48):19365–19370. doi:10.1073/pnas.1108515108

[133] Papageorgiou N, Spiliopoulou M, Nguyen T-H Van, Vaitsopoulou A, Laban EY, Alvarez K, Margiolaki I, Canard B, Ferron F. Brothers in Arms: Structure, Assembly and Function of Arenaviridae Nucleoprotein. Viruses. 2020;12(7):772. doi:10.3390/v12070772

[134] van der Zeijst BA, Noyes BE, Mirault ME, Parker B, Osterhaus AD, Swyryd EA, Bleumink N, Horzinek MC, Stark GR. Persistent infection of

some standard cell lines by lymphocytic choriomeningitis virus: transmission of infection by an intracellular agent. Journal of Virology. 1983;48(1):249–261. doi:10.1128/jvi.48.1.249-261.1983

[135] Young PR, Howard CR. Fine Structure Analysis of Pichinde Virus Nucleocapsids. Journal of General Virology. 1983;64(4):833–842. doi:10.1099/0022-1317-64-4-833

[136] Papageorgiou N, Vaitsopoulou A, Diop A, Nguyen TH Van, Canard B, Alvarez K, Ferron F. Observation of arenavirus nucleoprotein heptamer assembly. FEBS Open Bio. 2021;11(4):1076–1083. doi:10.1002/2211-5463.13106

[137] Pyle JD, Whelan SPJ. Isolation of Reconstructed Functional Ribonucleoprotein Complexes of Machupo Virus. Journal of Virology. 2021;95(22). doi:10.1128/JVI.01054-21

[138] Knopp KA, Ngo T, Gershon PD, Buchmeier MJ. Single Nucleoprotein Residue Modulates Arenavirus Replication Complex Formation. mBio. 2015;6(3). doi:10.1128/mBio.00524-15

[139] Stott RJ, Strecker T, Foster TL. Distinct Molecular Mechanisms of Host Immune Response Modulation by Arenavirus NP and Z Proteins. Viruses. 2020;12(7):784. doi:10.3390/v12070784

[140] Martiònez-Sobrido L, Giannakas P, Cubitt B, Garciòa-Sastre A, de la Torre JC. Differential Inhibition of Type I Interferon Induction by Arenavirus Nucleoproteins. Journal of Virology. 2007;81(22):12696–12703. doi:10.1128/JVI.00882-07

[141] Martiònez-Sobrido L, Emonet S, Giannakas P, Cubitt B, Garciòa-Sastre A, de la Torre JC. Identification of Amino Acid Residues Critical for the Anti-Interferon Activity of the Nucleoprotein of the Prototypic Arenavirus Lymphocytic Choriomeningitis Virus. Journal of Virology. 2009;83(21):11330–11340. doi:10.1128/JVI.00763-09

[142] Huang Q, Shao J, Lan S, Zhou Y, Xing J, Dong C, Liang Y, Ly H. In Vitro and In Vivo Characterizations of Pichinde Viral Nucleoprotein Exoribonuclease Functions. Journal of Virology. 2015;89(13):6595–6607. doi:10.1128/JVI.00009-15

[143] Jiang X, Huang Q, Wang W, Dong H, Ly H, Liang Y, Dong C. Structures of Arenaviral Nucleoproteins with Triphosphate dsRNA Reveal a Unique Mechanism of

Immune Suppression. Journal of Biological Chemistry. 2013;288(23):16949–16959. doi:10.1074/jbc.M112.420521

[144] Mateer EJ, Maruyama J, Card GE, Paessler S, Huang C. Lassa Virus, but Not Highly Pathogenic New World Arenaviruses, Restricts Immunostimulatory Double-Stranded RNA Accumulation during Infection. Journal of Virology. 2020;94(9). doi:10.1128/JVI.02006-19

[145] Martiònez-Sobrido L, Zuniga EI, Rosario D, Garciòa-Sastre A, de la Torre JC. Inhibition of the Type I Interferon Response by the Nucleoprotein of the Prototypic Arenavirus Lymphocytic Choriomeningitis Virus. Journal of Virology. 2006;80(18):9192–9199. doi:10.1128/JVI.00555-06

[146] Pythoud C, Rodrigo WWSI, Pasqual G, Rothenberger S, Martínez-Sobrido L, de la Torre JC, Kunz S. Arenavirus Nucleoprotein Targets Interferon Regulatory Factor-Activating Kinase IKKϵ. Journal of Virology. 2012;86(15):7728–7738. doi:10.1128/JVI.00187-12

[147] King BR, Hershkowitz D, Eisenhauer PL, Weir ME, Ziegler CM, Russo J, Bruce EA, Ballif BA, Botten J. A Map of the Arenavirus Nucleoprotein-Host Protein Interactome Reveals that Junín Virus Selectively Impairs the Antiviral Activity of Double-Stranded RNA-Activated Protein Kinase (PKR). Journal of Virology. 2017;91(15). doi:10.1128/JVI.00763-17

[148] Loureiro ME, Zorzetto-Fernandes AL, Radoshitzky S, Chi X, Dallari S, Marooki N, Lèger P, Foscaldi S, Harjono V, Sharma S, et al. DDX3 suppresses type I interferons and favors viral replication during Arenavirus infection. PLOS Pathogens. 2018;14(7):e1007125. doi:10.1371/journal.ppat.1007125

[149] Schröder M, Baran M, Bowie AG. Viral targeting of DEAD box protein 3 reveals its role in TBK1/IKKϵ-mediated IRF activation. The EMBO Journal. 2008;27(15):2147–2157. doi:10.1038/emboj.2008.143

[150] Soulat D, Bürckstümmer T, Westermayer S, Goncalves A, Bauch A, Stefanovic A, Hantschel O, Bennett KL, Decker T, Superti-Furga G. The DEAD-box helicase DDX3X is a critical component of the TANK-binding kinase 1-dependent innate immune response. The EMBO Journal. 2008;27(15):2135–2146. doi:10.1038/emboj.2008.126

[151] Meyer B, Groseth A. Apoptosis during arenavirus infection: mechanisms and evasion strategies. Microbes and Infection. 2018;20(2):65–80. doi:10.1016/j.micinf.2017.10.002

[152] Wolff S, Groseth A, Meyer B, Jackson D, Strecker T, Kaufmann A, Becker S. The New World arenavirus Tacaribe virus induces caspase-dependent apoptosis in infected cells. Journal of General Virology. 2016;97(4):855–866. doi:10.1099/jgv.0.000403

[153] Kolokoltsova OA, Grant AM, Huang C, Smith JK, Poussard AL, Tian B, Brasier AR, Peters CJ, Tseng C-TK, de la Torre JC, et al. RIG-I Enhanced Interferon Independent Apoptosis upon Junin Virus Infection. PLoS ONE. 2014;9(6):e99610. doi:10.1371/journal.pone.0099610

[154] Wolff S, Becker S, Groseth A. Cleavage of the Junin Virus Nucleoprotein Serves a Decoy Function To Inhibit the Induction of Apoptosis during Infection. Journal of Virology. 2013;87(1):224–233. doi:10.1128/JVI.01929-12

[155] Bostedt L, Fénéant L, Leske A, Holzerland J, Günther K, Waßmann I, Bohn P, Groseth A. Alternative translation contributes to the generation of a cytoplasmic subpopulation of the Junín virus nucleoprotein that inhibits caspase activation and innate immunity. Journal of Virology. 2024;98(2). doi:10.1128/jvi.01975-23

[156] Baize S, Kaplon J, Faure C, Pannetier D, Georges-Courbot M-C, Deubel V. Lassa Virus Infection of Human Dendritic Cells and Macrophages Is Productive but Fails to Activate Cells. The Journal of Immunology. 2004;172(5):2861–2869. doi:10.4049/jimmunol.172.5.2861

[157] Pythoud C, Rothenberger S, Martínez-Sobrido L, de la Torre JC, Kunz S. Lymphocytic Choriomeningitis Virus Differentially Affects the Virus-Induced Type I Interferon Response and Mitochondrial Apoptosis Mediated by RIG-I/MAVS. Journal of Virology. 2015;89(12):6240–6250. doi:10.1128/JVI.00610-15

[158] Kang H, Cong J, Wang C, Ji W, Xin Y, Qian Y, Li X, Chen Y, Rao Z. Structural basis for recognition and regulation of arenavirus polymerase L by Z protein. Nature Communications. 2021;12(1):4134. doi:10.1038/s41467-021-24458-1

[159] Ma J, Zhang S, Zhang X. Structure of Machupo virus polymerase in

complex with matrix protein Z. Nature Communications. 2021;12(1):6163. doi:10.1038/s41467-021-26432-3

[160] Wilda M, Lopez N, Casabona JC, Franze-Fernandez MT. Mapping of the Tacaribe Arenavirus Z-Protein Binding Sites on the L Protein Identified both Amino Acids within the Putative Polymerase Domain and a Region at the N Terminus of L That Are Critically Involved in Binding. Journal of Virology. 2008;82(22):11454–11460. doi:10.1128/JVI.01533-08

[161] Morin B, Coutard B, Lelke M, Ferron F, Kerber R, Jamal S, Frangeul A, Baronti C, Charrel R, de Lamballerie X, et al. The N-Terminal Domain of the Arenavirus L Protein Is an RNA Endonuclease Essential in mRNA Transcription. PLoS Pathogens. 2010;6(9):e1001038. doi:10.1371/journal.ppat.1001038

[162] Khamina K, Lercher A, Caldera M, Schliehe C, Vilagos B, Sahin M, Kosack L, Bhattacharya A, Májek P, Stukalov A, et al. Characterization of host proteins interacting with the lymphocytic choriomeningitis virus L protein. PLOS Pathogens. 2017;13(12):e1006758. doi:10.1371/journal.ppat.1006758

[163] Pyle JD, Whelan SPJ. RNA ligands activate the Machupo virus polymerase and guide promoter usage. Proceedings of the National Academy of Sciences. 2019;116(21):10518–10524. doi:10.1073/pnas.1900790116

[164] Kouba T, Vogel D, Thorkelsson SR, Quemin ERJ, Williams HM, Milewski M, Busch C, Günther S, Grünewald K, Rosenthal M, et al. Conformational changes in Lassa virus L protein associated with promoter binding and RNA synthesis activity. Nature Communications. 2021;12(1):7018. doi:10.1038/s41467-021-27305-5

[165] Kranzusch PJ, Schenk AD, Rahmeh AA, Radoshitzky SR, Bavari S, Walz T, Whelan SPJ. Assembly of a functional Machupo virus polymerase complex. Proceedings of the National Academy of Sciences. 2010;107(46):20069–20074. doi:10.1073/pnas.1007152107

[166] Vogel D, Rosenthal M, Gogrefe N, Reindl S, Günther S. Biochemical characterization of the Lassa virus L protein. Journal of Biological Chemistry. 2019;294(20):8088–8100. doi:10.1074/jbc.RA118.006973

[167] Kranzusch PJ, Whelan SPJ. Arenavirus Z protein controls viral RNA synthesis by locking a polymerase–promoter complex. Proceedings of the National Academy

of Sciences. 2011;108(49):19743–19748. doi:10.1073/pnas.1112742108

[168] Hara K, Schmidt FI, Crow M, Brownlee GG. Amino Acid Residues in the N-Terminal Region of the PA Subunit of Influenza A Virus RNA Polymerase Play a Critical Role in Protein Stability, Endonuclease Activity, Cap Binding, and Virion RNA Promoter Binding. Journal of Virology. 2006;80(16):7789–7798. doi:10.1128/JVI.00600-06

[169] Yuan P, Bartlam M, Lou Z, Chen S, Zhou J, He X, Lv Z, Ge R, Li X, Deng T, et al. Crystal structure of an avian influenza polymerase PAN reveals an endonuclease active site. Nature. 2009;458(7240):909–913. doi:10.1038/nature07720

[170] Dias A, Bouvier D, Crépin T, McCarthy AA, Hart DJ, Baudin F, Cusack S, Ruigrok RWH. The cap-snatching endonuclease of influenza virus polymerase resides in the PA subunit. Nature. 2009;458(7240):914–918. doi:10.1038/nature07745

[171] Rosenthal M, Gogrefe N, Vogel D, Reguera J, Rauschenberger B, Cusack S, Günther S, Reindl S. Structural insights into reptarenavirus cap-snatching machinery. PLOS Pathogens. 2017;13(5):e1006400. doi:10.1371/journal.ppat.1006400

[172] Lehmann M, Pahlmann M, Jérôme H, Busch C, Lelke M, Günther S. Role of the C Terminus of Lassa Virus L Protein in Viral mRNA Synthesis. Journal of Virology. 2014;88(15):8713–8717. doi:10.1128/JVI.00652-14

[173] Lenz O, ter Meulen J, Klenk HD, Seidah NG, Garten W. The Lassa virus glycoprotein precursor GP-C is proteolytically processed by subtilase SKI-1/S1P. Proceedings of the National Academy of Sciences of the United States of America. 2001;98(22):12701–5. doi:10.1073/pnas.221447598

[174] Rojek JM, Lee AM, Nguyen N, Spiropoulou CF, Kunz S. Site 1 Protease Is Required for Proteolytic Processing of the Glycoproteins of the South American Hemorrhagic Fever Viruses Junin, Machupo, and Guanarito. Journal of Virology. 2008;82(12):6045–6051. doi:10.1128/JVI.02392-07

[175] Kang JS, Zhou K, Wang H, Tang S, Lyles KVM, Luo M, Zhou ZH. Architectural organization and in situ fusion protein structure of lymphocytic choriomeningitis virus. Journal of Virology. 2024;98(10). doi:10.1128/jvi.00640-24

[176] Beyer WR, Pöpplau D, Garten W, von Laer D, Lenz O. Endoproteolytic

processing of the lymphocytic choriomeningitis virus glycoprotein by the subtilase SKI-1/S1P. Journal of virology. 2003;77(5):2866–72. doi:10.1128/jvi.77.5.2866-2872.2003

[177] Lenz O, ter Meulen J, Klenk H-D, Seidah NG, Garten W. The Lassa virus glycoprotein precursor GP-C is proteolytically processed by subtilase SKI-1/S1P. Proceedings of the National Academy of Sciences. 2001;98(22):12701–12705. doi:10.1073/pnas.221447598

[178] York J, Romanowski V, Lu M, Nunberg JH. The Signal Peptide of the Juniòn Arenavirus Envelope Glycoprotein Is Myristoylated and Forms an Essential Subunit of the Mature G1-G2 Complex. Journal of Virology. 2004;78(19):10783–10792. doi:10.1128/JVI.78.19.10783-10792.2004

[179] Hastie KM, Igonet S, Sullivan BM, Legrand P, Zandonatti MA, Robinson JE, Garry RF, Rey FA, Oldstone MB, Saphire EO. Crystal structure of the prefusion surface glycoprotein of the prototypic arenavirus LCMV. Nature Structural & Molecular Biology. 2016;23(6):513–521. doi:10.1038/nsmb.3210

[180] Katz M, Weinstein J, Eilon-Ashkenazy M, Gehring K, Cohen-Dvashi H, Elad N, Fleishman SJ, Diskin R. Structure and receptor recognition by the Lassa virus spike complex. Nature. 2022;603(7899):174–179. doi:10.1038/s41586-022-04429-2

[181] Enriquez AS, Buck TK, Li H, Norris MJ, Moon-Walker A, Zandonatti MA, Harkins SS, Robinson JE, Branco LM, Garry RF, et al. Delineating the mechanism of anti-Lassa virus GPC-A neutralizing antibodies. Cell Reports. 2022;39(8):110841. doi:10.1016/j.celrep.2022.110841

[182] Hastie KM, Zandonatti MA, Kleinfelter LM, Heinrich ML, Rowland MM, Chandran K, Branco LM, Robinson JE, Garry RF, Saphire EO. Structural basis for antibody-mediated neutralization of Lassa virus. Science. 2017;356(6341):923–928. doi:10.1126/science.aam7260

[183] Hastie KM, Cross RW, Harkins SS, Zandonatti MA, Koval AP, Heinrich ML, Rowland MM, Robinson JE, Geisbert TW, Garry RF, et al. Convergent Structures Illuminate Features for Germline Antibody Binding and Pan-Lassa Virus Neutralization. Cell. 2019;178(4):1004-1015.e14. doi:10.1016/j.cell.2019.07.020

[184] Eichler R, Lenz O, Strecker T, Eickmann M, Klenk H, Garten W. Identification

of Lassa virus glycoprotein signal peptide as a trans -acting maturation factor. EMBO reports. 2003;4(11):1084–1088. doi:10.1038/sj.embor.7400002

[185] Agnihothram SS, York J, Nunberg JH. Role of the Stable Signal Peptide and Cytoplasmic Domain of G2 in Regulating Intracellular Transport of the Juniòn Virus Envelope Glycoprotein Complex. Journal of Virology. 2006;80(11):5189–5198. doi:10.1128/JVI.00208-06

[186] Agnihothram SS, York J, Trahey M, Nunberg JH. Bitopic Membrane Topology of the Stable Signal Peptide in the Tripartite Juniòn Virus GP-C Envelope Glycoprotein Complex. Journal of Virology. 2007;81(8):4331–4337. doi:10.1128/JVI.02779-06

[187] Mahmutovic S, Clark L, Levis SC, Briggiler AM, Enria DA, Harrison SC, Abraham J. Molecular Basis for Antibody-Mediated Neutralization of New World Hemorrhagic Fever Mammarenaviruses. Cell Host & Microbe. 2015;18(6):705–713. doi:10.1016/j.chom.2015.11.005

[188] Cohen-Dvashi H, Cohen N, Israeli H, Diskin R. Molecular Mechanism for LAMP1 Recognition by Lassa Virus. Journal of Virology. 2015;89(15):7584–7592. doi:10.1128/JVI.00651-15

[189] Klewitz C, Klenk H-D, ter Meulen J. Amino acids from both N-terminal hydrophobic regions of the Lassa virus envelope glycoprotein GP-2 are critical for pH-dependent membrane fusion and infectivity. Journal of General Virology. 2007;88(8):2320–2328. doi:10.1099/vir.0.82950-0

[190] Igonet S, Vaney M-C, Vonrhein C, Bricogne G, Stura EA, Hengartner H, Eschli B, Rey FA. X-ray structure of the arenavirus glycoprotein GP2 in its postfusion hairpin conformation. Proceedings of the National Academy of Sciences. 2011;108(50):19967–19972. doi:10.1073/pnas.1108910108

[191] Eschli B, Quirin K, Wepf A, Weber J, Zinkernagel R, Hengartner H. Identification of an N-Terminal Trimeric Coiled-Coil Core within Arenavirus Glycoprotein 2 Permits Assignment to Class I Viral Fusion Proteins. Journal of Virology. 2006;80(12):5897–5907. doi:10.1128/JVI.00008-06

[192] Gregory SM, Harada E, Liang B, Delos SE, White JM, Tamm LK. Structure and function of the complete internal fusion loop from Ebolavirus glycoprotein

2. Proceedings of the National Academy of Sciences. 2011;108(27):11211–11216. doi:10.1073/pnas.1104760108

[193] Ito H, Watanabe S, Sanchez A, Whitt MA, Kawaoka Y. Mutational Analysis of the Putative Fusion Domain of Ebola Virus Glycoprotein. Journal of Virology. 1999;73(10):8907–8912. doi:10.1128/JVI.73.10.8907-8912.1999

[194] Nunberg JH, York J. The Curious Case of Arenavirus Entry, and Its Inhibition. Viruses. 2012;4(1):83–101. doi:10.3390/v4010083

[195] Von Heijne G. Signal sequences. Journal of Molecular Biology. 1985;184(1):99–105. doi:10.1016/0022-2836(85)90046-4

[196] Froeschke M, Basler M, Groettrup M, Dobberstein B. Long-lived Signal Peptide of Lymphocytic Choriomeningitis Virus Glycoprotein pGP-C. Journal of Biological Chemistry. 2003;278(43):41914–41920. doi:10.1074/jbc.M302343200

[197] Schlie K, Strecker T, Garten W. Maturation cleavage within the ectodomain of Lassa virus glycoprotein relies on stabilization by the cytoplasmic tail. FEBS Letters. 2010;584(21):4379–4382. doi:10.1016/j.febslet.2010.09.032

[198] York J, Nunberg JH. Distinct requirements for signal peptidase processing and function in the stable signal peptide subunit of the Junín virus envelope glycoprotein. Virology. 2007;359(1):72–81. doi:10.1016/j.virol.2006.08.048

[199] York J, Nunberg JH. A Novel Zinc-Binding Domain Is Essential for Formation of the Functional Juniòn Virus Envelope Glycoprotein Complex. Journal of Virology. 2007;81(24):13385–13391. doi:10.1128/JVI.01785-07

[200] York J, Nunberg JH. Role of the Stable Signal Peptide of Juniòn Arenavirus Envelope Glycoprotein in pH-Dependent Membrane Fusion. Journal of Virology. 2006;80(15):7775–7780. doi:10.1128/JVI.00642-06

[201] York J, Romanowski V, Lu M, Nunberg JH. The Signal Peptide of the Juniòn Arenavirus Envelope Glycoprotein Is Myristoylated and Forms an Essential Subunit of the Mature G1-G2 Complex. Journal of Virology. 2004;78(19):10783–10792. doi:10.1128/JVI.78.19.10783-10792.2004

[202] Parekh BS, Buchmeier MJ. Proteins of lymphocytic choriomeningitis virus: Antigenic topography of the viral glycoproteins. Virology. 1986;153(2):168–178. doi:10.1016/0042-6822(86)90020-6

[203] Borrow P, Oldstone MB. Characterization of lymphocytic choriomeningitis virus-binding protein(s): a candidate cellular receptor for the virus. Journal of Virology. 1992;66(12):7270–7281. doi:10.1128/jvi.66.12.7270-7281.1992

[204] Cao W, Henry MD, Borrow P, Yamada H, Elder JH, Ravkov E V., Nichol ST, Compans RW, Campbell KP, Oldstone MBA. Identification of α-Dystroglycan as a Receptor for Lymphocytic Choriomeningitis Virus and Lassa Fever Virus. Science. 1998;282(5396):2079–2081. doi:10.1126/science.282.5396.2079

[205] Spiropoulou CF, Kunz S, Rollin PE, Campbell KP, Oldstone MBA. New World Arenavirus Clade C, but Not Clade A and B Viruses, Utilizes α-Dystroglycan as Its Major Receptor. Journal of Virology. 2002;76(10):5140–5146. doi:10.1128/JVI.76.10.5140-5146.2002

[206] Kunz S, Sevilla N, McGavern DB, Campbell KP, Oldstone MBA. Molecular analysis of the interaction of LCMV with its cellular receptor α-dystroglycan. The Journal of Cell Biology. 2001;155(2):301–310. doi:10.1083/jcb.200104103

[207] Kunz S, Rojek JM, Perez M, Spiropoulou CF, Oldstone MBA. Characterization of the Interaction of Lassa Fever Virus with Its Cellular Receptor α-Dystroglycan. Journal of Virology. 2005;79(10):5979–5987. doi:10.1128/JVI.79.10.5979-5987.2005

[208] Sevilla N, Kunz S, Holz A, Lewicki H, Homann D, Yamada H, Campbell KP, de la Torre JC, Oldstone MBA. Immunosuppression and Resultant Viral Persistence by Specific Viral Targeting of Dendritic Cells. The Journal of Experimental Medicine. 2000;192(9):1249–1260. doi:10.1084/jem.192.9.1249

[209] Kunz S, Sevilla N, Rojek JM, Oldstone MBA. Use of alternative receptors different than α-dystroglycan by selected isolates of lymphocytic choriomeningitis virus. Virology. 2004;325(2):432–445. doi:10.1016/j.virol.2004.05.009

[210] Fedeli C, Moreno H, Kunz S. The Role of Receptor Tyrosine Kinases in Lassa Virus Cell Entry. Viruses. 2020;12(8):857. doi:10.3390/v12080857

[211] Radoshitzky SR, Abraham J, Spiropoulou CF, Kuhn JH, Nguyen D, Li W, Nagel J, Schmidt PJ, Nunberg JH, Andrews NC, et al. Transferrin receptor 1 is a cellular receptor for New World haemorrhagic fever arenaviruses. Nature. 2007;446(7131):92–96. doi:10.1038/nature05539

[212] Flanagan ML, Oldenburg J, Reignier T, Holt N, Hamilton GA, Martin VK,

Cannon PM. New World Clade B Arenaviruses Can Use Transferrin Receptor 1 (TfR1)-Dependent and -Independent Entry Pathways, and Glycoproteins from Human Pathogenic Strains Are Associated with the Use of TfR1. Journal of Virology. 2008;82(2):938–948. doi:10.1128/JVI.01397-07

[213] Parsy M-L, Harlos K, Huiskonen JT, Bowden TA. Crystal Structure of Venezuelan Hemorrhagic Fever Virus Fusion Glycoprotein Reveals a Class 1 Postfusion Architecture with Extensive Glycosylation. Journal of Virology. 2013;87(23):13070–13075. doi:10.1128/JVI.02298-13

[214] Koellhoffer JF, Dai Z, Malashkevich VN, Stenglein MD, Liu Y, Toro R, S. Harrison J, Chandran K, DeRisi JL, Almo SC, et al. Structural Characterization of the Glycoprotein GP2 Core Domain from the CAS Virus, a Novel Arenavirus-Like Species. Journal of Molecular Biology. 2014;426(7):1452–1468. doi:10.1016/j.jmb.2013.12.009

[215] Kielian M, Rey FA. Virus membrane-fusion proteins: more than one way to make a hairpin. Nature Reviews Microbiology. 2006;4(1):67–76. doi:10.1038/nrmicro1326

[216] Wright K. Post-translational processing of the glycoproteins of lymphocytic choriomeningitis virus. Virology. 1990;177(1):175–183. doi:10.1016/0042-6822(90)90471-3

[217] Bonhomme CJ, Knopp KA, Bederka LH, Angelini MM, Buchmeier MJ. LCMV Glycosylation Modulates Viral Fitness and Cell Tropism. PLoS ONE. 2013;8(1):e53273. doi:10.1371/journal.pone.0053273

[218] Bonhomme CJ, Capul AA, Lauron EJ, Bederka LH, Knopp KA, Buchmeier MJ. Glycosylation modulates arenavirus glycoprotein expression and function. Virology. 2011;409(2):223–233. doi:10.1016/j.virol.2010.10.011

[219] Eichler R, Lenz O, Garten W, Strecker T. The role of single N-glycans in proteolytic processing and cell surface transport of the Lassa virus glycoprotein GP-C. Virology Journal. 2006;3(1):41. doi:10.1186/1743-422X-3-41

[220] Koma T, Huang C, Coscia A, Hallam S, Manning JT, Maruyama J, Walker AG, Miller M, Smith JN, Patterson M, et al. Glycoprotein N-linked glycans play a critical role in arenavirus pathogenicity. PLOS Pathogens. 2021;17(3):e1009356.

doi:10.1371/journal.ppat.1009356

[221] Neuman BW, Adair BD, Burns JW, Milligan RA, Buchmeier MJ, Yeager M. Complementarity in the Supramolecular Design of Arenaviruses and Retroviruses Revealed by Electron Cryomicroscopy and Image Analysis. Journal of Virology. 2005;79(6):3822–3830. doi:10.1128/JVI.79.6.3822-3830.2005

[222] Cornu TI, de la Torre JC. RING Finger Z Protein of Lymphocytic Choriomeningitis Virus (LCMV) Inhibits Transcription and RNA Replication of an LCMV S-Segment Minigenome. Journal of Virology. 2001;75(19):9415–9426. doi:10.1128/JVI.75.19.9415-9426.2001

[223] Perez M, Craven RC, de la Torre JC. The small RING finger protein Z drives arenavirus budding: implications for antiviral strategies. Proceedings of the National Academy of Sciences of the United States of America. 2003;100(22):12978–83. doi:10.1073/pnas.2133782100

[224] Kentsis A, Dwyer EC, Perez JM, Sharma M, Chen A, Pan ZQ, Borden KLB. The RING domains of the promyelocytic leukemia protein PML and the arenaviral protein Z repress translation by directly inhibiting translation initiation factor eIF4E 1 1Edited by D. Draper. Journal of Molecular Biology. 2001;312(4):609–623. doi:10.1006/jmbi.2001.5003

[225] Shtanko O, Watanabe S, Jasenosky LD, Watanabe T, Kawaoka Y. ALIX/AIP1 Is Required for NP Incorporation into Mopeia Virus Z-Induced Virus-Like Particles. Journal of Virology. 2011;85(7):3631–3641. doi:10.1128/JVI.01984-10

[226] Ziegler CM, Dang L, Eisenhauer P, Kelly JA, King BR, Klaus JP, Manuelyan I, Mattice EB, Shirley DJ, Weir ME, et al. NEDD4 family ubiquitin ligases associate with LCMV Z's PPXY domain and are required for virus budding, but not via direct ubiquitination of Z. PLOS Pathogens. 2019;15(11):e1008100. doi:10.1371/journal.ppat.1008100

[227] Volpon L, Osborne MJ, Capul AA, de la Torre JC, Borden KLB. Structural characterization of the Z RING-eIF4E complex reveals a distinct mode of control for eIF4E. Proceedings of the National Academy of Sciences. 2010;107(12):5441–5446. doi:10.1073/pnas.0909877107

[228] Groseth A, Wolff S, Strecker T, Hoenen T, Becker S. Efficient Budding of the

Tacaribe Virus Matrix Protein Z Requires the Nucleoprotein. Journal of Virology. 2010;84(7):3603–3611. doi:10.1128/JVI.02429-09

[229] Fan L, Briese T, Lipkin WI. Z Proteins of New World Arenaviruses Bind RIG-I and Interfere with Type I Interferon Induction. Journal of Virology. 2010;84(4):1785–1791. doi:10.1128/JVI.01362-09

[230] Loureiro ME, Wilda M, Levingston Macleod JM, D'Antuono A, Foscaldi S, Buslje CM, Lopez N. Molecular Determinants of Arenavirus Z Protein Homo-Oligomerization and L Polymerase Binding. Journal of Virology. 2011;85(23):12304–12314. doi:10.1128/JVI.05691-11

[231] Capul AA, Perez M, Burke E, Kunz S, Buchmeier MJ, de la Torre JC. Arenavirus Z-Glycoprotein Association Requires Z Myristoylation but Not Functional RING or Late Domains. Journal of Virology. 2007;81(17):9451–9460. doi:10.1128/JVI.00499-07

[232] Perez M, Greenwald DL, de La Torre JC. Myristoylation of the RING Finger Z Protein Is Essential for Arenavirus Budding. Journal of Virology. 2004;78(20):11443–11448. doi:10.1128/JVI.78.20.11443-11448.2004

[233] Casabona JC, Levingston Macleod JM, Loureiro ME, Gomez GA, Lopez N. The RING Domain and the L79 Residue of Z Protein Are Involved in both the Rescue of Nucleocapsids and the Incorporation of Glycoproteins into Infectious Chimeric Arenavirus-Like Particles. Journal of Virology. 2009;83(14):7029–7039. doi:10.1128/JVI.00329-09

[234] Eichler R, Strecker T, Kolesnikova L, ter Meulen J, Weissenhorn W, Becker S, Klenk HD, Garten W, Lenz O. Characterization of the Lassa virus matrix protein Z: electron microscopic study of virus-like particles and interaction with the nucleoprotein (NP). Virus Research. 2004;100(2):249–255. doi:10.1016/j.virusres.2003.11.017

[235] Lee KJ, Perez M, Pinschewer DD, de la Torre JC. Identification of the Lymphocytic Choriomeningitis Virus (LCMV) Proteins Required To Rescue LCMV RNA Analogs into LCMV-Like Particles. Journal of Virology. 2002;76(12):6393–6397. doi:10.1128/JVI.76.12.6393-6397.2002

[236] Ziegler CM, Eisenhauer P, Bruce EA, Weir ME, King BR, Klaus

JP, Krementsov DN, Shirley DJ, Ballif BA, Botten J. The Lymphocytic Choriomeningitis Virus Matrix Protein PPXY Late Domain Drives the Production of Defective Interfering Particles. PLOS Pathogens. 2016;12(3):e1005501. doi:10.1371/journal.ppat.1005501

[237] Baillet N, Krieger S, Carnec X, Mateo M, Journeaux A, Merabet O, Caro V, Tangy F, Vidalain P-O, Baize S. E3 Ligase ITCH Interacts with the Z Matrix Protein of Lassa and Mopeia Viruses and Is Required for the Release of Infectious Particles. Viruses. 2019;12(1):49. doi:10.3390/v12010049

[238] Borden KLB, Campbell Dwyer EJ, Salvato MS. An Arenavirus RING (Zinc-Binding) Protein Binds the Oncoprotein Promyelocyte Leukemia Protein (PML) and Relocates PML Nuclear Bodies to the Cytoplasm. Journal of Virology. 1998;72(1):758–766. doi:10.1128/JVI.72.1.758-766.1998

[239] Campbell Dwyer EJ, Lai H, MacDonald RC, Salvato MS, Borden KLB. The Lymphocytic Choriomeningitis Virus RING Protein Z Associates with Eukaryotic Initiation Factor 4E and Selectively Represses Translation in a RING-Dependent Manner. Journal of Virology. 2000;74(7):3293–3300. doi:10.1128/JVI.74.7.3293-3300.2000

[240] Radoshitzky SR, Buchmeier MJ, Charrel RN, Gonzalez J-PJ, Günther S, Hepojoki J, Kuhn JH, Lukashevich IS, Romanowski V, Salvato MS, et al. ICTV Virus Taxonomy Profile: Arenaviridae 2023.

[accessed 2025 Feb 24]. https://ictv.global/report/chapter/arenaviridae/arenaviridae

[241] Fontana J, López-Montero N, Elliott RM, Fernández JJ, Risco C. The unique architecture of Bunyamwera virus factories around the Golgi complex. Cellular Microbiology. 2008;10(10):2012–2028. doi:10.1111/j.1462-5822.2008.01184.x

[242] Novoa RR, Calderita G, Cabezas P, Elliott RM, Risco C. Key Golgi Factors for Structural and Functional Maturation of Bunyamwera Virus. Journal of Virology. 2005;79(17):10852–10863. doi:10.1128/JVI.79.17.10852-10863.2005

[243] Salanueva IJ, Novoa RR, Cabezas P, Loòpez-Iglesias C, Carrascosa JL, Elliott RM, Risco C. Polymorphism and Structural Maturation of Bunyamwera Virus in Golgi and Post-Golgi Compartments. Journal of Virology. 2003;77(2):1368–1381. doi:10.1128/JVI.77.2.1368-1381.2003

[244] ICTV Genus: Innmovirus. [accessed 2025 Feb 24]. https://ictv.global/report/chapter/arenaviridae/arenaviridae/innmovirus

[245] Shi M, Lin X-D, Chen X, Tian J-H, Chen L-J, Li K, Wang W, Eden J-S, Shen J-J, Liu L, et al. The evolutionary history of vertebrate RNA viruses. Nature. 2018;556(7700):197–202. doi:10.1038/s41586-018-0012-7

[246] ICTV Genus: Antennavirus. [accessed 2025 Feb 24]. https://ictv.global/report/chapter/arenaviridae/arenaviridae/antennavirus

[247] Tani H, Iha K, Shimojima M, Fukushi S, Taniguchi S, Yoshikawa T, Kawaoka Y, Nakasone N, Ninomiya H, Saijo M, et al. Analysis of Lujo Virus Cell Entry using Pseudotype Vesicular Stomatitis Virus. Journal of Virology. 2014;88(13):7317–7330. doi:10.1128/JVI.00512-14

[248] Raaben M, Jae LT, Herbert AS, Kuehne AI, Stubbs SH, Chou Y, Blomen VA, Kirchhausen T, Dye JM, Brummelkamp TR, et al. NRP2 and CD63 Are Host Factors for Lujo Virus Cell Entry. Cell Host & Microbe. 2017;22(5):688-696.e5. doi:10.1016/j.chom.2017.10.002

[249] Jemielity S, Wang JJ, Chan YK, Ahmed AA, Li W, Monahan S, Bu X, Farzan M, Freeman GJ, Umetsu DT, et al. TIM-family Proteins Promote Infection of Multiple Enveloped Viruses through Virion-associated Phosphatidylserine. PLoS Pathogens. 2013;9(3):e1003232. doi:10.1371/journal.ppat.1003232

[250] Abraham J, Kwong JA, Albariño CG, Lu JG, Radoshitzky SR, Salazar-Bravo J, Farzan M, Spiropoulou CF, Choe H. Host-Species Transferrin Receptor 1 Orthologs Are Cellular Receptors for Nonpathogenic New World Clade B Arenaviruses. PLoS Pathogens. 2009;5(4):e1000358. doi:10.1371/journal.ppat.1000358

[251] Emonet SF, de la Torre JC, Domingo E, Sevilla N. Arenavirus genetic diversity and its biological implications. Infection, Genetics and Evolution. 2009;9(4):417–429. doi:10.1016/j.meegid.2009.03.005

[252] Fedeli C, Moreno H, Kunz S. Novel Insights into Cell Entry of Emerging Human Pathogenic Arenaviruses. Journal of Molecular Biology. 2018;430(13):1839–1852. doi:10.1016/j.jmb.2018.04.026

[253] Radoshitzky SR, Kuhn JH, Spiropoulou CF, Albariño CG, Nguyen DP, Salazar-Bravo J, Dorfman T, Lee AS, Wang E, Ross SR, et al. Receptor

determinants of zoonotic transmission of New World hemorrhagic fever arenaviruses. Proceedings of the National Academy of Sciences. 2008;105(7):2664–2669. doi:10.1073/pnas.0709254105

[254] Stenglein MD, Sanders C, Kistler AL, Ruby JG, Franco JY, Reavill DR, Dunker F, DeRisi JL. Identification, Characterization, and In Vitro Culture of Highly Divergent Arenaviruses from Boa Constrictors and Annulated Tree Boas: Candidate Etiological Agents for Snake Inclusion Body Disease. mBio. 2012;3(4). doi:10.1128/mBio.00180-12

[255] Korzyukov Y, Iheozor-Ejiofor R, Levanov L, Smura T, Hetzel U, Szirovicza L, de la Torre JC, Martinez-Sobrido L, Kipar A, Vapalahti O, et al. Differences in Tissue and Species Tropism of Reptarenavirus Species Studied by Vesicular Stomatitis Virus Pseudotypes. Viruses. 2020;12(4):395. doi:10.3390/v12040395

[256] Borrow P, Oldstone MBA. Mechanism of Lymphocytic Choriomeningitis Virus Entry into Cells. Virology. 1994;198(1):1–9. doi:10.1006/viro.1994.1001

[257] Rojek JM, Sanchez AB, Nguyen NT, de la Torre J-C, Kunz S. Different Mechanisms of Cell Entry by Human-Pathogenic Old World and New World Arenaviruses. Journal of Virology. 2008;82(15):7677–7687. doi:10.1128/JVI.00560-08

[258] Quirin K, Eschli B, Scheu I, Poort L, Kartenbeck J, Helenius A. Lymphocytic choriomeningitis virus uses a novel endocytic pathway for infectious entry via late endosomes. Virology. 2008;378(1):21–33. doi:10.1016/j.virol.2008.04.046

[259] Rojek JM, Perez M, Kunz S. Cellular Entry of Lymphocytic Choriomeningitis Virus. Journal of Virology. 2008;82(3):1505–1517. doi:10.1128/JVI.01331-07

[260] Iwasaki M, Ngo N, de la Torre JC. Sodium hydrogen exchangers contribute to arenavirus cell entry. Journal of virology. 2014;88(1):643–54. doi:10.1128/JVI.02110-13

[261] Martinez MG, Cordo SM, Candurra NA. Characterization of Junín arenavirus cell entry. Journal of General Virology. 2007;88(6):1776–1784. doi:10.1099/vir.0.82808-0

[262] Jae LT, Raaben M, Herbert AS, Kuehne AI, Wirchnianski AS, Soh TK, Stubbs SH, Janssen H, Damme M, Saftig P, et al. Lassa virus entry

requires a trigger-induced receptor switch. Science. 2014;344(6191):1506–1510. doi:10.1126/science.1252480

[263] Cohen-Dvashi H, Israeli H, Shani O, Katz A, Diskin R. Role of LAMP1 Binding and pH Sensing by the Spike Complex of Lassa Virus. Journal of Virology. 2016;90(22):10329–10338. doi:10.1128/JVI.01624-16

[264] Lippincott-Schwartz J, Fambrough DM. Cycling of the integral membrane glycoprotein, LEP100, between plasma membrane and lysosomes: Kinetic and morphological analysis. Cell. 1987;49(5):669–677. doi:10.1016/0092-8674(87)90543-5

[265] Amos B, Lotan R. Modulation of lysosomal-associated membrane glycoproteins during retinoic acid-induced embryonal carcinoma cell differentiation. Journal of Biological Chemistry. 1990;265(31):19192–19198. doi:10.1016/S0021-9258(17)30643-9

[266] Bakkers MJG, Moon-Walker A, Herlo R, Brusic V, Stubbs SH, Hastie KM, Saphire EO, Kirchhausen TL, Whelan SPJ. CD164 is a host factor for lymphocytic choriomeningitis virus entry. Proceedings of the National Academy of Sciences of the United States of America. 2022;119(10):e2119676119. doi:10.1073/pnas.2119676119

[267] Liu J, Knopp KA, Rackaityte E, Wang CY, Laurie MT, Sunshine S, Puschnik AS, DeRisi JL. Genome-Wide Knockout Screen Identifies Human Sialomucin CD164 as an Essential Entry Factor for Lymphocytic Choriomeningitis Virus. mBio. 2022;13(3). doi:10.1128/mbio.00205-22

[268] Enriquez AS, Buck TK, Li H, Norris MJ, Moon-Walker A, Zandonatti MA, Harkins SS, Robinson JE, Branco LM, Garry RF, et al. Delineating the mechanism of anti-Lassa virus GPC-A neutralizing antibodies. Cell Reports. 2022;39(8):110841. doi:10.1016/j.celrep.2022.110841

[269] Zhang Y, York J, Brindley MA, Nunberg JH, Melikyan GB. Fusogenic structural changes in arenavirus glycoproteins are associated with viroporin activity. PLOS Pathogens. 2023;19(7):e1011217. doi:10.1371/journal.ppat.1011217

[270] Markosyan RM, Marin M, Zhang Y, Cohen FS, Melikyan GB. The late endosome-resident lipid bis(monoacylglycero)phosphate is a cofactor for Lassa virus fusion. PLOS Pathogens. 2021;17(9):e1009488. doi:10.1371/journal.ppat.1009488

[271] Zhang Y, Carlos de la Torre J, Melikyan GB. Human LAMP1 accelerates Lassa virus fusion and potently promotes fusion pore dilation upon forcing viral fusion with non-endosomal membrane. PLOS Pathogens. 2022;18(8):e1010625. doi:10.1371/journal.ppat.1010625

[272] Stauffer S, Feng Y, Nebioglu F, Heilig R, Picotti P, Helenius A. Stepwise Priming by Acidic pH and a High K Concentration Is Required for Efficient Uncoating of Influenza A Virus Cores after Penetration. Journal of Virology. 2014;88(22):13029–13046. doi:10.1128/JVI.01430-14

[273] Pinto LH, Holsinger LJ, Lamb RA. Influenza virus M2 protein has ion channel activity. Cell. 1992;69(3):517–528. doi:10.1016/0092-8674(92)90452-I

[274] Jin H, Elliott RM. Characterization of Bunyamwera virus S RNA that is transcribed and replicated by the L protein expressed from recombinant vaccinia virus. Journal of Virology. 1993;67(3):1396–1404. doi:10.1128/jvi.67.3.1396-1404.1993

[275] Meyer BJ, Southern PJ. Concurrent sequence analysis of 5' and 3' RNA termini by intramolecular circularization reveals 5' nontemplated bases and 3' terminal heterogeneity for lymphocytic choriomeningitis virus mRNAs. Journal of Virology. 1993;67(5):2621–2627. doi:10.1128/jvi.67.5.2621-2627.1993

[276] Polyak SJ, Zheng S, Harnish DG. 5' termini of Pichinde arenavirus S RNAs and mRNAs contain nontemplated nucleotides. Journal of Virology. 1995;69(5):3211–3215. doi:10.1128/jvi.69.5.3211-3215.1995

[277] Reich S, Guilligay D, Pflug A, Malet H, Berger I, Crépin T, Hart D, Lunardi T, Nanao M, Ruigrok RWH, et al. Structural insight into cap-snatching and RNA synthesis by influenza polymerase. Nature. 2014;516(7531):361–366. doi:10.1038/nature14009

[278] De Vlugt C, Sikora D, Pelchat M. Insight into Influenza: A Virus Cap-Snatching. Viruses. 2018;10(11):641. doi:10.3390/v10110641

[279] Datta K, Wolkerstorfer A, Szolar OHJ, Cusack S, Klumpp K. Characterization of PA-N terminal domain of Influenza A polymerase reveals sequence specific RNA cleavage. Nucleic Acids Research. 2013;41(17):8289–8299. doi:10.1093/nar/gkt603

[280] Lamb RA, Choppin PW. Synthesis of influenza virus polypeptides in

cells resistant to alpha-amanitin: evidence for the involvement of cellular RNA polymerase II in virus replication. Journal of Virology. 1977;23(3):816–819. doi:10.1128/jvi.23.3.816-819.1977

[281] Ferron F, Weber F, de la Torre JC, Reguera J. Transcription and replication mechanisms of Bunyaviridae and Arenaviridae L proteins. Virus Research. 2017;234:118–134. doi:10.1016/j.virusres.2017.01.018

[282] Polyak SJ, Zheng S, Harnish DG. 5' termini of Pichinde arenavirus S RNAs and mRNAs contain nontemplated nucleotides. Journal of Virology. 1995;69(5):3211–3215. doi:10.1128/jvi.69.5.3211-3215.1995

[283] Szentirmay MN. Survey and summary: Spatial organization of RNA polymerase II transcription in the nucleus. Nucleic Acids Research. 2000;28(10):2019–2025. doi:10.1093/nar/28.10.2019

[284] Linero F, Welnowska E, Carrasco L, Scolaro L. Participation of eIF4F complex in Junin virus infection: blockage of eIF4E does not impair virus replication. Cellular Microbiology. 2013 Jun:n/a-n/a. doi:10.1111/cmi.12149

[285] Campbell Dwyer EJ, Lai H, MacDonald RC, Salvato MS, Borden KLB. The Lymphocytic Choriomeningitis Virus RING Protein Z Associates with Eukaryotic Initiation Factor 4E and Selectively Represses Translation in a RING-Dependent Manner. Journal of Virology. 2000;74(7):3293–3300. doi:10.1128/JVI.74.7.3293-3300.2000

[286] Cordo SM, Acuña MC y, Candurra NA. Polarized entry and release of Junín virus, a New World arenavirus. Journal of General Virology. 2005;86(5):1475–1479. doi:10.1099/vir.0.80473-0

[287] Schlie K, Maisa A, Freiberg F, Groseth A, Strecker T, Garten W. Viral Protein Determinants of Lassa Virus Entry and Release from Polarized Epithelial Cells. Journal of Virology. 2010;84(7):3178–3188. doi:10.1128/JVI.02240-09

[288] Urata S, Yasuda J, de la Torre JC. The Z Protein of the New World Arenavirus Tacaribe Virus Has Bona Fide Budding Activity That Does Not Depend on Known Late Domain Motifs. Journal of Virology. 2009;83(23):12651–12655. doi:10.1128/JVI.01012-09

1.4 Project Aims

The presented work of this thesis aimed to investigate the later stages of arenavirus infection. The thesis utilised LCMV as a biosafety level (BSL) 2 model pathogen, with the extrapolation to the more harmful BSL 4 arenaviruses. By understanding the requirements for later stages of arenavirus infection, specific therapeutic could be developed which may lessen pandemic potenital. Three main objectives were established for this project:

1. **Investigating the role of cellular COPI and AP-4 complexes in Lymphocytic choriomeningitis arenavirus infection.** Cellular COPI and AP-4 vesicle components were identified via an siRNA trafficking screen as important during LCMV infection. The aim was to investigate the which stages of infection required COPI and AP-4 complexes.

2. **Exploring the requirement of cell-cell connections within Lymphocytic choriomeningitis arenavirus infection.** Using live cell imaging alongside rLCMV-EGFP, an unusual spread of LCMV throughout an infected culture was observed. Interestingly, cells adjacent to infected cells would often become infected, despite the lack of a semi-solid overlay. This allowed the hypothesis that LCMV may utilise cell-cell modes of transmission. The aim was to investigate the reliance on cell-cell connections during infection.

3. **Investigating phosphorylation of Lymphocytic choriomeningitis arenavirus nucleoprotein during infection.** This objective was conceived due to the finding of a post-translational modification of LCMV NP. Through mass spectrometry analysis, it was identified that LCMV NP is phosphorylated. The aim was to investigate the role of this modification during LCMV infection.

   In summary, the focus of this project was on clarifying the viral and host requirements during the later stages of LCMV infection. Alongside these aims, rLCMV tools have been developed, such as the GP1-FLAG and L-cMYC tags, which assisted in these objectives, but can be applied to future investigations.

Chapter 2

Lymphocytic choriomeningitis arenavirus requires cellular COPI and AP-4 complexes for efficient virion production

Jounal of Virology: DOI: https://doi.org/10.1128/jvi.02006-23

Owen Byford [1,2] Amelia B. Shaw[1,2], Hiu Nam Tse [1,2] Eleanor J. A. A. Todd [1,2] Beatriz Álvarez-Rodríguez [1,2*] Roger Hewson[3] Juan Fontana[1,2] John N. Barr [1,2]

[1]School of Molecular and Cellular Biology, Faculty of Biological Sciences, University of Leeds, Leeds, LS2 9JT, United Kingdom

[2]Astbury Centre for Structural Molecular Biology, University of Leeds, Leeds, United Kingdom

[3]Virology and Pathogenesis Group, National Infection Service, Public Health England, Porton Down SP4 0JG, UK.

[*]Present address: Beatriz Álvarez-Rodríguez, Institute for Integrative Systems Biology, I2SysBio (Universitat de València-CSIC), Paterna, Spain.

2.1 Abstract

Lymphocytic choriomeningitis virus (LCMV) is a bisegmented negative-sense RNA virus classified within the *Arenaviridae* family of the *Bunyavirales* order. LCMV is associated with fatal disease in immunocompromized populations, and as the prototypical arenavirus, acts as a model for the many serious human pathogens within this group. Here, we examined the dependence of LCMV multiplication on cellular trafficking components using a recombinant LCMV expressing enhanced green fluorescent protein in conjunction with a curated siRNA library. The screen revealed a requirement for subunits of both the coat protein 1 (COPI) coatomer and adapter protein 4 (AP-4) complexes. By rescuing a recombinant LCMV harboring a FLAG-tagged glycoprotein (GP-1) envelope spike (rLCMV-GP1-FLAG), we showed infection resulted in marked co-localization of individual COPI and AP-4 components with both LCMV nucleoprotein (NP) and GP-1, consistent with their involvement in viral processes. To further investigate the role of both COPI and AP-4 complexes during LCMV infection, we utilized the ARF-I inhibitor brefeldin A (BFA) that prevents complex formation. Within a single 12-h cycle of virus multiplication, BFA pre-treatment caused no significant change in LCMV-specific RNA synthesis, alongside no significant change in LCMV NP expression, as measured by BFA time-of-addition experiments. In contrast, BFA addition resulted in a significant drop in released virus titers, approaching 50-fold over the same 12-h period, rising to over 600-fold over 24 h. Taken together, these findings suggest COPI and AP-4 complexes are important host cell factors required for the formation and release of infectious LCMV.

2.2 Importance

Arenaviruses are rodent-borne, segmented, negative-sense RNA viruses, with several members responsible for fatal human disease, with the prototypic member lymphocytic choriomeningitis virus (LCMV) being under-recognised as a pathogen capable of inflicting neurological infections with fatal outcome. A detailed understanding of how arenaviruses subvert host cell processes to complete their multiplication cycle is incomplete. Here, using a combination of gene ablation and

pharmacological inhibition techniques, we showed that host cellular COPI and AP-4 complexes, with native roles in cellular vesicular transport, were required for efficient LCMV growth. We further showed these complexes acted on late stages of the multiplication cycle, post-gene expression, with a significant impact on infectious virus egress. Collectively, our findings improve the understanding of arenaviruses host-pathogen interactions and reveal critical cellular trafficking pathways required during infection.

Keywords: AP-4; COPI; LCMV; arenavirus.

2.3 Chapter Introduction

The Arenaviridae family within the *Bunyavirales* order of segmented negative sense RNA viruses currently compromises 56 species, which are sub-divided into four genera: *Antennavirus*, *Hartmanivirus*, *Mammarenavirus* and *Reptarenavirus*. Members of the *Mammarenavirus* genus can infect mammals [1–3] and notable species include Lassa virus (LASV) and Junín virus (JUNV), for which infections can result in haemorrhagic fever and subsequent fatality in approximately 1-2 % and 30 % of human cases, respectively [4, 5]. Currently, no specific antiviral therapeutics or FDA-approved vaccines exist to target any member of the Arenaviridae family [6]. Combined, these factors contribute to the classification of LASV, JUNV and several other arenaviruses as hazard group 4 pathogens, requiring the highest BSL 4 containment for their study, which has hindered research progress.

Lymphocytic choriomeningitis virus (LCMV) is classified within the *Mammarenavirus* genus and causes a persistent infection within the common house mouse, *Mus musculus*, which acts as the primary host. Rodent-to-human transmission frequently occurs but rarely results in severe disease [7]. LCMV exhibits tropism for non-differentiated neuroblasts and in some populations, including immunocompromised patients or neonates, can lead to aseptic meningitis [8, 9]. Specifically, the LCMV Armstrong strain acts as an effective research model for more pathogenic mammarenaviruses due to shared structural and functional characteristics, and requirement for more amenable BSL-2 containment facilities for its study. The LCMV genome comprises small (S) and large (L)

segments and encodes four structural proteins using an ambi-sense transcription strategy. Following entry, the input virion-associated (vRNA) S and L segments are transcribed by the viral RNA-dependent RNA polymerase (RdRp) to generate mRNAs encoding nucleocapsid protein (NP) and RdRp, respectively. Subsequent vRNA replication yields S and L anti-genome (ag) RNAs, which act as templates for the transcription of mRNAs encoding a glycoprotein precursor (GPC) and matrix protein (Z) [10, 11]. Post-translational cleavage of GPC results in the production of N-terminal glycoprotein-1 (GP-1), C-terminal glycoprotein-2 (GP-2) and stable signal peptide (SSP), that remain associated as trimers [12–15].

Although LCMV has been studied heavily from an immunological perspective, many molecular details underpinning its multiplication are yet to be determined. It is thought that LCMV first attaches to the cell at the plasma membrane (PM) by binding to cellular receptor α-dystroglycan, although members of the Tyro3, Axl, and Mer (TAM) family and C-type lectins have also been implicated [16, 17]. LCMV is internalised, potentially via macropinocytosis due to the requirement of actin remodelling and Pak1 [18], after which virions are trafficked via multivesicular bodies (MVBs) to late endosomes. Here, following interaction with secondary receptor CD164, GP-2 mediates endosomal fusion and subsequent release of the vRNAs into the cytosol [19, 20]. The site of arenavirus RNA synthesis is unclear, with reports of newly made mRNAs located within processing bodies [21] and agRNA and vRNAs compartmentalised within specialised NP-induced organelles known as replication-transcription complexes [22]. Following translation, GPC is glycosylated within the endoplasmic reticulum (ER) then post-translationally cleaved by the resident ER signal peptidase to release the SSP, which remains associated with the GPC whilst it is trafficked to, and throughout, the Golgi [23]. Here, GPC is further cleaved by subtilisin kexin isozyme-1/site-1 protease (SKI-1/S1P) to release GP-1 and GP-2, which associate alongside SSP as trimers [24–26]. While the site of viral budding is unclear, virion assembly requires Z-mediated recruitment of endosomal sorting complex required for transport (ESCRT) components; Z is proposed to recruit RNPs via interaction with NP, and myristylation of Z is required for virion incorporation of glycoprotein trimers [27, 28].

Here, using a curated siRNA library targeting the expression of cellular proteins involved in vesicular trafficking we showed the efficient LCMV multiplication in

the neuronal cell line SH-SY5Y required components of the coat protein I (COPI) and adaptor protein 4 (AP-4) complexes. Disrupting the formation of these complexes using brefeldin A (BFA) resulted in redistribution of LCMV GP-1 and NP, corroborating a role for AP-4 and COPI components in LCMV protein trafficking. Quantification of LCMV-specific vRNA, protein expression and viral titres during single-step growth, alongside BFA time-of-addition assays, indicated COPI and AP-4 complexes are not required for efficient gene expression, but are important for LCMV assembly and egress. Overall, this study improves our understanding of arenavirus-host interactions, which may aid in the identification of targets for effective anti-arenaviral therapies.

2.4 Results

Identification of the trafficking components required during LCMV multiplication

The role of host cell trafficking components in LCMV multiplication and egress was assessed using a focused siRNA library comprising three different siRNAs specific for each of 87 host trafficking genes. To facilitate the screen, a recombinant LCMV expressing eGFP (rLCMV-eGFP) using a P2A-linked [29–32] eGFP open reading frame (ORF) appended to the NP ORF (Figure 2.1A) was used, rescued as previously described [32]. Using this virus, measurement of total integrated intensity of eGFP expression (TIIE) represented a surrogate for LCMV multiplication and infection progression (Figure 2.1B). Following reverse transfection of each individual siRNA, human-origin neuronal SH-SY5Y cells were infected with rLCMV-eGFP at a multiplicity of infection (MOI) of 0.2 and live-cell images were acquired to measure TIIE at 24 hpi (Figure 2.1C). At this time point, rLCMV-eGFP has undergone multiple infection cycles in these cells [32] thus, a significant reduction in TIIE relative to the positive control (virus plus transfection reagent only) could represent inhibition of any stage of the LCMV replication cycle encompassing binding, entry, replication, assembly or egress.

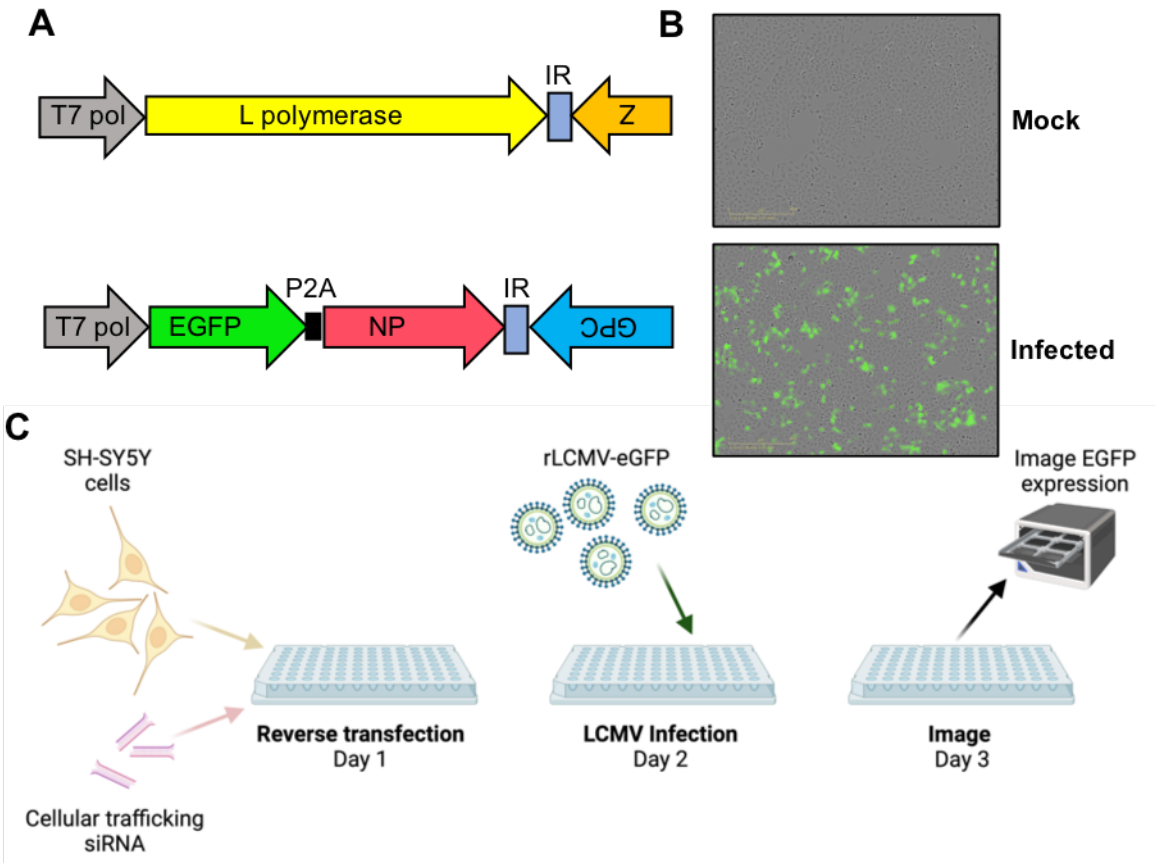

Figure 2.1: Rescue of a recombinant LCMV expressing eGFP used to perform an siRNA screen to identify cellular factors involved in LCMV multiplication.(A) Schematic of rLCMV segments, showing the location of the eGFP open reading frame within the S segment. (B) Live cell images of A549 cells infected with LCMV-eGFP showing eGFP fluorescence at 24 hpi. (C) Schematic of the siRNA screen protocol.

The impact of each individual siRNA on overall multiplication and infectious virion production was tested four times (supplementary data set S1) and the 30 genes with the greatest mean TIIE reduction across all three individual siRNAs are listed in Figure 2.2, alongside appropriate controls.

AP-4 and COPI vesicle components are required for productive LCMV infection.

rLCMV-eGFP-mediated TIIE in siRNA transfected cells was most-reduced following knockdown of AP-4 component AP4M1, with a mean TIIE level at 24 hpi of 44% compared to scrambled (Figure 2.2; siRNA 1 = 0.5771 [P = 0.0091]; siRNA 2 = 0.2412 [P = 0.0041]; siRNA 3 = 0.4935 [P=0.0013]). In addition, knockdown of a second AP-4 component, AP4B1, resulted in a mean TIIE level of 64%. The second most-reduced TIIE level was for COPI vesicle component COPA, with 45%

TIIE compared to scrambled (Figure 2.2; siRNA 1 = 0.5335 [P = 0.0006]; siRNA 2 = 0.2524 [P = 0.0013]; siRNA 3 = 0.5664 [P = 0.0029]), with these siRNAs proving effective for knockdown of the corresponding COPA target and also infection of the related Hazara nairovirus [33]. In addition, knockdown of a second COPI component, COPB1, resulted in 53% TIIE.

Interestingly siRNA knockdown of other components required indirectly to form both AP-4 and COPI vesicles, namely the small GTP-binding protein ADP-ribosylation factor 1 (ARF-1) and Golgi BFA-resistant guanine nucleotide exchange factor 1 (GBF-1) (30), also resulted in significantly reduced TIIE levels (Figure 2.2; ARF-1; siRNA 1 = 0.6543 [P = 0.0185]; siRNA 2 = 0.7418 [P = 0.0600]; siRNA 3 = 0.5500 [P = 0.0002] GBF-1; siRNA 1 = 0.7750 [P = 0.1478]; siRNA 2 = 0.3474 [P = 0.0001]; siRNA 3 = 0.77 [P = 0.0100]). GBF-1 is a guanine exchange factor (GEF) responsible for activation of ARF-1, which then binds GTP to allow recruitment of intact COPI heptameric complexes and their subsequent anchoring within membranes [34]. The recruitment of AP-4 vesicles to the TGN is also regulated by ARF-1, a process mediated by direct interaction between AP4M1 and ARF-1, following its activation [35]. Taken together, these findings suggested important roles for both AP-4 and COPI complexes in the LCMV multiplication cycle.

Gene ID	Full length name	siRNA 1	siRNA 2	siRNA 3	Avg.
AP4M1	adaptor-related protein complex 4, mu 1 subunit	58%	24%	49%	44%
COPA	coatomer protein complex, subunit alpha	53%	25%	57%	45%
PREB	prolactin regulatory element binding	64%	51%	32%	49%
STX10	syntaxin 10	50%	46%	58%	51%
COPB1	coatomer protein complex, subunit beta 1	45%	50%	63%	53%
AP3S2	adaptor-related protein complex 3, sigma 2 subunit	76%	40%	44%	53%
AP1S1	adaptor-related protein complex 1, sigma 1 subunit	59%	54%	55%	56%
STX1A	syntaxin 1A (brain)	87%	29%	53%	56%
SNAP25	synaptosomal-associated protein, 25kDa	63%	44%	65%	57%
AP2A2	adaptor-related protein complex 2, alpha 2 subunit	57%	58%	59%	58%
SYT7	synaptotagmin VII	61%	42%	74%	59%
VAMP7	vesicle-associated membrane protein 7	51%	51%	75%	59%
STX11	syntaxin 11	49%	43%	86%	59%
SYT1	synaptotagmin I	62%	28%	92%	61%
STXBP2	syntaxin binding protein 2	76%	62%	45%	61%
SEC23A	Sec23 homolog A (S. cerevisiae)	71%	44%	70%	62%
VAMP3	vesicle-associated membrane protein 3	70%	58%	59%	62%
CACNA1S	calcium channel, L type, alpha 1S subunit	78%	58%	52%	63%
GBF1	golgi BFA resistant guanine nucleotide exchange factor 1	77%	35%	77%	63%
ITGA3	integrin, alpha 3	40%	60%	92%	64%
CLTA	clathrin, light chain (Lca)	101%	44%	47%	64%
AP3D1	adaptor-related protein complex 3, delta 1 subunit	66%	70%	57%	64%
STXBP3	syntaxin binding protein 3	83%	23%	88%	64%
AP4B1	adaptor-related protein complex 4, beta 1 subunit	74%	60%	59%	64%
HUWE1	HECT, UBA and WWE domain containing 1	82%	35%	76%	64%
ARF1	ADP-ribosylation factor 1	65%	74%	55%	65%
AP3B2	adaptor-related protein complex 3, beta 2 subunit	96%	80%	19%	65%
VAPB	VAMP-associated protein B and C	76%	55%	65%	65%
STX3	syntaxin 3	66%	56%	74%	65%
AP3B1	adaptor-related protein complex 3, beta 1 subunit	83%	70%	44%	66%

Control	R1	R2	R3	R4	Avg.
Mock	0%	0%	0%	1%	0%
Reagent	100%	100%	100%	100%	100%
Scr1	128%	76%	88%	75%	92%
Scr2	95%	71%	76%	91%	83%
Scr3	69%	76%	95%	108%	87%

Figure 2.2: Top 30 gene targets impacting rLCMV-eGFP growth, identified using an siRNA screen of cellular factors involved in vesicle trafficking. Viral growth was measured by total integrated intensity of eGFP expression (TIIE) relative to virus plus transfection reagent control, following siRNA knockdown at 24 hpi. Percentage TIIE values are shown for three individual siRNAs against a single gene target. Each percentage value represents the mean of four experimental repeats, and the colours indicate the levels of reduction in TIIE from red (most reduction) to white (least reduction). Genes highlighted in boldface represent those associated with COPI and AP-4 vesicles. All transfections included scrambled (scr), mock infected and infected plus transfection reagent controls, from four repeats, tabulated below.

Generation of a recombinant infectious LCMV bearing a FLAG tagged GP-1.

AP-4 and COPI complexes localise within the Golgi [35–38] and given that LCMV GPC is known to be proteolytically-cleaved and post-translationally modified within this compartment [26], we wished to develop a tool to simultaneously assess GP distribution alongside NP during virus infection.

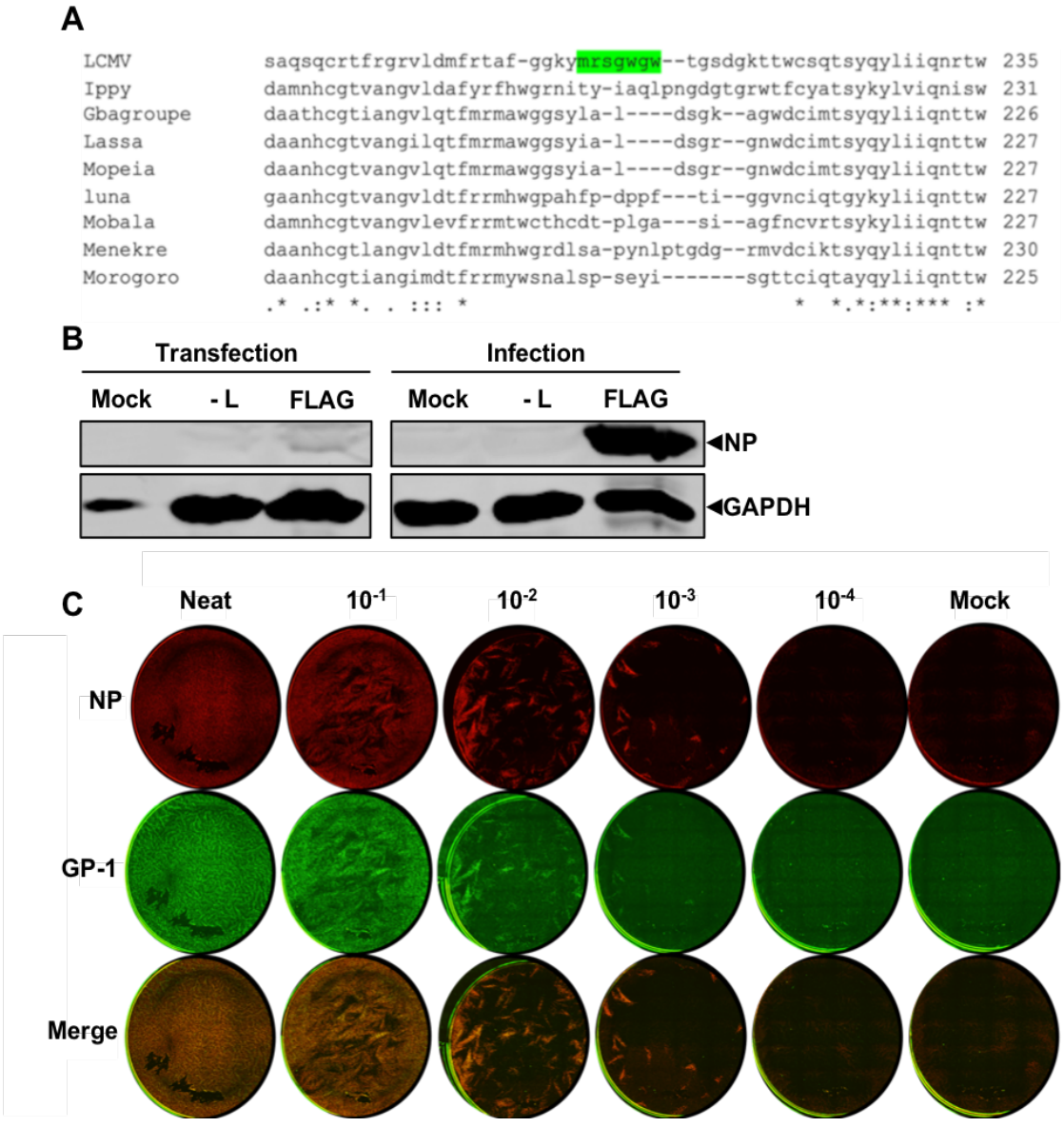

Figure 2.3: Generation of a recombinant LCMV expressing a FLAG-tagged GP-1. (A) Alignment of partial GP-1 sequence of selected Old-World arenaviruses identifying a region of low conservation as a potential FLAG tag insertion site (green). (B) Western blot analysis of transfected BSR-T7 and infected BHK-21 cell cultures confirming LCMV-GP1-FLAG rescue, using antisera specific for LCMV NP and GAPDH as loading control. (C) Immunofluorescence focus forming assay for rLCMV-GP1-FLAG showing foci by staining at 3 dpi for LCMV NP, GP-1 (FLAG) alongside merged channels.

To achieve this, we generated rLCMV with a FLAG epitope tag inserted within GP-1 (rLCMV-GP1-FLAG). The site for FLAG insertion was rationally selected by identification of regions of high sequence variation between various OW arenavirus members (Figure 2.3A) and a SWISS-MODEL prediction of the GP-1 structure, which revealed the selected site was within a flexible and surface exposed region, thus a suitable candidate for detection by immunofluorescence (IF). Subsequent virus rescue was confirmed by western blotting (Figure 2.3B) and using an immunofluorescent focus forming assay (FFA) utilising NP and FLAG (GP-1) antibody staining, which revealed the resulting virus rLCMV-GP1-FLAG was infectious, the FLAG epitope was confirmed as accessible to antibody detection and yielded viral titres of around 10^5 pfu/mL (Figure 2.3C).

Analysis of LCMV NP and GP-1 localization.

IF analysis of rLCMV-GP1-FLAG infected A549 cells at 24 hpi using NP and FLAG antisera revealed NP and GP-1 distribution was distinct; while NP was distributed widely in perinuclear regions with occasional dense puncta, GP-1 was mostly localised on one side of the nucleus, reminiscent of Golgi distribution (Figure 2.4A). To confirm Golgi localisation of GP-1, we performed IF using antisera specific for both FLAG and the *cis*-Golgi marker GM130, for which many peak intensities spatially corresponded, quantified by line scan analysis across a distance of approximately 20 µm (Figure 2.4B). This confirmed previous localization studies that used transient LCMV GPC expression [39], although here, we report for the first time the cellular location of GP-1 expressed from an infectious LCMV.

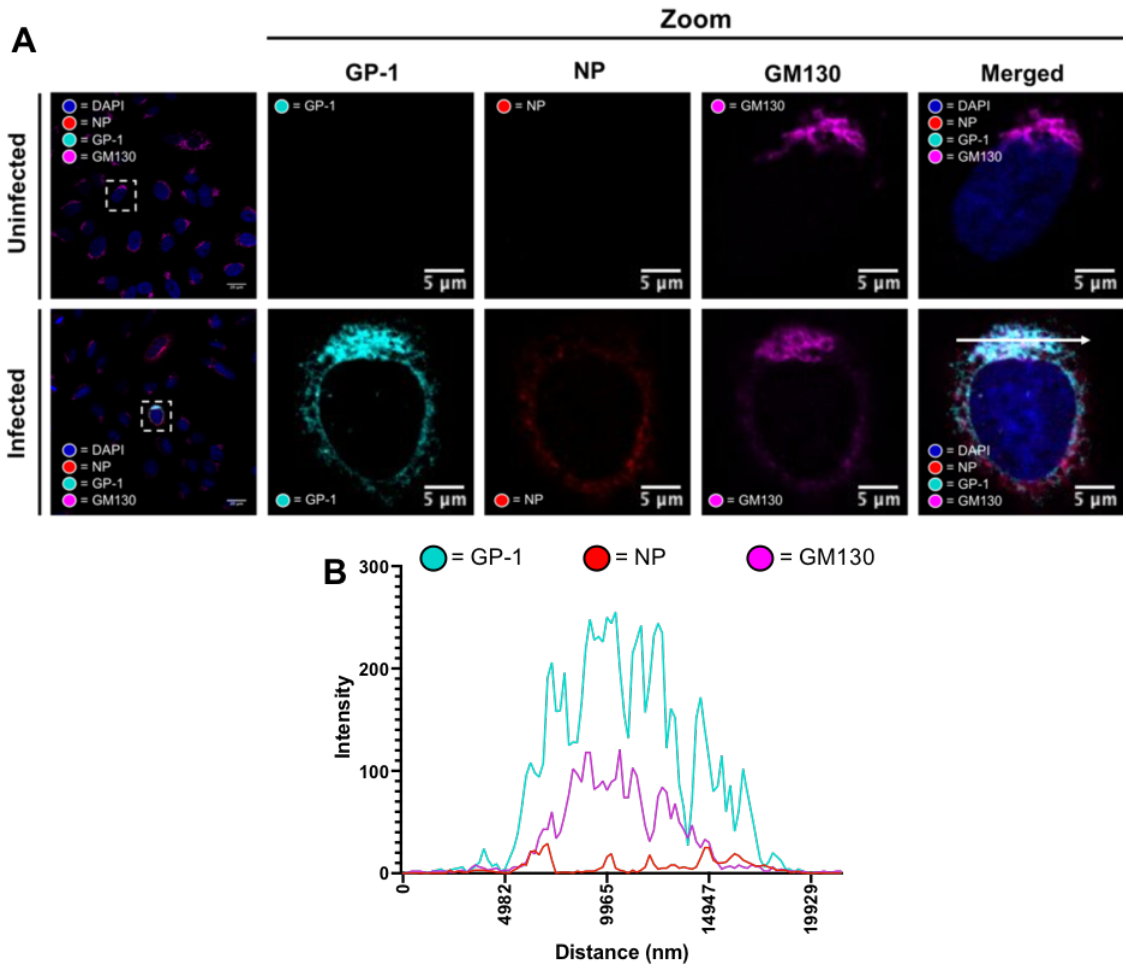

Figure 2.4: LCMV GP-1 co-localises with Golgi marker GM130 in rLCMV-GP1-FLAG infected cells. (A) Confocal microscopy of uninfected and rLCMV-GP1-FLAG infected cells at an MOI of 0.1 at 24 hpi. A549 cells were stained with antisera specific for GM130 (magenta), GP-1 (cyan), and NP (red) alongside DAPI. A zoomed image for both uninfected and infected (white boxes) for all channels is shown, alongside merged channels. (B) Line scan for the region highlighted in the zoomed merged image in panel A (scan line represented by a white arrow), showing intensities of channels corresponding to NP, GP-1 and GM130 across a 20 µm distance.

rLCMV infection results in redistribution of COPI complex components.

Using rLCMV-GP1-FLAG, we next examined the spatial proximity of NP and GP-1 alongside components of the COPI complex.

As expected, native COPA staining within uninfected cells presented as discrete puncta with characteristic ER/Golgi distribution (Figure 2.5A-B). In contrast, within rLCMV-GP1-FLAG infected cells, a portion of COPA staining exhibited this same native ER/Golgi localisation, but in these infected cells COPA staining was also detected outside perinuclear regions, extending throughout the cytoplasm.

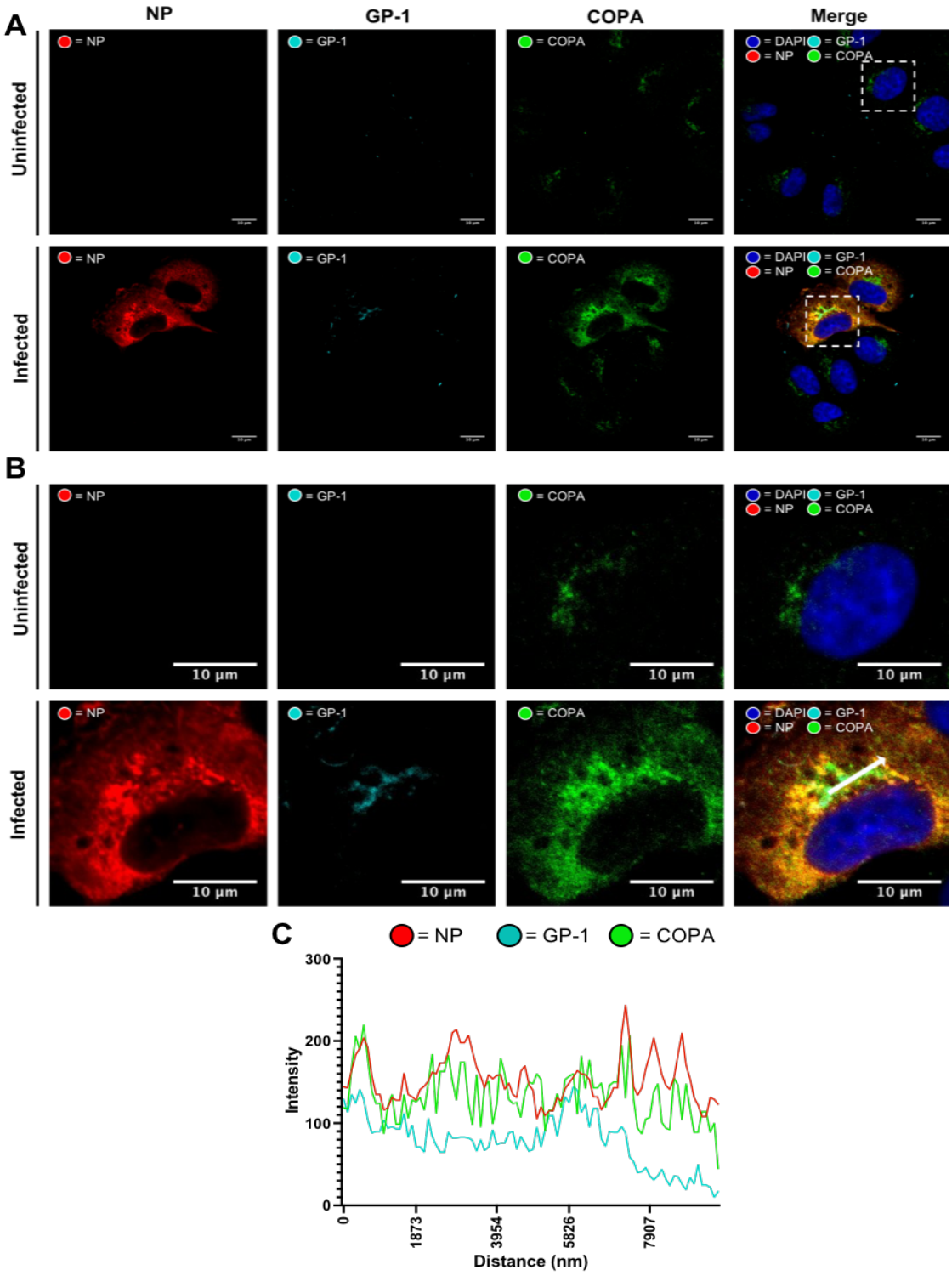

Figure 2.5: LCMV NP and the COPA component of COPI complexes co-localize in LCMV infected A549 cells. (A) Confocal microscopy of uninfected and rLCMV-GP1-FLAG infected cells at 15 hpi, MOI of 0.1. A549 cells were stained with antisera specific for COPA (green), GP-1 (cyan), and NP (red) alongside DAPI. (B) A zoomed image for both uninfected and infected (white boxes) for all channels is shown, alongside merged channels. (C) Line scan for the region highlighted in the zoomed image in panel B (scan line represented by a white arrow), showing intensities of channels corresponding to NP, GP-1 and COPA across a 10 µm distance.

This redistributed COPA staining closely corresponded with that of NP, which is represented in the merged image and associated line scan (Figure 2.5C). To examine whether COPA and NP interacted directly, we immunoprecipitated LCMV NP from infected cells and performed mass spectrometry analysis of the eluate, however COPA was not identified, suggesting any interaction between NP and COPA was indirect (data not shown).

Co-staining with FLAG antisera revealed GP-1 occupied a restricted area within that occupied by COPA, with many of the peak intensities of GP-1 and COPA being closely aligned, as shown by line scan analysis (Figure 2.5C). This GP-1 and COPA colocalization was consistently imaged across all infected cells analysed (Supplementary figure 6.1A). As with our previous observations, described above (Figure 2.4A and B), NP and GP-1 occupied distinct regions, and the positions of their peak intensities or general abundance did not precisely correspond.

Taken together, these findings suggest a close association between COPA and NP, as well as between COPA and GP-1, consistent with a role for COPI in LCMV NP and GPC functions.

rLCMV infection results in redistribution of AP-4 complex components.

As with components of the COPI complex described above, rLCMV-GP1-FLAG allowed examination of the spatial proximity of NP and GP-1 alongside components of the AP-4 complex. Staining uninfected cells with antisera for AP-4 subunit AP4E1 (Figure 2.6A-B) revealed its location within the *trans*-Golgi network, consistent with previous reports [37, 38]. In contrast, within rLCMV-GP1-FLAG infected cells, the majority of AP4E1 was located diffusely throughout the cytoplasm, suggestive of re-distribution.

Staining of rLCMV-GP1-FLAG infected cells with NP antisera revealed close co-localisation with AP4E1, suggesting NP was responsible for the observed AP4E1 redistribution (Figure 2.6C). In contrast, while GP-1 staining occupied a portion of that occupied by AP4E1/NP, its distribution was less extensive and more reminiscent of Golgi, as described above. To gain a better overall representation of GP-1, NP and AP4E1 distribution, colocalization of all these components was imaged in multiple different rLCMV-GP1-FLAG infected cells

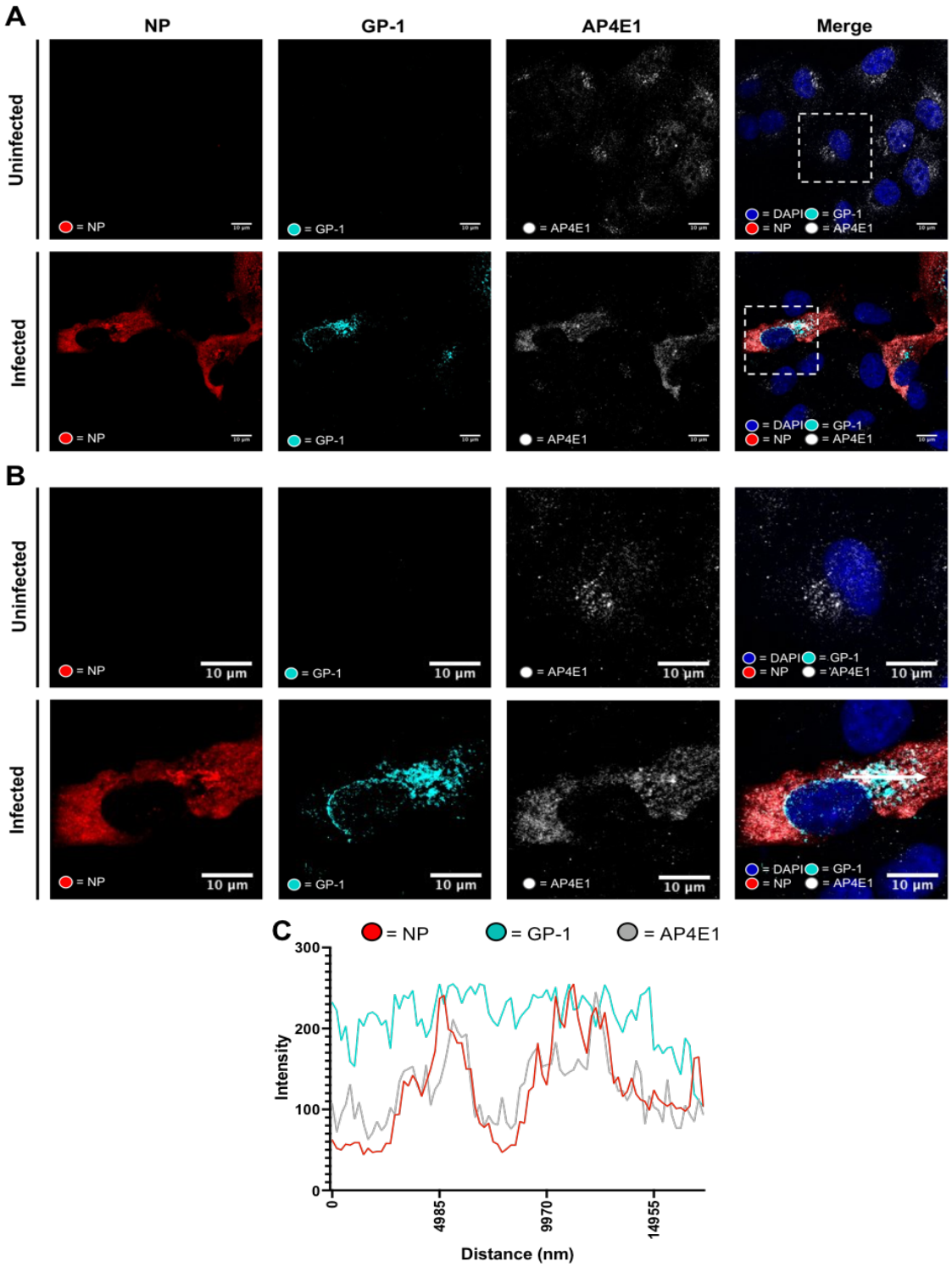

Figure 2.6: LCMV NP and the AP4E1 component of AP-4 complexes co-localize in rLCMV-GP1-FLAG infected A549 cells. (A) Confocal microscopy of uninfected and rLCMV-GP1-FLAG infected cells at 15 hpi, MOI of 0.1. A549 cells were stained with AP4E1 (white), GP-1 (cyan), and NP (red) and DAPI. (B) A zoomed image for regions of both uninfected and infected cells (white boxes) for all channels is shown, alongside merged channels. (C) Line scan analysis for the region highlighted in the merged zoomed image shown in panel B (scan line represented by a white arrow) showing intensities of channels corresponding to NP, GP-1 and AP4E1 across a 17 µm distance.

(Supplementary figure 6.1B), which revealed a consistent outcome.

Taken together, these findings suggest AP4E1 is redistributed during LCMV infection adopting a localization that closely matches that of NP, consistent with a role for AP-4 complexes during the viral multiplication cycle.

BFA treatment of LCMV infected cells during single-step growth does not significantly affect gene expression or genome RNA replication.

To further investigate the role of COPA and AP-4 complexes in the LCMV replication cycle, we used brefeldin-A (BFA), which inhibits ARF-1 activation, blocking formation of COPI and AP-4 complexes (Supplementary figure 6.2) [40, 41]. We determined that BFA was non-toxic for human-origin A549 cells in concentrations up to 5000 ng/mL (Supplementary figure 6.3A), at which NP and eGFP expression were impacted during multi-step growth measured at 24 hpi (Supplementary figure 6.3B-D). As a positive control, we showed BFA efficacy against influenza A virus (IAV) gene expression, measured by expression of IAV NP and eGFP expression, previously shown to be diminished by BFA treatment [33, 42].

We confirmed BFA resulted in the expected cellular changes by staining BFA-treated cells with antisera specific for COPA and AP4E1 components. Under normal cellular conditions, both COPA and AP4E1 localised in discrete perinuclear regions, consistent with Golgi/TGN localisation (Supplementary figure 6.4). However, upon addition of 5000 ng/mL BFA for 1 hour, both COPA and AP4E1 staining became diffusely distributed throughout the cytoplasm.

We next examined the effect of BFA on LCMV gene expression over a single cycle of LCMV infection, which we have previously determined to take 10-12 hours, when infectious virions are first released [32]. A549 cells were pre-treated for 45 min with BFA at 5000 ng/mL prior rLCMV-eGFP infection at an MOI of 5, chosen to facilitate detection of viral activities at early time points. To measure rLCMV-eGFP gene expression, TIIE was measured hourly, with BFA addition initially showing no significant impact on eGFP expression at times up to 7 hpi, and causing a small but significant drop in eGFP expression between 8-12 hpi of around 0.25 fold (Figure 2.7A).

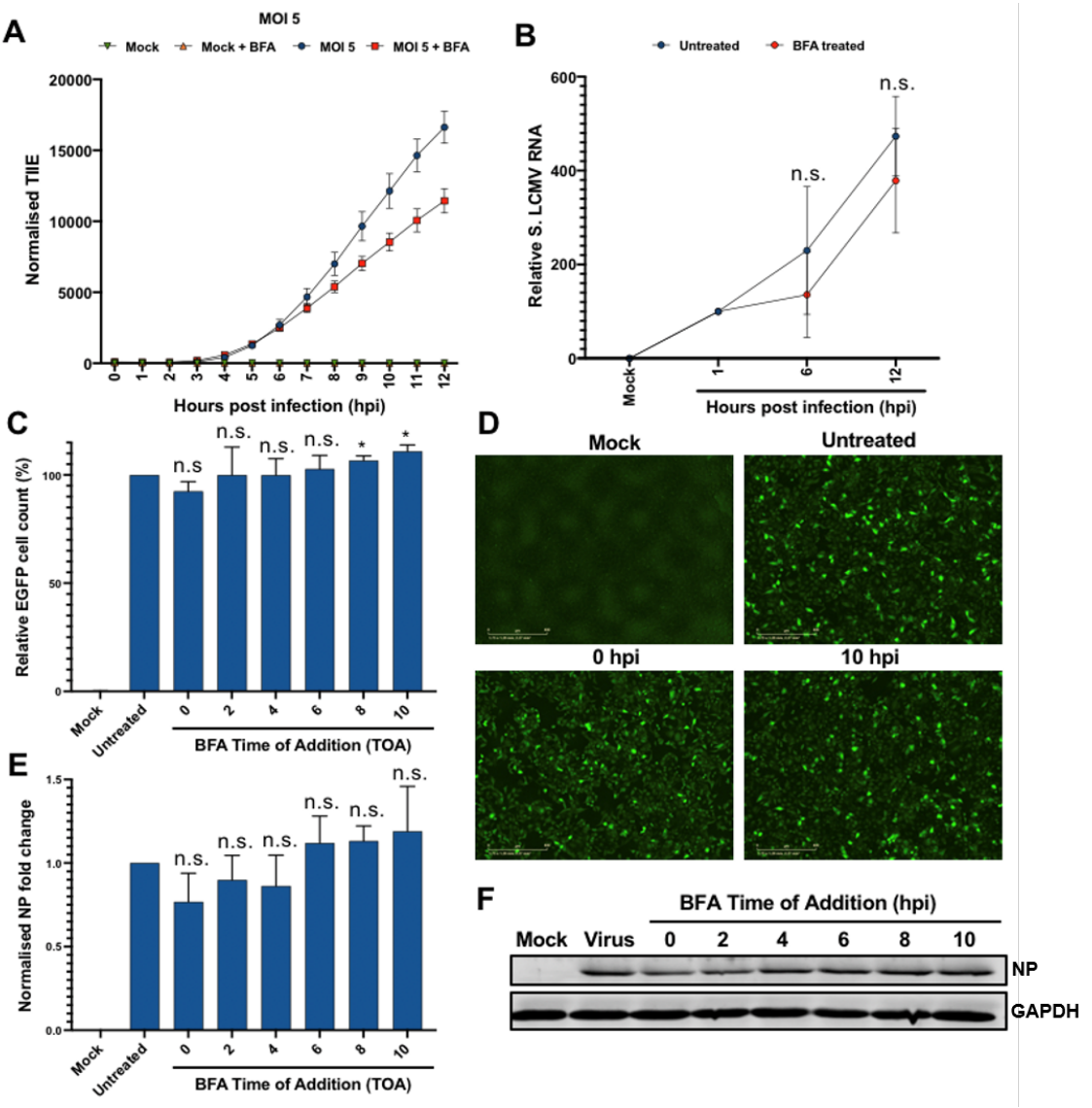

Figure 2.7: Temporal analysis of LCMV gene expression and vRNA synthesis suggests BFA treatment has little impact of LCMV gene expression. (A) A549 cells were pre-treated with BFA (5000 ng/mL) and then infected with rLCMV-eGFP at an MOI of 5. At hourly intervals, TIIE was quantified, normalised for confluency over three experimental repeats, with error bars showing deviation from the mean. (B) A549 cells were pre-treated with BFA (5000 ng/mL) and then infected with rLCMV-eGFP at an MOI of 5. At the indicated timepoints, cells were harvested for RNA extraction and RT-qPCR used to quantify S segment vRNA at each timepoint, normalised to the respective 1 hpi control. Four experimental repeats were performed, with error bars showing deviation from the mean. (C) For time of addition assays, A549 cells were infected with rLCMV-eGFP at an MOI of 5, with BFA added at bi-hourly intervals and remaining present for the duration of a single-round of infection. eGFP cell count was quantified, normalised to the untreated control, with three experimental repeats represented, with error bars showing deviation from the mean. (D) Live-cell fluorescence images of with mock, untreated, BFA added at 0 hpi and 10 hpi shown as examples. (E) Alongside, cell lysates were probed using antisera for LCMV NP and GAPDH as a loading control with band intensities quantified using densitometry and plotted showing relative fold-change of NP expression over three experimental repeats with error bars showing deviation from the mean, with a representative western blot shown in (F).

Next, to determine whether BFA treatment impaired LCMV RNA synthesis, we quantified S segment vRNA abundance during a single-round of infection, as above, achieved by limiting the time frame of analysis up to 12 hpi. rLCMV-eGFP infected cells were harvested for RNA extraction at 1, 6 and 12 hpi, with S segment vRNA abundance determined by qRT-PCR analysis, with the 1 hpi timepoint used to normalise variation in input vRNA quantity. This analysis revealed no significant difference in S segment vRNA abundance for any timepoint analysed between BFA treated and untreated samples (S vRNA; 6 hpi [$P = 0.104729$]; 12 hpi [$P = 0.061214$]) (Figure 2.7B). Thus, we conclude that BFA has no detectable effect on vRNA production within a single-round of infection.

Time-of-addition experiments suggest BFA treatment has no significant impact on LCMV NP production.

To corroborate our finding that BFA treatment had little or no impact on either LCMV gene expression or RNA synthesis, we performed time-of-addition (TOA) experiments, with BFA added to cultures at various times post infection. Cells were infected with LCMV-eGFP with an MOI of 5, then treated with BFA at time points of 0, 2, 4, 6 and 10 hpi, with sampling restricted to a 12 hpi window, chosen to span a single LCMV multiplication cycle [32], as above (Figure 2.7A and B). Impact of BFA treatment was first assessed by determining the eGFP cell count within infected cultures, measured by live cell fluorescence imaging and normalised for confluency over three independent experimental repeats (Figure 2.7C and D), with BFA treatment causing no significant decrease in eGFP expression.

As an orthogonal approach, we also assessed NP expression from TOA cultures (MOI of 5), with all lysates harvested at 12 hpi regardless of BFA-treatment times and analysed by Western blotting using NP antisera. Quantification of three independent experimental repeats (Figure 2.7E and F) revealed that LCMV NP expression was not significantly diminished by BFA treatment at any of the timepoints, even when BFA was present from the entire experimental period, from 0 hpi (Figure 2.7E; compare untreated and 0 hpi data points). Thus, the addition of BFA at temporally distinct phases of a single LCMV infection cycle had no significant impact on gene expression.

BFA treatment inhibits infectious virus assembly and release.

The results presented above showed BFA treatment of rLCMV-eGFP infected cells resulted in no significant change in LCMV NP expression (Figure 2.7E and F). Next, the affects of BFA treatment on infectious virus release were assessed. As for the previous experiments where gene expression was examined, we wanted to assess virus release during a single round of infection only. To achieve this, we performed a classical virus growth experiment with A549 cultures infected with LCMV-eGFP at an MOI of 5, with or without BFA pre-treatment, with supernatants harvested at 12 hpi when infectious virus is first released [32]. Supernatants were also harvested at additional 16, 20 and 24 hpi timepoints for completeness, and viral titres calculated by FFA represented relative to the untreated 24 hpi sample (Figure 2.8A), with the actual titres tabulated alongside (Figure 2.8B). In BFA treated cultures (Figure 2.8A; red data points) the titres at all timepoints were consistently less than 1% of the untreated control (Figure 2.8A; blue data points) (BFA viral titres; 12 hpi 0.62% [$P = 0.000006872$]; 16 hpi 0.49% [$P = 0.000004219$]; 20 hpi 0.26% [$P = 0.000000364$]; 24 hpi 0.21% [$P = 0.000000316$]) thus showing BFA treatment exerts major influence on virion production, with mean titres reduced by over 46-fold at the 12 hpi time point increasing to over 646-fold at 24 hpi (Figure 2.8B), with representative FFAs shown in Figure 2.8C.

Taken together, these data suggested that LCMV gene expression and vRNA production were not significantly affected by BFA treatment. In contrast, BFA treatment exerted major influence the production of infectious virus, suggesting an important role for COPI and AP-4 complexes in this process.

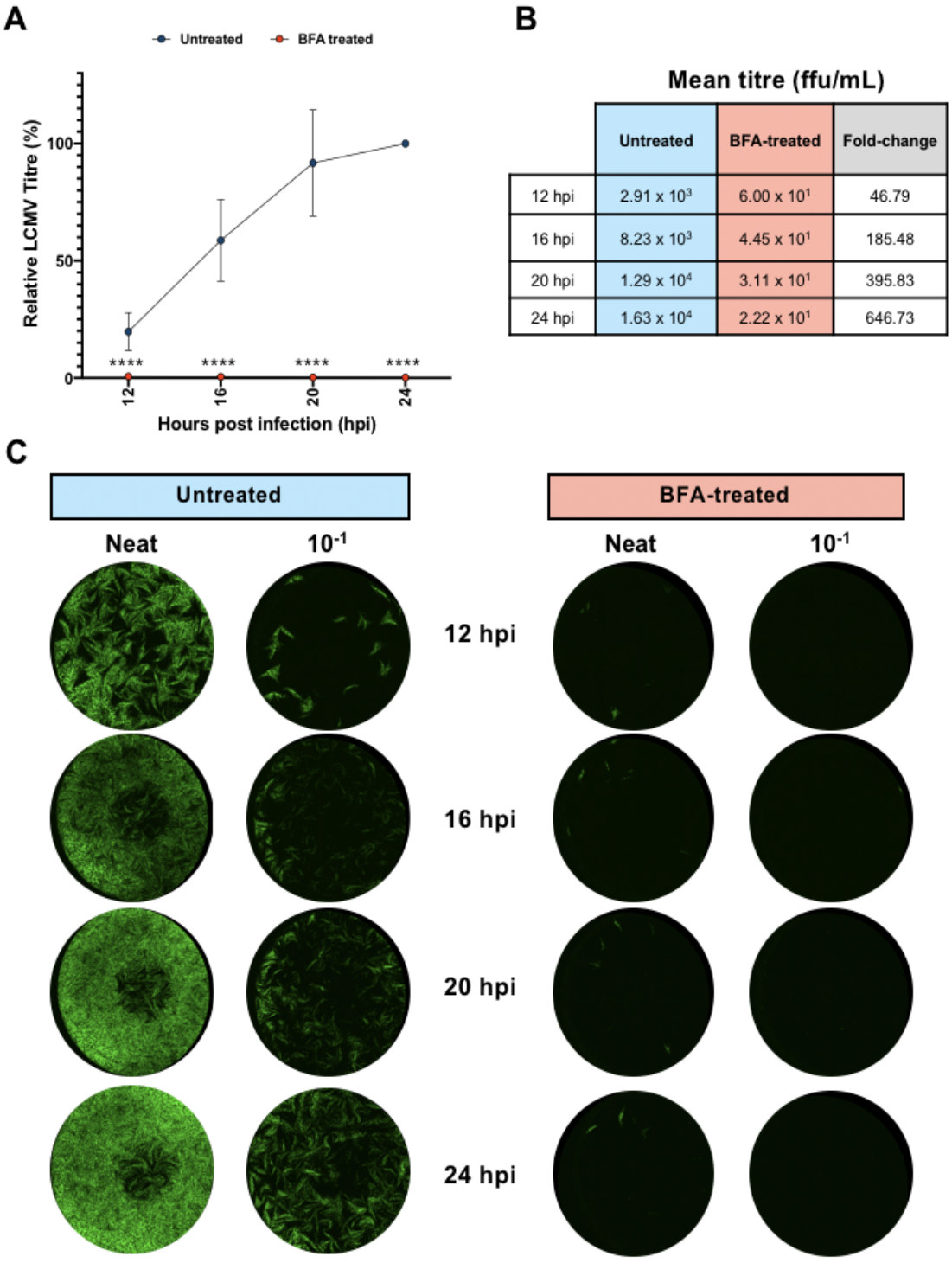

Figure 2.8: BFA-treatment has a major impact on LCMV growth. (A) A549 cells were either untreated or pre-treated with BFA (5000 ng/mL) and then infected with rLCMV-eGFP at an MOI of 5. At the indicated times post infection, viral supernatants were collected and subjected to titration via FFA, with titres from three experimental repeats plotted alongside the indicated timepoint, normalised to the 24 hpi untreated control, with error bars showing deviation from the mean. (B) Tabulated mean viral titres (ffu/mL) for three independent experimental repeats for supernatants harvested at 12, 16, 20 and 24 hpi, for both untreated (blue) and BFA-treated (red) conditions, with the mean fold-change ratio of untreated/BFA-treated, also shown. (C) Representative images of FFA wells, for both untreated and BFA-treated cultures, at dilutions of neat, and 10^{-1}

2.5 Discussion

Here, we used rLCMV-eGFP for identification of host cell trafficking factors required for LCMV multiplication, with measurement of virus-specific eGFP expression allowing high-throughput screening of siRNA-mediated gene knock down of host cellular genes on various stages of the LCMV multiplication cycle.

The siRNA screen comprised 261 siRNAs, specific for 87 target genes, and revealed an important role for multiple cellular factors, of which multiple components of AP-4 and COPI coatomer complexes were highly ranked, judged by the impact of expression knock down on virus-specific eGFP expression (Figure 2.1). Corroborating the importance of COPI and AP-4 components, ARF-1, and GBF-1, required by both AP-4 and COPI complexes for anchorage to Golgi membranes [43], were also high-ranking in terms of LCMV gene expression knock down. AP4M1 is one of four components of the AP4 complex that perform native cellular roles in trafficking of cargo proteins from the TGN to the plasma membrane [38], whereas COPA is one of seven components of the COPI complex, with well-characterised involvement in Golgi-ER retrograde transport and intra-Golgi trafficking, but also expression of cell surface receptors and maturation of early endosome to autophagic vacuoles [44]. To gain a better understanding of AP-4 and COPI involvement in the LCMV multiplication cycle, we generated a recombinant LCMV mutant rLCMV-GP1-FLAG containing a FLAG-tagged epitope within GP-1, which alongside our existing NP antisera allowed the spatial cellular distribution of these viral components to be examined alongside AP-4 and COPI complexes within virus-infected cells. First, using this virus we showed LCMV GP-1 was predominantly located within the Golgi compartment. This was distinct from NP staining, which was dispersed more widely throughout the cytoplasm, while also sharing some Golgi localization.

Next, we examined the cellular localisation of AP4E1, NP and GP-1, which showed virus infection led to redistribution of AP4E1 away from its characteristic *trans*-Golgi location, to occupy regions of the cell where GP-1 and in particular NP was most abundant, suggestive of a close interaction between these components. Selection of AP-4 cargo is known to be mediated through binding of a YXXØ or dileucine based motifs [(D/E)XXXL(L/I) and (LL/LI)] within the cytoplasmic tail

of cargo proteins to the AP4M1 subunit [38, 45]. LCMV NP has three YXXØ and eleven LCMV dileucine based motifs; GPC has six YXXØ and ten dileucine based motifs, although none lie within the predicted cytoplasmic tails, despite these tail domains being crucial in GP-1/GP-2 trafficking to the plasma membrane [46]. One possibility is that NP-mediated redistribution of AP-4 could be mediated by components of the GPC, for instance during transport of partially assembled RNPs in association with GPC components to a plasma membrane assembly site.

Currently there are many reports of viral subversion of members of the adapter protein complexes (AP1-5), although with few reports of viral roles specifically for the AP-4 complex [39, 47]. In the case of Hepatitis C virus (HCV), mutational studies showed that the HCV NS2 protein binds to the AP4M1 subunit via its dileucine motifs. When these motifs were mutated, HCV RNA replication was not impaired, yet extracellular viral titres were reduced [45]. This study also implicated AP-4 in promoting direct cell-to-cell spread [45]. Another example of viral AP-4 subversion is for Epstein-Barr virus (EBV) of the *Herpesviridae* family, which encodes a transmembrane glycoprotein BMRF-2 that has previously been shown to interact with the μsubunit of AP-4, permitting BMRF-2 trafficking from the TGN to the basolateral plasma membrane and thus EBV egress [48].

This study also focussed on the COPI coatomer complex, with knock down of two of its substituent components, COPA and COPB1, resulting in an approximately 50% reduction in LCMV-mediated eGFP expression within the siRNA screen protocol. Although components of COPI complexes have previously been described as important for the LCMV replication [49], this is the first report of COPI component involvement in a neuronal cell line that is relevant to the LCMV replication cycle. As described above for AP-4, using rLCMV-GP1-FLAG allowed examination of GP-1 and NP localization in relation to COPI components. This analysis revealed a high degree of colocation between COPA and NP in both dense puncta and also a more dispersed cytoplasmic distribution, as well as close co-localization between GP-1 and COPA, although within a more restricted region, characteristic of the Golgi. Taken together these findings are entirely consistent with COPI components playing important roles in virion assembly and egress, corroborating the results of the siRNA knock down analysis.

Also supportive of a role for COPI in LCMV multiplication was the finding that

BFA pre-treatment of infected cells resulted in no significant reduction in LCMV NP expression, within a single infectious cycle (Figure 2.7E) but almost 50-fold reduction in infectious virion production over the same period (Figure 2.8A and B), indicating a role for COPI and AP-4 complexes in the release of infectious virus. It is well-established that LCMV GPC is cleaved to GP-1/GP-2/SSP trimers by host cell protease SKI-1/S1P within the Golgi [26] and so one possibility is that canonical COPI complexes are utilised for intra-Golgi and retrograde Golgi-ER trafficking [50] that may be required for efficient GPC proteolytic processing.

The use of siRNA mediated depletion or BFA treatment has provided many examples where COPI components are required for efficient virus multiplication [44], with many examples from within the *Bunyavirales* order. We have previously reported a reliance on COPI complexes and ARF-1 involvement for the bunyavirus Hazara virus (HAZV), which is a species within the *Nairoviridae* family [33], a group that share many genetic and functional characteristics with the arenaviruses [51]. We showed HAZV requires COPI complexes in both ARF-I dependent and ARF-I independent processes, at early and late stages of the multiplication cycle [33], respectively. Particularly prominent was an influence of BFA on infectious virus production, similar to our current findings for LCMV. In addition to this, and likely related to COPI complex involvement, Uukuneimi virus, a member of the *Phenuiviridae* family within the *Bunyavirales* order, has been shown to require GBF-1 activation, and thus ARF-1 activation, for viral replication and particle assembly [52]. It is therefore possible that COPI complex involvement is a common requirement for all bunyaviruses. Whether this relates to a critical reliance on entirely functioning Golgi compartment for formation of the bunyaviral factory, or a more general requirement for the formation of other lipid-based compartments that depend on COPI complex activity is an interesting topic for future research [53, 54].

Collectively, our findings improve the understanding of arenaviruses host-pathogen interactions and reveal the involvement of important cellular trafficking pathways required during infection. Moreover, this study may lead to the discovery of novel therapeutic targets for arenaviruses to prevent serious human disease.

2.6 Materials and Methods

2.6.1 Plasmid design

Plasmids for rLCMV-WT and rLCMV-eGFP viral rescue were previously generated and described [32]. rLCMV-GP1-FLAG plasmid was generated by first performing sequence alignment of GP-1 alongside closely related OW arenaviruses to select a location for FLAG tag insertion. The predicated structure of GP-1 for rLCMV-GP1-FLAG was investigated using SWISS-MODEL and mapped alongside the solved LCMV GP-1 structure, which showed the FLAG insertion site to be within an unsolved flexible loop of GP-1, likely accessible for antibody recognition. rLCMV-GP1-FLAG was generated by insertion PCR utilising Q5 site-directed mutagenesis kit (New England BioLabs) and FLAG primers, according to the manufacturer's instructions. Positive colonies were verified via colony PCR and DNA sequencing (Genewiz).

2.6.2 Recovery of rLCMV-WT, rLCMV-eGFP and rLCMV-GP1-FLAG

Recovery of infectious variants of LCMV has previously been described [32], based on the work of the de la Torre group [55]. In brief, six-well plates were seeded with 2 x 10^5 BSR-T7/well 1 day prior to transfection in 2 mL of Dulbecco modified Eagle medium (DMEM) supplemented with 2.5% fetal bovine serum (FBS), 100 U/mL penicillin and 100 µg/mL streptomycin (2.5% DMEM). After 24 h, the cells were transfected with 1.6 µg pUC57-S-WT, 1.6 µg pUC57-NP (+), 2.8 µg pUC57-L, 2.0 µg pUC57-L (+) and 0.6 µg pCAG-T7pol, combined with 2.5µL of Mirus TransIT-LT1 transfection reagent (Mirus Bio) per µg of DNA, in 200µL of Opti-MEM. For rLCMV-eGFP recovery, the WT plasmid was replaced with pUC57-S-eGFP. A control sample, in which pUC57-L and pUC57-L (+) was omitted, was included for each virus recovery experiment. At 24 hours post transfection (hpt), media containing the transfection mix was removed and replaced with fresh 2.5% DMEM. Reinfection of fresh monolayers was carried out in six-well plates seeded with 2×10^5 BHK cells/well 1 day prior to infection in 2 mL of DMEM supplemented with

2.5% FBS, 100 U/mL penicillin and 100µg/mL streptomycin. Fresh BHK cells were washed with phosphate-buffered saline (PBS) twice prior to infection. Supernatants from transfected BSR-T7 cells were collected at 120 hpt, centrifuged at 4000 x *g* for 15 min and 1 mL used to infect fresh BHK cells in a 6-well plate in DMEM with 2.5% FBS. Cell supernatant from infected BHK cells was collected at 72 hours post infection (hpi), centrifuged at 4000 x *g* for 15 min and viral stocks were stored as aliquots at -80°C. This protocol was followed for successful recovery of the newly developed mutant rLCMV-GP1-FLAG, with the S plasmid of LCMV being replaced with the recently generated pUC57-RQ-S-FLAG. The viral supernatant gained from successful infection following transfection was centrifuged at 4000 x *g*, aliquoted (80 µL) and frozen for subsequent viral titration and bulking.

2.6.3 Virus infections

For the generation of a bulk stock of rLCMV-GP1-FLAG, a T175 flask was seeded with 5 x 10^6 BHK-21 cells one day prior to infection at an MOI 0.001. At 3 days post infection, viral supernatant was harvested and centrifuged at 4000 x *g* to remove cell debris, aliquoted (80 µL) and frozen for subsequent viral titration. For viral infections, cell monolayers were infected with LCMV at the specified MOI in either serum-free (SFM), 2.5% or 10% FBS DMEM, depending on cellular requirements, at 37°C. After 1 h, the inoculum was removed and SFM, fresh 2.5% or 10% DMEM was then applied for the duration of the infection. For synchronised infections, LCMV incubated on ice for 1 h to facilitate adsorption. Subsequently, the inoculum was removed, monolayers washed three times with PBS and SFM, fresh 2.5% or 10% DMEM was then applied for the duration of the infection.

2.6.4 Virus titration

Virus titres were determined by focus forming assays. Viral stocks requiring titration were serially diluted in SFM to infect fresh monolayers of BHK cells seeded at 1 x 10^5 in a 24 well-plate and incubated at 37°C for 1 h. After infection, medium containing virus was removed and 2 mL of overlay containing 10% FBS DMEM and 1.6% methylcellulose at a 1:1 ratio was reapplied to cells, then incubated for a further 3 days at 37°C. For rLCMV-eGFP titration, whole-well images were taken using an

Incucyte S3 live cell imaging system (Sartorius) and rLCMV-eGFP foci were then counted and virus titres were determined as focus forming units/mL (FFU/mL). For rLCMV-WT titration, cells were fixed using 4% (vol/vol) paraformaldehyde (PFA) for 15 min and washed three times with PBS. Cells were then incubated with permeabilisation buffer (0.1% [vol/vol] Triton X-100, 2% [wt/vol] FBS in 1 x PBS) for a further 15 min and washed three times with PBS. After permeabilisation, cells were incubated with 1 mL blocking buffer (2% [wt/vol] FBS in PBS) for 1 h, then incubated for 1 h with 150 µL/well LCMV NP primary antibody (in-house, 1:1000 in blocking buffer), and washed three times with PBS. Following this, cells were incubated for 1 h with 594 Alexa Fluor secondary antibody (Life Technologies; 1:500 in blocking buffer) and washed four times with PBS. The Incucyte S3 live cell imaging system (Sartorius) was then used to image whole wells of the plate to detect red rLCMV-WT foci, which were counted, and virus titres determined. For rLCMV-FLAG titration, cells were also stained with 150 µL/well FLAG (Sigma, 1:500 in blocking buffer) primary antibody and 488 (FLAG) Alexa Fluor secondary antibody (Life Technologies; 1:500 in blocking buffer), then washed and imaged as described above.

2.6.5 Reverse transfection of siRNA library

Trypsinised SH-SY5Y cells in 10% FBS DMEM were counted using a haemocytometer and used to make a cell suspension containing 1 x 10^5 cells/mL. A master mix was made resulting in 0.3 µL of Lipofectamine RNAiMAX reagent (Invitrogen) and 16.7 µL of Opti-MEM per well and 17 µL of this master mix was pipetted into each well of a 96-well plate. All siRNAs were taken from the 'silencer' human membrane trafficking siRNA library (thermo). A 3 µL volume of working stock siRNA (1 µM) was pipetted into the transfection master mix and mixed, resulting in a final concentration of 3 pmol of siRNA per well. Transfection master mix and siRNA were incubated for 20 min, following which 1 × 10^5 cells in 10% DMEM (100 µL total volume) was then applied per well. Cells were incubated with the transfection and siRNA mix for 24 h at 37°C, following which 60 µL of the medium was removed and replaced with 200 µL of fresh 10% FBS DMEM to dilute out any potential toxic effects of the siRNAs or transfection reagent. At 6 h post dilution, the medium was removed, and cells were washed in PBS prior to

infection with rLCMV-eGFP at an MOI of 0.2 in 100 µL of 10% FBS DMEM for 1 h. Following infection, virus was removed, and cells were washed twice with PBS to remove any unbound virus, then supplemented with 200 µL 10% FBS DMEM. At 24 hpi, eGFP fluorescence intensity was determined using the Incucyte S3 live cell imaging software as a measure of virus multiplication. The total integrated intensity of eGFP (TIIE; green count units [GCU] × μm^2/image) was first normalised to confluency per well and then analysed as a percentage of the total green integrated intensity in positive control wells containing virus and lipofectamine but omitting siRNA. Normalised values were averaged between four experimental repeats.

2.6.6 Immunofluorescence (confocal microscopy)

Trypsinised A549 cells were seeded onto a 19-mm round glass coverslip (VWR) in a 12-well plate at 1 x 10^5 cells/well, followed by incubation at 37°C. After 14 h, BFA was added to cells (5000 ng/mL) for 1 h prior to fixation. For IF (omitting AP4E1, see below), cells were washed twice in PBS prior to fixation in 4% (vol/vol) paraformaldehyde in PBS for 15 min at room temperature. After fixation, the cells were washed three times in PBS and then incubated in permeabilisation buffer (0.1% [vol/vol] Triton X-100, 1% [wt/vol] bovine serum albumin [BSA] in PBS) for 15 min at room temperature. Following permeabilisation, the monolayers were washed three times with PBS and incubated with blocking buffer (1% [wt/vol] BSA in PBS) for 1 h. Subsequently, primary antibody was diluted in BSA blocking buffer as follows: NP (1:500, in house [sheep]), FLAG (Sigma; 1:250 [mouse]) and COPA primary antibody (GeneTex; 1:100 [rabbit]) and incubated for 1 h at room temperature. The cells were then washed three times with PBS and incubated with corresponding Alexa Fluor 488, 594 and 647 secondary antibodies (Life Technologies; 1:500 in BSA blocking buffer) for 1 h at room temperature in a light protected vessel. Cell monolayers were then washed three times with PBS and mounted onto glass coverslips with the addition of Prolong Gold Antifade reagent with DAPI (Thermo Fisher Scientific), cured, sealed and stored at 4°C. Images were then taken on an LSM 880 confocal microscope (Zeiss) and processed using Zen (Blue Edition) software and Fiji (Image J). Line scan analysis was performed utilising Zen (Blue Edition).

For AP4E1 IF, cells were washed twice with PBS and fixed with 100% methanol for 5 min on ice. After fixation, the cells were washed three times in PBS and then incubated with blocking buffer (0.1% [wt/vol] Saponin, 1% [wt/vol] BSA in PBS) for 30 min. Subsequently, primary antibodies diluted in saponin/BSA blocking buffer containing NP (1:500, in house [sheep]), FLAG (Sigma; 1:250 [rabbit]) and AP4E1 primary antibody (BD Biosciences; 1:75 [mouse]) was incubated for 1 h at room temperature. The cells were then washed three times with PBS and incubated with corresponding Alexa Fluor 488, 594 and 647 secondary antibodies (Life Technologies; 1:500 in saponin/BSA blocking buffer) for 1 h at room temperature in a light protected vessel. Cell monolayers were then washed three times with PBS and mounted onto glass coverslips with the addition of Prolong Gold Antifade reagent with DAPI (Thermo Fisher Scientific), cured, sealed and stored at 4°C. Images were then taken on an LSM 880 confocal microscope and processed as described above.

2.6.7 Inhibition of retrograde transport

Trypsinised A549 cells were seeded into 24-well plates at 1 x 10^5 cells/well and incubated at 37°C. After 16 to 24 h, the cells were pre-treated with BFA at the indicated concentration for 45 min in SFM. Following this, rLCMV, rLCMV-eGFP, A/WSN/33 H1N1 (denoted as rIAV herein) and rIAV-eGFP was added directly to each well at an MOI of 0.1. For WT viruses, 24 hpi cells were lysed for analysis via western blotting. Densitometry was performed using Fiji software and NP expression normalised to confluency per well, then analysed as a percentage of virus only DMSO control. Normalised values were averaged between three biological repeats for WT viruses (n=3). For eGFP viruses, at 24 hpi the Incucyte S3 live cell imaging system (Sartorius) was utilised to measure eGFP fluorescence. The total integrated intensity of eGFP (TIIE; green count units [GCU] × µm2/image) was first normalized to confluency per well and then analysed as a percentage of the total green integrated intensity in virus only DMSO control. Normalized values were averaged between three biological repeats for eGFP mutant virus (n=3). For titration following BFA treatment, viral supernatant was collected for mock, virus, 50, 500 and 5000 ng/mL. Focus forming assays were performed for each BFA condition as previously described for LCMV-eGFP (n=3).

2.6.8 Temporal kinetic analysis of inhibition of retrograde transport

For gene expression analysis, trypsinised A549 cells were seeded into 12-well plates at 1 x 10^5 cells/well and incubated at 37°C. After 16 to 24 h, the cells were pre-treated with BFA at 5000 ng/mL for 45 min. Following this, rLCMV-eGFP was added directly to each well at an MOI of 1 and 5. Incucyte S3 live cell imaging system (Sartorius) was utilised to measure eGFP fluorescence at hourly intervals. The total integrated intensity of eGFP (TIIE; green count units [GCU] × µm^2/image) was first normalized to confluency per well and then analysed as a percentage of the total green integrated intensity for untreated 24 hpi control. Normalized values were averaged between three biological repeats (n=3).

For qPCR analysis, A549 cells were seeded into a 12-well plate at 1.5 x 10^5 cells/well. Following 16-24 h cells were pre-treated with BFA at 5000 ng/mL for 45 min. Subsequently, drug media was collected, and cells were infected at an MOI of 5 with rLCMV-WT in minimum volume 10% FBS DMEM media (250 µL) for 1 h. Following this, infection media was removed, and monolayers washed four times with 1 x PBS, and drug media replaced. At each indicated timepoint, cells lysates were washed with 1 x PBS, trypsinised and pelleted (500 x *g*) for 5 mins. RNA extraction was performed following the manufacturer's instructions for Monarch Total RNA Miniprep Kit (New England BioLabs). Two step qPCR was carried out firstly by converting RNA into cDNA following the manufacturer's instruction for LunaScript RT SuperMix Kit (New England BioLabs). Subsequently, qPCR was performed using the cDNA following the manufacturer's instructions for Luna Universal qPCR Master Mix. Analysis of S segment vRNA expression via qPCR for mock and virus (MOI 5) in untreated and BFA-treated conditions was performed, alongside GAPDH as the house keeping control. The primer sequences used were as follows: S vRNA (5' - CAG CCA ACA ACT CCC ACC AT - 3' and 5' - GAA GGC AGA GGT CAG ATT GCA - 3') and GAPDH (5' - TCA CCA CCA TGG AGA AGG CT – 3' and 5' - GCC ATC CAC AGT CTT CTG GG – 3'). vRNA levels, for each timepoint, in untreated and BFA treated were normalised for their respective input (1 hpi). Normalised values were averaged between four experiment repeats.

For viral titration, A549 cells were seeded into a 12-well plate at 1 x 10^5 cells/well. Following 16-24 h cells were pre-treated with BFA at 5000 ng/mL for 45 min. Subsequently, drug media was collected, and cells were infected at an MOI of 5 with rLCMV-eGFP in minimum volume 10% FBS DMEM media (250 µL) for 1 h. Following this, infection media was removed, and monolayers washed four times with 1 x PBS, and drug media replaced. At each indicated timepoint, viral supernatants were collected and titre via FFA for each untreated and BFA-treated sample, as previously described for LCMV-eGFP (n=3). Each sample was normalised against untreated 24 hpi titre and averaged between three biological repeats.

2.6.9 Time-of-addition addition experiments

Trypsinised A549 cells were seeded into 12-well plates at 1 x 10^5 cells/well and incubated at 37°C. Following 16-24 h, for the 0 hpi timepoint, cells were pre-treated with 500 µL BFA at 5000 ng/mL for 45 min. Subsequently, cells were infected with rLCMV-eGFP at an MOI of 5 in 500 µL in 10% FBS DMEM media. Of note, for the 0 hpi timepoint, the 500 µL virus infection media was made in 5000 ng/mL BFA media. For each timepoint, 500 µL of BFA at 10000 ng/mL was added to each well (1:1) to give a final concentration of 5000 ng/mL. At 12 hpi, for eGFP fluorescence was imaged, cell lysates harvested, and viral supernatants collected.

The eGFP was determined using the Incucyte S3 live cell imaging software. Total green cell count was recorded, normalised to confluency per well and then analysed as a percentage of untreated control. Normalised values were averaged between three biological repeats (n=3). Cells were lysed for analysis via western blotting. Densitometry was performed using Fiji software and NP expression normalised to confluency per well, then analysed as a percentage of untreated control. Normalised values were averaged between three biological repeats (n=3). Titre was calculated via FFA for each BFA time-of-addition, as previously described for LCMV-eGFP. Each sample was normalised against the untreated control, and averaged between three biological repeats (n=3).

2.7 Acknowledgements

We acknowledge funding from MRC grant MR/T016159/1 in support of JNB, JF, AS and HNT, BBSRC PhD studentship grant to AS, UKHSA PhD studentship grant to OB, and Wellcome trust studentship 102174/B/13/Z to EJAAT. BAR was supported by EU Marie Skłodowska-Curie Actions (MSCA) Innovative Training Network (ITN) H2020-MSCA-ITN-2016, grant agreement 721367 (HONOURS). The authors thank Dr Ruth Hughes and Dr Sally Boxall of the bioimaging facility, Faculty of Biological Sciences, University of Leeds, for their expert assistance and use of the Zeiss LSM880 confocal microscope, funded by Wellcome Trust grant WT104918MA. We also acknowledge Wellcome trust equipment grant 221538/Z/20/Z, which supports the use of the Incucyte live cell imaging platform.

2.8 References

[1] International Committee on Taxonomy of Viruses (ICTV). Taxonomy [online]. 2019 [accessed 2023 May 12]. https://talk.ictvonline.org/taxonomy/

[2] Centers for Disease Control and Prevention (CDC). Viral Hemorrhagic Fevers. Bunyavirales. [online]. [accessed 2023 May 12]. https://www.cdc.gov/vhf/virus-families/bunyaviridae.htmL

[3] Sheli R. Radoshitzky, Michael J. Buchmeier, Juan Carlos de la Torre. Fields Virology. 7th ed. Peter M. Howley, David M. Knipe, Sean P.J. Whelan, editors. Wolters Kluwer; 2021.

[4] Richmond JK, Baglole DJ. Lassa fever: epidemiology, clinical features, and social consequences. BMJ (Clinical research ed.). 2003;327(7426):1271–5. doi:10.1136/bmj.327.7426.1271

[5] Stanley A. Plotkin, Walter A. Orenstein, Paul A. Offit, Kathryn M. Edwards, Errnvphglfrv Ruj. Plotkin's Vaccines. Elsevier; 2018. doi:10.1016/C2013-0-18914-3

[6] Cheng BYH, Nogales A, de la Torre JC, Martínez-Sobrido L. Development of live-attenuated arenavirus vaccines based on codon deoptimization of the viral glycoprotein. Virology. 2017;501:35–46. doi:10.1016/j.virol.2016.11.001

[7] Bonthius DJ. The Arenaviruses. In: Neurotropic Viral Infections. Cham: Springer International Publishing; 2016. p. 149–174. doi:10.1007/978-3-319-33133-1_6

[8] Bonthius DJ, Nichols B, Harb H, Mahoney J, Karacay B. Lymphocytic choriomeningitis virus infection of the developing brain: critical role of host age. Annals of Neurology. 2007;62(4):356–374. doi:10.1002/ana.21193

[9] Bonthius DJ. Lymphocytic Choriomeningitis Virus: An Underrecognized Cause of Neurologic Disease in the Fetus, Child, and Adult. Seminars in Pediatric Neurology. 2012;19(3):89–95. doi:10.1016/j.spen.2012.02.002

[10] Meyer BJ, de la Torre JC, Southern PJ. Arenaviruses: genomic RNAs, transcription, and replication. Current topics in microbiology and immunology. 2002;262:139–57. doi:10.1007/978-3-642-56029-3_6

[11] Maria S. Salvato. Arenaviridae. In: Virus Taxonomy. Elsevier; 2012. p. 715–723. doi:10.1016/B978-0-12-384684-6.00058-6

[12] Riviere Y, Ahmed R, Southern PJ, Buchmeier MJ, Dutko FJ, Oldstone MB. The S RNA segment of lymphocytic choriomeningitis virus codes for the nucleoprotein and glycoproteins 1 and 2. Journal of virology. 1985;53(3):966–8. doi:10.1128/JVI.53.3.966-968.1985

[13] Hastie KM, Zandonatti MA, Kleinfelter LM, Heinrich ML, Rowland MM, Chandran K, Branco LM, Robinson JE, Garry RF, Saphire EO. Structural basis for antibody-mediated neutralization of Lassa virus. Science. 2017;356(6341):923–928. doi:10.1126/science.aam7260

[14] Hastie KM, Cross RW, Harkins SS, Zandonatti MA, Koval AP, Heinrich ML, Rowland MM, Robinson JE, Geisbert TW, Garry RF, et al. Convergent Structures Illuminate Features for Germline Antibody Binding and Pan-Lassa Virus Neutralization. Cell. 2019;178(4):1004-1015.e14. doi:10.1016/j.cell.2019.07.020

[15] Moon-Walker A, Zhang Z, Zyla DS, Buck TK, Li H, Diaz Avalos R, Schendel SL, Hastie KM, Crotty S, Saphire EO. Structural basis for antibody-mediated neutralization of lymphocytic choriomeningitis virus. Cell Chemical Biology. 2023;30(4):403-411.e4. doi:10.1016/j.chembiol.2023.03.005

[16] Cao W, Henry MD, Borrow P, Yamada H, Elder JH, Ravkov E V, Nichol ST,

Compans RW, Campbell KP, Oldstone MB. Identification of alpha-dystroglycan as a receptor for lymphocytic choriomeningitis virus and Lassa fever virus. Science (New York, N.Y.). 1998;282(5396):2079–81. doi:10.1126/science.282.5396.2079

[17] Shimojima M, Kawaoka Y. Cell surface molecules involved in infection mediated by lymphocytic choriomeningitis virus glycoprotein. The Journal of veterinary medical science. 2012;74(10):1363–6. doi:10.1292/jvms.12-0176

[18] Iwasaki M, Ngo N, de la Torre JC. Sodium hydrogen exchangers contribute to arenavirus cell entry. Journal of virology. 2014;88(1):643–54. doi:10.1128/JVI.02110-13

[19] Pasqual G, Rojek JM, Masin M, Chatton J-Y, Kunz S. Old World Arenaviruses Enter the Host Cell via the Multivesicular Body and Depend on the Endosomal Sorting Complex Required for Transport. PLoS Pathogens. 2011;7(9):e1002232. doi:10.1371/journal.ppat.1002232

[20] Bakkers MJG, Moon-Walker A, Herlo R, Brusic V, Stubbs SH, Hastie KM, Saphire EO, Kirchhausen TL, Whelan SPJ. CD164 is a host factor for lymphocytic choriomeningitis virus entry. Proceedings of the National Academy of Sciences of the United States of America. 2022;119(10):e2119676119. doi:10.1073/pnas.2119676119

[21] Modrow S, Falke D, Truyen U, Schätzl H. Molecular Virology. Berlin, Heidelberg: Springer Berlin Heidelberg; 2013. doi:10.1007/978-3-642-20718-1

[22] Baird NL, York J, Nunberg JH. Arenavirus infection induces discrete cytosolic structures for RNA replication. Journal of virology. 2012;86(20):11301–10. doi:10.1128/JVI.01635-12

[23] Burri DJ, Pasquato A, da Palma JR, Igonet S, Oldstone MBA, Kunz S. The role of proteolytic processing and the stable signal peptide in expression of the Old World arenavirus envelope glycoprotein ectodomain. Virology. 2013;436(1):127–33. doi:10.1016/j.virol.2012.10.038

[24] Lenz O, ter Meulen J, Klenk HD, Seidah NG, Garten W. The Lassa virus glycoprotein precursor GP-C is proteolytically processed by subtilase SKI-1/S1P. Proceedings of the National Academy of Sciences of the United States of America. 2001;98(22):12701–5. doi:10.1073/pnas.221447598

[25] Freigang S, Eschli B, Harris N, Geuking M, Quirin K, Schrempf S, Zellweger

R, Weber J, Hengartner H, Zinkernagel RM. A lymphocytic choriomeningitis virus glycoprotein variant that is retained in the endoplasmic reticulum efficiently cross-primes CD8(+) T cell responses. Proceedings of the National Academy of Sciences of the United States of America. 2007;104(33):13426–31. doi:10.1073/pnas.0704423104

[26] Beyer WR, Pöpplau D, Garten W, von Laer D, Lenz O. Endoproteolytic processing of the lymphocytic choriomeningitis virus glycoprotein by the subtilase SKI-1/S1P. Journal of virology. 2003;77(5):2866–72. doi:10.1128/jvi.77.5.2866-2872.2003

[27] Perez M, Craven RC, de la Torre JC. The small RING finger protein Z drives arenavirus budding: implications for antiviral strategies. Proceedings of the National Academy of Sciences of the United States of America. 2003;100(22):12978–83. doi:10.1073/pnas.2133782100

[28] Capul AA, Perez M, Burke E, Kunz S, Buchmeier MJ, de la Torre JC. Arenavirus Z-Glycoprotein Association Requires Z Myristoylation but Not Functional RING or Late Domains. Journal of Virology. 2007;81(17):9451–9460. doi:10.1128/JVI.00499-07

[29] Funston GM, Kallioinen SE, de Felipe P, Ryan MD, Iggo RD. Expression of heterologous genes in oncolytic adenoviruses using picornaviral 2A sequences that trigger ribosome skipping. Journal of General Virology. 2008;89(2):389–396. doi:10.1099/vir.0.83444-0

[30] Donnelly MLL, Luke G, Mehrotra A, Li X, Hughes LE, Gani D, Ryan MD. Analysis of the aphthovirus 2A/2B polyprotein 'cleavage' mechanism indicates not a proteolytic reaction, but a novel translational effect: a putative ribosomal 'skip.' Journal of General Virology. 2001;82(5):1013–1025. doi:10.1099/0022-1317-82-5-1013

[31] Kim JH, Lee S-R, Li L-H, Park H-J, Park J-H, Lee KY, Kim M-K, Shin BA, Choi S-Y. High Cleavage Efficiency of a 2A Peptide Derived from Porcine Teschovirus-1 in Human Cell Lines, Zebrafish and Mice. PLoS ONE. 2011;6(4):e18556. doi:10.1371/journal.pone.0018556

[32] Shaw AB, Tse HN, Byford O, plahe grace, Moon-Walker A, Saphire EO, Whelan SPJ, Mankouri J, Fontana J, Barr JN.

Cellular endosomal potassium ion flux regulates arenavirus uncoating during virus entry. bioRxiv. 2023 Jan 1:2023.06.23.546275. http://biorxiv.org/content/early/2023/06/26/2023.06.23.546275.abstract. doi:10.1101/2023.06.23.546275

[33] Fuller J, Álvarez-Rodríguez B, Todd EJAA, Mankouri J, Hewson R, Barr JN. Hazara Nairovirus Requires COPI Components in both Arf1-Dependent and Arf1-Independent Stages of Its Replication Cycle. Journal of Virology. 2020;94(17). doi:10.1128/JVI.00766-20

[34] Deng Y, Golinelli-Cohen M, Smirnova E, Jackson CL. A COPI coat subunit interacts directly with an early-Golgi localized Arf exchange factor. EMBO reports. 2009;10(1):58–64. doi:10.1038/embor.2008.221

[35] Boehm M, Aguilar RC, Bonifacino JS. Functional and physical interactions of the adaptor protein complex AP-4 with ADP-ribosylation factors (ARFs). The EMBO journal. 2001;20(22):6265–76. doi:10.1093/emboj/20.22.6265

[36] Beck R, Ravet M, Wieland FT, Cassel D. The COPI system: Molecular mechanisms and function. FEBS Letters. 2009;583(17):2701–2709. doi:10.1016/j.febslet.2009.07.032

[37] Fuji K, Shirakawa M, Shimono Y, Kunieda T, Fukao Y, Koumoto Y, Takahashi H, Hara-Nishimura I, Shimada T. The Adaptor Complex AP-4 Regulates Vacuolar Protein Sorting at the trans-Golgi Network by Interacting with vacuolar sorting receptor 1. Plant Physiology. 2016;170(1):211–219. doi:10.1104/pp.15.00869

[38] Mattera R, De Pace R, Bonifacino JS. The role of AP-4 in cargo export from the trans -Golgi network and hereditary spastic paraplegia. Biochemical Society Transactions. 2020;48(5):1877–1888. doi:10.1042/BST20190664

[39] Rojek JM, Pasqual G, Sanchez AB, Nguyen N-T, de la Torre J-C, Kunz S. Targeting the proteolytic processing of the viral glycoprotein precursor is a promising novel antiviral strategy against arenaviruses. Journal of virology. 2010;84(1):573–84. doi:10.1128/JVI.01697-09

[40] Helms JB, Rothman JE. Inhibition by brefeldin A of a Golgi membrane enzyme that catalyses exchange of guanine nucleotide bound to ARF. Nature. 1992;360(6402):352–354. doi:10.1038/360352a0

[41] Donaldson JG, Finazzi D, Klausner RD. Brefeldin A inhibits Golgi membrane-catalysed exchange of guanine nucleotide onto ARF protein. Nature. 1992;360(6402):350–352. doi:10.1038/360350a0

[42] Sun E, He J, Zhuang X. Dissecting the role of COPI complexes in influenza virus infection. Journal of virology. 2013;87(5):2673–85. doi:10.1128/JVI.02277-12

[43] Zhao L, Helms JB, Brügger B, Harter C, Martoglio B, Graf R, Brunner J, Wieland FT. Direct and GTP-dependent interaction of ADP ribosylation factor 1 with coatomer subunit beta. Proceedings of the National Academy of Sciences of the United States of America. 1997;94(9):4418–23. doi:10.1073/pnas.94.9.4418

[44] Thompson JA, Brown JC. Role of Coatomer Protein I in Virus Replication. Journal of virology & antiviral research. 2012;1(2). doi:10.4172/2324-8955.1000102

[45] Xiao F, Wang S, Barouch-Bentov R, Neveu G, Pu S, Beer M, Schor S, Kumar S, Nicolaescu V, Lindenbach BD, et al. Interactions between the Hepatitis C Virus Nonstructural 2 Protein and Host Adaptor Proteins 1 and 4 Orchestrate Virus Release. mBio. 2018;9(2). doi:10.1128/mBio.02233-17

[46] Kunz S, Edelmann KH, de la Torre J-C, Gorney R, Oldstone MBA. Mechanisms for lymphocytic choriomeningitis virus glycoprotein cleavage, transport, and incorporation into virions. Virology. 2003;314(1):168–78. doi:10.1016/s0042-6822(03)00421-5

[47] Strazic Geljic I, Kucan Brlic P, Musak L, Karner D, Ambriović-Ristov A, Jonjic S, Schu P, Rovis TL. Viral Interactions with Adaptor-Protein Complexes: A Ubiquitous Trait among Viral Species. International journal of molecular sciences. 2021;22(10). doi:10.3390/ijms22105274

[48] Xiao J, Palefsky JM, Herrera R, Berline J, Tugizov SM. EBV BMRF-2 facilitates cell-to-cell spread of virus within polarized oral epithelial cells. Virology. 2009;388(2):335–343. doi:10.1016/j.virol.2009.03.030

[49] Panda D, Das A, Dinh PX, Subramaniam S, Nayak D, Barrows NJ, Pearson JL, Thompson J, Kelly DL, Ladunga I, et al. RNAi screening reveals requirement for host cell secretory pathway in infection by diverse families of negative-strand RNA viruses. Proceedings of the National Academy of Sciences of the United States of America. 2011;108(47):19036–41. doi:10.1073/pnas.1113643108

[50] Lee C, Goldberg J. Structure of Coatomer Cage Proteins and the Relationship among COPI, COPII, and Clathrin Vesicle Coats. Cell. 2010;142(1):123–132. doi:10.1016/j.cell.2010.05.030

[51] Guo Y, Wang W, Ji W, Deng M, Sun Y, Zhou H, Yang C, Deng F, Wang H, Hu Z, et al. Crimean-Congo hemorrhagic fever virus nucleoprotein reveals endonuclease activity in bunyaviruses. Proceedings of the National Academy of Sciences of the United States of America. 2012;109(13):5046–51. doi:10.1073/pnas.1200808109

[52] Uckeley ZM, Moeller R, Kühn LI, Nilsson E, Robens C, Lasswitz L, Lindqvist R, Lenman A, Passos V, Voss Y, et al. Quantitative Proteomics of Uukuniemi Virus-host Cell Interactions Reveals GBF1 as Proviral Host Factor for Phleboviruses. Molecular & cellular proteomics: MCP. 2019;18(12):2401–2417. doi:10.1074/mcp.RA119.001631

[53] Wilfling F, Thiam AR, Olarte M-J, Wang J, Beck R, Gould TJ, Allgeyer ES, Pincet F, Bewersdorf J, Farese R V, et al. Arf1/COPI machinery acts directly on lipid droplets and enables their connection to the ER for protein targeting. eLife. 2014;3:e01607. doi:10.7554/eLife.01607

[54] Beller M, Sztalryd C, Southall N, Bell M, Jäckle H, Auld DS, Oliver B. COPI Complex Is a Regulator of Lipid Homeostasis. PLoS Biology. 2008;6(11):e292. doi:10.1371/journal.pbio.0060292

[55] Sánchez AB, de la Torre JC. Rescue of the prototypic Arenavirus LCMV entirely from plasmid. Virology. 2006;350(2):370–380. doi:10.1016/j.virol.2006.01.012

Chapter 3

Lymphocytic choriomeningitis arenavirus utilises intercellular connections for cell to cell spread

Scientific Reports; DOI https://doi.org/10.1038/s41598-024-79397-w

Owen Byford[1,2] Amelia B. Shaw[1,2] Hiu Nam Tse[1,2] Alex Moon-Walker [3,4,5,$] Erica Ollmann Saphire[3], Sean P. J. Whelan[4], Martin Stacey[1], Roger Hewson[6], Juan Fontana [1,2] John N. Barr[1,2]

[1]School of Molecular and Cellular Biology, Faculty of Biological Sciences, University of Leeds, Leeds, LS2 9JT, United Kingdom

[2]Astbury Centre for Structural Molecular Biology, University of Leeds, Leeds, LS2 9JT, United Kingdom

[3]Center for Infectious Disease and Vaccine Research, La Jolla Institute for Immunology, La Jolla, CA, 92037 USA

[4]Department of Molecular Microbiology, Washington University in St. Louis, St. Louis, MO, 63110 USA

[5]Program in Virology, Harvard Medical School, Boston, MA 02115 USA

[6]Virology and Pathogenesis Group, National Infection Service, Public Health England, Porton Down SP4 0JG, UK.

$Present address: Merck Research Laboratories, Merck & Co., Cambridge, MA 02141, USA

3.1 Abstract

The *Arenaviridae* family of segmented RNA viruses contains nearly 70 species with several associated with fatal haemorrhagic fevers, including Lassa, Lujo and Junin viruses. Lymphocytic choriomeningitis arenavirus (LCMV) is associated with fatal neurologic disease in humans and additionally represents a tractable model for studying arenavirus biology. Within cultured cells, a high proportion of LCMV spread is between directly neighbouring cells, suggesting infectivity may pass through intercellular connections, bypassing the canonical extracellular route involving egress from the plasma membrane. Consistent with this, we visualized abundant actin- and tubulin-rich connections conjoining LCMV-infected and uninfected cells within cultures, resembling tunnelling nanotubes (TNTs). Within these TNT-like connections, confocal and STED microscopy identified puncta containing the major structural components of LCMV virions alongside genomic RNA, consistent with intercellular transit of assembled virions or ribonucleoprotein genome segments. Blocking the extracellular route of infection by adding potent LCMV neutralising antibody M28 to supernatants during infection revealed around 50% of LCMV transmission was via intercellular connections. These results show arenaviruses transmission is more complex than previously thought involving both extracellular and intercellular routes.

Keywords: Arenavirus; Intercellular transmission; LCMV; Tunnelling nanotubes.

3.2 Chapter Introduction

The *Bunyaviricetes* class of segmented RNA viruses comprises over 500 named viruses divided into 15 families, of which the *Arenaviridae* family currently contains 69 species subdivided into five genera: *Antennavirus*, *Hartmanivirus*, *Innmovirus*, *Mammarenavirus* and *Reptarenavirus* [1]. Mammarenaviruses are designated as Old World (OW) or New World (NW) viruses based on geographical location of their isolation and prevalence, which also correlates with distinctive genetic lineage [2]. Several mammarenaviruses cause serious human disease, such as the OW Lassa virus (LASV) and NW Junín virus (JUNV) [1, 2], both notable for their association with fatal haemorrhagic fevers [3]. Currently, no specific antiviral therapeutics or FDA-approved vaccines exist to target any member of the *Arenaviridae* family [4]. Together, these factors have contributed to LASV, JUNV and other arenaviruses being defined as hazard group 4 pathogens, requiring the highest biosafety level (BSL) 4 containment.

The prototypic species within the *Mammarenavirus* genus is the OW lymphocytic choriomeningitis virus (LCMV; and formally, *Mammarenavirus choriomeningitidis*) for which rodents are the main vector, with the common house mouse *Mus musculus* acting as primary host [2]. Rodent-to-human LCMV transmission frequently occurs, yet severe disease only arises in rare cases. This is most often in immunocompromised patients or neonates, where infection can result in aseptic meningitis [5, 6], with LCMV described as an under-recognised agent of neurological disease [6]. Specifically, the LCMV Armstrong strain is a hazard group 2 virus, requiring only BSL-2 containment, thus acting as a relevant research model for the more pathogenic species of the *Mammarenavirus* genus, due to similarities in structure and function.

Within mature virions, the viral-associated RNA (vRNA) is coated by the viral nucleoprotein (NP) and interacts with the viral RNA-dependent RNA polymerase (RdRp, L protein) to form the viral ribonucleoproteins (RNPs). These are surrounded by a lipid bilayer, which is lined by the viral matrix (Z) protein and contains protruding viral spikes. All species within the *Mammarenavirus* genus have genomes consisting of two segments, small (S) and large (L), which together encode four structural proteins. All species of this genus express their genes using

an ambi-sense strategy; initially, input viral RNA (vRNA) S and L segments are transcribed by the viral RdRp, following entry and uncoating, to generate mRNAs that encode the NP and RdRp, respectively. Subsequently, replication of the full-length S and L vRNAs produces S and L anti-genome RNAs (agRNA), which act as templates for synthesis of mRNAs encoding glycoprotein precursor (GPC) and Z proteins [7, 8]. The GPC is post-translationally cleaved to form a trimeric assembly of structural proteins glycoprotein-1 (GP-1), glycoprotein-2 (GP-2) and a stable signal peptide (SSP) [9].

Although LCMV has been intensively studied from an immunological perspective, many molecular aspects of its replication cycle remain poorly understood. One such area is the dependence of viral multiplication on host cell components. While the catalogue of critical cellular factors is increasing, with recent additions to the list including components of the coat protein complex I (COPI) and adaptor protein complex 4 (AP-4) [10], the chaperonin TCP-1 Ring Complex TRiC/CCT [11] and sialomucin core protein 24 (CD164) as a secondary receptor for entry [12], many gaps in our knowledge remain.

Here, we investigated the ability of LCMV to infect cells via intercellular connections rather than the canonical extracellular infection route that involves egress into the extracellular space and subsequent entry. Many viruses, including coronaviruses [13], retroviruses [14–17], alphaviruses [18] and orthomyxoviruses [19], have all been shown to utilise intercellular connections as a method of cell-to-cell spread. Possibly this mechanism represents an efficient means of transmission that does not require intact virion formation and allowing evasion of the host immune response [20]. One such class of connections are tunnelling nanotubes (TNTs), which are membranous tubular structures possessing a backbone rich in filamentous-actin (F-actin) that vary in diameter between 50 to 200 nm and can extend for distances of up to 100 µm [21]. TNT connecting A549 cells have previously been described in the literature, which contain both actin and tubulin, and require HGF/c-Met/ β1-integrin signalling for cell-cell formation [22]. TNTs allow cellular connectivity and have been shown to permit the transfer of varied components between distant cells, including organelles, vesicles, signalling molecules, and ions [17].

Using recombinant LCMV variants with engineered epitope tags, we showed the three major LCMV structural proteins, NP, GP-1 and Z, all colocalised within

TNT-like structures during infection. Furthermore, fluorescent in situ hybridisation (FISH) showed these connections also contained LCMV genomic sense RNA. Taken together, these observations suggest LCMV may utilize such connections to allow intact virions or RNPs to pass between cells. Blocking the extracellular route of infection by adding the potent LCMV neutralising antibody M28 to supernatants during infection revealed almost half of all LCMV transmission events were by intercellular connections. Consistent with this, by blocking extracellular transmission using M28 alongside simultaneous disruption of TNT formation using pharmacological inhibition, LCMV transmission was reduced to background levels.

This is the first report of cell-to-cell infection via TNT-like connections for any species within the *Bunyaviricetes* class, which reveals arenavirus transmission is more complex than originally thought. This study furthers our understanding of how arenaviruses manipulate the host to establish infection, which may aid in the development of effective antiviral therapies.

3.3 Results

Observation of rLCMV-eGFP infection of cultured cells suggests transmission may involve direct cell-to-cell connectivity.

During routine LCMV infection of cultured cells, when omitting semi-solid media overlay, we noted that infected cells formed discrete foci rather than being widely dispersed throughout the culture. To further examine LCMV spread, cells were seeded and infected with previously described recombinant LCMV expressing eGFP (rLCMV-eGFP) [23] at MOI 0.001, without semi-solid media overlay. Whole well live-cell fluorescent microscopy analysis was then used to continuously monitor infected cell clusters every 6 hours post infection (hpi) (Figure 3.1A). At 6 hpi, eGFP expression was first visualised within a single infected cell (Figure 3.1A; white arrow). As infection progressed with time, an increasing number of neighbouring cells became infected, culminating at 42 hpi when a discrete fluorescent focus was visualised, with few cells outside of this showing evidence of infection. This finding suggested that LCMV spread within a culture may involve transmission via direct cell-to-cell contact.

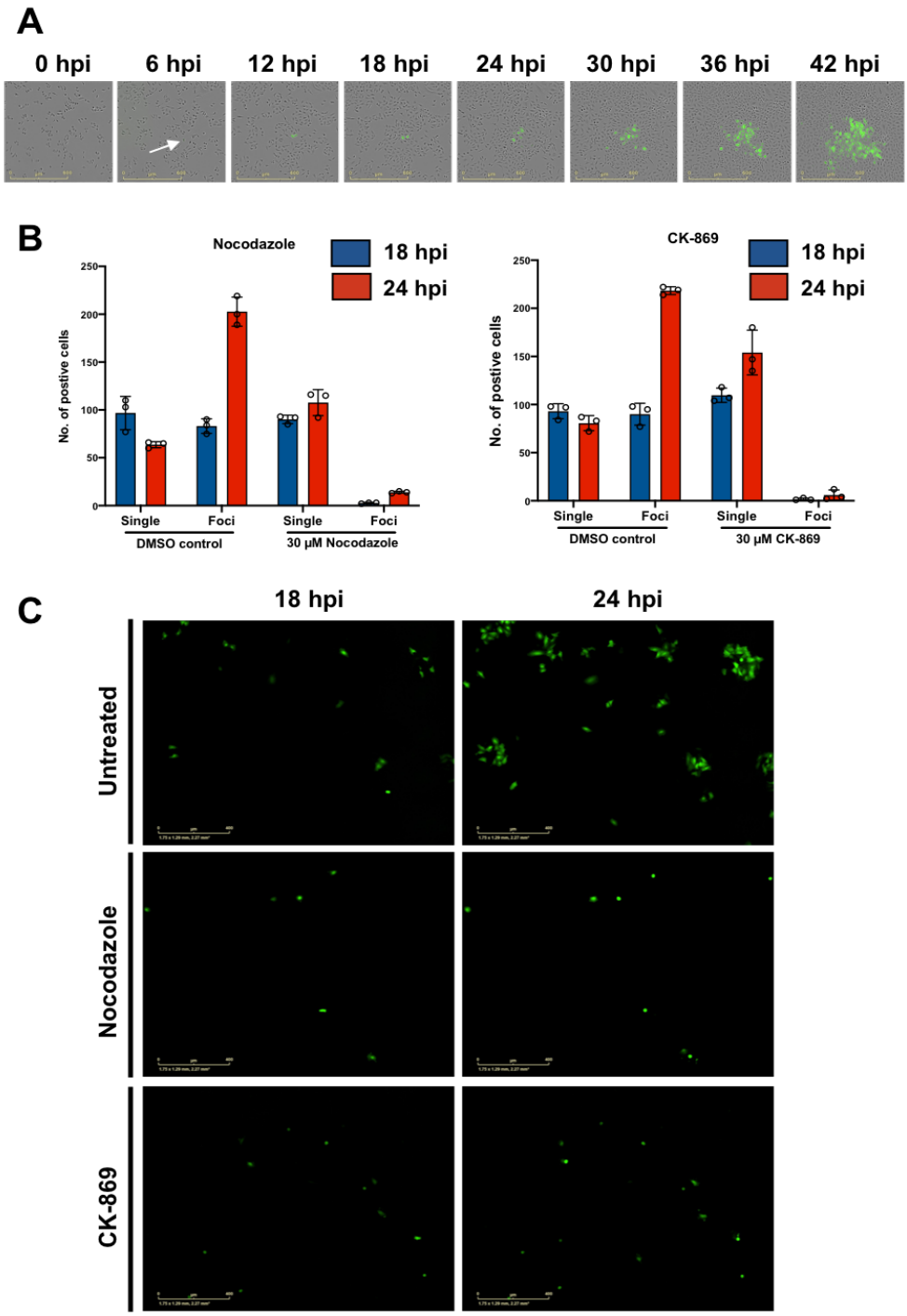

Figure 3.1: LCMV transmission within a culture involves cell-to-cell spread and is blocked by inhibitors of actin and tubulin cytoskeleton formation. (A) A549 cells were seeded and simultaneously infected with rLCMV-eGFP at a 0.001 multiplicity of infection (MOI). Phase and eGFP whole well images were taken every 6 hours, and subsets cells monitored until 42 hpi. A single infected cell (white arrow) was monitored for the duration of the experiment. (B) A549 cells were infected with rLCMV-eGFP at an MOI of 0.01. At 3 hpi, 30 µM nocodazole or CK-869 was added to infected culturescultures and present for the duration of time analysed. Infected cells were counted at both 18 and 24 hpi and represented as single cells or multicellular foci. The average of three independent experimental repeats is shown (n=3). Statistical analysis (T test) was performed for each inhibitor condition against the respective DMSO control. (C) Representative single image for untreated, nocodazole and CK-869-treated cultures, at both 18 and 24 hpi.

Disruption of cellular connections significantly attenuates LCMV cell-to-cell transmission.

Previous studies have shown that transmission of the related influenza virus can occur via intercellular connections built around a rearranged cytoskeletal scaffold, and pharmacological disruption of these structures inhibits infectivity [19]. To test for the possible involvement of such structures in LCMV cell-to-cell transmission, A549 cells were [24, 25] infected with rLCMV-eGFP at an MOI of 0.01, after which non-toxic concentrations of both microtubule inhibitor nocodazole and F-actin polymerization inhibitor CK-869 [24, 25] were added at 3 hpi (Supplementary figure 7.1A), when internalization is known to be complete [23]. Transmission was assessed using live cell fluorescence microscopy to count multicellular foci, indicative of intercellular transmission, or single infected cells, indicative of spread involving extracellular egress (Figure 3.1B and C). Visualization of DMSO-treated control cultures at 24 hpi revealed a high relative abundance of multi-cellular foci compared to single cells suggesting direct transmission between adjacent cells was a frequent event. In cells treated with either CK-869 or nocodazole, foci formation was significantly impaired at 24 hpi, with the most abundant infected cells detected as single entities, with few multicellular foci. The fold change reduction in foci formation was 14.5 for nocodazole and 36.5 for CK-869 treated cultures. To ensure this reduction in foci formation related to a block in cell-to-cell connectivity rather than overall virion production, we tested the extracellular titre from a single-round of infection in the presence of nocodazole and CK-869, and the observed effect was modest (Supplementary figure 7.1B). Taken together, these data suggest that LCMV cell-to-cell transmission, and foci formation depend on a functional cytoskeletal network, consistent with the involvement of intercellular connections.

Cell-to-cell connections contain both actin and tubulin.

To further investigate the role of cell-to-cell contacts in LCMV spread, we first needed to visualize such connections, and confirm that viral components could be detected within. To do this, A549 cells were infected with our previously described rLCMV-GP1-FLAG [10] expressing a FLAG tagged GP-1 and fixed at 24 hpi with staining to detect the cellular distribution of the LCMV GP-1 spike (cyan) alongside

the cytoskeletal components F-actin (red) and β-tubulin (green), visualised using indirect immunofluorescence (IF) confocal microscopy. For clarity, two successive magnifications of intercellular connections are shown; zoom-1 (Figure 3.2; middle row) and zoom-2 (Figure 3.2; bottom row).

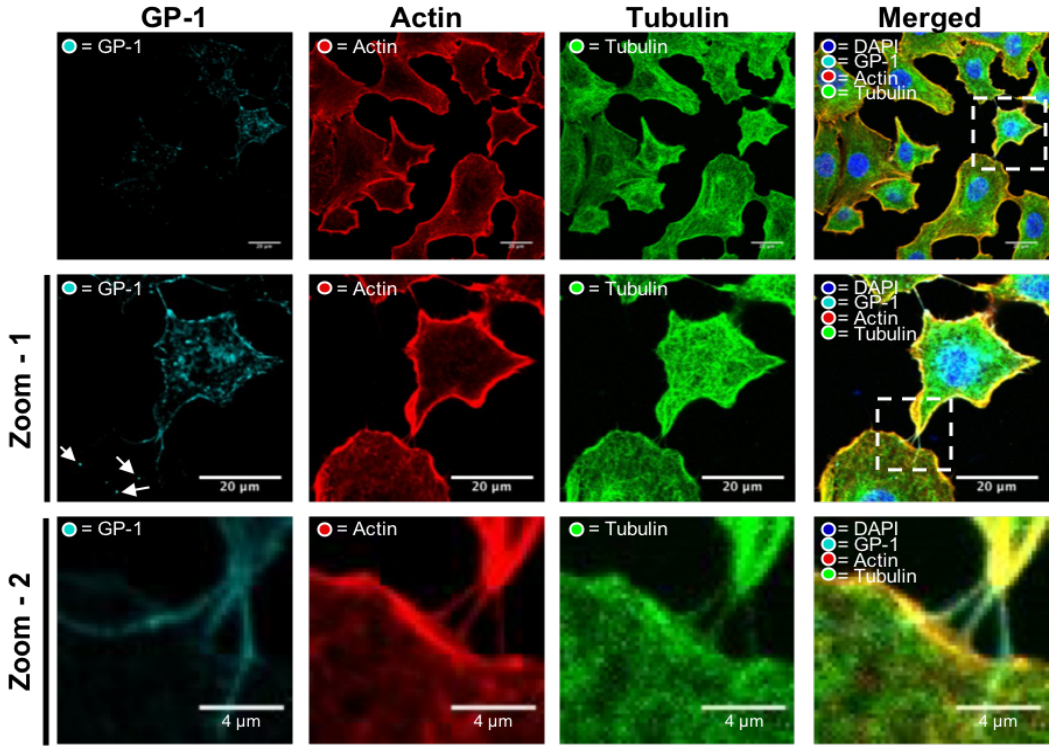

Figure 3.2: Intercellular connections between LCMV-GP-1-FLAG infected cells contain both F-actin and tubulin, as well as virion component GP-1 A549 cells were infected with rLCMV-GP1-FLAG at an MOI of 0.2. At 24 hpi, cells were fixed and then stained with DAPI and phalloidin (actin) alongside antisera specific for GP-1 (cyan) and a β-tubulin-specific Affimer (green), and then visualized by confocal microscopy. A magnified region of interest (white box in the central row) is shown on the middle row, zoom-1, where multiple cell-cell connections are visualized by staining with both tubulin and F-actin, shown further magnified in the bottom row, zoom-2. Additional points of interest are indicated by arrows to highlight punctate regions of LCMV GP-1 present in uninfected neighbouring cells, extending beyond F-actin and β-tubulin staining.

At 24 hpi, GP-1 was predominantly localised within perinuclear regions, but also within puncta throughout the cytosol and proximal to the plasma membrane (Figure 3.2; zoom-1). As expected, inspection of the intercellular spaces revealed GP-1 was also present within filamentous projections that extended between adjacent cells (Figure 3.2; zoom-1 and zoom-2). In addition, IF analysis revealed that both F-actin and β-tubulin were present within the tubular cell-to-cell connections. These cell-to-cell connections varied in size but often appeared to connect an infected cell containing abundant GP-1 to cells devoid of GP-1, likely uninfected. To view these connections more clearly, we routinely used phase-contrast

imaging alongside IF confocal microscopy to reveal the boundary of the TNT-like structures, with further representative cell images shown in Supplementary figure 7.2A. In many cases, multiple GP-1 puncta were observed extending beyond cell-to-cell connections into the cytosol of the uninfected cell (Figure 3.2; zoom-1 white arrows), consistent with the connections being open-ended. As these intercellular connections share some of, but not all, the distinguishing characteristics of TNTs, namely rich in F-actin and open-endedness, hereafter we refer to these connections as 'TNT-like'.

To understand if LCMV induced the formation of TNT-like connections, we quantified the total number of connections between 50 cell pairs for both uninfected and infected cultures (MOI 0.5), which revealed no significant difference in the total numbers in response to infection (Supplementary figure 7.2B). These results suggest that LCMV infection does not induce the formation of TNT-like connections, but instead LCMV likely subverts existing connections for transmission.

Visualization of intercellular connections within LCMV-infected cultures using stimulated emission depletion (STED) microscopy.

To view intercellular connections with greater detail, we next observed A549 cells infected with rLCMV-GP1-FLAG using stimulated emission depletion (STED) microscopy, with staining for F-actin alongside LCMV spike component GP-1. This analysis revealed intercellular connections between cells to comprise a complex F-actin architecture, typically with multiple F-actin bundles running parallel with the long axis of the tubes, both bordering the tube as well as forming an internal central core.

In the image shown, one prominent F-actin filament emanated from within the cell on the right of the image and extend through the connection (Figure 3.3A, bottom row arrows). The staining of GP-1 within the two interconnected cells was different; in the right-hand cell, GP-1 was widely-distributed with abundant intense signal suggestive of a late-stage infection, whereas in the left–hand cell, the GP-1 signal was of low intensity, suggestive of an early-stage infection. Within the cell-to-cell connection, the GP-1 signal exhibited a gradient of abundance, which decreased with distance away from the late-stage infected cell. The majority of

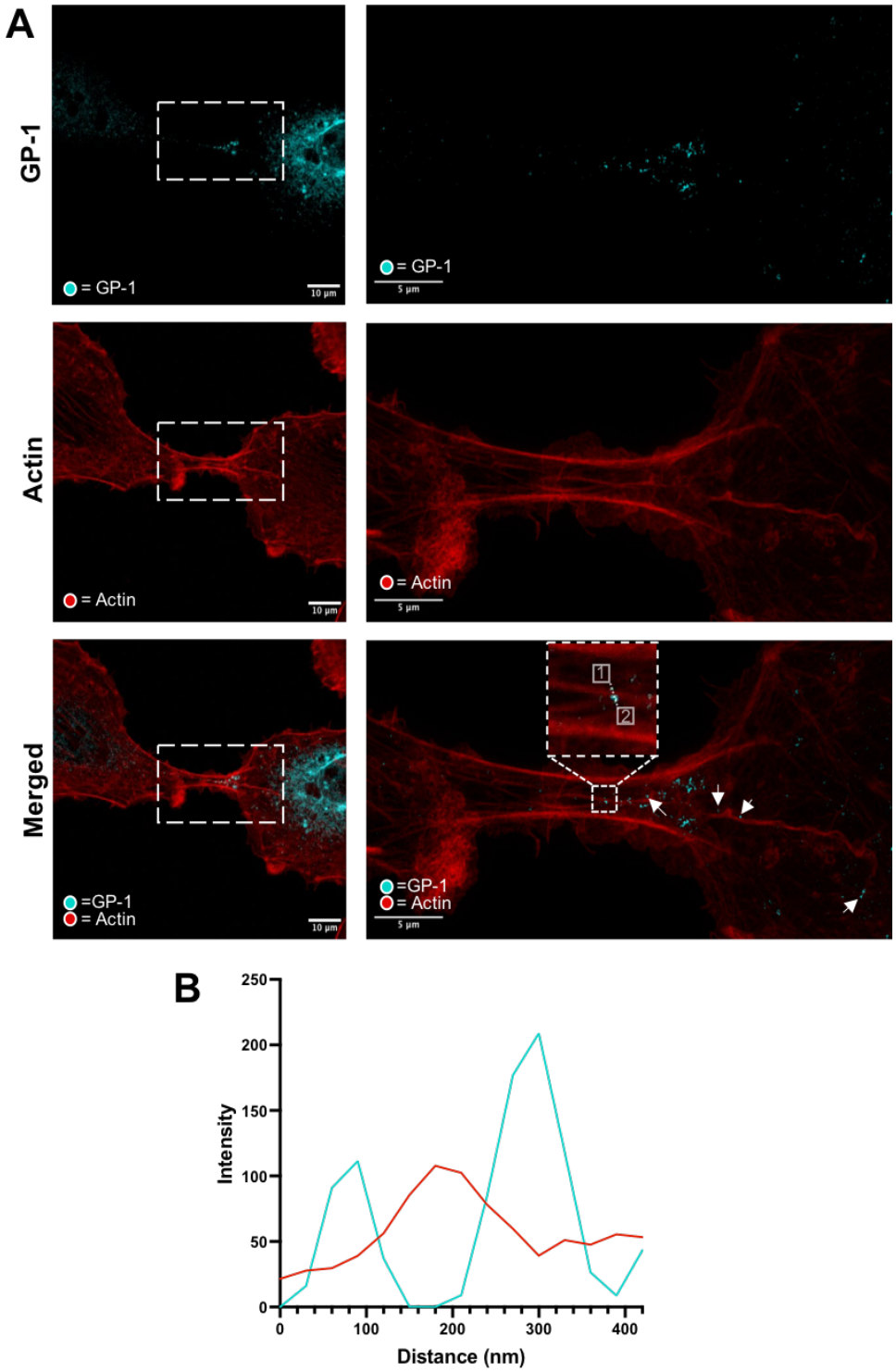

Figure 3.3: Stimulated emission depletion microscopy reveals the structural organisation of cell-to-cell connections between A549 cells infected with rLCMV-GP1-FLAG. (A) A549 cells were infected with rLCMV-GP1-FLAG at an MOI of 0.2. and at 24 hpi, cells were fixed, stained for GP-1-FLAG (cyan) and F-actin (red), then visualized by stimulated emission depletion microscopy (STED). An infected cell (left) and a zoom (right) region of interest (white box) are shown. Points of interest are indicated (arrows) to highlight punctate regions of LCMV GP-1 that exist along an F-actin branch. The bottom right panel is a magnified version of the region within the white box from the bottom left panel. (B) Line scan analysis of the region of interest in the zoomed merged image (white box), showing GP-1 peak intensities do not closely correspond to those of F-actin at this resolution.

GP-1 was located proximal to, but not coincident with, the central F-actin fibres (Figure 3.3A, arrows). This observation was corroborated with line scan analysis (Figure 3.3B; corresponding to dotted line in panel A [start 1, end 2]), which showed the peak signals corresponding to F-actin did not precisely overlap with GP-1, but instead were separated by approximately 90 nm. Interestingly, super resolution measurement of regions within the cell-to-cell connection confirmed GP-1 puncta were of a size (100-150 nm) expected for intact virions, but we cannot rule out the possibility that these objects are composed of GP-1 only. Taken together, these findings suggest that intercellular connections may act as conduits for the transport of LCMV components, or even intact virions, between neighbouring cells.

Rescue of a recombinant LCMV variant with GP-1 FLAG-tag alongside Z HA-tag (rLCMV-GP1-FLAG-Z-HA).

The results of the previous section showed that viral component GP-1 can travel through TNT-like connections. To investigate whether other viral components could similarly pass within TNT-like connections, we combined segments from two previously described infectious rLCMV variants, namely rLCMV-Z-HA [23] and rLCMV-GP1-FLAG [10], generating the rLCMV reassortant rLCMV-GP1-FLAG-Z-HA (Figure 3.4A). For this virus, the S segment expressed FLAG-tagged GP-1 and the L segment expressed a C-terminally HA-tagged Z, allowing simultaneous detection of LCMV NP (using NP antisera), Z and GP-1, the three major structural components of the virion, within infected cells (Figure 3.4B). Western blot analysis confirmed successful rescue of rLCMV-GP1-FLAG-Z-HA (Figure 3.4C and supplementary figure 7.3), with the presence of LCMV NP at 5 days post transfection indicating successful recovery of rLCMV-GP1-FLAG-Z-HA. Subsequently, supernatants were transferred to fresh BHK cells and harvested at 2 days post infection (dpi). Western blot analysis revealed successful recovery of rLCMV-GP1-FLAG-Z-HA, and the relative NP abundance for all mutants recovered were comparable to WT (Figure 3.4C). Subsequently, rLCMV-GP1-FLAG-Z-HA stocks were amplified and titrated in BHK cells, reaching a titre of 5 x 10^5.

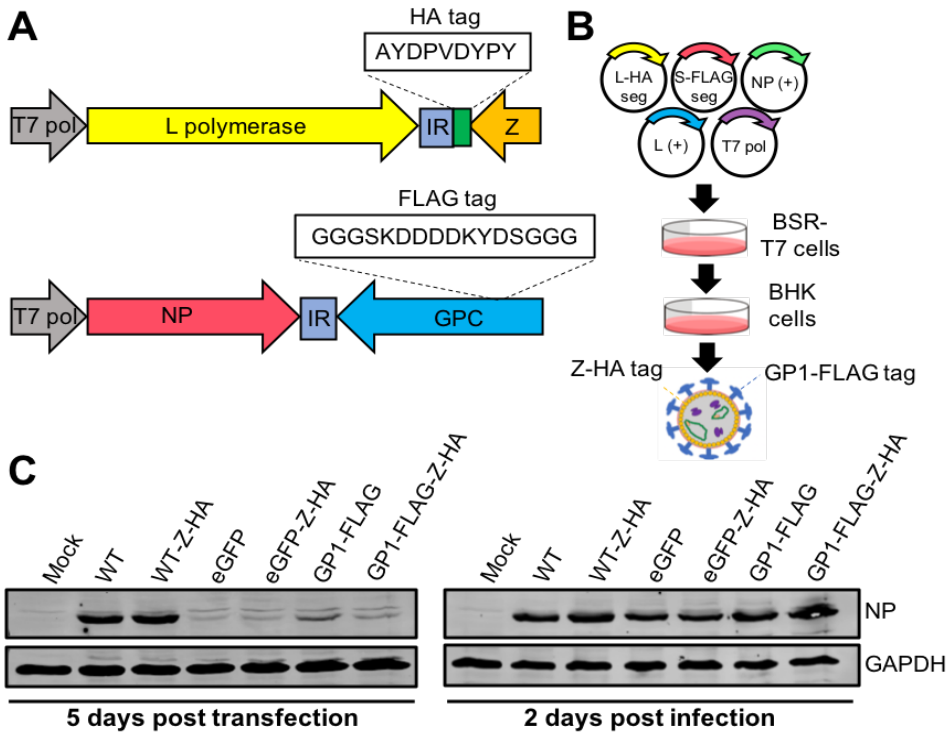

Figure 3.4: Rescue of a recombinant LCMV variant with GP-1 FLAG tag alongside Z HA tag (rLCMV-GP1-FLAG-Z-HA). (A) Schematic of LCMV S and L segments with respective tag insertions. (B) BSR-T7 cells were transfected with cDNAs expressing a LCMV S segment encoding a FLAG tagged GP-1 (S-FLAG segment), an L segment encoding a HA tagged Z (L-HA segment), as well as NP and L open reading frames (support plasmids, L+ and NP+) and a plasmid expressing T7 RNA polymerase. At 5 days post transfection (5 dpt), cellular supernatants were transferred to BHK cells, and at 3 days post infection (3 dpi), cell lysates were analysed by western blotting using NP antisera, with viral supernatants harvested and subject to focus forming assays (FFA). (C) Western blot analysis of transfected BSR-T7 and infected BHK-21 cell cultures confirmed rLCMV-GP1-FLAG-Z-HA rescue (alongside all other mutants), using antisera specific for LCMV NP and GAPDH as loading control.

LCMV GP-1, NP and Z puncta co-localise within TNTs during infection.

Next, rLCMV-GP1-FLAG-Z-HA was used to assess the presence of NP, Z and GP-1 within infected cells and TNT-like connections. A549 cells were infected with rLCMV-GP1-FLAG-Z-HA at a MOI of 0.25, and at 24 hpi cells were fixed and the cellular localisation of NP (red), GP-1 (cyan) and Z (green) was assessed using specific antisera via confocal IF microscopy (Figure 3.5).

At 24 hpi the distribution of each of NP, GP-1 and Z was distinctive. In agreement with our previous findings, LCMV NP formed discrete perinuclear puncta, as well as being widespread throughout the cytoplasm [23].

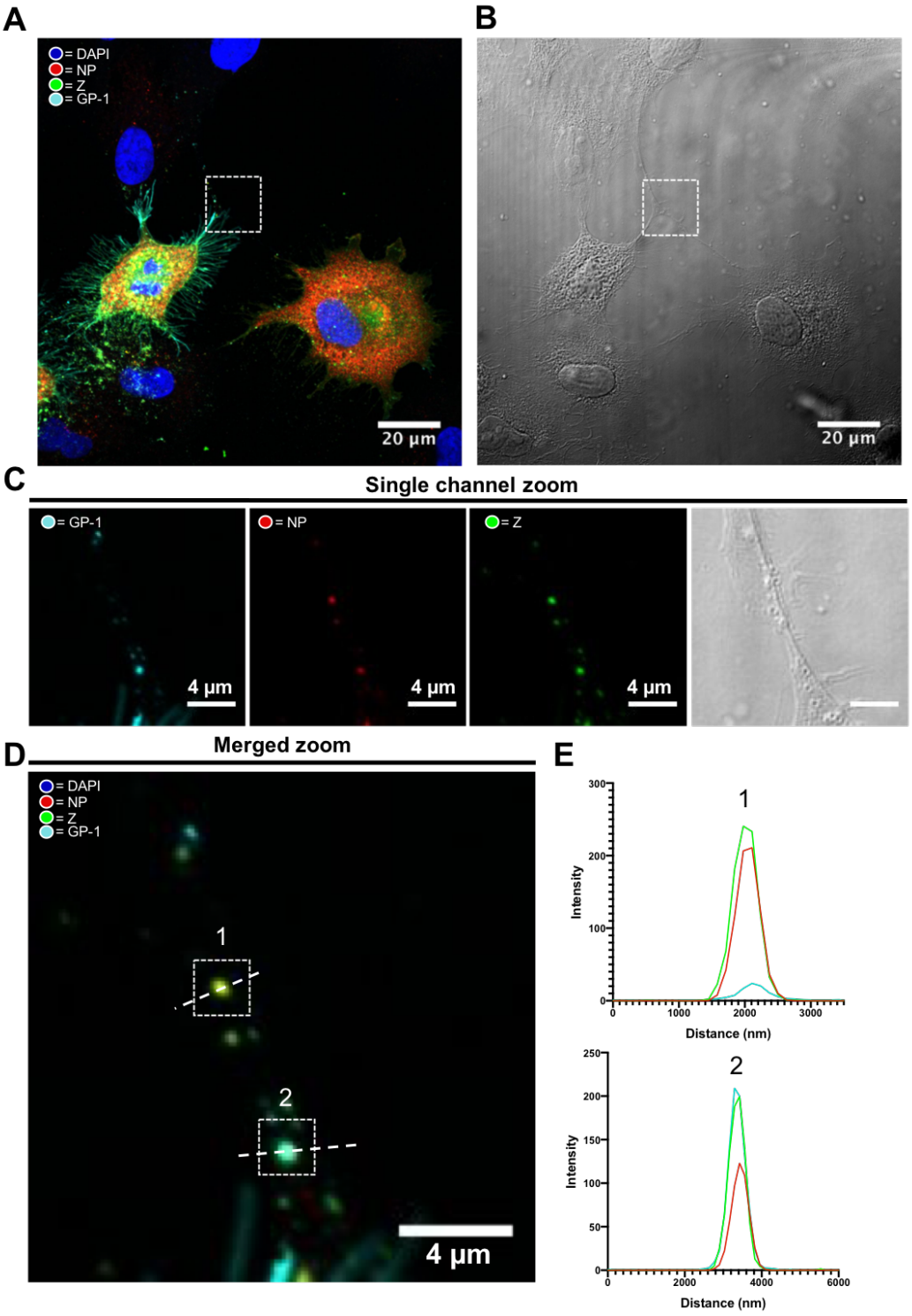

Figure 3.5: GP-1, NP and Z puncta co-localise within TNT-like connections during rLCMV-GP1-FLAG-Z-HA infection. (A) At 24 hpi A549 cells infected with rLCMV-GP1-FLAG-Z-HA at an MOI of 0.25 were fixed, stained for GP-1 (cyan), NP (red) and Z (green) and visualized by confocal microscopy, also imaged using phase contrast, shown in (B) alongside. (C) A TNT-like connection between an infected and uninfected cell is boxed in both confocal and phase images, shown magnified as separate channels with the same zoomed image shown with channels merged in (D). (E) Line scan analysis of the region of interest in the zoomed merged image showing alignment the intensity peaks for NP, GP-1 and Z.

LCMV GP-1 localisation differed to that of NP, being predominantly punctate and perinuclear as well as being abundantly distributed along the plasma membrane. Interestingly, Z showed a similar cellular distribution to GP-1, with clear and abundant Z/GP-1 co-localisation in perinuclear regions, and co-localization at discrete locations proximal to the plasma membrane, possibly representing virus assembly sites.

In addition, multiple puncta were observed within TNT-like connections between LCMV infected and uninfected cells (Figure 3.5A; white boxes in top row) containing NP, GP-1 and Z. Line scan analysis across two discrete puncta (Figure 3.5D; white boxes in bottom row) showed the peak intensities for NP, GP-1 and Z viral components were spatially closely aligned (Figure 3.5E) although interestingly, the relative composition of these three proteins within the puncta was not consistent. Taken together, these observations show that in addition to the GP-1 envelope spike protein, internal virion components NP and Z are also able to pass through TNT-like connections as discrete punctate objects. These observations raise the interesting possibility that assemblies of multiple viral proteins, or even intact virions, may pass between cells through intercellular connections.

LCMV NP and viral genomes co-localize within TNT-like connections.

For infectivity to transmit between cells via intercellular connections, we reasoned these connections must contain, at minimum, the LCMV genome enwrapped in NP to form the RNP. To test this, we performed fluorescent in situ hybridisation (FISH) using probes designed to detect negative sense LCMV vRNA genomes, which represents the LCMV genetic material found within infecting virions.

To achieve this, we generated a set of fluorescently labelled probes specific for the NP coding region of the negative sense rLCMV S RNA segment (list of probes; table 7.1), with which we performed FISH on A549 cells infected with rLCMV at an MOI of 1.0 at 24 hpi using wide-field microscopy. To specifically detect assembled LCMV RNPs, which represent the form in which vRNAs are packaged within virions, cells were also co-stained with antisera specific for LCMV NP.

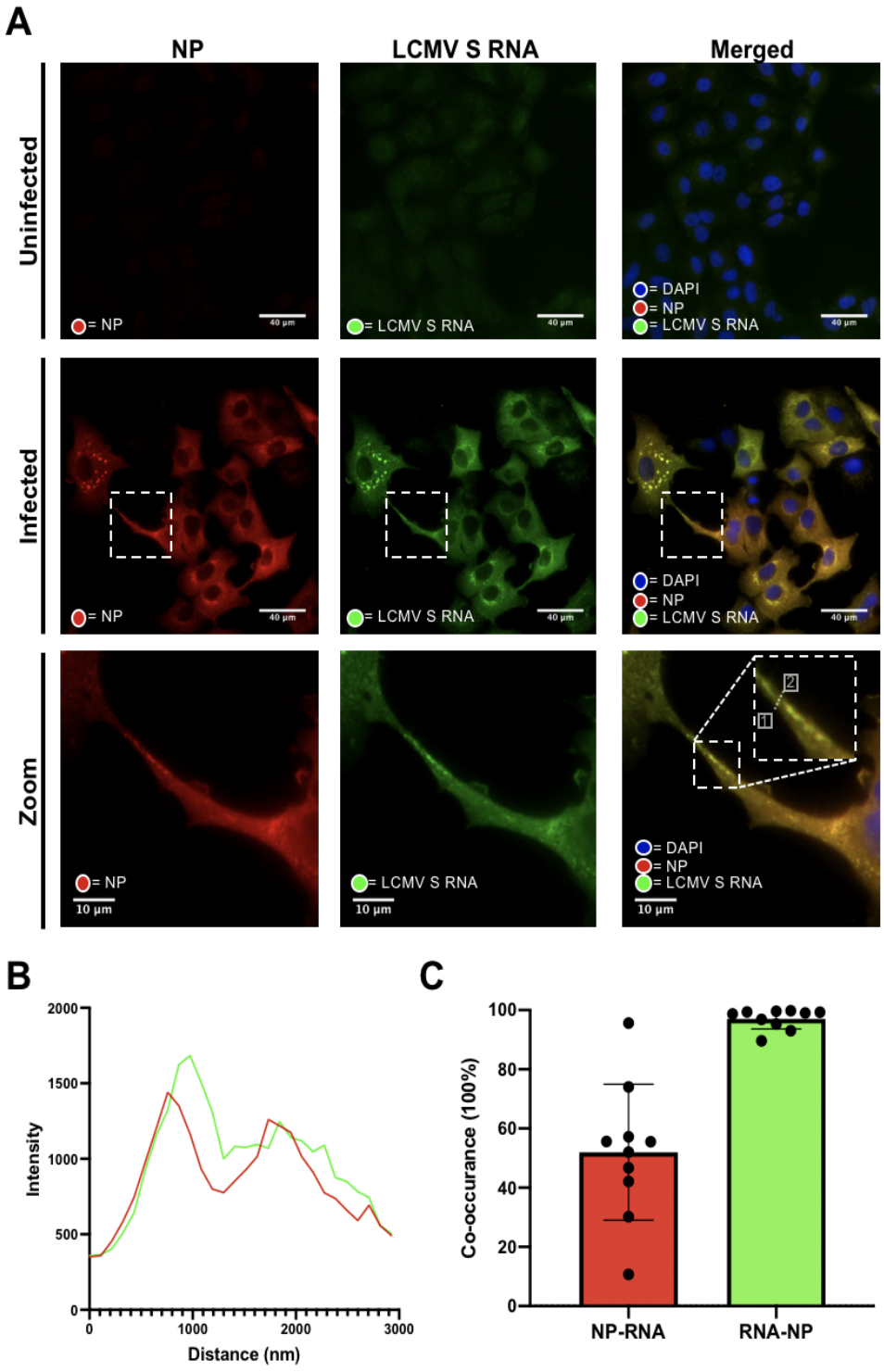

Figure 3.6: LCMV vRNA is present alongside NP in TNT-like connections. (A) At 24 hpi rLCMV infected A549 cells at an MOI of 1 were fixed and then stained for NP (red). Subsequently, coverslips were hybridised overnight with 48 specific FISH probes designed to hybridize with LCMV S vRNA (green). Widefield microscopy was then utilised to visualise NP and S vRNA within TNT-cell connections. Cell nuclei were DAPI stained. Uninfected cells and infected cells are shown. A zoomed-in region of interest (white box in the central row) is shown on the bottom row. (B) Line scan analysis of the region of interest in the zoomed merged image (dashed line in the bottom right panel of A) revealed peaks in intensity of NP and S vRNA were similar. (C) Co-occurrence analysis using the Manders coefficient method was performed for 10 TNT-like connections. The percentage of LCMV NP to S vRNA (Red) and S vRNA to LCMV NP (green) is shown, and individual images plotted.

As anticipated for an MOI of 1.0 at this time point, most cells appeared infected as evidenced by staining by FISH and NP (Figure 3.6A, middle row). Within cells, NP distribution was consistent with previous findings, and FISH analysis revealed close co-localisation of NP and LCMV S segment vRNA at several locations within the infected cells (Figure 3.6A, middle bottom rows; zoom) sometimes in perinuclear locations, but also as dense puncta throughout the cytosol. Within TNT-like connections, signals corresponding to NP and S segment vRNA were visualised (Figure 3.6A, white boxes in middle and bottom rows) as discrete puncta, within which NP and RNA signals appeared to closely co-localize. This was corroborated using line scan analysis, which revealed peaks corresponding to both NP and S vRNA were closely coincident (Figure 3.6B; corresponding to the dotted line in panel A, bottom row; start 1, end 2). Such punctate objects were common within TNT-like structures and further representatives are shown, along with corresponding line scans, in supplementary figure 7.4. The proximity of the LCMV NP and S segment vRNA signals was consistent with their location within the assembled RNP, with the small offset in peak spatial intensity likely a reflection of the differing approaches used for target detection; the FISH probes bind directly to the S vRNA target and emit signal from fluorogenic probe-bound dyes. In contrast, the NP signal results from binding of primary and fluorescent secondary antibodies, thus some spatial separation between target and fluorophore was expected.To quantify the extent of S vRNA and LCMV NP co-localisation within connections, we performed co-occurrence analysis of 10 different TNT-like tubes (Figure 3.6C), which revealed an RNA/NP mean co-occurrence of 97%, consistent with the presence of RNPs. In contrast, mean co-occurrence of NP/RNA was 52%, suggesting some NP may also be trafficked through connections in an RNA-free state.

Taken together, the results of this analysis are consistent with a scenario in which LCMV RNP components, namely vRNA and NP, can travel within TNT-like connections between cells. These RNPs likely have the capacity to initiate infection, as has recently been shown for the related segmented negative sense RNA virus, influenza A virus (IAV) [19].

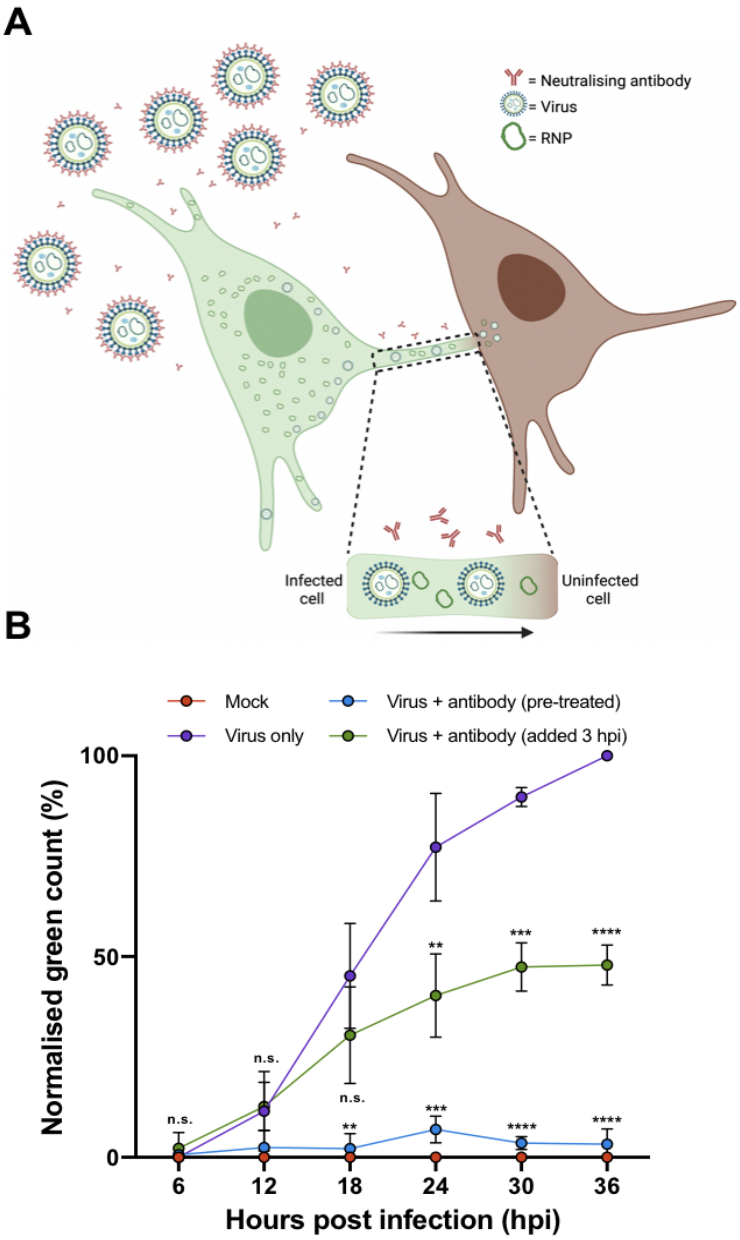

Figure 3.7: LCMV can efficiently spread through a culture despite blocking extracellular transmission using a potent neutralising antibody. (A) Schematic representation of the model for intercellular LCMV transmission in the presence of potent neutralizing antibody M28 that targets GP-2. Virus released via the canonical plasma membrane egress mechanism are rendered non-infectious through M28 binding the GP-2 portion of the spike complex. Only virions or RNPs that pass-through TNT-like connections can transmit infectivity to new cells. Image created with Biorender. (B) A549 cells were infected with rLCMV-eGFP at an MOI of 0.1 that was either pre-treated with antibody M28 (blue plotted points; 5 µg/mL antibody for 1 h) or virus only (in the absence of antibody; purple plotted points). For virus + antibody (green plotted points), 5 µg/mL antibody was added to cultures at 3 hpi, following LCMV entry and uncoating, which remained for the duration of infection. The total green count (number of green cells) was measured every 6 h and normalised against virus only (purple) cultures at 36 hpi. The average of three independent experimental repeats is shown (n=3), with error bars showing standard deviation at each time point. Statistical analysis (T test) was performed for each condition against the respective virus only control timepoint.

Blocking extracellular LCMV transmission with a potent neutralising antibody reveals that LCMV utilises cell-to-cell spread during infection.

To confirm that LCMV infectivity can pass between cells via TNT-like connections, we made use of a recently described LCMV neutralising antibody (M28) that targets GP-2 [26]. We reasoned that when added to infected cell supernatants, this antibody would block LCMV infection via the extracellular route but would not hinder cell-to-cell transmission via intercellular connections (Figure 3.7A).

First, to confirm the potency of this neutralising antibody under the selected experimental conditions, M28 at 5 µg/mL was pre-incubated with rLCMV-eGFP prior to infection of A549 cultures. To measure virus transmission throughout the culture the total green cell count (TGC) was determined at successive 6 hpi time points up to 36 hpi, at which time a TCG value of just 3% was recorded (Figure 3.7B; blue plotted points) and normalized to that of the virus only (in the absence of antibody) control (Figure 3.7B; purple plotted points). This was statistically indistinguishable from the TCG of mock infected cultures (Figure 3.7B; red plotted points) and thus confirmed that the antibody effectively blocked extracellular transmission in the culture to background levels of detection.

Next, to investigate whether rLCMV-eGFP could spread within the culture when extracellular transmission was blocked, cultures were infected with rLCMV-eGFP at an MOI of 0.1, with M28 added at 3 hpi, at which time virus entry is complete but virion assembly has not yet commenced [23]. This protocol would allow virus to enter these initial cells, but the presence of antibody in the media thereafter would block any subsequent transmission by the extracellular route. To further demonstrate that M28 was able to neutralize any viruses that might be released, supernatants of rLCMV-eGFP infected cells were collected at 18 hpi, treated with 5 µg/mL antibody and titrated via focus forming assays (Supplementary figure 7.5), which revealed no infectivity.

Blocking extracellular transmission using these experimental conditions resulted in a TCG value of 47% at 36 hpi (Figure 3.7B; green plotted points) when normalized to the virus only control. This showed that significant transmission had occurred throughout the culture despite the continued presence of potent neutralizing antibody.

Taken together, these results show that a major fraction of LCMV transmission within a culture occurs without involvement of the extracellular space, and the detection of LCMV components NP, Z, GP-1 and vRNA within TNT-like connections, strongly suggests these structures represent effective conduits of infectivity.

3.4 Discussion

Curious as to why LCMV spread throughout cultured cells appeared to be spatially restrained thus forming infected cell foci, we reasoned that infectivity may pass between cells by TNT-like intercellular connections. To investigate this, we first used epitope tagged LCMV variants rLCMV-GP1 and rLCMV-GP1-FLAG-Z-HA to confirm that viral proteins GP-1, Z and NP were present within these connections, colocalized within discrete punctate objects. Furthermore, FISH analysis showed these TNT-like connections also contained LCMV S genomic vRNA in close proximity to NP, indicative of RNP structures that would be expected to be found within infectious virions, or that could themselves represent the infecting entity. Although LCMV NP alone has previously been detected between cells [27], our current study is the first to reveal the co-localization of all major LCMV structural components namely NP, genomic RNA, Z and GP1 as discrete puncta within intercellular connections. Furthermore, we showed LCMV could transmit within a culture in the presence of a potent neutralising antibody, which effectively blocked extracellular transmission. This revealed that LCMV transmission could occur without involvement of the extracellular space and that cell-to-cell LCMV transmission may represent up to around 50% of total spread during infection. Taken together, our data suggests that LCMV infectivity can traffic between cells through intercellular connections, and this mode of virus spread represents a significant proportion of total virus transmission during infection.

This work is the first report describing cell-to-cell transmission via TNT-like connections for any species of the *Bunyaviricetes* class. Nevertheless, many other viruses have been revealed to rely on TNT or TNT-like structures during infection including species of retroviruses, herpesviruses, alphaviruses, pneumoviruses, orthomyxoviruses, paramyxoviruses, flaviviruses and picornaviruses [28].

Within the *Coronaviridae* family, SARS-CoV-2 virions have recently been visualised to 'surf' on the outside of TNTs, connecting cells during infection, along with evidence to suggest mature virions are also present within the interior of the same structures [13]. Furthermore, this study demonstrated transmission of SARS-CoV-2 between permissive and non-permissive neuronal cells via TNT connections. Thus, TNT connections could potentially act as a mechanism for widespread dissemination of viruses within a host, circumventing different cellular or tissue-type restrictions, such as the requirement for specific entry receptors, allowing spread to tissues and organs distinct from the initially infected target cells.

The reliance of SARS-CoV-2 on TNTs was further investigated with the use of neutralising antibody to block extracellular transmission of a pseudotyped lentivirus, resulting in no significant decrease in cell-cell spread [29]. Thus, it was proposed that cell-to-cell TNT connections may represent an efficient mode of transmission, allowing evasion of host immune cell responses. It will be interesting to test whether LCMV also exploits TNT-like structures during infection of target host tissues, and also, whether this mode of transmission occurs during infection of intact organisms. Since LCMV has been extensively studied from the perspective of immune evasion and the balance between chronic or acute infections [30] it would be interesting to investigate whether cell-to-cell transmission plays a significant role in these processes. In addition, a greater understanding of how LCMV propagates in the natural host, where multiple cell types are susceptible to infection, may help explain how LCMV is able to grow to high titres in suspension cultures [31] which likely preclude the formation of interconnected cells.

Interestingly, IAV, which like LCMV is an enveloped negative-sense segmented RNA virus, has been shown to utilise TNT connections for spread during infection. However, for IAV the infectious entity is not proposed to be a fully assembled mature virion, but instead is believed to comprise solely the RNP, devoid of both matrix and the spike-embedded envelope [19, 32]. Rab11a is known to be involved in transport of RNPs to assembly sites at the plasma membrane for subsequent budding and transmission involving extracellular release, and Rab11 was also shown to play a role in movement of IAV vRNPs across TNT connections [19]. Interestingly, analysis of IAV infection outcome revealed the movement of IAV segments through TNT connections acted to facilitate genome reassortment during co-infections, with

important consequences for virus evolution and possible emergence of pathogenic variants [19].

For LCMV, we are interested in determining the composition of the intercellular infecting entity. While our data shows that the internal RNP as well as Z and GPC components are colocalised within TNT-like connections, we are unable to determine whether the RNP alone, or the RNP in combination with one or more of the matrix or envelope components are required to transmit infectivity. What is probable, and consistent with our data, is that both intact virions and non-enveloped RNPs can traffic through TNT-like connections. Further investigations are required to understand if only one or both options results in productive infection within subsequent cells, but clearly, the distinction between these two possibilities has implications for infection of the connected cell. If the transmitting object is an RNP, then presumably this would be able to initiate infection in the same way as if just released from an endocytic vesicle. In contrast, if the transmitting object is an intact enveloped virion, it must follow an infection pathway in the new cells that allows virion disassembly and RNP release by interaction with its secondary receptor CD164, that is specifically located within late-endosomal compartments, and how this could be achieved is unclear. It is interesting to note that as arenaviruses assemble at the plasma membrane, non-enveloped RNPs must necessarily transit across the cytosol from their replication site, as occurs for IAV, where they acquire their envelope, matrix and spike complex. This allows the possibility that non-enveloped RNPs may be substrates for cytoskeletal trafficking pathways that lead to the plasma membrane, but alternatively, these cytoskeletal pathways may also lead through intercellular connections delivering RNPs to new cells. If intact virions are indeed capable of passing through cell-to-cell connections, it is intriguing to speculate how such particles can be generated, given the plasma membrane site of virion assembly. One possibility is that some cell-to-cell connections are not open-ended tubes, but instead possess membranous structures at one or both ends that could potentially allow formation and subsequent passage of an enveloped virion into the interior of the connecting structure. Such closed tubes have been described alongside open-ended tubes [33].

Further investigations are required to understand if the movement of virus components within TNT-like connections is an active or passive process, or if there

is a reliance on host cell components for this transport, such as Rab11, as described for IAV, above [19] . Interestingly, STED analysis of rLCMV infected cells stained for GP-1 and F-actin (Figure 3.2B) showed the corresponding signals were proximal but not coincident. This observation raises the possibility that F-actin associated proteins such as the resident myosin motors may play a role. The host cell motor protein myosin II has been implicated in 'viral surfing' for several viruses including murine leukaemia virus, avian sarcoma leukosis virus and vesicular stomatitis virus [34]. In the context of HIV infection, host cell motor protein non-muscle myosin II (NMMII), has been implicated in the movement of Gag and Env through cell-cell TNTs during infection [16]. It is unclear if LCMV requires the involvement of any cellular motors, or if an association with growing F-actin fibres is sufficient for TNT trafficking, and experiments to investigate this are underway. Developing a clear understanding of transmission routes is important in order to formulate antiviral strategies. The role of cell-cell transmission of hepatitis C virus (HCV) for evasion of neutralising antibodies is well understood [35]. Direct acting antivirals (DAAs) are effective therapeutics for HCV, yet resistance can occur. In a recent study, cell-cell transmission was shown to be the primary route of HCV DAA-resistance, leading to infection persistence. By targeting cell-cell transmission alongside DAA treatment, resistance was overcome, and HCV was again eliminated in a cell culture model [35].

Overall, this study reveals that a major fraction of LCMV transmission within cultured cells occurs via intercellular transmission, without involvement of the extracellular space. It will be interesting to examine whether other arenaviruses from both OW and NW clades utilise TNT-like connections as transmission conduits, and also to test whether these connections are formed in the context of intact tissues with an infected host.

3.5 Materials and Methods

3.5.1 Plasmid design and virus rescue.

Construction of plasmids expressing S and L segments for rescue of rLCMV-WT, rLCMV-eGFP, LCMV-Z-HA [23] and LCMV-GP1-FLAG [10] have been

previously described, along with corresponding rescue protocols. Rescue of rLCMV-GP1-FLAG-Z-HA was achieved using these same protocols, by transfection of BSR-T7 cells with cDNAs expressing the S segment of rLCMV-GP1-FLAG along with the L segment of rLCMV-Z-HA (Figure 3.4). Also transfected were supporting plasmids expressing the ORFs of LCMV NP and LCMV L proteins, as well as bacteriophage T7 RNA polymerase. At 5 days post transfection (dpt), cell supernatants were transferred to BHK cells allowing amplification of any rescued viruses. At 2 days post infection (dpi), viral supernatants were collected and subject to focus forming assays (FFA). Titred viral stocks gained were utilised for bulking in BHK cells at an MOI of 0.001, and subsequently harvested at 3 dpi.

3.5.2 Virus infections.

To generate virus stocks, T175 flasks of BHK cells seeded at $5x10^6$ the day prior were infected at an MOI 0.001. At 3 days post infection, viral supernatant was harvested and centrifuged to remove cell debris (x4000 g), aliquoted (80 µL) and frozen for subsequent viral titration. For all other viral infections, cell monolayers were infected with LCMV at the specified MOI in either serum-free (SFM), 2.5% or 10% FBS DMEM, depending on cellular requirements, at 37 °C. After 1 h, the inoculum was removed and SFM, fresh 2.5% or 10% DMEM was then applied for the duration of the infection. For synchronised infections, LCMV was bound on ice to cells for 1 h. Subsequently, the inoculum was removed, monolayers washed x3 with PBS and SFM, fresh 2.5% or 10% DMEM was then applied for the duration of the infection.

3.5.3 Viral titration.

Determination of virus titres was achieved through focus forming assays (FFA).Viral stocks requiring titration were serially diluted in SFM to infect fresh monolayers of BHK cells seeded at 1 x 10^5 in a 24 well-plate. After infection, medium containing virus was removed and 1 mL 1:1 ratio of 10% FBS DMEM to 1.6% methylcellulose was reapplied, and the cells incubated for a further 3 days. For rLCMV-eGFP titration, the Incucyte Zoom S3 live cell imaging system (Sartorius) was used to image whole wells and detect fluorescent rLCMV-eGFP foci, which were then

counted for titre determination. For rLCMV-WT titration, cells are fixed using 4% (vol/vol) paraformaldehyde (PFA) for 15 mins and washed three times with PBS. Cells were then incubated with permeabilisation buffer (0.3% [vol/vol] Triton X-100, 2% [wt/vol] FBS in 1 x PBS) for a further 10 mins, and then washed three times with PBS. Following this, cells were incubated with 1 mL blocking buffer (1% [wt/vol] BSA in PBS) for 1 h. The cells were then incubated for 1 h with 150 µL/well LCMV NP primary antibody (generated in-house, 1:1000 in blocking buffer), and washed three times with PBS. Following this, cells were incubated for 1 h with 594 Alexa Fluor secondary antibody (Life Technologies; 1:500 in blocking buffer), and subsequently washed four times with PBS. The Incucyte Zoom S3 live cell imaging system was then used to image whole wells of the plate to detect red rLCMV-WT focus forming plaques. Plaques were quantified, and virus titres determined. For rLCMV-FLAG titration, the protocol for rLCMV-WT was followed, yet cells were incubated for 1 h with 150 µL/well LCMV NP (in-house, 1:1000 in blocking buffer) and FLAG (Sigma, 1:500 in blocking buffer) primary antibodies. Following this, cells were incubated for 1 h with 488 (FLAG) and 594 (LCMV NP) Alexa Fluor antibodies (Life Technologies; 1:500 in blocking buffer), then washed four times with PBS.

3.5.4 Analysis of LCMV infection progression

Trypsinised A549 cells were seeded in a 12-well plate at 1 x 10^5 cells/well in 1 mL 10% FBS DMEM; simultaneously, cells were infected with rLCMV-eGFP, at an MOI of 0.001. To investigate spread throughout a culture, whole well images were taken at 6 h intervals using an Incucyte Zoom S3 live cell imaging system (Sartorius).

3.5.5 Immunofluorescence (widefield and confocal microscopy)

Trypsinised A549 cells were seeded onto a 19-mm round glass coverslips (VWR) in a 12-well plate at 1 x 10^5 cells/well, followed by incubation at 37 °C. At 24 hpi, 1 mL 4% (vol/vol) paraformaldehyde in PBS was added directly on top of the 1 mL infection media for 20 mins at room temperature. After fixation, the cells were washed three times in PBS and then incubated in permeabilisation buffer

(0.3% [vol/vol] Triton X-100, 1% [wt/vol] bovine serum albumin [BSA] in PBS) for 10 mins at room temperature. Following permeabilisation, the monolayers were washed three times with PBS and incubated with blocking buffer (1% [wt/vol] BSA in PBS) for 1 h. Subsequently, primary antibody made in the BSA blocking buffer containing NP (1:500, in house [sheep]), FLAG (1:100 [mouse/rabbit]) and HA (1:500 [mouse/rabbit]) was incubated for 1 h at room temperature. The cells were then washed three times with PBS and incubated with corresponding Alexa Fluor 488, 594 and 647 secondary antibodies (Life Technologies; 1:500 in BSA blocking buffer) for 1 h at room temperature in a light protected vessel. Cell monolayers were then washed four times with PBS before addition of appropriate stain/dye; F-actin (Phalloidins, Texas Red, 5 µL/well in 500 µL blocking buffer) and β-tubulin (affimer; 1:200; A gift from Professor Michelle Peckham, University of Leeds, UK), for 1 h in a light protected vessel. Cell monolayers were then washed four times with PBS and mounted onto glass coverslips with the addition of Prolong Gold Antifade reagent with DAPI (Thermo Fisher Scientific), cured, sealed, and stored at 4 °C. Images were then taken on either Zeiss LSM 880 confocal microscopy or Olympus Widefield Deconvolution Microscope and processed using Zen (Blue Edition) software and Fiji (Image J). Line scan analysis was performed utilising Zen (Blue Edition).

3.5.6 TNT-like connection inhibition utilising nocodazole and CK-869.

Trypsinised A549 cells were seeded in a 12-well plate at 1 x 10^5 cells/well in 1 mL 10% FBS DMEM and incubated for 16- to 24- h. Cells were subsequently infected with 500 µL rLCMV-eGFP at an MOI of 0.01, and at 3 hpi 500 µL of nocodazole (60 µM) or CK-869 (60 µM) was added to give a 30 µM final concentration. To investigate spread throughout a culture, 16-images were taken for each condition at 18- and 24- hpi using an Incucyte Zoom S3 live cell imaging system (Sartorius). For each condition, at both 18- and 24 hpi, infected cells were manually counted and represented as single or foci (defined as a minimum of two infected adjacent cells). The average of three independent experimental repeats is shown, with error bars showing standard deviation at each time point (n = 3). To ensure nocodazole and CK-869 major effect is on cell-cell connections, viral egress was analysed after

a single round of infection. A549 cells were infected at an MOI of 1 and infection incubated for 1 h at 37 °C. Subsequently, infection medium was removed and cells washed with 1 x PBS four times prior to replacement with 1 mL 10 % FBS DMEM. At 3 hpi, nocodazole or CK-869 (30 µM) was added to the cultures. At 12 hpi, viral supernatants were collected and subject to focus forming assay analysis, and results expressed as normalised untreated titres. The average of three independent experimental repeats is shown, with error bars showing standard deviation at each time point (n = 3).

3.5.7 Immunofluorescence (FISH)

FISH probes used were identical to a set previously described [36] and synthesised by Stellaris. The protocol was followed according to manufacturer's instructions, with probes hybridized overnight at 37 °C. As recommended by the manufacturer, FISH probes were visualized using widefield microscopy.

3.5.8 Immunofluorescence (STED)

Trypsinised A549 cells were seeded onto a 19-mm round glass coverslip (VWR) in a 12-well plate at 1 x 10^5 cells/well, followed by incubation at 37 °C. At 24 hpi, 1 mL 4% (vol/vol) paraformaldehyde in PBS was added directly on top of the 1 mL infection media for 20 mins at room temperature. After fixation, the cells were washed three times in PBS and the incubated in permeabilisation buffer (0.3% [vol/vol] Triton X-100, 1% [wt/vol] bovine serum albumin [BSA] in PBS) for 10 mins at room temperature. Following permeabilisation, the monolayers were washed three times with PBS and incubated with blocking buffer (1% [wt/vol] BSA in PBS) for 1 h. Subsequently, primary antibody in BSA blocking buffer containing FLAG, (1:100 [rabbit/mouse]) and HA (1:500 [rabbit/mouse]) was incubated for 1 h at room temperature. The cells were then washed three times with PBS and incubated with Fluro 647 secondary antibodies (Abberior STAR red; 1:500 in BSA blocking buffer) for 1 h at room temperature in a light protected vessel. Cell monolayers were then washed four times with PBS before addition of F-actin stain (Phalloidins, Texas Red, 5 µL/well in 500 µL blocking buffer) for 1 h in a light protected vessel. Cell monolayers were then washed four times with PBS and mounted onto glass coverslips

with the addition of Prolong Gold Antifade reagent (Thermo Fisher Scientific), cured, sealed, and stored at 4 °C.

3.5.9 Neutralising antibody assay

Trypsinised A549 cells were seeded in a 12-well plate at 1 x 10^5 cells/well, followed by incubation at 37 °C for 16-24 h. For pre-treated condition, rLCMV-eGFP (MOI of 0.2) was incubated with 1 mL neutralising antibody (5µg/mL; made in 10% FBS DMEM) for 1 h. Remaining conditions (mock, virus only, virus + antibody [added at 3 hpi]) were subject to incubation with 1 mL 10% FBS DMEM for 1 h. Subsequently, the total 1 mL for each condition was added to A549s, and infection allowed to progress. At 3hpi, 5µg/mL neutralising antibody was added inhibiting extracellular viral spread. Total green cell count was measured every 6 h using an Incucyte Zoom S3 live cell imaging system (Sartorius) and normalised for confluency variation. The average of three independent experimental repeats is shown, with error bars showing standard deviation at each time point (n = 3). To confirm the effectiveness of antibody M28 in neutralization of any newly released viruses, supernatants were collected for 18 hpi, and then subject to treatment with 5µg/mL neutralising antibody for 1 h. Subsequently, virus with and without neutralising antibody were subject to focus forming assays and titres expressed as normalised virus titres. The average of three independent experimental repeats is shown, with error bars showing standard deviation at each time point (n = 3).

3.6 Acknowledgements

We acknowledge funding from MRC grant MR/T016159/1 in support of JNB, JF, AS and HNT, BBSRC PhD studentship grant to AS, UKHSA PhD studentship grant to OB. The authors thank Dr Ruth Hughes and Dr Sally Boxall of the bioimaging facility, Faculty of Biological Sciences, University of Leeds, for their expert assistance. We acknowledge the support of Wellcome Trust grant WT104918MA, for provision of the Zeiss LSM880 confocal microscope, the BBRSC grant BB/S019464/1 for the STEDYCon STED microscope, and equipment grant 221538/Z/20/Z from The Wellcome Trust, which supports the use of the Incucyte

live cell imaging platform.

3.7 References

[1] International Committee on Taxonomy of Viruses (ICTV). . Taxonomy. 2022 [accessed 2024 Mar 12]. https://talk.ictvonline.org/taxonomy/.

[2] Centers for Disease Control and Prevention (CDC). Viral Hemorrhagic Fevers. Bunyavirales. [online]. [accessed 2023 May 12]. https://www.cdc.gov/vhf/virus-families/bunyaviridae.htmL

[3] González PH, Cossio PM, Arana R, Maiztegui JI, Laguens RP. Lymphatic tissue in Argentine hemorrhagic fever. Pathologic features. Archives of pathology & laboratory medicine. 1980;104(5):250–4.

[4] Cheng BYH, Nogales A, de la Torre JC, Martínez-Sobrido L. Development of live-attenuated arenavirus vaccines based on codon deoptimization of the viral glycoprotein. Virology. 2017;501:35–46. doi:10.1016/j.virol.2016.11.001

[5] Bonthius DJ, Nichols B, Harb H, Mahoney J, Karacay B. Lymphocytic choriomeningitis virus infection of the developing brain: critical role of host age. Annals of Neurology. 2007;62(4):356–374. doi:10.1002/ana.21193

[6] Bonthius DJ. Lymphocytic Choriomeningitis Virus: An Underrecognized Cause of Neurologic Disease in the Fetus, Child, and Adult. Seminars in Pediatric Neurology. 2012;19(3):89–95. doi:10.1016/j.spen.2012.02.002

[7] Meyer BJ, de la Torre JC, Southern PJ. Arenaviruses: genomic RNAs, transcription, and replication. Current topics in microbiology and immunology. 2002;262:139–57. doi:10.1007/978-3-642-56029-3_6

[8] Maria S. Salvato. Arenaviridae. In: Virus Taxonomy. Elsevier; 2012. p. 715–723. doi:10.1016/B978-0-12-384684-6.00058-6

[9] Riviere Y, Ahmed R, Southern PJ, Buchmeier MJ, Dutko FJ, Oldstone MB. The S RNA segment of lymphocytic choriomeningitis virus codes for the nucleoprotein and glycoproteins 1 and 2. Journal of virology. 1985;53(3):966–8. doi:10.1128/JVI.53.3.966-968.1985

[10] Byford O, Shaw AB, Tse HN, Todd EJAA, Álvarez-Rodríguez B, Hewson

R, Fontana J, Barr JN. Lymphocytic choriomeningitis arenavirus requires cellular COPI and AP-4 complexes for efficient virion production. Journal of Virology. 2024 Feb 9. doi:10.1128/jvi.02006-23

[11] Sakabe S, Witwit H, Khafaji R, Cubitt B, de la Torre JC. Chaperonin TRiC/CCT Participates in Mammarenavirus Multiplication in Human Cells via Interaction with the Viral Nucleoprotein. Journal of Virology. 2023;97(2). doi:10.1128/jvi.01688-22

[12] Bakkers MJG, Moon-Walker A, Herlo R, Brusic V, Stubbs SH, Hastie KM, Saphire EO, Kirchhausen TL, Whelan SPJ. CD164 is a host factor for lymphocytic choriomeningitis virus entry. Proceedings of the National Academy of Sciences of the United States of America. 2022;119(10):e2119676119. doi:10.1073/pnas.2119676119

[13] Pepe A, Pietropaoli S, Vos M, Barba-Spaeth G, Zurzolo C. Tunneling nanotubes provide a route for SARS-CoV-2 spreading. Science advances. 2022;8(29):eabo0171. doi:10.1126/sciadv.abo0171

[14] Aggarwal A, Iemma TL, Shih I, Newsome TP, McAllery S, Cunningham AL, Turville SG. Mobilization of HIV Spread by Diaphanous 2 Dependent Filopodia in Infected Dendritic Cells. PLoS Pathogens. 2012;8(6):e1002762. doi:10.1371/journal.ppat.1002762

[15] Souriant S, Balboa L, Dupont M, Pingris K, Kviatcovsky D, Cougoule C, Lastrucci C, Bah A, Gasser R, Poincloux R, et al. Tuberculosis Exacerbates HIV-1 Infection through IL-10/STAT3-Dependent Tunneling Nanotube Formation in Macrophages. Cell Reports. 2019;26(13):3586-3599.e7. doi:10.1016/j.celrep.2019.02.091

[16] Kadiu I, Gendelman HE. Human Immunodeficiency Virus type 1 Endocytic Trafficking Through Macrophage Bridging Conduits Facilitates Spread of Infection. Journal of Neuroimmune Pharmacology. 2011;6(4):658–675. doi:10.1007/s11481-011-9298-z

[17] Eugenin EA, Gaskill PJ, Berman JW. Tunneling nanotubes (TNT) are induced by HIV-infection of macrophages: a potential mechanism for intercellular HIV trafficking. Cellular immunology. 2009;254(2):142–8. doi:10.1016/j.cellimm.2008.08.005

[18] Martinez MG, Kielian M. Intercellular Extensions Are Induced by the Alphavirus Structural Proteins and Mediate Virus Transmission. PLOS Pathogens. 2016;12(12):e1006061. doi:10.1371/journal.ppat.1006061

[19] Ganti K, Han J, Manicassamy B, Lowen AC. Rab11a mediates cell-cell spread and reassortment of influenza A virus genomes via tunneling nanotubes. PLoS pathogens. 2021;17(9):e1009321. doi:10.1371/journal.ppat.1009321

[20] Mothes W, Sherer NM, Jin J, Zhong P. Virus Cell-to-Cell Transmission. Journal of Virology. 2010;84(17):8360–8368. doi:10.1128/JVI.00443-10

[21] Rustom A, Saffrich R, Markovic I, Walther P, Gerdes H-H. Nanotubular Highways for Intercellular Organelle Transport. Science. 2004;303(5660):1007–1010. doi:10.1126/science.1093133

[22] Kumar A, Kim JH, Ranjan P, Metcalfe MG, Cao W, Mishina M, Gangappa S, Guo Z, Boyden ES, Zaki S, et al. Influenza virus exploits tunneling nanotubes for cell-to-cell spread. Scientific Reports. 2017;7(1):40360. doi:10.1038/srep40360

[23] Shaw AB, Tse HN, Byford O, Plahe G, Moon-Walker A, Hover SE, Saphire EO, Whelan SPJ, Mankouri J, Fontana J, et al. Cellular endosomal potassium ion flux regulates arenavirus uncoating during virus entry Duggal NK, editor. mBio. 2024;15(7):2023.06.23.546275. https://journals.asm.org/doi/10.1128/mbio.01684-23. doi:10.1128/mbio.01684-23

[24] Yamagishi Y, Oya K, Matsuura A, Abe H. Use of CK-548 and CK-869 as Arp2/3 complex inhibitors directly suppresses microtubule assembly both in vitro and in vivo. Biochemical and Biophysical Research Communications. 2018;496(3):834–839. doi:10.1016/j.bbrc.2018.01.143

[25] Hetrick B, Han MS, Helgeson LA, Nolen BJ. Small Molecules CK-666 and CK-869 Inhibit Actin-Related Protein 2/3 Complex by Blocking an Activating Conformational Change. Chemistry & Biology. 2013;20(5):701–712. doi:10.1016/j.chembiol.2013.03.019

[26] Moon-Walker A, Zhang Z, Zyla DS, Buck TK, Li H, Diaz Avalos R, Schendel SL, Hastie KM, Crotty S, Saphire EO. Structural basis for antibody-mediated neutralization of lymphocytic choriomeningitis virus. Cell Chemical Biology. 2023;30(4):403-411.e4. doi:10.1016/j.chembiol.2023.03.005

[27] Labudová M, Čiampor F, Pastoreková S, Pastorek J. Cell-to-cell transmission of lymphocytic choriomeningitis virus MX strain during persistent infection and its influence on cell migration. Acta virologica. 2018;62(04):424–434. doi:10.4149/av_2018_411

[28] Jansens RJJ, Tishchenko A, Favoreel HW. Bridging the Gap: Virus Long-Distance Spread via Tunneling Nanotubes. Journal of virology. 2020;94(8). doi:10.1128/JVI.02120-19

[29] Zeng C, Evans JP, King T, Zheng Y-M, Oltz EM, Whelan SPJ, Saif LJ, Peeples ME, Liu S-L. SARS-CoV-2 spreads through cell-to-cell transmission. Proceedings of the National Academy of Sciences. 2022;119(1). doi:10.1073/pnas.2111400119

[30] Kahan SM, Zajac AJ. Immune Exhaustion: Past Lessons and New Insights from Lymphocytic Choriomeningitis Virus. Viruses. 2019;11(2):156. doi:10.3390/v11020156

[31] Staneck LD, Trowbridge RS, Welsh RM, Wright EA, Pfau CJ. Arenaviruses: Cellular Response to Long-Term In Vitro Infection with Parana and Lymphocytic Choriomeningitis Viruses. Infection and Immunity. 1972;6(4):444–450. doi:10.1128/iai.6.4.444-450.1972

[32] Kumar A, Kim JH, Ranjan P, Metcalfe MG, Cao W, Mishina M, Gangappa S, Guo Z, Boyden ES, Zaki S, et al. Influenza virus exploits tunneling nanotubes for cell-to-cell spread. Scientific Reports. 2017;7(1):40360. doi:10.1038/srep40360

[33] Sartori-Rupp A, Cordero Cervantes D, Pepe A, Gousset K, Delage E, Corroyer-Dulmont S, Schmitt C, Krijnse-Locker J, Zurzolo C. Correlative cryo-electron microscopy reveals the structure of TNTs in neuronal cells. Nature Communications. 2019;10(1):342. doi:10.1038/s41467-018-08178-7

[34] Lehmann MJ, Sherer NM, Marks CB, Pypaert M, Mothes W. Actin- and myosin-driven movement of viruses along filopodia precedes their entry into cells. Journal of Cell Biology. 2005;170(2):317–325. doi:10.1083/jcb.200503059

[35] Xiao F, Fofana I, Heydmann L, Barth H, Soulier E, Habersetzer F, Doffoël M, Bukh J, Patel AH, Zeisel MB, et al. Hepatitis C Virus Cell-Cell Transmission and Resistance to Direct-Acting Antiviral Agents. PLoS Pathogens. 2014;10(5):e1004128.

[36] King BR, Kellner S, Eisenhauer PL, Bruce EA, Ziegler CM, Zenklusen D, Botten JW. Visualization of the lymphocytic choriomeningitis mammarenavirus (LCMV) genome reveals the early endosome as a possible site for genome replication and viral particle pre-assembly. The Journal of general virology. 2017;98(10):2454–2460. doi:10.1099/jgv.0.000930

Chapter 4

Lymphocytic choriomeningitis arenavirus nucleoprotein phosphorylation as an antiviral response

Unpublished

Owen Byford[1,2] Amelia B. Shaw[1,2] Marine-Noel Klamke[3] Richard Küchler[3] Axel Karger [3] Hiu Nam Tse [1,2] Lee Kipling [1] Martin Stacey [1] Roger Hewson 4,5 Allison Groseth 3 Juan Fontana 6 John N. Barr 1,2

[1]School of Molecular and Cellular Biology, Faculty of Biological Sciences, University of Leeds, Leeds, LS2 9JT, United Kingdom

[2]Astbury Centre for Structural Molecular Biology, University of Leeds, Leeds, LS2 9JT, United Kingdom

[3]Laboratory for Arenavirus Biology, Institute of Molecular Virology and Cell Biology, Friedrich-Loeffler-Institut, Greifswald-Insel Riems, Germany

[4]UK Health Security Agency (UK), Porton Down, Salisbury SP4 0JG, UK

[5]Faculty Infectious and Tropical Diseases, London School of Hygiene and Tropical Medicine, Keppel Street, London WC1E 7HT, UK

[6]Instituto Biofisika, CSIC-UPV/EHU, Barrio Sarriena s/n, Leioa, Bizkaia, Spain

4.1 Abstract

The newly formed *Bunyaviricetes* class of segmented negative-sense RNA viruses contains the *Arenaviridae* family, for which the prototypic species is lymphocytic choriomeningitis virus (LCMV), a recognised model for members able to cause fatal haemorrhagic fevers such as Lassa and Junín viruses. Here, we examine the phosphorylation of LCMV nucleoprotein (NP) with particular focus on the S343 residue. Through mass spectrometry, we detected phosphorylation at 6 NP residues, with modification at S343 identified as most abundant. To test the consequence of charge acquisition at S343, infectious LCMV bearing NP with phospho-ablantant (S343A) and phospho-mimetic (S343E) substitutions were generated, and analysis of their growth kinetics during infection of BHK, A549, SH-SY5Y and NIH3T3 cell lines, revealed no significant differences in virus fitness. In contrast, infection of the mouse macrophage cell line RAW264.7 with rLCMV-S343E resulted in a significantly diminished titre and NP expression compared to rLCMV-WT. Interestingly, LCMV-WE (pathogenic) NP is unable to be phosphorylated at S343, thus this modification is specific to LCMV-Arm (non-pathogenic), which may contribute to the differences in pathogenicity. Taken together, these findings shown that LCMV NP can be phosphorylated, and residue S343 phosphorylation acts as an antiviral response.

4.2 Importance

Arenavirus species can cause human fatality and currently there are no specific preventatives or treatments available. Here, we utilise LCMV and provide evidence that the NP is phosphorylated. We further examined the role of NP residue S343, revealing that NP S343 phosphorylation is not required for any viral-dependent stage of LCMV infection, but instead acts in an antiviral manner. Our data suggests that S343 phosphorylation of NP is LCMV strain specific, which may contribute to the differing pathogenicity.

Keywords: Arenavirus; LCMV; nucleoprotein, phosphorylation, antiviral.

4.3 Chapter Introduction

The *Arenaviridae* family within the *Bunyavirricetes* class of segmented negative-sense RNA viruses presently contains 69 species grouped into five genera; *Antennavirus*, *Hartmanivirus*, *Innmovirus*, *Mammarenavirus* and *Reptarenavirus* [1]. Species of the *Mammarenavirus* genus typically establish latent infections within rodents, but can spill-over into humans resulting in severe disease. In some cases, infection can result in haemorrhagic fever with potentially fatal outcomes, most notably for Lassa virus (LASV) and Junín virus (JUNV) [2, 3]. To date, there are no FDA-approved vaccines or antiviral therapies to prevent or mitigate infection by any member of the *Arenaviridae* family. Consequently, several arenaviruses are classified as hazard group 4 pathogens, requiring biosafety level (BSL) 4 containment for handling, which has hindered research advancements.

Lymphocytic choriomeningitis virus (LCMV), the prototypic species of the *Mammarenavirus* genus, acts as a research model for highly pathogenic arenaviruses, with the Armstrong strain requiring only BSL-2 containment for study. The common host mouse Mus musculus is the primary host for LCMV, with rodent-human transmission frequently occurring [4]. Multiple serology studies conducted within urbanised areas have reported a prevalence of LCMV antibodies within the human population as 2-9% [5–7]. Although LCMV infection is considered as less pathogenic, severe disease can arise within immunocompromised patients or neonates [8, 9]. In these cases, patients often present with aseptic meningitis, and as such LCMV has been identified as an underrecognised agent of neurological disease [9].

All species within the *Mammarenavirus* genus possess bi-segmented genomes comprising small (S) and large (L) segments, which collectively encode four structural proteins. S encodes the nucleoprotein (NP) and glycoprotein precursor (GPC), whereas L encodes the viral RNA-dependent RNA polymerase (RdRp, L protein) and matrix protein (Z). Nascent virion-associated RNAs (vRNA) are coated by NP, and together associate with L to form viral ribonucleoprotein (vRNPs). Within mature virions, vRNPs are enclosed within a cell-derived lipid bilayer; Z coats the interior, with viral spikes protruding from the surface. In relation to gene expression, entry and uncoating releases input S and L vRNAs into the cytoplasm, which are transcribed to yield mRNAs encoding for NP and L,

respectively. Succeeding this, replication of full-length S and L vRNAs generates S and L anti-genome RNAs (agRNA), and using an ambi-sense coding strategy, these S and L agRNAs act as templates for transcription of mRNAs encoding GPC and Z, respectively.

The interplay between virus infection and both the innate and adaptive immune system has been well studies for arenaviruses, with LCMV being used extensively as a model system, in particular for understanding the establishment latent or persistent infections at the organismal level, using the natural rodent host. In addition, many arenaviruses express a potent immune modulatory factor in the form of the NP. The LASV NP been shown possess an exonuclease activity specific for dsRNA that acts to restrict translocation of IFN regulatory factor 3 (IRF3) and block activation of innate immune responses [10]. The exonuclease domain (ExoN) of NP belongs to the DEDDh family of 3'-5' exonucleases and functional residues D382 and G385 are highly conserved between arenavirus species [11, 12]. The ExoN regions of NP has also been shown to bind directly to Inhibitor Of Nuclear Factor Kappa B Kinase Subunit Epsilon (IKKϵ) [13]. Sequestering of IKKϵ was shown in vitro to prevent IRF3 phosphorylation, and thus blocks IRF3 activation [13]. The NP-IKKϵ interaction is retained for both Old and New World arenavirus species including LCMV, LASV, WWAV, LATV and JUNV, indicating this mechanism of immune inhibition may be conserved [13].

Proteomic analysis of NP binding partners has identified multiple other cellular interacting proteins involved in immune signalling including Retinoic acid-inducible gene I (RIG-I), melanoma differentiation-associated protein 5 (MDA-5) and DEAD-Box Helicase 3 (DDX3) [14–17]. Investigation for RIG-I and MDA-5 highlighted how NP may prevent nuclear translocation of IRF3, ultimately preventing IFN-β production [14–16]. Intriguingly, DDX3 has previously been described as antiviral, by causing activation of IFN-I [18, 19]. However, for LCMV, the NP-DDX3 interaction was shown to be pro-viral supressing IFN-I [20].

Interestingly, despite retaining this exonuclease domain, JUNV NP is unable to degrade dsRNA [21]. Thus, JUNV employs a different strategy to modulate induction of apoptosis and interferon expression. Firstly, within native JUNV infection, NP cleavage and alternative translation of NP mRNA results in three additional NP isoforms, and these products act as a caspase decoys for modulating

the induction of apoptosis and interferon expression [22, 23]. Additionally, to control immune activation via the protein kinase R (PKR) signalling pathway, which is activated by increased levels of dsRNA, JUNV NP binds directly to PKR preventing phosphorylation of eIF2a [24]. Taken together, this highlights how arenavirus NP has multifunctional roles for immune modulation during infection.

Phosphorylation of LCMV NP during native infection has been reported previously, [25]. Within this work, five NP phosphorylation sites were identified through mass spectrometry of purified LCMV virions: S116, S122, Y125, S343, and T330 [25]. Alongside these identified sites, phosphorylation algorithms highlighted four other residues as predicted site: S9, S82, T206, and S233 [25]. The investigations primarily focused on phosphorylation of T206, and the requirement of this modification for the formation of punctate replication and transcription complexes (RTCs) during LCMV infection [25].

Here, we sought to further investigate LCMV NP phosphorylation. Using LC-MS we identified novel phosphorylation sites at residues S2, T73, T76, S138 and S263, alongside the previously reported S343, which became the focus of our study due to its relative abundance and its location within a potential region of disorder separating the N- and C-terminal domains. To test the importance of S343 phosphorylation on virus fitness, infectious phospho-ablatant (rLCMV-S343A) and phospho-mimetic (rLCMV-S343E) LCMV variants were generated, revealing rLCMV-S343E possessed a significant growth deficiency in the mouse macrophage cell line RAW264.7, establishing the acquisition of charge at residue S343 by phosphorylation as a possible antiviral determinant. Interestingly, while residue S343 is conserved in the pathogenic LCMV strain WE (LCMV-WE), we showed it cannot be phosphorylated, thus opening the interesting possibility that acquisition of charge at S343 may represent a previously unrecognised determinant of LCMV pathogenicity.

Overall, this study improves our understanding of arenavirus NP post-translational modifications and highlights how phosphorylation of viral proteins may act as a host counter-defence.

4.4 Results

Phosphorylation of LCMV NP

Previous mass spectrometric analysis of purified LCMV showed NP was phosphorylated at residues S116, S122, Y125, S343, and T330 [25], with residues S9, S82, T206, and S233 predicted to be phosphorylated, despite not being detected [25]. The phenotypic consequences of phosphorylation at only T206 were examined further, with this residue shown to be essential for virus rescue.

To investigate LCMV NP phosphorylation further, we adopted a virus-like particle (VLP) approach, chosen to allow the detection of NP phosphorylation events independent of virus multiplication. As such, we transfected HEK293T cells with plasmids expressing NP and Z proteins, with subsequently generated virus-like particles (VLPs) harvested and purified, then subject to liquid chromatography-tandem mass spectrometry analysis (LC-MS). Tryptic and chymotryptic digests of NP resulted in peptides that were independently examined for the presence of phosphorylation, with 6 residues identified, namely S2, T73, T76, S138, S263 and S343. Of these, S2, T73, T76, S138 and S263 are novel phosphorylation sites, with only S343 being previously identified [25] (Figure 4.1A; Mass spectra; Supplementary figure 8.1). While S2, T73, T76, S138, S263 were detected as phosphorylated with a single peptide, phosphorylation at S343 was identified through multiple peptides. Interestingly, all the newly identified phosphorylated residues were located within the NP-core domain, with the exception of S343, which was located within the accessible flexible linker region connecting the NP-core and ExoN domains (Figure 4.1B).

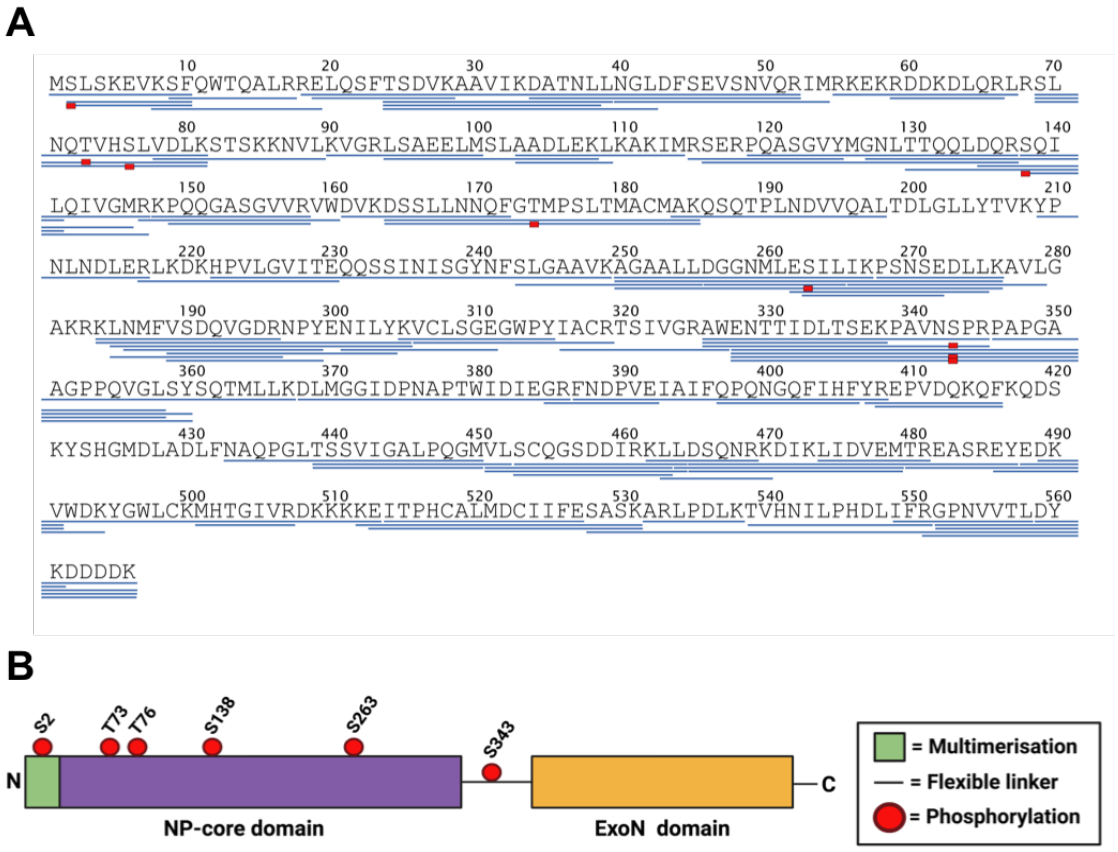

Figure 4.1: LCMV NP phosphorylated residues. (A) Peptide map of LCMV NP-flag. Sequence regions matching identified unique peptides and phosphosite positions are shown with blue lines and red boxes, respectively. The proteomics experiment resulted in a total coverage of 96.6%. (B) Schematic depicting the NP domains and flexible linkers, alongside the positions of identified phosphorylated residues (red circles).

F-actin disruption via CK-869 causes phosphorylation of LCMV NP at S343.

When performing western blot analysis of NP from rLCMV-infected A549 cells using NP antisera, we routinely detect a doublet comprising a major NP species in addition to a minor species of reduced mobility (Supplemental Figure 8.2), potentially representing NP with a post-translational modification. Interestingly, during recent work where we intentionally disrupted actin or tubulin cytoskeleton integrity using CK-869 or nocodazole, we noticed an increased abundance of an equivalent slower migrating species (Figure 4.2A-B). We postulated that cytoskeletal disruption, and the subsequent induction of cellular kinase activity that this brings [26, 27] may promote NP phosphorylation. Consistent with this hypothesis, virus-induced remodelling of the actin cytoskeleton is known to alter the activity of the PP1-R12C

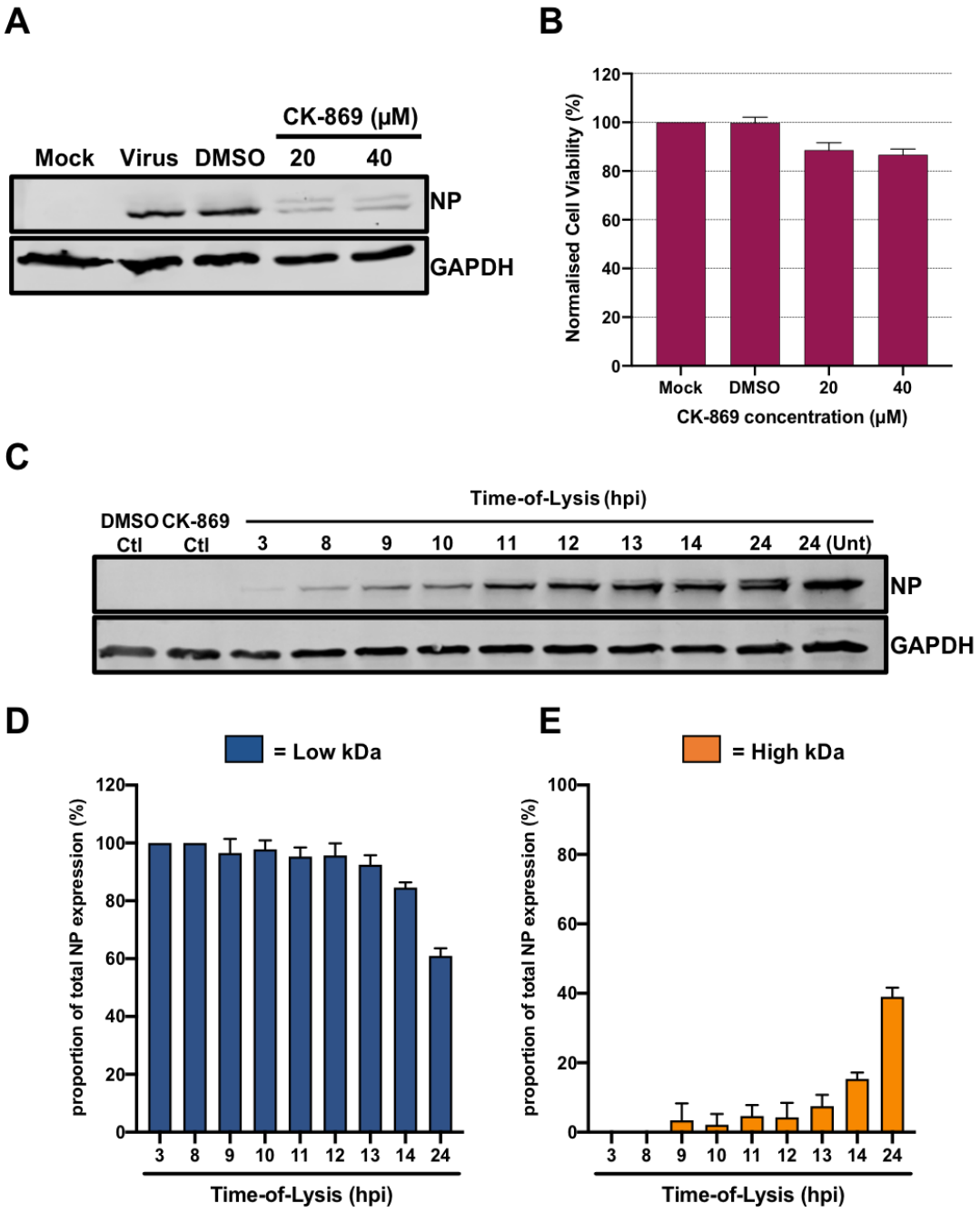

Figure 4.2: CK-869 causes an increased post-translational modification of LCMV NP. (A) A549 cells were pre-treated with 20- and 40 μM CK-869 and then infected with LCMV at an multiplicity of infection (MOI) of 0.2. Lysates were collected at 24 hpi, and subject to western blot analysis using anti-sera specific for LCMV NP and GAPDH as loading control. (B) Analysis of CK-869 toxicity in A549 at 20- and 40 μM as measured by MTT assay, normalised to mock untreated cells. (C) Representative western blot from time-of-lysis analysis. A549 cells were infected with LCMV at an MOI of 0.2, with CK-869 (20 μM) added at 3 hpi. Subsequently, lysates were collected at hourly intervals (8-14 hpi), alongside input (3 hpi) and known (24 hpi) controls, which were then subject to western blot analysis. (D and E) Densitometry histograms of the NP proportion representing the lower (D) and higher (E) molecular weight. The proportion was quantified for three independent experimental repeats, with error bars representing deviation from the mean.

phosphatase complex, which primes and activates the RIG-I-like receptor, mediating an increased antiviral IFN response [28]. An increased antiviral IFN response could confer increased NP phosphorylation as a consequence of cellular kinases, relating to antiviral signalling pathways such as STAT1/3, IRF3/7 and MAVS [29–31].

To investigate the origin of this reduced mobility NP species, we wanted to understand the kinetics of its induction, and to this end we performed a time-of-lysis experiment. Cells were infected with rLCMV-WT at an MOI of 0.2, and at 3 hpi, 20 µM CK-869 was added, with cell lysates harvested hourly from 8 to 24 hpi and subjected to western blotting (Figure 4.2C). LCMV NP was first detectable at 3 hpi and with increasing abundance thereafter, as quantified by densitometry of three western blots (Figure 4.2D). In contrast, the reduced mobility band was first detected at around 9 hpi, subsequently increasing in both abundance and relative proportion until reaching approximately 40% abundance at 24 hpi (Figure 4.2D). This temporal appearance of the minor reduced mobility species was consistent with kinase induction.

To identify the modification responsible for the appearance of the reduced mobility species in CK-869 treated cells, we performed LC-MS analysis of chymotrypsin-digested NP co-immunoprecipitated (co-IP) from LCMV infected cell lysates (Figure 4.3A). This analysis identified residue S343 to be the sole phosphorylation site within NP, with a certainty of over 97% (Figure 4.3B). Interestingly, in untreated conditions, we were unable to detect phosphorylation at S343, likely a result of low abundance of the corresponding peptide following NP pull-down. No other modifications were detected in these samples, leading us to conclude that the reduced mobility NP species detected by western blotting corresponded in major part to NP phosphorylated at residue S343.

A

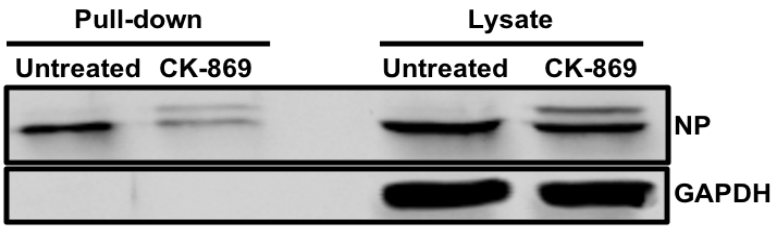

B

Peptide generated (chemotryptic)	Modification	Residue	Probability (%)
TSEKPAVN**S**PRPAPGAAGPPQVGL	Phosphorylation	S343	97.47
TSEKPAVNSPRPAPGAAGPPQVGL	Phosphorylation	T335	2.53

Figure 4.3: NP is phosphorylated with S343 representing the likely residue. (A) Co-Immunoprecipitation was performed from infected LCMV untreated and CK-869 cultures, lysates and pull-down products were then subject to western blot analysis. (B) Liquid chromatography–mass spectrometry (LC-MS) analysis was performed on chemotryptic digested untreated and CK-869 treated pull-down samples. The highlighted peptides was identified as phosphorylated in CK-869 treated cultures, with the probability for each residue shown.

Recovery of recombinant LCMV expressing NP with S343 phospho-ablatant and phospho-mimetic mutations.

The results of the previous sections identified residue S343 as a consistently phosphorylated site within NP, either in native conditions, or following cytoskeletal disruption. These observations, combined with the location of S343 within the inter-domain unstructured region, prompted us to investigate the consequences of S343 phosphorylation, and subsequent acquisition of negative charge, in LCMV multiplication.

To do this, we attempted to recover infectious recombinant LCMV bearing phospho-ablatant (S343A) and phospho-mimetic (S343E) substitutions [32, 33] (Figure 4.4A), intended to mimic the constitutive loss or gain of negative charge that phosphorylation at S343 would impart, respectively [34].

Recovery of both rLCMV-S343A and rLCMV-S343E was successful, evidenced by the detection of NP following subsequent infection in BHK cells (Figure 4.4B and Supplimentary figure 8.3), with both viruses reaching titres of around 10^7 focus forming units/mL (FFU/mL) in subsequently amplified stocks.

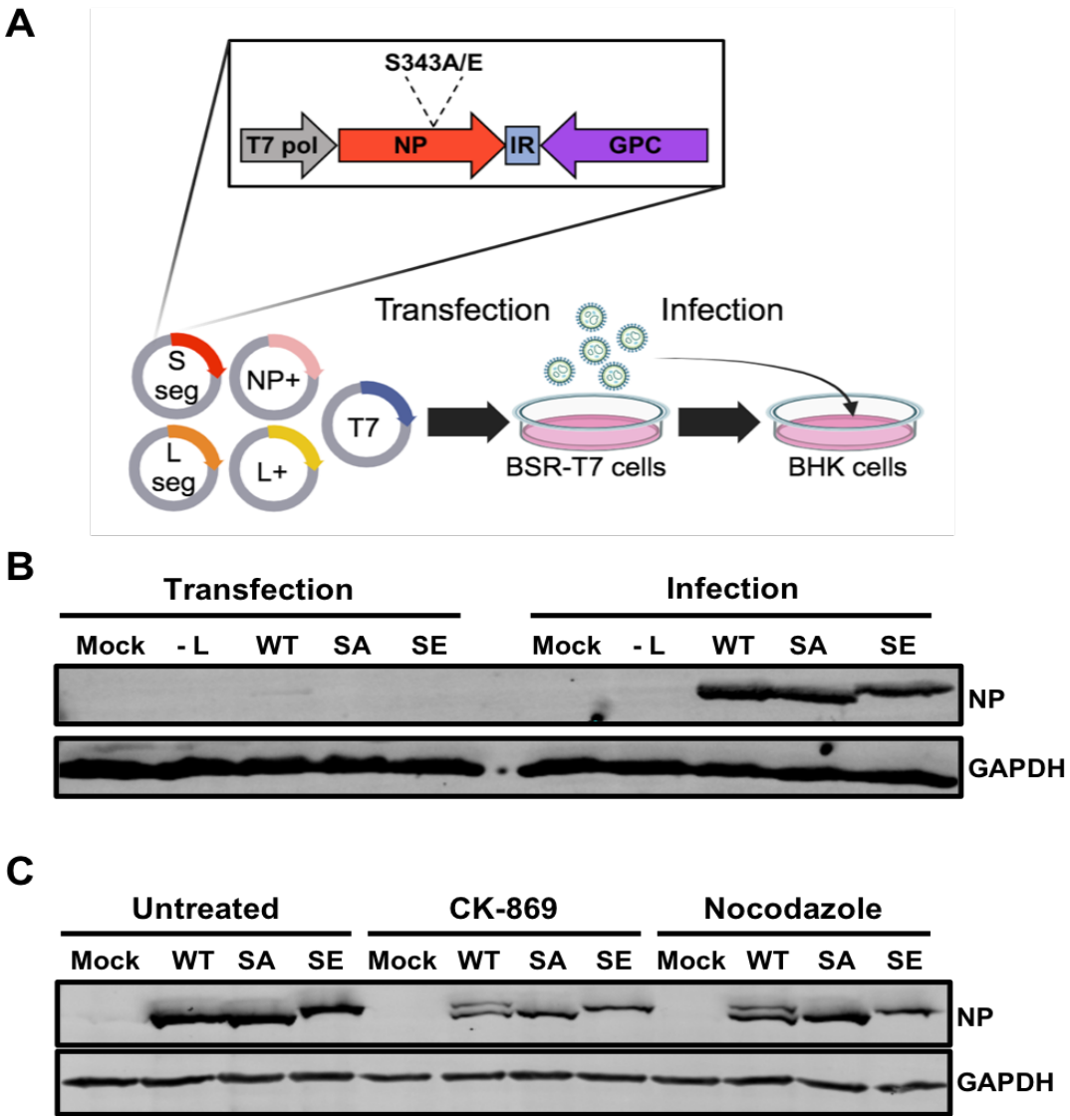

Figure 4.4: Recovery of LCMV NP phospho-ablatant (S343A) and phospho-mimetic (S343E) mutants. (A) Schematic highlighting rescue of recombinant LCMV harbouring NP S343A/E mutations within the S segment. (B) Western blot analysis of transfected BSR-T7 alongside infected BHK-21 cell cultures confirmed rLCMV-S343A/E (alongside rLCMV-WT rescue). (C) Validation of S343 as the site of phosphorylation. A549 cells were infected with rLCMV-WT, rLCMV-S343A and rLCMV-S343E, with CK-869 (20 µM) or nocodazole (20 µM) added at 3 hpi. Lysates were harvested at 24 hpi and subjected to western blot analysis.

Next, to test whether the specified mutations were stably retained, rLCMV-S343A and rLCMV-S343E infected cells were treated with CK-869 and nocodazole. As expected, NP generated in rLCMV-S343A infected cells migrated as a single major species with equivalent mobility to that of WT NP, indicating it had lost the capacity to acquire phosphorylation, and thus charge (Figure 4.4C). Also in line with expectations, NP generated in rLCMV-S343E infected cells migrated as a single species, but with a reduced mobility corresponding to that of NP phosphorylated at S343, consistent with acquisition of negative charge through the

S343E substitution. Taken together, the mobility of NP expressed in rLCMV-S343A and rLCMV-S343E infected cells was consistent with their respective loss or gain of negative charge and further confirmed that residue S343 was the target of modification by a phosphorylation event.

Phosphorylation of LCMV NP at S343 is not required for viral propagation.

To elucidate the role of S343 phosphorylation during LCMV infection, we investigated the propagation of rLCMV-WT, rLCMV-S343A and rLCMV-S343E in multiple cell lines including BHK, SH-SY5Y, NIH3T3, A549 and the LCMV permissible mouse macrophage cell line RAW264.7, which exhibit fundamental macrophage-like immune related functions such as phagocytosis and pinocytosis. Cells were infected with each virus with an MOI of 0.2. and viral supernatants were collected at 48 hpi, which were then subject to titration via focus forming assay. The mean titre for rLCMV-WT, rLCMV-S343A and rLCMV-S343E for each cell line is shown, alongside standard deviation of the three independent experimental repeats (Figure 4.5 and 4.6A). Consistent with previous virus rescue experiments, when propagated in BHK-21 cells (red) there was no significant difference between the growth of rLCMV-WT, rLCMV-S343A or rLCMV-S343E, with all capable of virus propagation to around 10^7 FFU/mL. The lack of difference in propagation between rLCMV-WT, rLCMV-S343A and rLCMV-S343E was also conserved for SH-SY5Y (blue), NIH3T3 (purple) and A549 (green) cells (Figure 4.5).

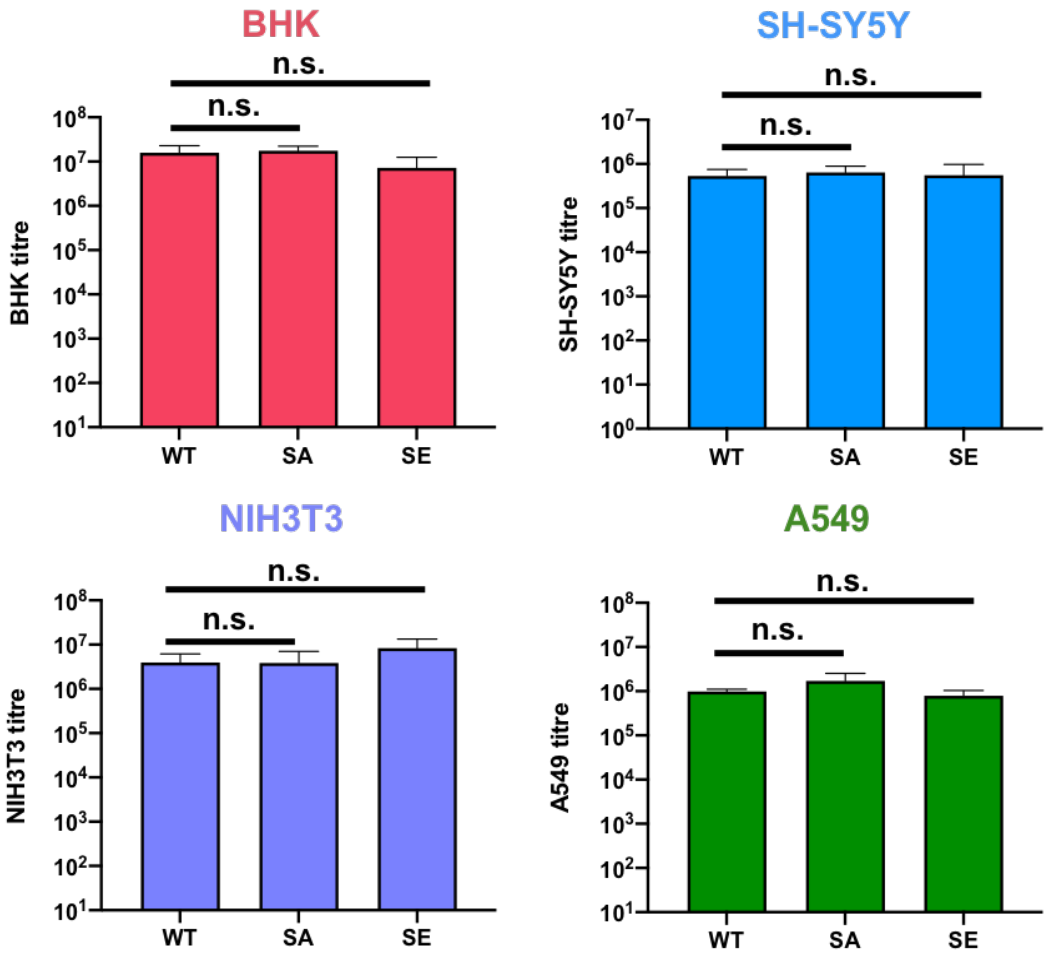

Figure 4.5: LCMV growth is not dependent on NP S343 phosphorylation. BHK (red), SH-SY5Y (blue), NIH3T3 (purple) or A549 (green) cells were infected with either rLCMV-WT, rLCMV-S343A or rLCMV-S343E at an MOI of 0.2, viral supernatants were then collected at 48 hpi. Three independent experimental repeats were performed with the mean represented, and error bars representing deviation.

Next, we examined LCMV and the two variant viruses following infection of the mouse macrophage cell line RAW264.7, utilised for investigating LCMV persistence and immune evasion. Here, rLCMV-S343A and LCMV-WT showed no significant difference in mean viral titre (Figure 4.6A), rLCMV-S343E had a significantly reduced (10-fold) mean titre compared to rLCMV-WT (Figure 4.6A). This reduced titre was also mirrored in reduced expression of LCMV NP, with quantification of three independent experimental repeats (Figure 4.6B and C) revealing NP expression levels 19.9% that of LCMV-WT (Figure 4.6B). Taken together, these data show the acquisition of negative change at 343 correlates with the reduced fitness of rLCMV-S343E, which is consistent with phosphorylation at this site being an antiviral outcome, The fact that this phenotype was only identified in RAW264.7 cells suggests it is related to the innate immune competency of these cells.

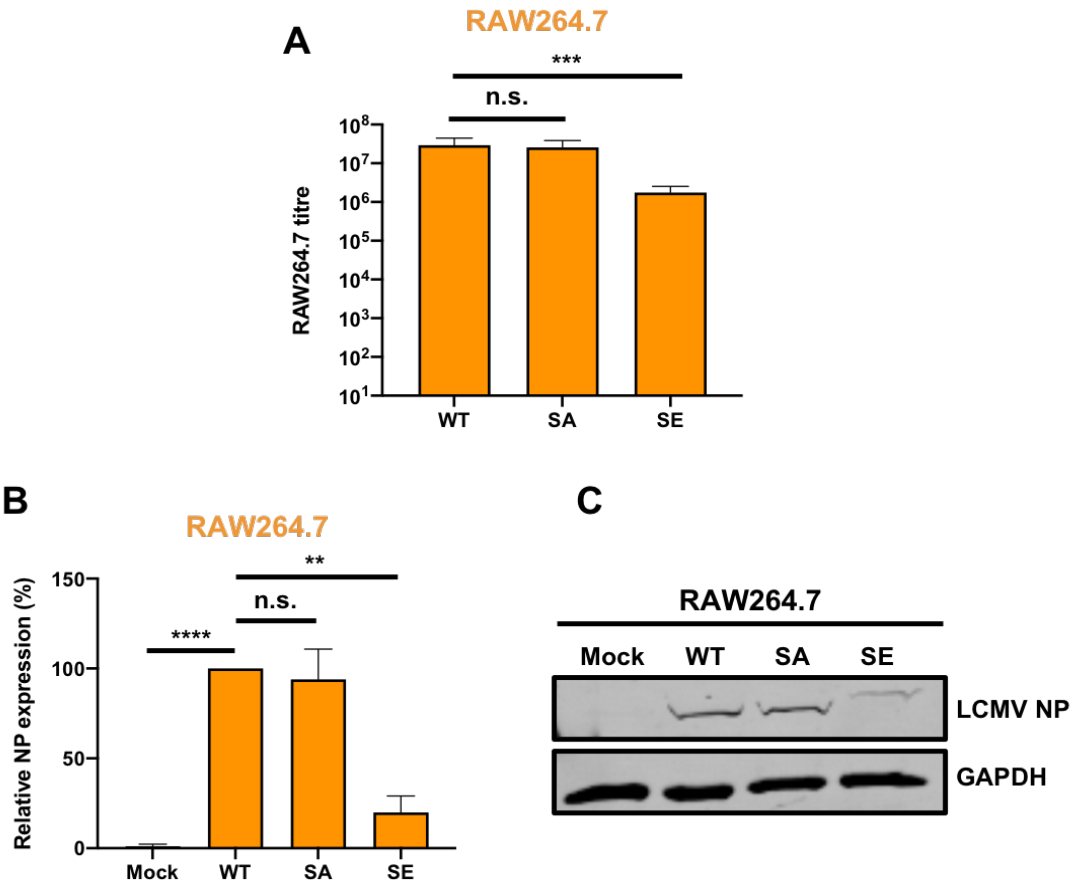

Figure 4.6: Analysis of S343A and S343E within the mouse macrophage cell line RAW264.7. (A) RAW264.7 cells (orange) were infected with either rLCMV-WT, rLCMV-S343A or rLCMV-S343E at an MOI of 0.2, viral supernatants were then collected at 48 hpi. Three independent experimental repeats were performed with the mean represented, and error bars representing deviation. (B and C) Lysates from (A) were collected and subject to western blot analysis (represented in C). Densitometry was plotted showing relative fold-change of NP expression, normalised to rLCMV-WT, over three experimental repeats with error bars showing deviation from the mean.

Co-localisation of LCMV-S343E NP and lysosomes.

LCMV NP was shown to have similar diffuse cytoplasmic localisation within RAW264.7 cultures for LCMV-WT, LCMV-S343A and LCMV-S343E, despite a reduction in NP expression and titre following LCMV-S343E infection. We hypothesised that NP may be expressed and distributed similar initially in all cultures, yet phosphorylation targets NP for lysosomal degradation [35]. To investigate this, we performed IF to examine the spatial proximity of NP and LAMP-1, a lysosomal cell marker, for RAW264.7 cultures infected with LCMV-WT, LCMV-S343A and LCMV-S343E (Figure 4.7).

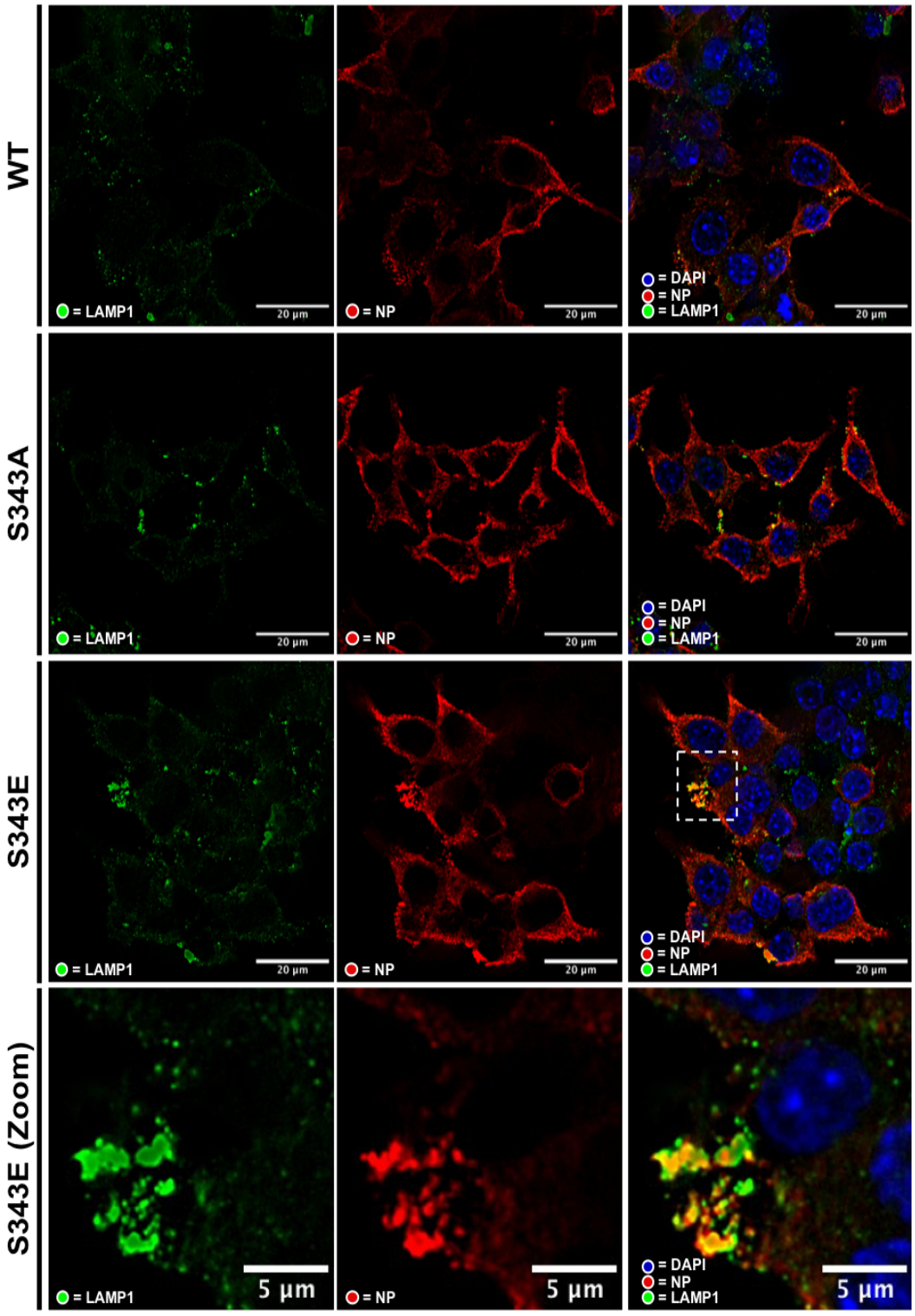

Figure 4.7: LCMV NP and LAMP-1 (lysosomes) co-localise in rLCMV-S343E infected RAW264.7 cells. Confocal microscopy of rLCMV-WT, rLCMV-S343A and rLCMV-S343E RAW264.7 infected cells at 48 hpi, MOI of 0.2. RAW264.7 cells were stained with NP (red), LAMP-1 (green) and DAPI (blue), scale bar 20 µm. A zoomed image for rLCMV-S343 NP/LAMP co-localisation (white boxes) is shown, scale bar 5 µm.

Consistent with the previous IF analysis, for RAW264.7 cells infected with LCMV-WT, LCMV-S343A or LCMV-S343E, the distribution of NP (red) alone was comparable. Infected cells showed diffuse cytoplasmic NP distribution, with

specific regions that had increased intensity. Interestingly, the LAMP-1 (lysosomal) localisation and distribution differed between LCMV-WT, LCMV-S343A and LCMV-S343E. For the RAW264.7 culture infected with LCMV-WT, LAMP-1 (green) was mainly distributed within infrequent small puncta throughout the cytoplasm (Figure 4.7). Within this culture, no clear co-localisation between LCMV NP and LAMP-1 was evident. For the LCMV-S343A infected culture, LAMP-1 showed localisation within discrete cytosolic regions, which were of higher intensity compared to LCMV-WT. However, comparable to LCMV-WT, NP from LCMV-S343A cultures had little evidence of co-localisation with LAMP-1. Of emphasis, the LCMV-S343E infected culture showed major differences compared to both LCMV-WT and LCMV-S343A. Firstly, the LAMP-1 localisation differed, showing diffuse cytoplasmic distribution alongside regions with clusters of discrete puncta (Figure 4.7). Secondly, within S343E infected cultures, the LAMP-1 regions of increased intensity revealed close co-localisation with LCMV NP (Figure 4.7; zoom).

Taken together, these findings suggest a close association between NP and LAMP-1 within RAW264.7 cells infected with LCMV-S343E, which is not evident in LCMV-WT or LCMV-S343A cultures. Thus, this is consistent with phosphorylation of NP performing in an antiviral manner, through the targeting of NP for degradation via lysosomes.

NP phosphorylation is strain specific.

The previous findings were all performed using the apathogenic LCMV-Arm strain. Recent work has revelated that infection with LCMV-Arm strain or LCMV-WE strain corresponds to differing immune responses, giving possible explanation for the difference in respective apathogenic or pathogenic outcomes [36]. Given that NP is well established to interfere with innate immune signalling by virtue of its ExoN activity, alongside our finding that S343 phosphorylation of NP may be a host antiviral response, we wished to examine whether NP from both LCMV-Arm and LCMV-WE strains can be phosphorylated. First, sequence alignment confirmed residue S343 was conserved in both strains despite differences in the surrounding residues (Figure 4.8A).

To investigate the ability of NP from rLCMV-Arm and rLCMV-WE to be phosphorylated, A549 cells were infected with either strain, and at 3 hpi, 20 µM CK-869 was added to the cultures, with cellular lysates harvested at 24 hpi and subjected to western blotting using NP antisera (Figure 4.8B). As shown above (Figure 4.2), NP from rLCMV-Arm can be phosphorylated, resulting in detection of NP with reduced mobility by western blotting in both untreated and CK-869 treated conditions (Figure 4.8B). Interestingly, when examining NP from LCMV-WE infected lysates, there was no such NP doublet, showing phosphorylation at S343 was not possible, despite this residue being conserved.

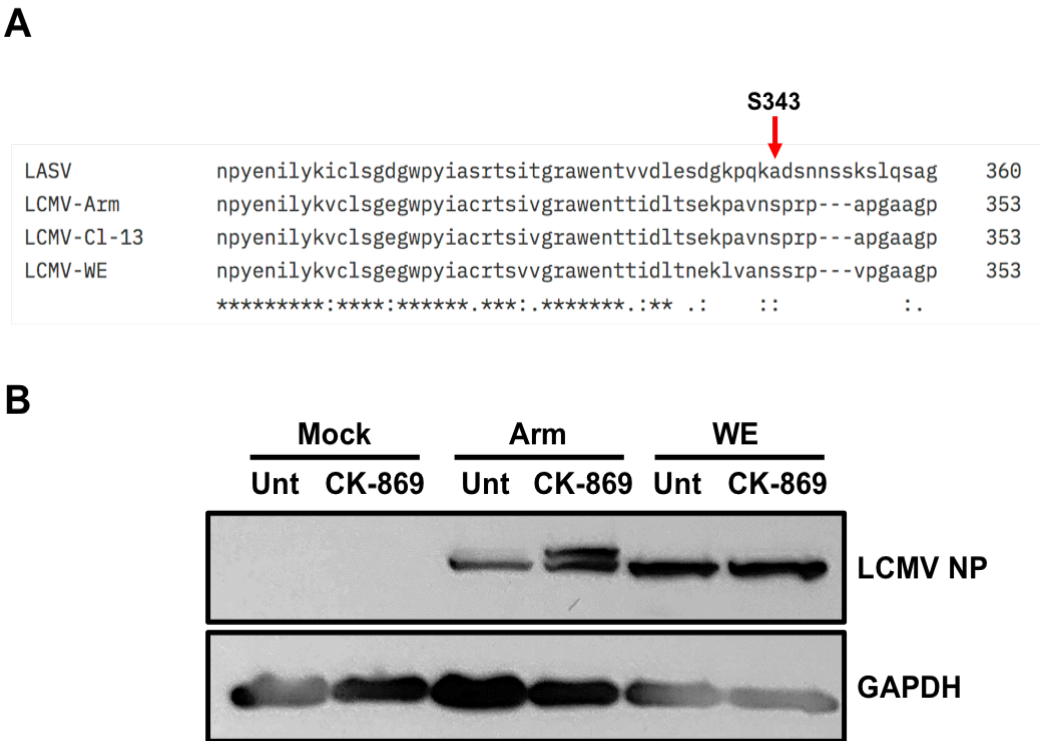

Figure 4.8: LCMV NP S343 phosphorylation is strain specific. (A) Sequence alignment of apathogenic (Arm/Cl-13) and pathogenic (WE) LCMV strains and LASV was performed, with S343 shown (red arrow). (B) A549 cells were infected with LCMV-Arm and LCMV-WE at an MOI of 0.2, with CK-869 (20 µM) was added to cultures at 3 hpi. Lysates were harvested at 24 hpi and subject to western blot analysis.

Taken together, these findings show phosphorylation of LCMV NP at S343 is a strain specific outcome, likely dictated by local sequences surrounding this residue and raises the interesting possibility that phosphorylation at this residue may have consequences for LCMV pathogenicity.

4.5 Discussion

Here, we investigated the impact of S343 phosphorylation of LCMV NP. Through VLP data and LC-MS of CK-869-treated cultures, it was identified that LCMV NP can be phosphorylated at residue S343. To investigate this further, infectious recombinant LCMV was recovered with S343 phospho-ablatant (S343A) and phosphor-mimetic (S343E) NPs. Intriguingly, initial investigations revealed that S343 phosphorylation of NP is not a viral-dependent process, with similar growth kinetics of rLCMV-S343A/E compared with rLCMV-WT in multiple different cell lines. Consequently, we investigated whether NP phosphorylation is a host defence mechanism; thus, immune competent RAW264.7 (mouse macrophage) cells were infected with rLCMV-WT, rLCMV-S343A and rLCMV-S343E, and growth kinetics monitored. Interestingly, rLCMV-S343E had significantly diminished titres (10-fold) and NP expression (19.9%) compared to rLCMV-WT, with no significant differences observed for rLCMV-S343A. This revealed that S343 phosphorylation of LCMV NP is an antiviral response, being detrimental for LCMV growth. Mechanistically, IF analysis suggests that phosphorylation may target NP for degradation by lysosomes, since there was increased co-localisation between NP and LAMP-1 within rLCMV-S343E infected cultures (Figure 4.7).

This work is the first report describing phosphorylation of LCMV NP from infected cultures, and the only report that phosphorylation of NP is detrimental to LCMV propagation *in vitro*. Nevertheless, may viral proteins have been shown to be phosphorylated during viral infection for species of orthomyxoviruses [37–44], alphaviruses [45–47], retroviruses [48–51], filoviruses [52–54], coronaviruses [55–57] and flaviviruses [58–61]. Generally, many instances involve phosphorylation of a viral protein subsequently ensures the protein becomes "active", allowing for specific functions within distinct stages of the viruses replication cycle including transcription, replication, viral-host protein interactions, viral protein multimerisation, assembly, budding, apoptosis [62].

However, for Hepatitis C virus (HCV), phosphorylation of nonstructural 2 (NS2) protein has been shown to target the protein for degradation [63]. Here, the residue S168 was identified as being critical for NS2 for proteasomal degradation [63]. A host cell kinase, casein kinase 2 (CK2), was recognised for its potential

to phosphorylate NS2, with inhibitors against CK2 increasing NS2 stability [63]. Furthermore, the consensus S/TXXE motif, which enables recognition by CK2, was identified as highly conserved between all HCV genotypes [63]. Subsequent mutagenesis studies have revealed that S168 (S168A/G) of NS2 is important for infectious HCV virion production [64]. In the context of our findings, we propose that S343 phosphorylation targets NP for degradation via lysosomes. Additionally, we did not observe any viral process dependent on phosphorylation of S343 *in vitro*, but we cannot rule out if this post-translational modification may be required for dissemination of LCMV into differing host tissues, resulting in efficient spread *in vivo*.

Host cell kinases phosphorylate proteins using consensus motifs, whereby amino acids surrounding the phosphorylation site enable kinase recognition [65]. We utilised kinase prediction algorithms to predict the host cell kinase responsible for S343 phosphorylation (data not shown). The most prominent members belonged to the CMGC family of kinases, yet this encompasses a vast number of kinases including cyclin-dependent kinases (CDKs), mitogen-activated protein kinases (MAPKs), glycogen synthase kinases (GSKs), and CDC-like kinases (CLKs) [66]. As such, any attempts to utilise kinase inhibitors alongside CK-869 treatment during LCMV infection (to investigate the restoration of a single band due to the lack of phosphorylation) were unsuccessful, and we were unable to identify the specific kinases involved in S343 phosphorylation.

Intriguingly, we reveal that phosphorylation of NP is LCMV strain specific, with LCMV-Arm being capable of modification, yet LCMV-WE is not (Figure 4.8). Given that LCMV-WE has been established to be more pathogenic compared to LCMV-Arm, it is interesting to consider whether S343 phosphorylation of NP contributes to this difference in pathogenicity [36, 67–69]. Of note, in the case of guinea pigs, LCMV-Arm is non-lethal even at doses of greater than 10,000 PFU, yet LCMV-WE caused 100% mortality with a dose of less than 10 PFU [70]. Recently, the innate immune activation pathways of LCMV-Arm and LCMV-WE were examined [71]. One particular finding was that LCMV-Arm has stronger activation of NF-κB signalling compared to LCMV-WE [71]. In the context of our findings, this could be justified since phosphorylated NP (S343E), specific to LCMV-Arm, co-localises with lysosomes. When lysosomal degradation is impaired,

NF-κB may become activated through persistent toll-like receptors (TLR) activation [72]. Interestingly, TLR-2 was identified as being critical for NF-κB activation during LCMV-Arm infection [71]. In normal squamous esophagus cells, long-term activation of TLR-2 has been shown to increase the abundance and size of lysosomes, alongside increased LAMP-1 expression [73]. Thus, the increased requirement for lysosomes to degrade phosphorylated NP, in specifically LCMV-Arm infection, could confer increased activation of TLR-2, and consequently NF-κB. Since strain LCMV-Arm is apathogenic yet LCMV-WE is pathogenic [71], it is also plausible that LCMV NP degradation could contribute to the decreased pathogenicity of LCMV-Arm by limiting the spread of the virus *in vivo*, and this should be further examined.

The antiviral phenotype observed only during infection of the macrophage (RAW264.7) cell line with rLCMV-S343E is thought-provoking, given macrophages are a key target cells of LCMV for persistence and immune suppression [74]. CD169+ macrophages have been shown to be important for determining LCMV clearance vs persistence [75]. Here, the investigations suggests that CD169+ macrophages release a secondary wave of IFN-I, which functions for the induction of inflammatory macrophages, effector CD8+ T cells generation and viral clearance [75]. The antiviral nature of S343 phosphorylated NP, which only observed in the macrophage cell lines, points towards the requirement of specific immune pathways. Whether the subsequent degradation of NP has implications for persistence and immune suppression should be further investigated.

Overall, this study highlights that NP can be phosphorylated, with particular focus on residue S343 which is revealed to act in an antiviral manner. It will be interesting to examine whether NPs of other OW and NW arenaviruses also can be phosphorylated and determine if these act in a pro- or antiviral manner. The described ability of macrophage cells to degrade NP during LCMV infection improves our understanding of host-defences against arenavirus infection, which may improve antiviral therapies for effective treatments.

4.6 Future directions

To further understand the role of LCMV NP phosphorylation additional experiments could be performed. One such experiment could be to investigate S343A/E co-localisation with LAMP1 within infected A549 cells, since this cell line did not show any significant differences for NP S343A/E when compared to WT. Additionally, it may be important to understand whether the observed phenotype in RAW264.7 cells relates to LCMV cell-cell spread. To investigate this, foci forming assays could be performed using RAW264.7 cells, to assess for any changes between WT, S343A and S343E NP. Current investigations to identify the host cell kinase(s) responsible for S343 NP phosphorylation were unsuccessful (data not presented); thus, additional experiments are also required to understand the cellular machinery responsible for this post-translational modification. Finally, since NP S343 phosphorylation was not observed within infected cellular lysates, it could be important to examine whether this modification is present within infected rodent tissues.

4.7 Materials and Methods

4.7.1 Plasmid design and virus rescue.

Throughout rLCMV-WT was utilised in all experiments described, and rescue protocols have previously been described [33]. The phospho-ablatant (S343A) and phospho-mimetic (S343E) recombinant viruses were achieved utilising the same protocol. Briefly, BSR-T7 cells were transfected with the appropriate cDNA (Figure 4.4A), with the Opti-MEM transfection medium being replaced for 2.5% DMEM at 24 hours post transfection (hpt). At 5 days post transfection (dpt), viral supernatants BHKs were infected with transfection viral supernatant for virus propagation. At 2 days post infection (dpi), viral supernatants were harvested, clarified (4000 x g for 30 mins) and subjected to focus forming assay (FFA). Lysates were also collected from both transfection and infection, and subject to western blotting. In order to gain a bulk stock BHK cells were infected at an MOI of 0.001, and subsequently harvested at 3 dpi.

4.7.2 Virus infections and titration.

For virus stock generation, BHKs were seeded in a T175 at 5 x 10^6 in 10% FBS DMEM media, and simultaneously infected in suspension at an MOI of 0.001. Viral supernatants were harvested at 3 dpi, clarified and aliquoted prior to freezing. For general infections the inoculum containing viruses for the desired MOI was added to cell monolayers in either serum-free media (SFM), 2.5 % FSB or 10 % FBS depending on cellular requirement. For titration of virus, previously detailed methods were utilised [32, 33].

4.7.3 VLP production.

HEK293T cells were transfected with 1000 µg of a pCAGGS expression plasmid containing the Z or NP ORF of LCMV (strain Armstrong). VLPs were harvested after 72 h and transferred to a 50 mL tube and kept on ice. Cells were centrifuged at 1200 x g for 20 min at 4°C to remove cell debris. Supernatants were collected and layered onto a 3 ml 20% sucrose/HM cushion in an SW32ti ultracentrifugation tube (Beckmann Polyallomer Centrifuge tubes 25x89 mm, Cat. No.: 32623), followed by ultracentrifugation at 170000 x g for 3 h at 4°C using a Beckmann Coulter Optima LE-80K ultracentrifuge. Pellets were resuspended in 500 µL Tris-buffered saline (TBS) overnight at 4°C. The next day a 5-20% iodixanol gradient (OptiPrep, Stemcell Technologies) was prepared by diluting a commercial OptiPrep stock solution of 50% iodixanol in 1x TBS (prepared by diluting 5 volumes of the 60% commercial OptiPrep solution with 6x TBS, in which all components were used in a 6x concentration except NaCl, which is 1x concentrated to maintain iso-osmotic conditions). The diluted OptiPrep solutions were then placed in SW 40 ti ultracentrifugation tubes (Seton Scientific; 14x95 mm; Cat. 7031). These solutions were filtered through a 22 µm filter (Merck Millipore) after which the two solutions were overlaid, and the gradient was prepared with a gradient maker (Gradient Master108, BioLabs). The resuspended VLP pellets were carefully placed on top of the gradient and ultracentrifuged at 200000 x g for 1.5 h at 4°C. Fractions containing the highest concentration of viral particles (4 of 13) were pooled and placed on a 3 ml 20% sucrose/HM cushion in an SW 32 ti ultracentrifugation tube. Ultracentrifugation was then performed at 170000 x g for 3 h at 4°C. The resulting

pellet was resuspended overnight in 80 µl 2% SDC lysis buffer at 4°C. Protein content was determined by BCA.

4.7.4 VLP proteomics sample preparation.

10 µg of LCMV VLP lysate was digested using a modified in-solution digestion protocol [76, 77]. Reduction and alkylation were performed by addition of 1:10 reduction/alkylation solution (100 mM TCEP, 400 mM CAM) and 10 min incubation at 45°C with 800 rpm shaking. Digestion was performed by addition of either 1:50 trypsin (Promega, V5111), 1:50 GluC (Promega, V1651), or 1:20 chymotrypsin (Promega, V1061) and incubated at 37°C over night. SDC was precipitated by addition of 1:10 10% TFA and removed by 10 min centrifugation at 14000 x g. Peptides were subjected to Stage tip clean-up according to [78] with in-house prepared C18 Stage tips (Empore^{TM} SPE discs, 66883-U). Eluted peptides were dried in a vacuum centrifuge and reconstituted in 8 µL 0.1% FA, before being subjected to LC-MS measurement.

4.7.5 VLP LC-MS measurements.

Peptides were separated on a NanoELute 2 (Bruker Daltonics, Germany) using a 30 min gradient (4-25% solvent B (0-27 min), 25-32% B (27-30 min), 32%-95% B (30-31 min), and 95% B (31-35 min)) on a Bruker PepSep Max column (10 cm, ID 150 µm, 1.5 µm C18) (Bruker Daltonics, Germany) at a 0.5 µL min-1 flow rate using 0.1% FA in water and 0.1% FA in ACN as solvent A and B, respectively. Column was operated at 40°C. Mass spectrometry measurements were performed on a TimsTOF HT (Bruker Daltonics, Germany) using the standard Parallel Accumulation and Serial Fragmentation (PASEF) method with a 1.1 s cycle time.

4.7.6 VLP Data analysis.

Raw data were analysed with MaxQuant v2.4.2.0 [79] using a sequence database assembled from the proteome of the transfected cells (Homo sapiens, UniProt ID: UP000005640), as well as LCMV NP (GeneBank: AAX49342.1) and Z (GeneBank: AAX49343.1) sequences, including their C-terminal flag tag. The search was FDR

controlled (1%) and performed using the Andromeda search engine. 3 and 5 missed cleavages were allowed for trypsin and the other proteases (GluC, Chymotrypsin), respectively. Carbamidomethylation of cysteine was set as fixed modification, and methionine oxidation, protein N-term acetylation, as well as phosphorylation of serine, threonine and tyrosine was chosen as variable modifications with a maximum of 5 modifications per peptide.

4.7.7 Analysis of CK-869 pre-treatment.

A549 cells were trypsinised and seeded into a 12-well plate at 1 x 105 cells/well, and then incubated at 37 °C overnight. Cells were then infected pre-treated with 500 µL 20- or 40- µM CK-869 for 45 mins, and then infected with rLCMV-WT (made in 500 µL drug media) at an MOI of 0.2. At 24 hpi, cell lysates were collected and subject to western blotting utilising an in-house LCMV NP anti-sera for detection (1:1000). To assess cell viability following CK-869 treatment, an MTS assay (Promega CellTiter 96® AQueous One Solution Cell Proliferation Assay) was performed following the manufacturer's instructions.

4.7.8 CK-869 time-of-lysis experiment.

A549 cells were trypsinised and seeded into a 12-well plate at 1 x 10^5 cells/well, and then incubated at 37 °C overnight. Cells were the infected with rLCMV-WT at an MOI of 5 in 500 µL inoculum. At 3 hpi, 500 µL of 40 µM CK-869 was added to the 500 µL virus inoculum to give a final concentration of 20 µM for the duration of the experiment. Subsequently, cells were lysed at 3 hpi as a control for input LCMV NP to allow the visualisation of newly synthesised NP. Subsequent to 8 hpi, cells were then lysed at hourly intervals (8-14 hpi) alongside a 24 hpi control. Densitometry was performed using Fiji software and abundance of low/high molecular weight NP expressed as a percentage of total NP for each individual timepoint. Normalised values were averaged between three biological repeats (n = 3).

4.7.9 Co-immunoprecipitation and LC-MS.

Trypsinised A549 cells were seeded into a T175 flask at 1.15 x 10^7 cells/well, and then incubated at 37 °C overnight. Subsequently, cells were infected with rLCMV-WT at an MOI of 0.2. At 24 hpi, cells were lysed (1.5 mL RIPA buffer) for 30 mins on ice, scraped and collected. For successful IP, Invitrogen ™ Dynabead™ Protein G were utilised. Per reaction, 200 µL of the resuspended magnetic beads were placed in a tube and separated from suspension buffer using a magnet. The remaining beads were resuspended in 800 µL PBS-T (0.02%), and 20 µL of LCMV-NP anti-sera (in-house). The bead/antibody solution was then incubated with rotation for 2 hrs at room temperature. Subsequently, the antibody solution was removed from the beads, which were then washed three times with 800 µL PBS-T (0.02%). Next, the appropriate lysates were incubated with the beads at 4 °C overnight with rotation. Following this, the sample was removed, and the bead mixture then washed four times with 800 µL PBS-T (0.02%). In the final wash buffer, beads were transferred to a separate tube, to ensure specificity of the assay. Subsequently, the magnetic beads were then resuspended in 50 µL PBS-T (0.02%) and stored at -80 °C prior to LC-MS sampling. LC-MS analysis was then performed by the University of Bristol, whereby a chymotryptic digest isolate a peptide of appropriate length for subsequent analysis.

4.7.10 Phospho-ablatant and Phospho-mimetic, alongside CK-869 and nocodazole treatment.

Recovery of rLCMV-WT, rLCMV-S343A and rLCMV-S343E was performed as aforementioned, and three independent recoveries performed for completeness (n = 3). To investigate the presence of a 'doublet' LCMV NP band alongside these viruses, CK-869 and nocodazole treatment was utilised. Trypsinised A594 cells were seeded into a 12-well plate at 1.5 x 10^5 cells/well and incubated at 37 °C overnight. Subsequently, cells were then infected with rLCMV-WT, rLCMV-S343A or rLCMV-S343E at an MOI of 0.2 in 500 µL inoculum. At 3 hpi, 500 µL 40 µM of CK-869 or nocodazole (MTS previously performed [80]) was added to the virus inoculum to give a final concentration of 20 µM. Lysates were collected at 24 hpi and subject to western blotting with NP anti-sera utilised for detection. For titration of

these virus, focus forming assays were performed as previously described.

4.7.11 LCMV-S343A/E propagation in varying cell lines.

Trypsinised BHKs, SH-SY5Ys, NIH3T3s, A549s and RAW264.7 cells were seeded into a 12-well plate at 1.5 x 10^5 cells/well and then incubated at 37 °C overnight. Subsequently, cells were then infected with rLCMV-WT, rLCMV-S343A or rLCMV-S343E at an MOI of 0.2 in 1 mL inoculum. At 48 hpi, viral supernatants were collected and subject to FFA utilising an in-house NP antisera and appropriate fluorescent secondary antibody. The mean titre for each virus, and cell line, is shown alongside the standard deviation for the three individual experimental repeats (n = 3). For RAW264.7 cells, lysates were collected and subject to Western blot analysis, utilising the NP antisera. Densitometry was performed using Fiji software and NP abundance expressed as a percentage normalised to LCMV-WT. Normalised values were averaged between three biological repeats (n = 3).

4.7.12 RAW264.7 immunofluorescence.

Trypsinised RAW264.7 cells were seeded onto 19-mm round glass coverslip (VWR) in a 12-well plate at 1.5 x 10^5 cells/well and then incubated at 37 °C. Subsequently, cells were then infected with rLCMV-WT, rLCMV-S343A or rLCMV-S343E at an MOI of 0.2 in 1 mL inoculum. At 48 hpi, cells were fixed with 8% (vol/vol) paraformaldehyde in PBS for 15 min at room temperature. Following fixative, cells were washed with PBS three times and then incubated with permeabilisation buffer (0.1% [vol/vol] Triton X-100, 1% [wt/vol] bovine serum albumin [BSA] in PBS) for 10 min at room temperature. After permeabilisation, cells were washed twice with PBS and incubated with blocking buffer [1% (wt/vol) BSA in PBS] for 1 h. Primary antibody containing LCMV NP [1:500, in house (sheep)] and/or LAMP-1 [Cell Signalling Technology; 1:100 (mouse)] were diluted with BSA blocking buffer and incubated with cells for 1 h at room temperature. Coverslips were then washed with PBS for 5 minutes, repeated three times. Secondary antibodies were diluted in BSA blocking buffer [Life Technologies; 1:500 (alexafluor 488 and 594)] and then added to coverslips for 1 h at room temperature protected from light. Cell monolayers were then washed four times with PBS prior to mounting with Prolong Gold Antifade

reagent with DAPI (Thermo Fisher Scientific). Slides were cured overnight at 4 °C, prior to being imaged the following day. Images were acquired using an LSM 880 confocal microscope (Zeiss), with subsequent processing via Fiji (ImageJ).

4.7.13 Analysis of phosphorylation of NP from differing LCMV strains.

A549 cells were trypsinised and seeded into a 12-well plate at 1 x 10^5 cells/well, and then incubated at 37 °C overnight. Cells were the infected with LCMV-Arm or LCMV-WE at an MOI of 0.2 in 500 µL inoculum. At 3 hpi, 500 µL of 40 µM CK-869 was added to the 500 µL virus inoculum to give a final concentration of 20 µM for the duration of the experiment. Subsequently, cells were lysed at 24 hpi, with cell lysates harvested prior to Western blot analysis utilising an in-house LCMV NP anti-sera for detection (1:1000).

4.8 References

[1] Taxonomy [online] 2024. International Committee on Taxonomy of Viruses (ICTV). 2024.

[2] González PH, Cossio PM, Arana R, Maiztegui JI, Laguens RP. Lymphatic tissue in Argentine hemorrhagic fever. Pathologic features. Archives of pathology & laboratory medicine. 1980;104(5):250–4.

[3] Centers for Disease Control and Prevention (CDC). Viral Hemorrhagic Fevers. Bunyavirales. [online]. [accessed 2023 May 12]. https://www.cdc.gov/vhf/virus-families/bunyaviridae.htmL

[4] Bonthius DJ. The Arenaviruses. In: Neurotropic Viral Infections. Cham: Springer International Publishing; 2016. p. 149–174. doi:10.1007/978-3-319-33133-1_6

[5] Fevola C, Kuivanen S, Smura T, Vaheri A, Kallio-Kokko H, Hauffe HC, Vapalahti O, Jääskeläinen AJ. Seroprevalence of lymphocytic choriomeningitis virus and Ljungan virus in Finnish patients with suspected neurological infections. Journal of Medical Virology. 2018;90(3):429–435. doi:10.1002/jmv.24966

[6] Alburkat H, Jääskeläinen AJ, Barakat AM, Hasony HJ, Sironen T, Al-hello H, Smura T, Vapalahti O. Lymphocytic Choriomeningitis Virus Infections and Seroprevalence, Southern Iraq. Emerging Infectious Diseases. 2020;26(12):3002–3006. doi:10.3201/eid2612.201792

[7] Park JY, Peters CJ, Rollin PE, Ksiazek TG, Katholi CR, Waites KB, Gray B, Maetz HM, Stephensen CB. Age distribution of lymphocytic choriomeningitis virus serum antibody in Birmingham, Alabama: evidence of a decreased risk of infection. The American journal of tropical medicine and hygiene. 1997;57(1):37–41. doi:10.4269/ajtmh.1997.57.37

[8] Bonthius DJ, Nichols B, Harb H, Mahoney J, Karacay B. Lymphocytic choriomeningitis virus infection of the developing brain: critical role of host age. Annals of Neurology. 2007;62(4):356–374. doi:10.1002/ana.21193

[9] Bonthius DJ. Lymphocytic Choriomeningitis Virus: An Underrecognized Cause of Neurologic Disease in the Fetus, Child, and Adult. Seminars in Pediatric

Neurology. 2012;19(3):89–95. doi:10.1016/j.spen.2012.02.002

[10] Hastie KM, Kimberlin CR, Zandonatti MA, MacRae IJ, Saphire EO. Structure of the Lassa virus nucleoprotein reveals a dsRNA-specific 3' to 5' exonuclease activity essential for immune suppression. Proceedings of the National Academy of Sciences. 2011;108(6):2396–2401. doi:10.1073/pnas.1016404108

[11] Papageorgiou N, Spiliopoulou M, Nguyen T-H Van, Vaitsopoulou A, Laban EY, Alvarez K, Margiolaki I, Canard B, Ferron F. Brothers in Arms: Structure, Assembly and Function of Arenaviridae Nucleoprotein. Viruses. 2020;12(7):772. doi:10.3390/v12070772

[12] Martínez-Sobrido L, Emonet S, Giannakas P, Cubitt B, Garciòa-Sastre A, de la Torre JC. Identification of Amino Acid Residues Critical for the Anti-Interferon Activity of the Nucleoprotein of the Prototypic Arenavirus Lymphocytic Choriomeningitis Virus. Journal of Virology. 2009;83(21):11330–11340. doi:10.1128/JVI.00763-09

[13] Pythoud C, Rodrigo WWSI, Pasqual G, Rothenberger S, Martínez-Sobrido L, de la Torre JC, Kunz S. Arenavirus Nucleoprotein Targets Interferon Regulatory Factor-Activating Kinase IKKϵ. Journal of Virology. 2012;86(15):7728–7738. doi:10.1128/JVI.00187-12

[14] Stott RJ, Strecker T, Foster TL. Distinct Molecular Mechanisms of Host Immune Response Modulation by Arenavirus NP and Z Proteins. Viruses. 2020;12(7):784. doi:10.3390/v12070784

[15] Martínez-Sobrido L, Zúñiga EI, Rosario D, García-Sastre A, de la Torre JC. Inhibition of the Type I Interferon Response by the Nucleoprotein of the Prototypic Arenavirus Lymphocytic Choriomeningitis Virus. Journal of Virology. 2006;80(18):9192–9199. doi:10.1128/JVI.00555-06

[16] Zhou S, Cerny AM, Zacharia A, Fitzgerald KA, Kurt-Jones EA, Finberg RW. Induction and Inhibition of Type I Interferon Responses by Distinct Components of Lymphocytic Choriomeningitis Virus. Journal of Virology. 2010;84(18):9452–9462. doi:10.1128/JVI.00155-10

[17] Loureiro ME, Zorzetto-Fernandes AL, Radoshitzky S, Chi X, Dallari S, Marooki N, Lèger P, Foscaldi S, Harjono V, Sharma S, et al. DDX3 suppresses type

I interferons and favors viral replication during Arenavirus infection. PLOS Pathogens. 2018;14(7):e1007125. doi:10.1371/journal.ppat.1007125

[18] Schröder M, Baran M, Bowie AG. Viral targeting of DEAD box protein 3 reveals its role in TBK1/IKKϵ-mediated IRF activation. The EMBO Journal. 2008;27(15):2147–2157. doi:10.1038/emboj.2008.143

[19] Soulat D, Bürckstümmer T, Westermayer S, Goncalves A, Bauch A, Stefanovic A, Hantschel O, Bennett KL, Decker T, Superti-Furga G. The DEAD-box helicase DDX3X is a critical component of the TANK-binding kinase 1-dependent innate immune response. The EMBO Journal. 2008;27(15):2135–2146. doi:10.1038/emboj.2008.126

[20] Loureiro ME, Zorzetto-Fernandes AL, Radoshitzky S, Chi X, Dallari S, Marooki N, Lèger P, Foscaldi S, Harjono V, Sharma S, et al. DDX3 suppresses type I interferons and favors viral replication during Arenavirus infection. PLOS Pathogens. 2018;14(7):e1007125.

[21] Mateer EJ, Maruyama J, Card GE, Paessler S, Huang C. Lassa Virus, but Not Highly Pathogenic New World Arenaviruses, Restricts Immunostimulatory Double-Stranded RNA Accumulation during Infection. Journal of Virology. 2020;94(9). doi:10.1128/JVI.02006-19

[22] Wolff S, Becker S, Groseth A. Cleavage of the Junin Virus Nucleoprotein Serves a Decoy Function To Inhibit the Induction of Apoptosis during Infection. Journal of Virology. 2013;87(1):224–233. doi:10.1128/JVI.01929-12

[23] Bostedt L, Fénéant L, Leske A, Holzerland J, Günther K, Waßmann I, Bohn P, Groseth A. Alternative translation contributes to the generation of a cytoplasmic subpopulation of the Junín virus nucleoprotein that inhibits caspase activation and innate immunity. Journal of Virology. 2024;98(2). doi:10.1128/jvi.01975-23

[24] King BR, Hershkowitz D, Eisenhauer PL, Weir ME, Ziegler CM, Russo J, Bruce EA, Ballif BA, Botten J. A Map of the Arenavirus Nucleoprotein-Host Protein Interactome Reveals that Junín Virus Selectively Impairs the Antiviral Activity of Double-Stranded RNA-Activated Protein Kinase (PKR). Journal of Virology. 2017;91(15). doi:10.1128/JVI.00763-17

[25] Knopp KA, Ngo T, Gershon PD, Buchmeier MJ. Single Nucleoprotein

Residue Modulates Arenavirus Replication Complex Formation. mBio. 2015;6(3). doi:10.1128/mBio.00524-15

[26] Samaj J. From signal to cell polarity: mitogen-activated protein kinases as sensors and effectors of cytoskeleton dynamicity. Journal of Experimental Botany. 2003;55(395):189–198. doi:10.1093/jxb/erh012

[27] Lim Y, Kang S, An WG, Lee Y, Chun J, Sonn JK. Chondrogenesis induced by actin cytoskeleton disruption is regulated via protein kinase C-dependent p38 mitogen-activated protein kinase signaling. Journal of Cellular Biochemistry. 2003;88(4):713–718. doi:10.1002/jcb.10389

[28] Acharya D, Reis R, Volcic M, Liu G, Wang MK, Chia BS, Nchioua R, Groß R, Münch J, Kirchhoff F, et al. Actin cytoskeleton remodeling primes RIG-I-like receptor activation. Cell. 2022;185(19):3588-3602.e21. doi:10.1016/j.cell.2022.08.011

[29] Yoshizumi T, Imamura H, Taku T, Kuroki T, Kawaguchi A, Ishikawa K, Nakada K, Koshiba T. RLR-mediated antiviral innate immunity requires oxidative phosphorylation activity. Scientific Reports. 2017;7(1):5379. doi:10.1038/s41598-017-05808-w

[30] Li Z, Liu G, Sun L, Teng Y, Guo X, Jia J, Sha J, Yang X, Chen D, Sun Q. PPM1A Regulates Antiviral Signaling by Antagonizing TBK1-Mediated STING Phosphorylation and Aggregation. PLOS Pathogens. 2015;11(3):e1004783. doi:10.1371/journal.ppat.1004783

[31] Liu S, Liu S, Yu Z, Zhou W, Zheng M, Gu R, Hong J, Yang Z, Chi X, Guo G, et al. STAT3 regulates antiviral immunity by suppressing excessive interferon signaling. Cell Reports. 2023;42(7):112806. doi:10.1016/j.celrep.2023.112806

[32] Byford O, Shaw AB, Tse HN, Todd EJAA, Álvarez-Rodríguez B, Hewson R, Fontana J, Barr JN. Lymphocytic choriomeningitis arenavirus requires cellular COPI and AP-4 complexes for efficient virion production. Journal of Virology. 2024 Feb 9. doi:10.1128/jvi.02006-23

[33] Shaw AB, Tse HN, Byford O, Plahe G, Moon-Walker A, Hover SE, Saphire EO, Whelan SPJ, Mankouri J, Fontana J, et al. Cellular endosomal potassium ion flux regulates arenavirus uncoating during

virus entry Duggal NK, editor. mBio. 2024;15(7):2023.06.23.546275. https://journals.asm.org/doi/10.1128/mbio.01684-23. doi:10.1128/mbio.01684-23

[34] Kliche J, Garvanska DH, Simonetti L, Badgujar D, Dobritzsch D, Nilsson J, Davey NE, Ivarsson Y. Large-scale phosphomimetic screening identifies phospho-modulated motif-based protein interactions. Molecular Systems Biology. 2023;19(7). doi:10.15252/msb.202211164

[35] Paudel RR, Lu D, Roy Chowdhury S, Monroy EY, Wang J. Targeted Protein Degradation via Lysosomes. Biochemistry. 2023;62(3):564–579. doi:10.1021/acs.biochem.2c00310

[36] Johnson DM, Khakhum N, Wang M, Warner NL, Jokinen JD, Comer JE, Lukashevich IS. Pathogenic and Apathogenic Strains of Lymphocytic Choriomeningitis Virus Have Distinct Entry and Innate Immune Activation Pathways. Viruses. 2024;16(4):635. doi:10.3390/v16040635

[37] Cui L, Zheng W, Li M, Bai X, Yang W, Li J, Fan W, Gao GF, Sun L, Liu W. Phosphorylation Status of Tyrosine 78 Residue Regulates the Nuclear Export and Ubiquitination of Influenza A Virus Nucleoprotein. Frontiers in Microbiology. 2019;10. doi:10.3389/fmicb.2019.01816

[38] Mondal A, Potts GK, Dawson AR, Coon JJ, Mehle A. Phosphorylation at the Homotypic Interface Regulates Nucleoprotein Oligomerization and Assembly of the Influenza Virus Replication Machinery. PLOS Pathogens. 2015;11(4):e1004826. doi:10.1371/journal.ppat.1004826

[39] Liu L, Weber A, Linne U, Shehata M, Pleschka S, Kracht M, Schmitz ML. Phosphorylation of Influenza A Virus Matrix Protein 1 at Threonine 108 Controls Its Multimerization State and Functional Association with the STRIPAK Complex. mBio. 2023;14(1). doi:10.1128/mbio.03231-22

[40] Hutchinson EC, Denham EM, Thomas B, Trudgian DC, Hester SS, Ridlova G, York A, Turrell L, Fodor E. Mapping the Phosphoproteome of Influenza A and B Viruses by Mass Spectrometry. PLoS Pathogens. 2012;8(11):e1002993. doi:10.1371/journal.ppat.1002993

[41] Hale BG, Knebel A, Botting CH, Galloway CS, Precious BL, Jackson D, Elliott RM, Randall RE. CDK/ERK-mediated phosphorylation of the human

influenza A virus NS1 protein at threonine-215. Virology. 2009;383(1):6–11. doi:10.1016/j.virol.2008.10.002

[42] Hsiang T-Y, Zhou L, Krug RM. Roles of the Phosphorylation of Specific Serines and Threonines in the NS1 Protein of Human Influenza A Viruses. Journal of Virology. 2012;86(19):10370–10376. doi:10.1128/JVI.00732-12

[43] Patil A, Anhlan D, Ferrando V, Mecate-Zambrano A, Mellmann A, Wixler V, Boergeling Y, Ludwig S. Phosphorylation of Influenza A Virus NS1 at Serine 205 Mediates Its Viral Polymerase-Enhancing Function. Journal of Virology. 2021;95(6). doi:10.1128/JVI.02369-20

[44] Wang S, Zhao Z, Bi Y, Sun L, Liu X, Liu W. Tyrosine 132 Phosphorylation of Influenza A Virus M1 Protein Is Crucial for Virus Replication by Controlling the Nuclear Import of M1. Journal of Virology. 2013;87(11):6182–6191. doi:10.1128/JVI.03024-12

[45] Peranen J, Takkinen K, Kalkkinen N, Kaariainen L. Semliki Forest Virus-specific Non-structural Protein nsP3 Is a Phosphoprotein. Journal of General Virology. 1988;69(9):2165–2178. doi:10.1099/0022-1317-69-9-2165

[46] Liu N, Brown DT. Phosphorylation and Dephosphorylation Events Play Critical Roles in Sindbis Virus Maturation. Virology. 1993;196(2):703–711. doi:10.1006/viro.1993.1527

[47] Li G, La Starza MW, Reef Hardy W, Strauss JH, Rice CM. Phosphorylation of sindbis virus nsP3 in vivo and in vitro. Virology. 1990;179(1):416–427. doi:10.1016/0042-6822(90)90310-N

[48] Meggio F, D'Agostino DM, Ciminale V, Chieco-Bianchi L, Pinna LA. Phosphorylation of HIV-1 Rev Protein: Implication of Protein Kinase CK2 and Pro-Directed Kinases. Biochemical and Biophysical Research Communications. 1996;226(2):547–554. doi:10.1006/bbrc.1996.1392

[49] Coates K, Harris M. The human immunodeficiency virus type 1 Nef protein functions as a protein kinase C substrate in vitro. Journal of General Virology. 1995;76(4):837–844. doi:10.1099/0022-1317-76-4-837

[50] Burnette B, Yu G, Felsted RL. Phosphorylation of HIV-1 gag proteins by protein kinase C. The Journal of biological chemistry. 1993;268(12):8698–703.

[51] Ammosova T, Berro R, Jerebtsova M, Jackson A, Charles S, Klase Z, Southerland W, Gordeuk VR, Kashanchi F, Nekhai S. Phosphorylation of HIV-1 Tat by CDK2 in HIV-1 transcription. Retrovirology. 2006;3(1):78. doi:10.1186/1742-4690-3-78

[52] Modrof J, Möritz C, Kolesnikova L, Konakova T, Hartlieb B, Randolf A, Mühlberger E, Becker S. Phosphorylation of Marburg Virus VP30 at Serines 40 and 42 Is Critical for Its Interaction with NP Inclusions. Virology. 2001;287(1):171–182. doi:10.1006/viro.2001.1027

[53] Lötfering B, Mühlberger E, Tamura T, Klenk H-D, Becker S. The Nucleoprotein of Marburg Virus Is Target for Multiple Cellular Kinases. Virology. 1999;255(1):50–62. doi:10.1006/viro.1998.9577

[54] Modrof J, Mühlberger E, Klenk H-D, Becker S. Phosphorylation of VP30 Impairs Ebola Virus Transcription. Journal of Biological Chemistry. 2002;277(36):33099–33104. doi:10.1074/jbc.M203775200

[55] Wu C-H, Yeh S-H, Tsay Y-G, Shieh Y-H, Kao C-L, Chen Y-S, Wang S-H, Kuo T-J, Chen D-S, Chen P-J. Glycogen Synthase Kinase-3 Regulates the Phosphorylation of Severe Acute Respiratory Syndrome Coronavirus Nucleocapsid Protein and Viral Replication. Journal of Biological Chemistry. 2009;284(8):5229–5239. doi:10.1074/jbc.M805747200

[56] Peng T, Lee K, Tarn W. Phosphorylation of the arginine/serine dipeptide-rich motif of the severe acute respiratory syndrome coronavirus nucleocapsid protein modulates its multimerization, translation inhibitory activity and cellular localization. The FEBS Journal. 2008;275(16):4152–4163. doi:10.1111/j.1742-4658.2008.06564.x

[57] Surjit M, Kumar R, Mishra RN, Reddy MK, Chow VTK, Lal SK. The Severe Acute Respiratory Syndrome Coronavirus Nucleocapsid Protein Is Phosphorylated and Localizes in the Cytoplasm by 14-3-3-Mediated Translocation. Journal of Virology. 2005;79(17):11476–11486. doi:10.1128/JVI.79.17.11476-11486.2005

[58] Bhuvanakantham R, Cheong YK, Ng M-L. West Nile virus capsid protein interaction with importin and HDM2 protein is regulated by protein kinase C-mediated phosphorylation. Microbes and Infection. 2010;12(8–9):615–625. doi:10.1016/j.micinf.2010.04.005

[59] Forwood JK, Brooks A, Briggs LJ, Xiao C-Y, Jans DA, Vasudevan SG. The 37-Amino-Acid Interdomain of Dengue Virus NS5 Protein Contains a Functional NLS and Inhibitory CK2 Site. Biochemical and Biophysical Research Communications. 1999;257(3):731–737. doi:10.1006/bbrc.1999.0370

[60] Morozova O V, Tsekhanovskaya NA, Maksimova TG, Bachvalova VN, Matveeva VA, Kit YY. Phosphorylation of tick-borne encephalitis virus NS5 protein. Virus Research. 1997;49(1):9–15. doi:10.1016/S0168-1702(96)01433-5

[61] Bhattacharya D, Ansari IH, Striker R. The flaviviral methyltransferase is a substrate of Casein Kinase 1. Virus Research. 2009;141(1):101–104. doi:10.1016/j.virusres.2009.01.002

[62] Keating JA, Striker R. Phosphorylation events during viral infections provide potential therapeutic targets. Reviews in Medical Virology. 2012;22(3):166–181. doi:10.1002/rmv.722

[63] Franck N, Le Seyec J, Guguen-Guillouzo C, Erdtmann L. Hepatitis C Virus NS2 Protein Is Phosphorylated by the Protein Kinase CK2 and Targeted for Degradation to the Proteasome. Journal of Virology. 2005;79(5):2700–2708. doi:10.1128/JVI.79.5.2700-2708.2005

[64] Yi M, Ma Y, Yates J, Lemon SM. trans-Complementation of an NS2 Defect in a Late Step in Hepatitis C Virus (HCV) Particle Assembly and Maturation. PLoS Pathogens. 2009;5(5):e1000403. doi:10.1371/journal.ppat.1000403

[65] Miller CJ, Turk BE. Rapid Identification of Protein Kinase Phosphorylation Site Motifs Using Combinatorial Peptide Libraries. 2016. p. 203–216. doi:10.1007/978-1-4939-3073-9_15

[66] Chowdhury I, Dashi G, Keskitalo S. CMGC Kinases in Health and Cancer. Cancers. 2023;15(15):3838. doi:10.3390/cancers15153838

[67] Zinkernagel RM, Haenseler E, Leist T, Cerny A, Hengartner H, Althage A. T cell-mediated hepatitis in mice infected with lymphocytic choriomeningitis virus. Liver cell destruction by H-2 class I-restricted virus-specific cytotoxic T cells as a physiological correlate of the 51Cr-release assay? The Journal of experimental medicine. 1986;164(4):1075–1092. doi:10.1084/jem.164.4.1075

[68] Beier JI, Jokinen JD, Holz GE, Whang PS, Martin AM, Warner NL, Arteel GE,

Lukashevich IS. Novel Mechanism of Arenavirus-Induced Liver Pathology. PLOS ONE. 2015;10(3):e0122839. doi:10.1371/journal.pone.0122839

[69] Lukashevich IS, Rodas JD, Tikhonov II, Zapata JC, Yang Y, Djavani M, Salvato MS. LCMV-mediated hepatitis in rhesus macaques: WE but not ARM strain activates hepatocytes and induces liver regeneration. Archives of Virology. 2004;149(12):2319–2336. doi:10.1007/s00705-004-0385-9

[70] Riviere Y, Ahmed R, Southern PJ, Buchmeier MJ, Oldstone MB. Genetic mapping of lymphocytic choriomeningitis virus pathogenicity: virulence in guinea pigs is associated with the L RNA segment. Journal of Virology. 1985;55(3):704–709. doi:10.1128/jvi.55.3.704-709.1985

[71] Johnson DM, Khakhum N, Wang M, Warner NL, Jokinen JD, Comer JE, Lukashevich IS. Pathogenic and Apathogenic Strains of Lymphocytic Choriomeningitis Virus Have Distinct Entry and Innate Immune Activation Pathways. Viruses. 2024;16(4):635. doi:10.3390/v16040635

[72] Saftig P, Puertollano R. How Lysosomes Sense, Integrate, and Cope with Stress. Trends in Biochemical Sciences. 2021;46(2):97–112. doi:10.1016/j.tibs.2020.09.004

[73] Verbeek RE, Siersema PD, Vleggaar FP, Ten Kate FJ, Posthuma G, Souza RF, De Haan J, Van Baal JWPM. Toll-like Receptor 2 Signalling and the Lysosomal Machinery in Barrett's Esophagus. Journal of Gastrointestinal and Liver Diseases. 2016;25(3):273–282. doi:10.15403/jgld.2014.1121.253.rc2

[74] Matloubian M, Kolhekar SR, Somasundaram T, Ahmed R. Molecular determinants of macrophage tropism and viral persistence: importance of single amino acid changes in the polymerase and glycoprotein of lymphocytic choriomeningitis virus. Journal of Virology. 1993;67(12):7340–7349. doi:10.1128/jvi.67.12.7340-7349.1993

[75] Casella V, Domenjo-Vila E, Esteve-Codina A, Pedragosa M, Cebollada Rica P, Vidal E, de la Rubia I, López-Rodríguez C, Bocharov G, Argilaguet J, et al. Differential kinetics of splenic CD169+ macrophage death is one underlying cause of virus infection fate regulation. Cell Death & Disease. 2023;14(12):838. doi:10.1038/s41419-023-06374-y

[76] Lin Y, Liu Y, Li J, Zhao Y, He Q, Han W, Chen P, Wang X, Liang

S. Evaluation and optimization of removal of an acid-insoluble surfactant for shotgun analysis of membrane proteome. Electrophoresis. 2010;31(16):2705–13. doi:10.1002/elps.201000161

[77] Zhou J, Zhou T, Cao R, Liu Z, Shen J, Chen P, Wang X, Liang S. Evaluation of the application of sodium deoxycholate to proteomic analysis of rat hippocampal plasma membrane. Journal of proteome research. 2006;5(10):2547–53. doi:10.1021/pr060112a

[78] Rappsilber J, Mann M, Ishihama Y. Protocol for micro-purification, enrichment, pre-fractionation and storage of peptides for proteomics using StageTips. Nature protocols. 2007;2(8):1896–906. doi:10.1038/nprot.2007.261

[79] Cox J, Mann M. MaxQuant enables high peptide identification rates, individualized p.p.b.-range mass accuracies and proteome-wide protein quantification. Nature biotechnology. 2008;26(12):1367–72. doi:10.1038/nbt.1511

[80] Byford O, Shaw AB, Tse HN, Moon-Walker A, Saphire EO, Whelan SPJ, Stacey M, Hewson R, Fontana J, Barr JN. Lymphocytic choriomeningitis arenavirus utilises intercellular connections for cell to cell spread. Scientific Reports. 2024;14(1):28961. doi:10.1038/s41598-024-79397-w

Chapter 5

Concluding remarks

The main goal of this project was to investigate the assembly and egress of arenaviruses, utilising LCMV as the prototypic mammarenavirus. Three different aims, previously detailed in section 1.2 were established for this purpose. Each aim was addressed and fulfilled during the project, as briefly outlined below.

Aim 1: Lymphocytic choriomeningitis arenavirus requires cellular COPI and AP-4 complexes for efficient virion production.

The later stages of mammarenavirus multiplication are not well defined, with key pieces of information lacking. The sub-cellular or virus-induced compartments utilised for processing each viral protein is known, but it is unclear how these proteins are trafficked between the compartments prior to assembly. Chapter 2 'Lymphocytic choriomeningitis arenavirus requires cellular COPI and AP-4 complexes for efficient virion production' provides evidence for the cellular trafficking vesicles required during LCMV infection. Within this study, an siRNA screen was performed to investigate silencing of a range of host cell trafficking components, and this revealed that members of the COPI and AP-4 complexes are required. Detailed investigations revealed that entry, replication, and protein expression remained unaffected following COPI and AP-4 complex disruption, suggesting a role for these complexes in viral protein trafficking.

IF analysis utilising a novel infectious recombinant LCMV variant harbouring a FLAG-tag within GP-1 corroborates the Golgi localisation of GP-1 from native infection rather than transient expression. Since the availability of arenavirus glycoprotein antibodies is limited, beyond this study, the rLCMV-GP1-FLAG variant may aid in further understanding the processing of glycoproteins prior to assembly and the required interacting partners. Utilising this virus alongside staining for the COPI (COPA) and AP-4 (AP4E1) complexes, co-localisation of

both NP and GP-1 was identified, confirming a role for these during multiplication. However, co-IP of the LCMV NP (Figure 5.1), did not isolate any COPI or AP-4 complexes interacting partners. Thus, this suggests that either the interaction with NP is either indirect, or that COPI and AP-4 complexes may be required for trafficking of GPC or Z. Whilst further experiments are required to corroborate the exact mechanisms, utilising information regarding the native function of COPI and AP-4 complexes, it is reasonable to propose that COPI complexes may be required for intra-Golgi trafficking of SSP/GP-1/GP-2 trimers, and that AP-4 complexes subsequently transport these viral glycoprotein trimers to the PM. To investigate this, co-IP could be performed alongside the GP1-FLAG tagged protein, which would determined whether LCMV glycoproteins interact with any COPI/AP-4 complex components. Our data is consistent with this hypothesis, since disruption of these complexes has no impact on entry or gene expression, but significantly impairs virus release. Here, experiments show evidence for the requirement of COPI complexes during LCMV infection, but HAZV, UUKV, IAV and VSV have also all been shown to require these complexes, thus suggesting that they may be required in a wide-range of negative-sense RNA viruses, and could potentially be a pan-bunyavirus requirement [1–5].

This work firstly identified the COPI and AP-4 complexes as required during the LCMV multiplication cycle. Further investigations were able to pinpoint required stage of multiplication to specifically assembly and egress. There are some questions which remain, and answering these would elucidate the exact requirement of COPI and AP-4 during mammarenavirus infection, potentially allowing the development of an effective therapeutic. Further work should be perform to identify which viral protein(s) are trafficked within these two complexes, and subsequently determine whether any interactions are direct or indirect. If the binding is direct, it would also be interesting to find which motifs within the viral proteins regulate this. Furthermore, it would be beneficial to extend these studies to *in vivo* models, to investigate whether persistent LCMV infection occurs within $COPA^{-/-}$ or $AP4M1^{-/-}$ knockout mice. Finally, the requirement of COPI and AP-4 complexes should be studied within LASV and NW mammarenavirus infections, to determine whether these complexes are required across the entire family.

Aim 2: Lymphocytic choriomeningitis arenavirus utilises intercellular connections for cell to cell spread.

Chapter 3 'Lymphocytic choriomeningitis arenavirus utilises intercellular connections for cell to cell spread' highlights an alternative transmission mode of arenaviruses through intercellular connections. It has been established previously that vRNPs alone are sufficient in arenavirus infection to establish viral persistence [6]. Here, this objective reports that this may be possible since vRNPs can be trafficked through TNT-like structures, which likely establishes infection of neighbouring uninfected cells. However, LCMV structural proteins NP, GP-1 and Z co-localise within TNT-like structures, raising the possibility that intact virions may also be trafficked across these intercellular connections. Nevertheless, application of a potent neutralising antibody (M28) revealed a significant proportion of LCMV transmission utilises cell-cell transmission. One possibility for transmission discussed was the initiation of infection via active transport of the vRNPs across TNT-like connections by cytoskeletal proteins. In order to investigate this further, co-IP was performed of LCMV NP from infected A549 cell lysates (Figure 5.1).

Description	Coverage	# Peptides	# PSMs	# Unique Peptides
Unconventional myosin-VI OS=Homo sapiens OX=9606 GN=MYO6 PE=1 SV=1	74.7295209	100	536	1
Nucleoprotein OS=Lymphocytic choriomeningitis virus (strain Armstrong) OX=11624 GN=N PE=1 SV=1	87.2759857	46	368	46
Polyadenylate-binding protein OS=Homo sapiens OX=9606 GN=PABPC1 PE=1 SV=2	66.6110184	33	139	1
Pericentriolar material 1 protein (Fragment) OS=Homo sapiens OX=9606 GN=PCM1 PE=1 SV=1	38.317757	26	75	1
Myosin regulatory light chain 12B OS=Homo sapiens OX=9606 GN=MYL12B PE=1 SV=2	86.0465116	17	662	1
Polyadenylate-binding protein 3 OS=Homo sapiens OX=9606 GN=PABPC3 PE=1 SV=2	25.6735341	16	66	1
Heterogeneous nuclear ribonucleoprotein K (Fragment) OS=Homo sapiens OX=9606 GN=HNRNPK PE=1 SV=1	45.9102902	16	86	1
Chromodomain-helicase-DNA-binding protein 5 OS=Homo sapiens OX=9606 GN=CHD5 PE=1 SV=1	6.24360287	11	19	1
Double-stranded RNA-binding protein Staufen homolog 1 (Fragment) OS=Homo sapiens OX=9606 GN=STAU1 PE=1 SV=1	34.6733668	8	19	1
Macrophage-capping protein (Fragment) OS=Homo sapiens OX=9606 GN=GSN PE=1 SV=1	42.2413793	7	67	1
RING-type E3 ubiquitin transferase OS=Homo sapiens OX=9606 GN=ZNF598 PE=1 SV=1	11.1725664	6	7	1
E3 ubiquitin-protein ligase Itchy homolog OS=Homo sapiens OX=9606 GN=ITCH PE=1 SV=2	6.75526024	6	19	2
Poly(rC)-binding protein 3 OS=Homo sapiens OX=9606 GN=PCBP3 PE=1 SV=2	17.5202156	5	14	1
Bifunctional glutamate/proline--tRNA ligase OS=Homo sapiens OX=9606 GN=EPRS1 PE=1 SV=5	4.6957672	5	6	5
CAP-Gly domain-containing linker protein 2 OS=Homo sapiens OX=9606 GN=CLIP2 PE=1 SV=1	5.83173996	5	5	5
NAD(P)H dehydrogenase [quinone] 1 OS=Homo sapiens OX=9606 GN=NQO1 PE=1 SV=1	23.0483271	5	17	1

Figure 5.1: co-IP of LCMV NP co-IP of LCMV NP from cell lysates was performed alongside a mock sample. Mock and infected samples were then subject to LC-MS and peptides reported. Any peptides present from mock sample were excluded, and proteins ranked based on total peptides, but also considering PSMs and unique peptides.

Interestingly, the identified NP interacting partner with the most abundant peptides was unconventional myosin-VI (MYO6), with myosin regulatory light chain 12B (MYL12B) also appearing in the top 5. The motor protein myosin has been implicated in HIV-1 infection for movement of viral proteins through cell-cell connections [7]. Whether the interaction with NP-MYO6/MYL12B interaction is responsible for the active movement of vRNPs across TNT-like connections for

LCMV, and thus other potential arenaviruses, should be investigated.

Additionally, although the L protein would be presumed to be alongside NP and vRNA, forming vRNPs, there was no direct evidence that L was present within the TNT-like connections. In order to investigate this, a recombinant version of LCMV which harbours a c-Myc-tag within L was developed. LASV L has a described L-HA-TurboID tag, which was shown to have 70 % functional polymerase activity [8]. Sequence alignment was performed to highlight the residues within LCMV that correspond to this same LASV L tag insertion, and thus c-Myc was inserted between residues V404 and S405.

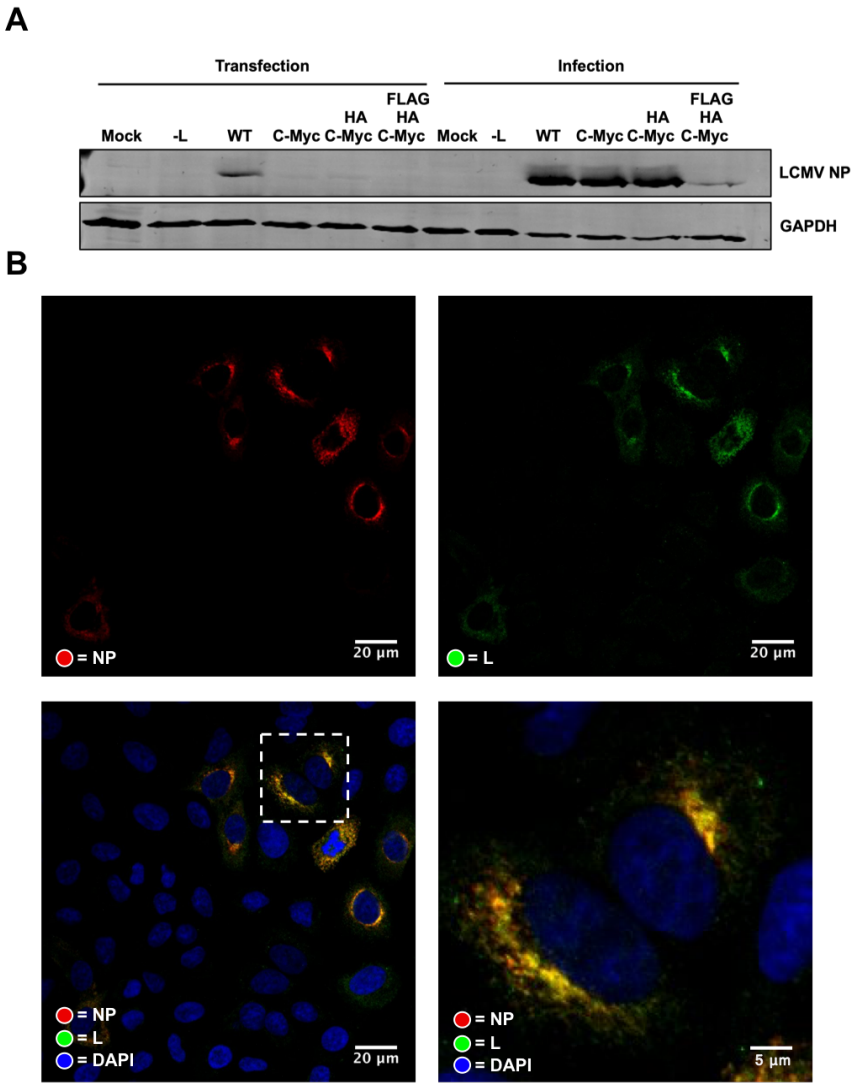

Figure 5.2: Rescue of rLCMV-L-cMyc (A) Recovery of a variety of rLCMV varients habouring epitope tags. Western blot analysis of transfected BSR-T7 and infected BHK-21 cell cultures confirmed rLCMV-L-cMyc, rLCMV-L-cMyc-Z-HA and rLCMV-L-cMyc-Z-HA-GP1-FLAG rescue (alongside rLCMV-WT), using antisera specific for LCMV NP and GAPDH as loading control. (B) At 24 hpi A549 cells infected with rLCMV-L-cMyc at an MOI of 0.2 were fixed, stained for NP (red) and L (green) and visualised by confocal microscopy.

Rescue of recombinant LCMV was then performed, in isolation and alongside other previously described tags Z-HA and GP-1-FLAG. Western blot analysis revealed recovery of all three mutants (Figure 5.2A), with similar NP expression for rLCMV-WT, rLCMV-L-cMyc and rLCMV-L-cMyc-Z-HA, but rLCMV-L-cMyc-Z-HA-GP1-FLAG appears moderately attenuated. This was reflected in titres following FFA, with the rLCMV-L-cMyc and rLCMV-L-cMyc-Z-HA reaching 10^7 FFU/mL, but only 10^4 FFU/mL for rLCMV-L-cMyc-Z-HA-GP1-FLAG. IF analysis of rLCMV-L-cMyc showed consistent NP (red) staining, with dense perinuclear regions but also widespread diffuse cytoplasmic localisation (Figure 5.2B).

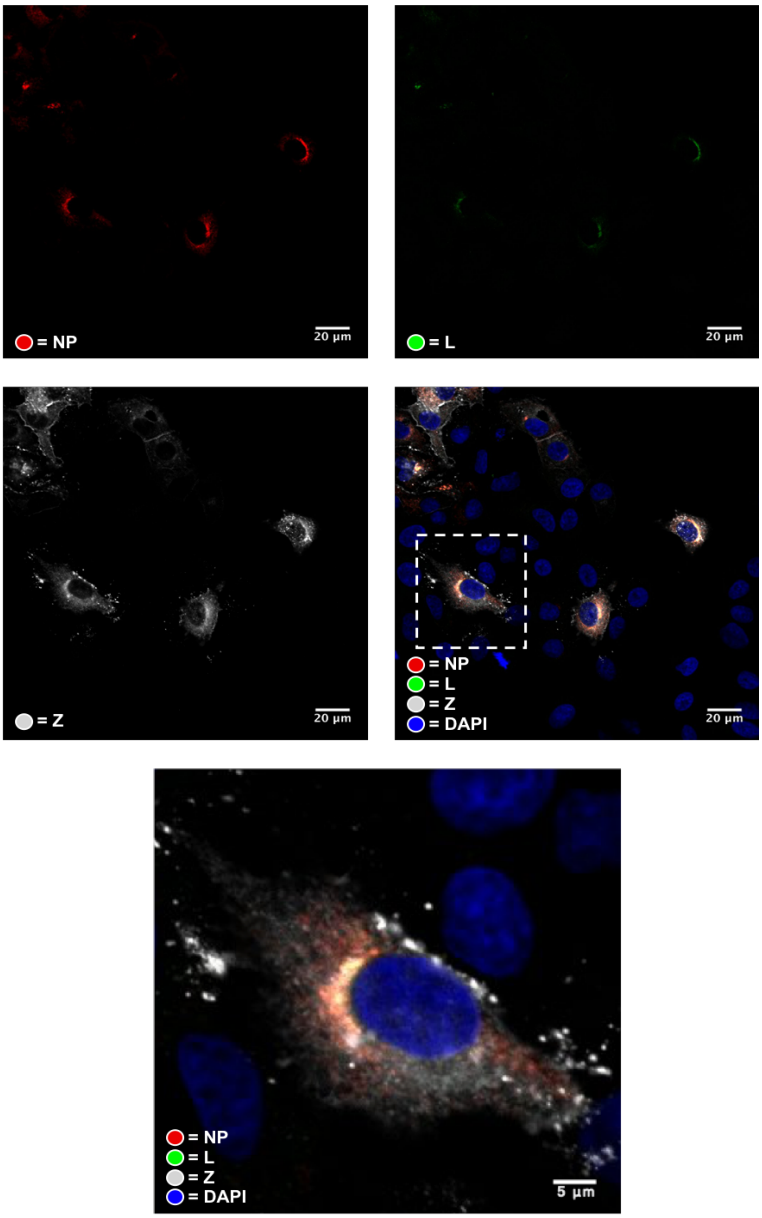

Figure 5.3: IF of rLCMV-L-cMyc-Z-HA At 24 hpi A549 cells infected with rLCMV-L-cMyc-Z-HA at an MOI of 0.2 were fixed, stained for NP (red), L (green) and Z (white) and visualised by confocal microscopy.

As expected, L (green) showed close co-localisation with NP, with the vast majority of NP always occupying the same sub-cellular space as L. Use of the Z/GP-1 mutants revealed that both Z (white; (Figure 5.3) and GP-1 (cyan; (Figure 5.4) broadly occupy the same regions as NP/L, but also extend towards the plasma membrane of cells. Overall, these findings display how the newly-described recombinant L mutants could be useful for investigating functional vRNP movement throughout TNT-like connections, alongside other LCMV structural proteins.

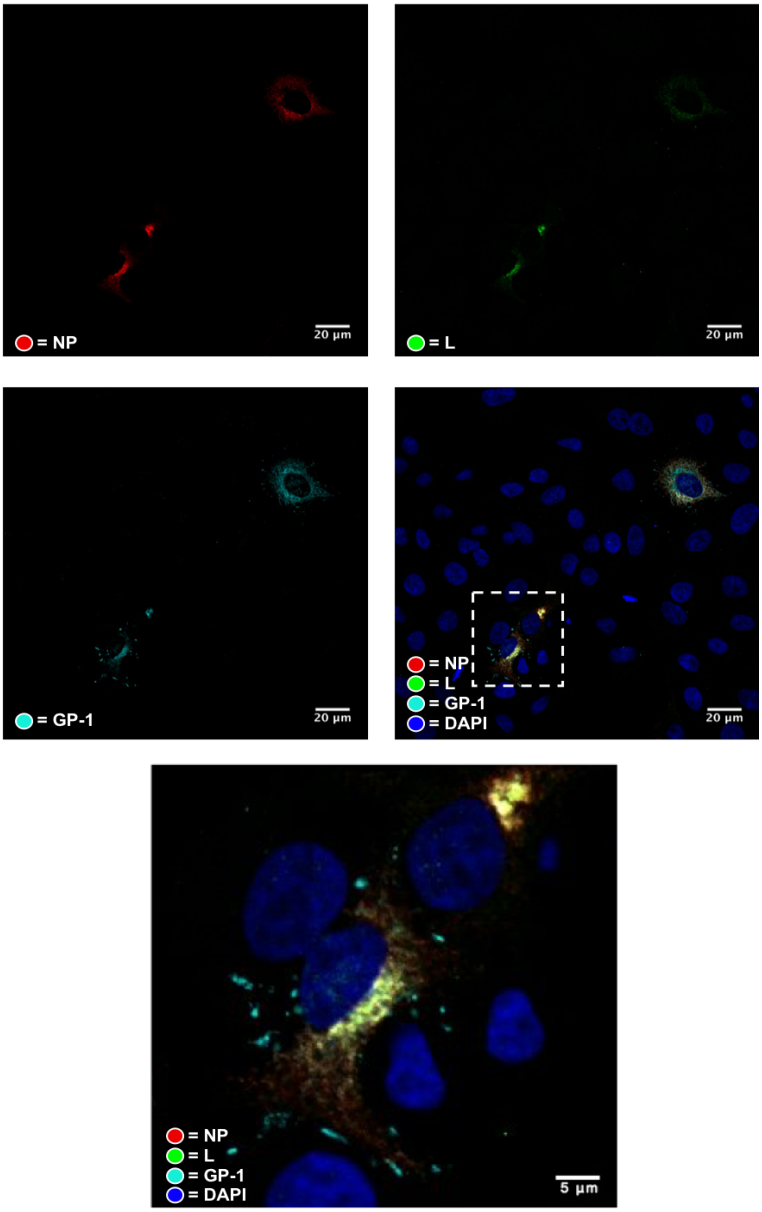

Figure 5.4: IF of rLCMV-L-cMyc-GP1-FLAG At 24 hpi A549 cells infected with rLCMV-L-cMyc-GP1-FLAG at an MOI of 0.2 were fixed, stained for NP (red), L (green) and GP-1 (cyan) and visualised by confocal microscopy.

Taken together, numerous findings surrounding the cell-cell spread of arenaviruses were addressed within this study. Further investigations into whether the movement of viral proteins through TNT-like connections is either an active or passive process, involving cytoskeletal proteins, are currently underway. It will also be important to investigate whether the use of TNT-like connections is a conserved feature of mammarenavirus infection. Inhibition of TNT-like connections with compounds such as nocodazole could also be applied to mouse models, which would allow us to understand how the cell-cell spread of LCMV occurs *in vivo.* Additionally, cryo-electron tomography could be utilised, as has been applied to other viruses, to investigate the content of TNT-like connections during infection. Here, high-resolution images would allow the visualisation of vRNP and/or intact virions within the intercellular connections, which may uncover the predominant mechanism of cell-cell infection.

Aim 3: Lymphocytic choriomeningitis arenavirus nucleoprotein phosphorylation is an antiviral response.

Within Chapter 4 'Lymphocytic choriomeningitis arenavirus nucleoprotein phosphorylation is an antiviral response' it was revealed that NP can be phosphorylated, but phosphorylation at residue S343 is detrimental to LCMV growth. It has previously been reported that phosphorylation of LCMV NP occurs; however, only residue T206 was investigated for its role in LCMV RTC formation [9]. Here, the aim was to investigate phosphorylation of LCMV NP and define the role of this post-translational modification at residue S343 during LCMV infection. Initially, a 'doublet' NP band was identified following CK-869 treatment, and subsequent MS analysis highlighted additional phosphorylation, with S343 being the likely residue. Through the generation of rLCMV-S343A and rLCMV-S343E, it was determined that phosphorylation of S343 is not required for any stage of LCMV multiplication. However, infection of RAW264.7 cells (mouse macrophage) with rLCMV-S343E resulted in diminished NP expression and viral titre compared to rLCMV-WT and rLCMV-S343A, implying an immune related antiviral role of phosphorylation. Interestingly, IF analysis of RAW264.7 cells showed that NP of rLCMV-S343E co-localises with LAMP-1, suggesting that NP S343 phosphorylation acts to target NP for degradation via lysosomes. Interestingly, the ability of NP to

be phosphorylated at residue S343 was identified as LCMV strain specific; only the NP of LCMV-Arm/Cl-13 can be phosphorylated, not LCMV-WE. It is intriguing to speculate whether this has any impact on the different disease outcomes between LCMV-Arm and LCMV-WE, and this could be investigated by introducing the S343 A/E mutations into the LCMV-WE strain and determining disease outcome of LCMV-WE mutants *in vivo*.

Overall, the results presented improve our understanding of arenavirus NP post-translational modifications and provide evidence that phosphorylation of LCMV NP may be an anti-viral response. Since IKKϵ has already been identified as a binding partner of NP, it would be interesting to investigate whether this kinase is responsible for S343 phosphorylation [10]. It will be important to consider whether the NP of more pathogenic mammarenaviruses can also be phosphorylated, or whether the inability of NP to be phosphorylated contributes to their increased pathogenicity.

In conclusion, the results presented in this project represent a step forward in understanding the later stages of arenaviruses infection. With this gained knowledge and by filling some of the gaps in the multiplication cycle, these objectives may assist in the development of effective mammarenavirus specific therapeutics. The discoveries made within this project could be translated to those emerging or novel mammarenaviruses which possess pandemic potential and may contribute to the prevention of future outbreaks.

References

[1] Sun E, He J, Zhuang X. Dissecting the role of COPI complexes in influenza virus infection. Journal of virology. 2013;87(5):2673–85. doi:10.1128/JVI.02277-12

[2] Byford O, Shaw AB, Tse HN, Todd EJAA, Álvarez-Rodríguez B, Hewson R, Fontana J, Barr JN. Lymphocytic choriomeningitis arenavirus requires cellular COPI and AP-4 complexes for efficient virion production. Journal of Virology. 2024 Feb 9. doi:10.1128/jvi.02006-23

[3] Fuller J, Álvarez-Rodríguez B, Todd EJAA, Mankouri J, Hewson R, Barr JN. Hazara Nairovirus Requires COPI Components in both Arf1-Dependent and Arf1-Independent Stages of Its Replication Cycle. Journal of Virology. 2020;94(17).

doi:10.1128/JVI.00766-20

[4] Uckeley ZM, Moeller R, Kühn LI, Nilsson E, Robens C, Lasswitz L, Lindqvist R, Lenman A, Passos V, Voss Y, et al. Quantitative Proteomics of Uukuniemi Virus-host Cell Interactions Reveals GBF1 as Proviral Host Factor for Phleboviruses. Molecular & cellular proteomics: MCP. 2019;18(12):2401–2417. doi:10.1074/mcp.RA119.001631

[5] Cureton DK, Burdeinick-Kerr R, Whelan SPJ. Genetic Inactivation of COPI Coatomer Separately Inhibits Vesicular Stomatitis Virus Entry and Gene Expression. Journal of Virology. 2012;86(2):655–666. doi:10.1128/JVI.05810-11

[6] van der Zeijst BA, Noyes BE, Mirault ME, Parker B, Osterhaus AD, Swyryd EA, Bleumink N, Horzinek MC, Stark GR. Persistent infection of some standard cell lines by lymphocytic choriomeningitis virus: transmission of infection by an intracellular agent. Journal of Virology. 1983;48(1):249–261. doi:10.1128/jvi.48.1.249-261.1983

[7] Kadiu I, Gendelman HE. Human Immunodeficiency Virus type 1 Endocytic Trafficking Through Macrophage Bridging Conduits Facilitates Spread of Infection. Journal of Neuroimmune Pharmacology. 2011;6(4):658–675. doi:10.1007/s11481-011-9298-z

[8] Fang J, Pietzsch C, Witwit H, Tsaprailis G, Crynen G, Cho KF, Ting AY, Bukreyev A, Saphire EO, de la Torre JC. Proximity interactome analysis of Lassa polymerase reveals eRF3a/GSPT1 as a druggable target for host-directed antivirals. Proceedings of the National Academy of Sciences. 2022;119(30). doi:10.1073/pnas.2201208119

[9] Knopp KA, Ngo T, Gershon PD, Buchmeier MJ. Single Nucleoprotein Residue Modulates Arenavirus Replication Complex Formation. mBio. 2015;6(3). doi:10.1128/mBio.00524-15

[10] Pythoud C, Rodrigo WWSI, Pasqual G, Rothenberger S, Martínez-Sobrido L, de la Torre JC, Kunz S. Arenavirus Nucleoprotein Targets Interferon Regulatory Factor-Activating Kinase IKKϵ. Journal of Virology. 2012;86(15):7728–7738. doi:10.1128/JVI.00187-12

I'm just tough

Jessica Pegula

Chapter 6

Appendix A

Supplementary data set 1 avaliable at:

https://journals.asm.org/doi/10.1128/jvi.02006-23

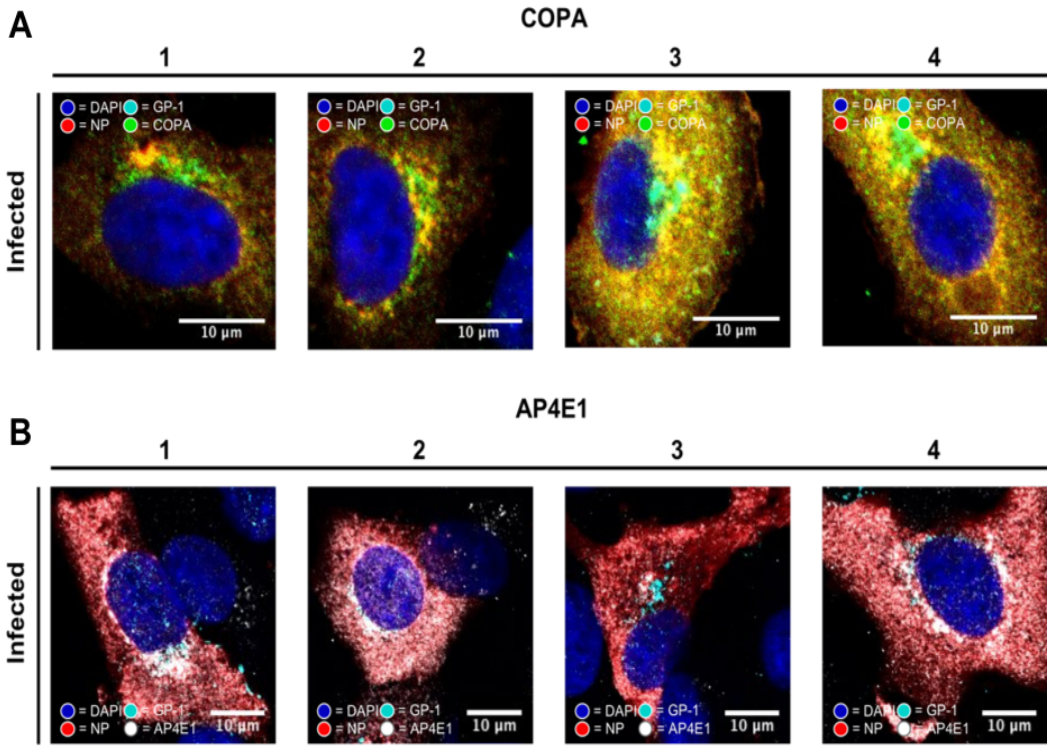

Figure 6.1: Co-localization of LCMV components with COPA and AP4E1. (A) Confocal microscopy of four different A549 cells infected with rLCMV-eGFP and stained at 24 hpi with COPA (green), GP-1 (cyan), and NP (red) and DAPI. (B) Confocal microscopy of four different A549 cells infected with rLCMV-eGFP and stained at 24 hpi stained with AP4E1 (white), GP-1 (cyan), and NP (red) and DAPI.

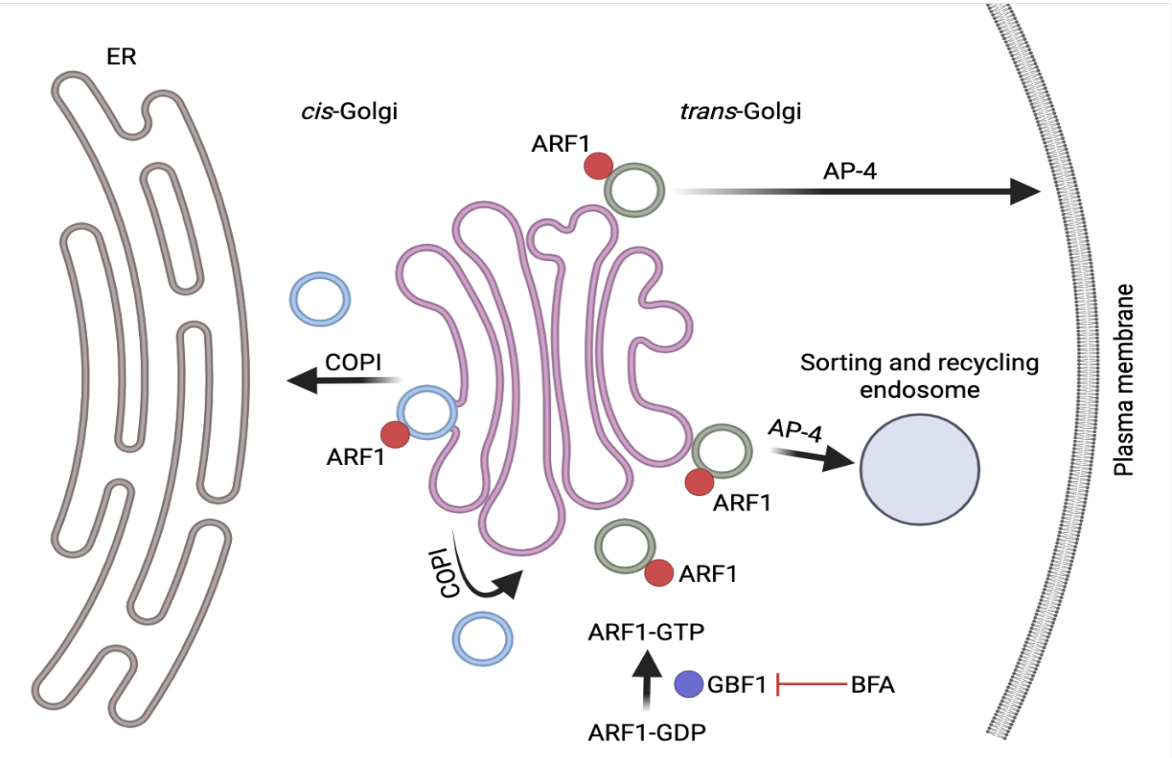

Figure 6.2: COPI and AP-4 pathways, including BFA mode of action. COPI complexes mediate transport of cellular components in a *cis*-Golgi to ER retrograde manner, and are also utilised for *intra*-Golgi trafficking. AP-4 complexes transport cellular components from the *trans*-Golgi network to the plasma membrane, and to sorting and recycling endosomes. Both AP-4 and COPI complex formation requires ARF1, which is disrupted by BFA through the inhibition of GBF1.

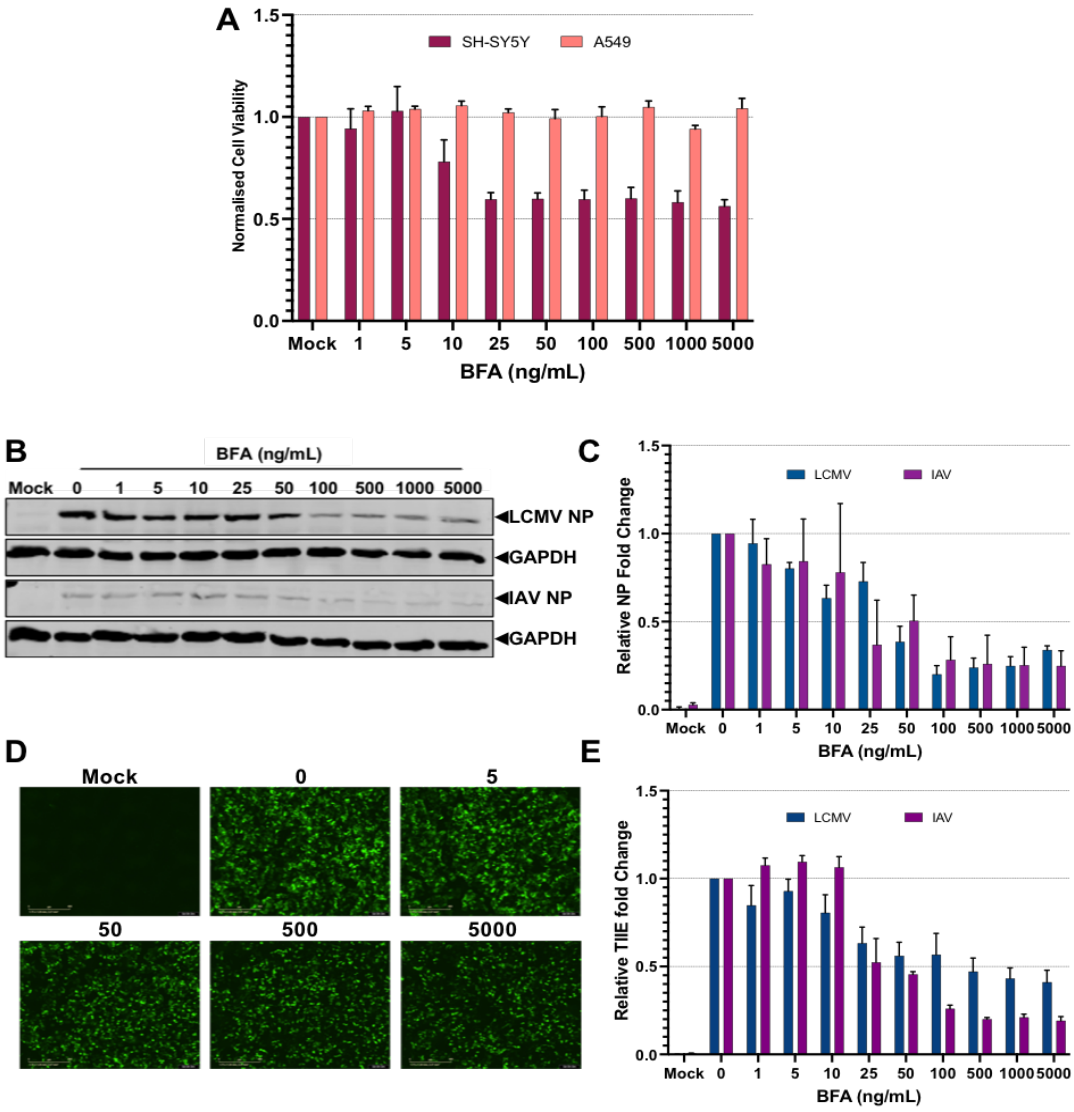

Figure 6.3: Treatment of LCMV infected cells with BFA inhibits viral processes during multistep growth. (A) Analysis of BFA toxicity in A549 and SH-SY5Y cells at various concentrations as measured by MTT assay, normalized to mock untreated cells. (B) Representative western blot analysis of A549 cells pre-treated with BFA 45 minutes prior to WT LCMV and IAV infection at an MOI of 0.1, with lysates harvested at 24 hpi. Samples were probed against antisera for their respective NPs (LCMV NP, IAV NP) and GAPDH as a loading control. (C) Densitometry histograms of the relative fold change in NP expression for LCMV (blue) and IAV (green) of cultures shown in panel A. Expression was quantified for three independent experimental repeats, with error bars representing deviation from the mean. (D) Representative fluorescent microscopy images of A549 cells pre-treated with BFA at indicated concentrations (0, 5, 50, 500 and 5000 ng/mL) and infected with rLCMV-eGFP at an MOI of 0.1 or uninfected (mock). (E) Histogram of the relative fold change in normalized TIIE in A549 cells pre-treated with BFA, and then infected with rLCMV-eGFP (blue) and rIAV-eGFP (green) at an MOI of 0.1. TIIE expression was quantified for three independent experimental repeats, with error bars representing deviation from the mean.

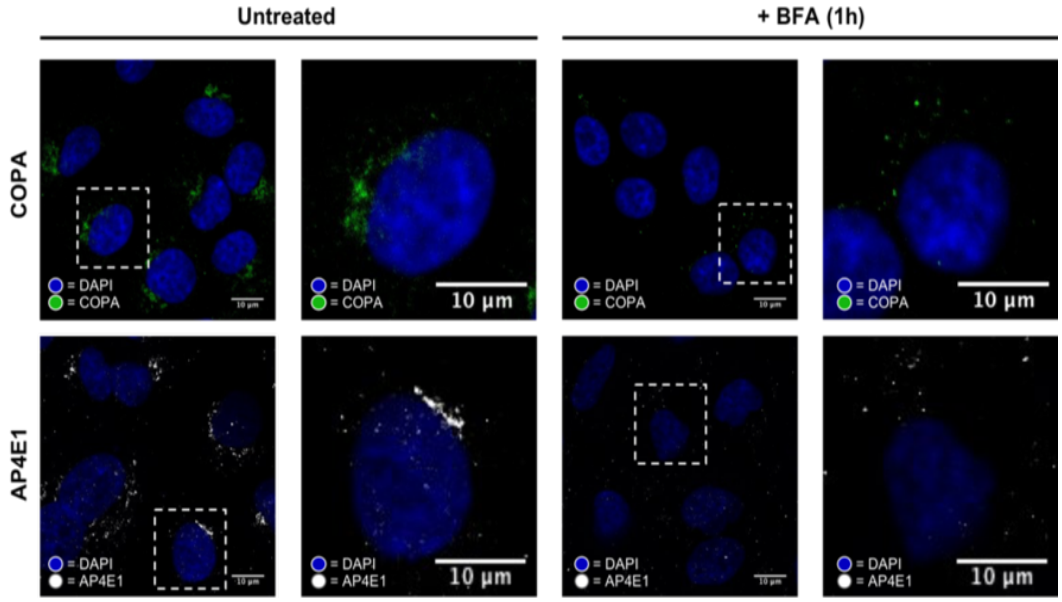

Figure 6.4: Addition of BFA at late stages of rLCMV-GP1-FLAG infection results in changes in the cellular distribution of COPA and AP4E1. Confocal microscopy images of untreated and BFA-treated A549 cells (5000 ng/mL) infected with rLCMV-GP1-FLAG at an MOI of 0.1, at 24 hpi. The infected cells were stained with DAPI and using antisera specific for either COPA (green; top panels) or AP4E1 (white, bottom panels). A zoomed image for both untreated and BFA-treated cells is shown corresponding to the white boxed area.

Chapter 7

Appendix B

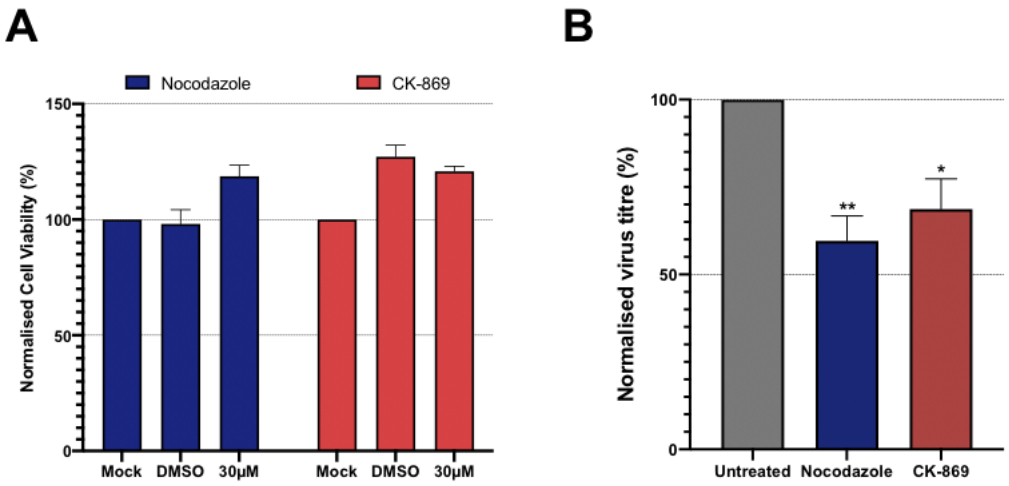

Figure 7.1: Cell viability of A549 cells with TNT-like connection inhibitors. Analysis of 30 µM nocodazole (blue) and 30 µM CK-869 (red) toxicity in A594 cells. We performed MTT assay, normalised to mock untreated cells; the average of three independent experiments is represented (n=3), with error bars showing standard deviation.

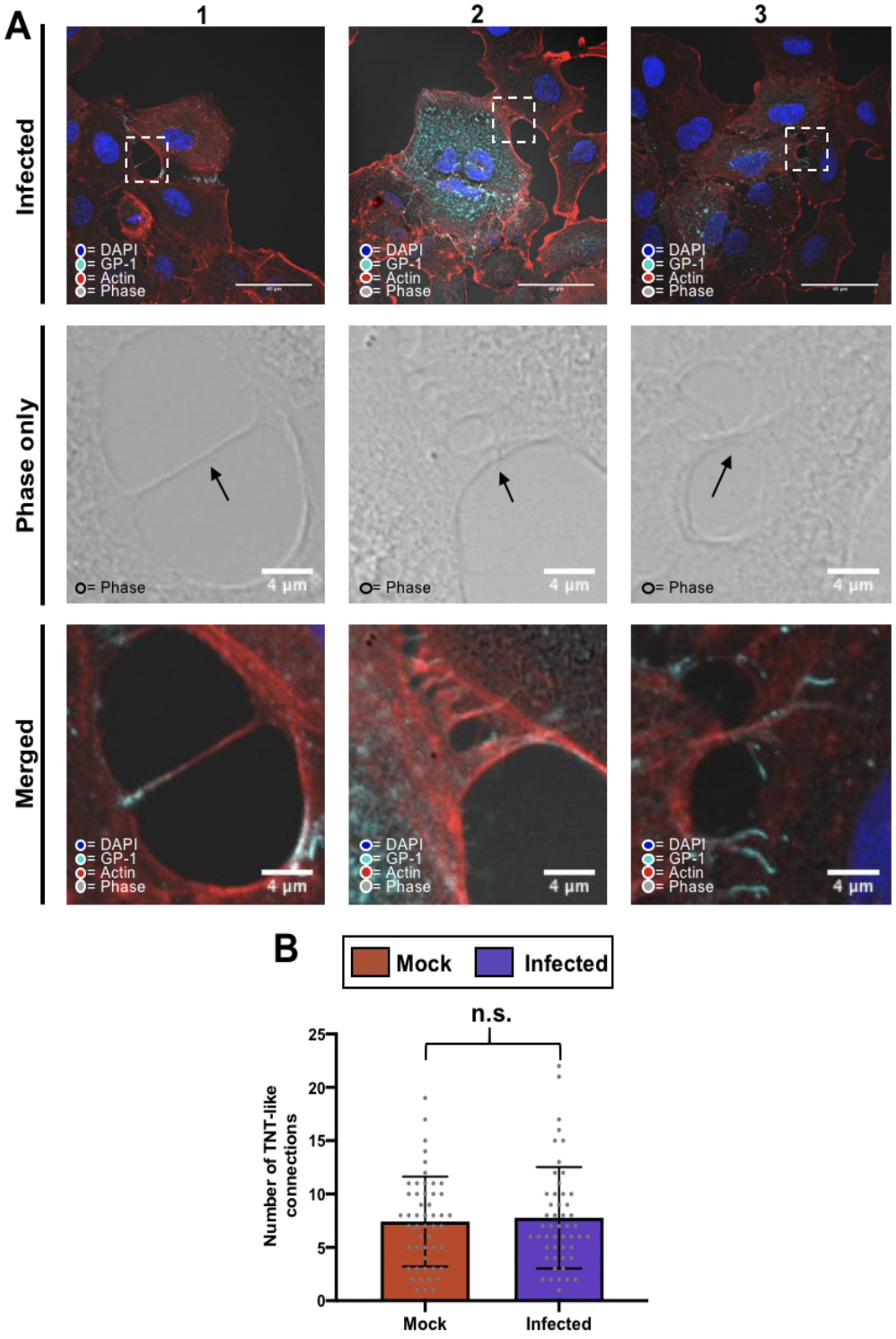

Figure 7.2: Phase-contrast microscopy of TNT-like connections during LCMV infection. (A) A549 cells were infected with rLCMV-GP1-FLAG at an MOI of 0.2. At 24 hpi, cells were fixed and then stained for GP-1 (cyan) and F-actin (red). Confocal microscopy was then utilised to visualise GP-1 and F-actin for TNT-like structures connecting cells. To better visualise the cell membrane of such structures (black arrows), phase-contrast microscopy was utilised. An overlay of GP-1, F-actin and phase-contrast is provided within merged panels. (B) TNT-like connections between 50 cell pairs were counted in both LCMV and mock infected cultures, with no statistical significance between resulting numbers.

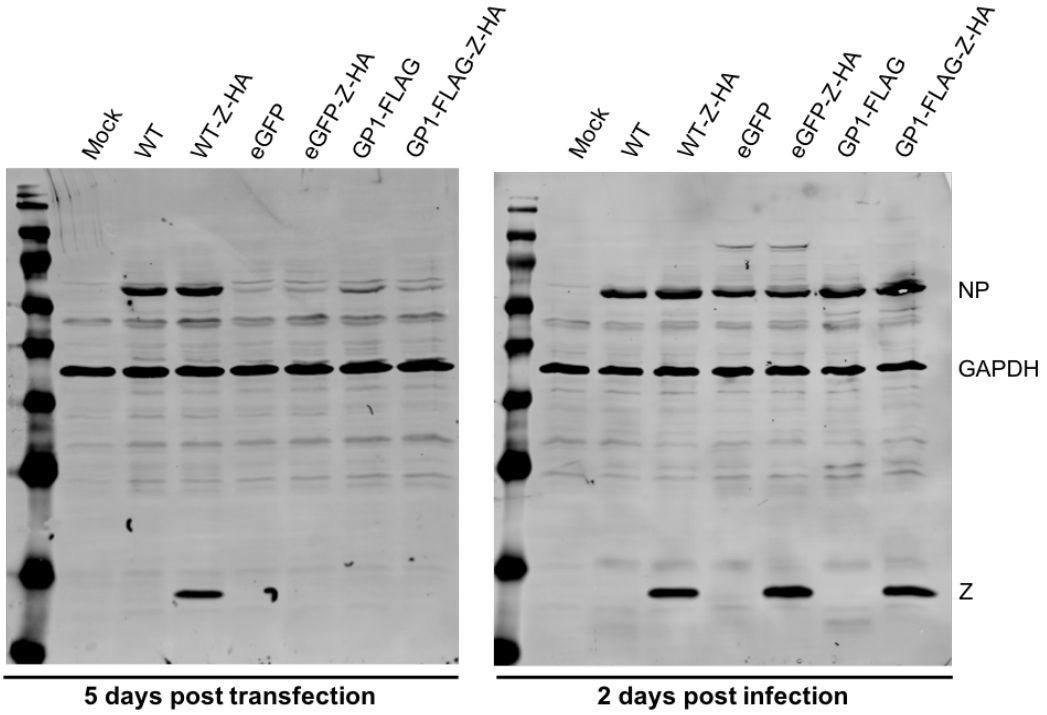

Figure 7.3: Uncropped Western blots of those shown in Figure 4C.

Table 7.1: FISH probes

Target	Probe Sequence	Probe Name	Fluorophore
LCMV S Genome	tttagaggcccaaatgttgt	LCMV_S_Genome_1	Quasar 670
LCMV S Genome	gctcccagatctgaaaactg	LCMV_S_Genome_2	Quasar 670
LCMV S Genome	cactcatggactgcatcatt	LCMV_S_Genome_3	Quasar 670
LCMV S Genome	tcgatgttgaaatgaccagg	LCMV_S_Genome_4	Quasar 670
LCMV S Genome	ggactcacagaataggaagg	LCMV_S_Genome_5	Quasar 670
LCMV S Genome	ccgatgacatcagaaagctt	LCMV_S_Genome_6	Quasar 670
LCMV S Genome	atggttctaagctgtcaagg	LCMV_S_Genome_7	Quasar 670
LCMV S Genome	tcgtcagttataggtgctct	LCMV_S_Genome_8	Quasar 670
LCMV S Genome	gatcttgccgacctcttcaa	LCMV_S_Genome_9	Quasar 670
LCMV S Genome	gattccaagtactcacacgg	LCMV_S_Genome_10	Quasar 670
LCMV S Genome	ggaacccgttgatcaaaaac	LCMV_S_Genome_11	Quasar 670
LCMV S Genome	cgggcagttcatacactttt	LCMV_S_Genome_12	Quasar 670
LCMV S Genome	tgatccagtggaaatagcaa	LCMV_S_Genome_13	Quasar 670
LCMV S Genome	caacgctcctacatggattg	LCMV_S_Genome_14	Quasar 670
LCMV S Genome	tacagccagacaatgctttt	LCMV_S_Genome_15	Quasar 670
LCMV S Genome	agaaacctgcagtcaattca	LCMV_S_Genome_16	Quasar 670
LCMV S Genome	gcatgggaaaacacaacaat	LCMV_S_Genome_17	Quasar 670
LCMV S Genome	gatggccatacatagcttgt	LCMV_S_Genome_18	Quasar 670
LCMV S Genome	aaagtttgcctttcaggtga	LCMV_S_Genome_19	Quasar 670
LCMV S Genome	caggaacccttatgaaaaca	LCMV_S_Genome_20	Quasar 670
LCMV S Genome	ttgtttcagaccaagttggg	LCMV_S_Genome_21	Quasar 670
LCMV S Genome	ggccaagagaaaactcaaca	LCMV_S_Genome_22	Quasar 670
LCMV S Genome	gacctcttgaaggcagttct	LCMV_S_Genome_23	Quasar 670
LCMV S Genome	ttttgatcaagccaagcaac	LCMV_S_Genome_24	Quasar 670
LCMV S Genome	aactttagtcttggtgctgc	LCMV_S_Genome_25	Quasar 670
LCMV S Genome	gtcatcactgaacagcagtc	LCMV_S_Genome_26	Quasar 670
LCMV S Genome	tcttgaaaggctgaaagaca	LCMV_S_Genome_27	Quasar 670
LCMV S Genome	ggcttgctttacacagtcaa	LCMV_S_Genome_28	Quasar 670
LCMV S Genome	tcaatgacgttgtacaagcg	LCMV_S_Genome_29	Quasar 670
LCMV S Genome	ctatggcttgtatggccaaa	LCMV_S_Genome_30	Quasar 670
LCMV S Genome	aatcaatttggcacaatgcc	LCMV_S_Genome_31	Quasar 670
LCMV S Genome	gggatgtgaaagactcatca	LCMV_S_Genome_32	Quasar 670
LCMV S Genome	ttgggatgagaaagcctcag	LCMV_S_Genome_33	Quasar 670
LCMV S Genome	gaccaaagatctcagatcct	LCMV_S_Genome_34	Quasar 670
LCMV S Genome	gggaacttaacaacacagca	LCMV_S_Genome_35	Quasar 670
LCMV S Genome	ccaggcttcaggggtatata	LCMV_S_Genome_36	Quasar 670
LCMV S Genome	ccaagatcatgaggtctgaa	LCMV_S_Genome_37	Quasar 670
LCMV S Genome	gctgaccttgagaagctgaa	LCMV_S_Genome_38	Quasar 670
LCMV S Genome	cagtgcagaagaactgatgt	LCMV_S_Genome_39	Quasar 670
LCMV S Genome	actgtacattctcttgtgga	LCMV_S_Genome_40	Quasar 670
LCMV S Genome	gagactcagaagtctcaacc	LCMV_S_Genome_41	Quasar 670
LCMV S Genome	aagagagatgacaaagacct	LCMV_S_Genome_42	Quasar 670
LCMV S Genome	cttctctgaggtcagcaatg	LCMV_S_Genome_43	Quasar 670
LCMV S Genome	ccaaccttctgaatgggttg	LCMV_S_Genome_44	Quasar 670
LCMV S Genome	ggctgctgtcattaaggatg	LCMV_S_Genome_45	Quasar 670
LCMV S Genome	gcagagcttcacatcagatg	LCMV_S_Genome_46	Quasar 670
LCMV S Genome	cgcaagcattgagaagagaa	LCMV_S_Genome_47	Quasar 670
LCMV S Genome	aggaagttaagagcttccaa	LCMV_S_Genome_48	Quasar 670

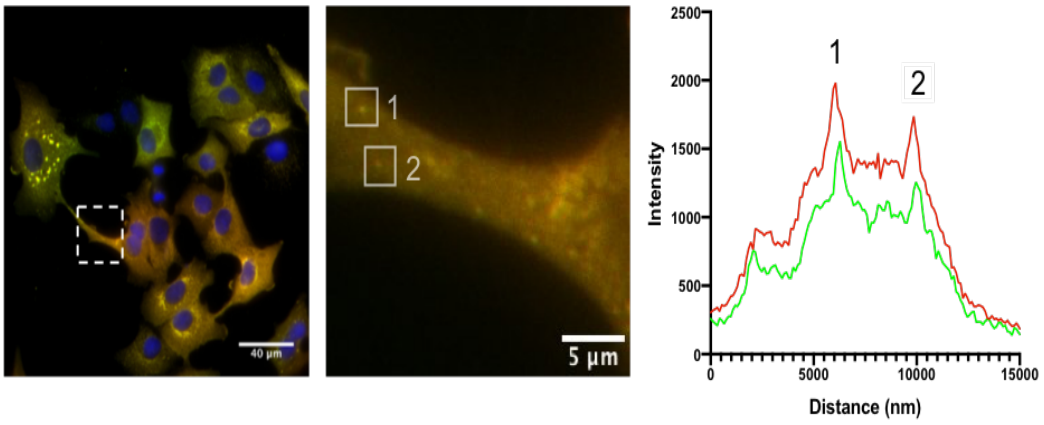

Figure 7.4: Representative TNT-like structures visualized within rLCMV-infected A549 cells, revealing co-localisation of LCMV NP (red) and S vRNA (green) as detected by FISH analysis . Line scan analysis was performed within the zoomed images represented by the dashed boxes, with the end points marked with the beginning (1) and end (2) of the scan line that correspond to the numbered peaks on the scan plot. Colours of the scan lines correspond to those in the cell images.

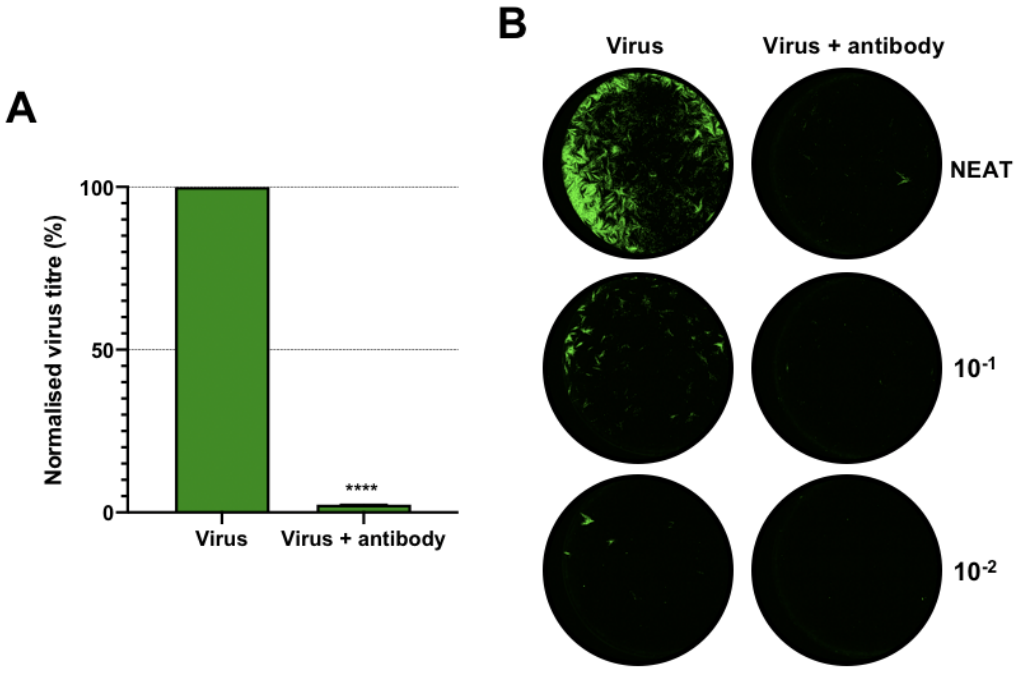

Figure 7.5: Analysis of neutralising antibodies affect on extracellular viruses. (A) To examine the neutralising antibody effectiveness in neutralising virus released within Figure 7 experiment, viral supernatants at 18 hpi for virus only were collected. Subsequently, 5 µg/mL antibody was incubated with samples for 1 h and focus forming assays performed. The normalised viral titre is represented for virus with and without antibody, and the average of three independent experimental repeats is shown (n=3), with error bars showing standard deviation. (B) Representative images for virus and virus with antibody for the neat, 10^{-1} and 10^{-2} dilutions.

Chapter 8

Appendix C

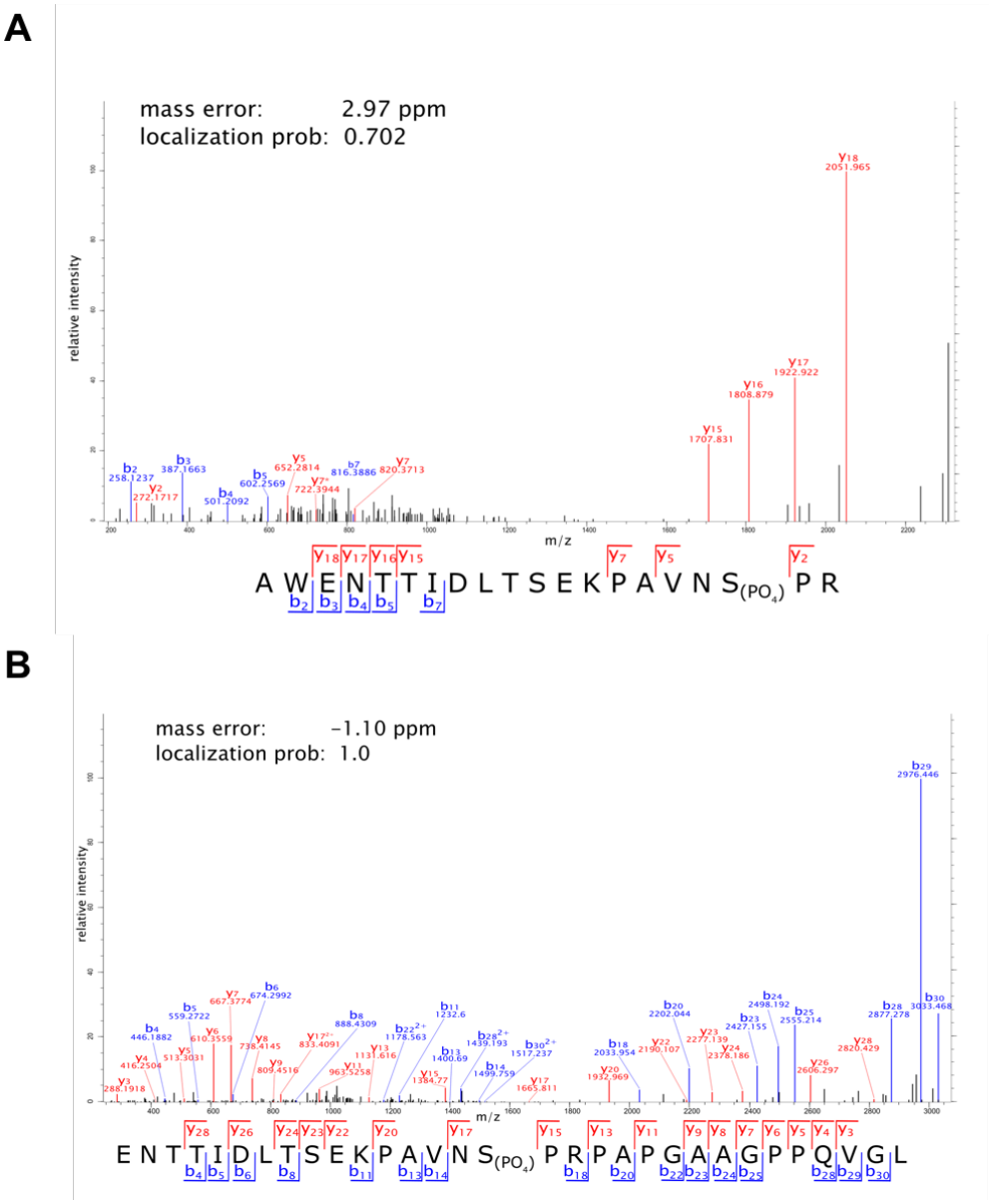

Figure 8.1: Mass spectra of LCMV NP S343 phosphorylated peptides. (A) Showing the detected y- and b-fragmentation series of the tryptic AWENTTIDLTSEKPAVNSPO4PR peptide. (B) Showing the detected y- and b-fragmentation series of the chymotryptic ENTTIDLTSEKPAVNSPO4PRPAPGAAGPPQVGL peptide. Phosphorylation site localization probability scores of the S343 and the mass error of the observed precursor mass are given in the upper left of the spectra.

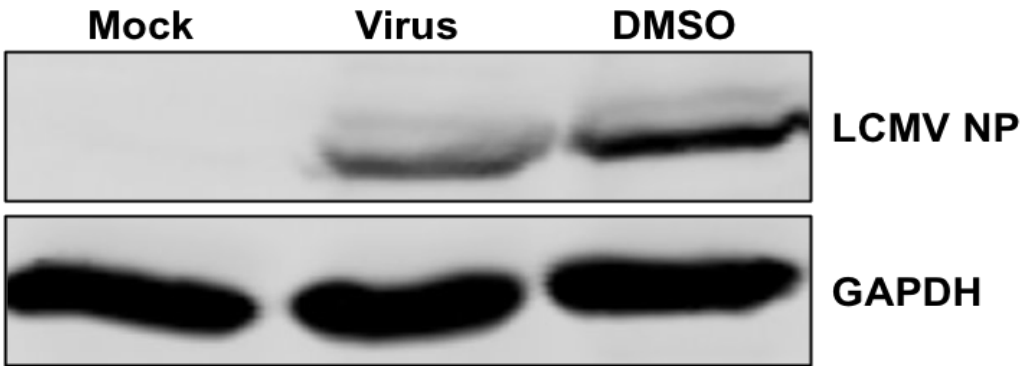

Figure 8.2: Minor 'doublet' LCMV band from native infection. A549 cells were infected with rLCMV-WT at an MOI of 0.2, and lysates gathered at 24 hpi prior to western blot analysis.

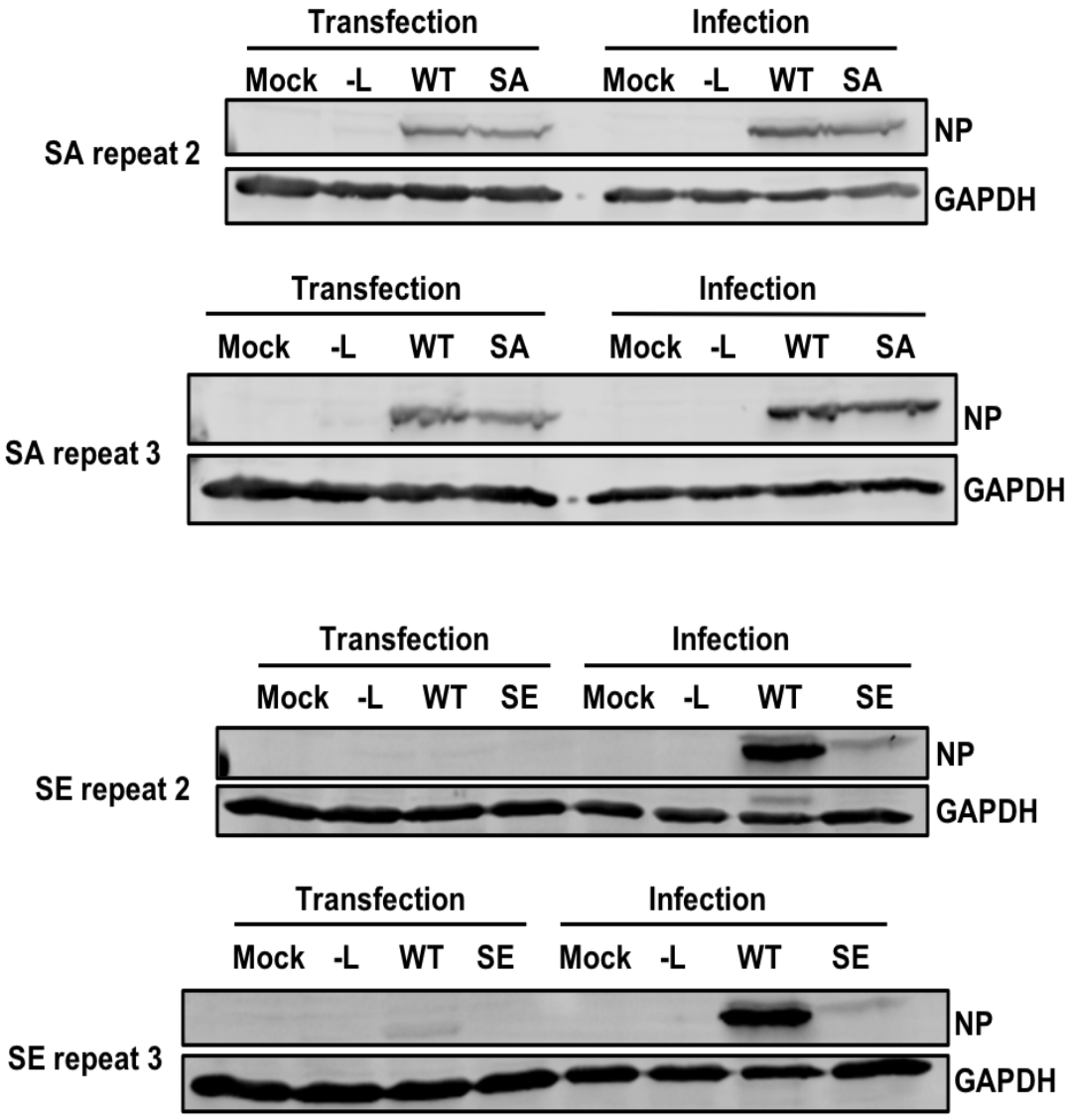

Figure 8.3: Additional rLCMV-S343A/E rescues (alongside rLCMV-WT). For completeness, three independent experimental recoveries of rLCMV-WT, rLCMV-S343A and rLCMV-S343E were performed identical to Figure 4.4B.